A Study of Dry Frictional Contacts

ABSTRACT

A Study of Dry Frictional Contacts **Richard Munisamy**

Lincoln College

D. Phil Thesis **Hilary 1994**

This study addresses a range of phenomena associated with dry frictional contacts. Particular emphasis is devoted to elastic dissimilarity. Problems are formulated such that coupling between normal and tangential tractions is permitted and the results, which must often be found by numerical means, are compared with classical solutions.

The manipulation of objects in contact with frictional surfaces is investigated. The main focus is on objects resting upon a plane at three discrete points of support. When displaced by an arbitrary force such objects have a tendency to rotate about these points of support. The motion of both planar and three dimensional objects is predicted and the effect of friction at the pushing contact is considered.

Rolling contact between two elastically dissimilar cylinders is addressed. By allowing full coupling between normal and tangential tractions it is found that an offset in the contact patch may result. This often leads to a significant resistive moment which balances the nett power supplied and the frictional losses.

Three dimensional contacts form a major part of the study and a numerical method is developed to facilitate their solution. The evolution of an incomplete contact is evaluated to demonstrate how contact boundaries may be determined. The method is then applied to sliding contact between elastically dissimilar spheres. The traction distributions which result from a fully coupled formulation are compared with those predicted by a Hertzian solution. The parameters which cause the greatest differences are found.

A Mindlin-type contact is re-evaluated and traction distributions are calculated which are compatible with local slip directions for both elastically similar and dissimilar bodies. A comprehensive set of results is presented revealing how material parameters influence the solution.

Interactions between cracks and contacts are analyzed. It is shown that although the change in compliance of a flawed body may modify the traction distribution compared with a flawless one, the stress intensity factors at the crack tip are rarely affected.

Finally, a method of determining the fracture toughness of brittle materials is explored based on the observation of surface cracks in the wake of a sliding indenter. Material characteristics are related to crack initiation, spacing and depth.

Acknowledgements

I am deeply indebted to Dr D A Hills for his unceasing encouragement and guidance throughout my time of study.

Thanks is also due to the members of the Structural Integrity Department of AEA Consultancy Services for their understanding and support during the writing of this thesis.

Richard Munisamy, 25 February 1994

Contents

Chapter 1

Introduction

1.1 Friction

Experience attests to the fact that when two bodies are pressed into normal contact, a force may be generated at the interface which tends to oppose any relative tangential motion. This force is known as friction and a dry frictional contact results when there is no significant lubrication at the interface.

General laws of friction have been developed from experimental observations originating with Leonardo da Vinci, Amontons (1699) and Coulomb (1785). They have been summarised by Prescott (1923) and are repeated here in a slightly modified form:

1. When two bodies in contact are in relative motion, the friction acting on either body at a point of contact is in the direction opposite to the motion of that point relative to the contiguous point of the other body.

2. The frictional traction at any point of contact of two given bodies cannot exceed a certain fraction of the normal pressure between the two bodies at that point. This maximum fraction is known as the coefficient of friction and, in general, depends upon the material of the two bodies and the condition of the two surfaces.

3. The coefficient of friction is independent of the intensity of the normal pressure.

An inference from the third law is that the frictional force is independent of the contact area.

The surfaces of engineering materials are not topologically smooth and for many years, following the lead of Amontons and Coulomb, it was assumed that friction was the result of lifting one surface over the roughnesses of the other. More recently, however, the hypothesis that adhesion between the two bodies plays a significant role was established by Hardy (1919) and Tomlinson (1929). This hypothesis implies that friction is due to the shearing of junctions at the asperity scale and hence should depend upon the area of contact, which accounts for its rejection by the earlier workers. This discrepancy was cleared up by Holm (1938), Ernst and Merchant (1940), and Bowden and Tabor (1942), who pointed out that only the tips of asperities within the interface are in actual contact. Hence, the real area of contact is much less than the nominal one. Greenwood and Williamson (1966), modelling the surface of rough bodies by a Gaussian distribution of elastically deformable asperities with spherical tips, have shown that the real contact area increases in proportion to the normal load. Much experimental evidence has confirmed this. Hence, the empirical rules of Amontons and Coulomb can be explained.

It is useful at the outset to draw a distinction between sliding and slipping. Every contact takes place over a distributed area no matter how small this is with respect to the characteristic dimensions of the two bodies. Sliding occurs when there is gross translation of one body over the surface of the other. If there is no rolling or spin associated with the relative motion of the bodies then the frictional tractions all act parallel to the direction of slide. It is such a model of sliding that leads to the potentially misleading, traditional definition of the coefficient of friction $f = Q/P$, where Q and P are tangential and normal forces respectively.

Slip occurs when there is relative motion of contiguous points in each body. Within

a contact there may be points which are slipping and different points which are simultaneously adhered. In addition the relative direction of relative motion of separate points within the contact may be different. This gives rise to the pointwise definition of the coefficient of friction at a point of slip $f = q(x,y)/p(x,y)$, where $q(x,y)$ and $p(x,y)$ are the local tangential and normal tractions.

The distinction between the traditional and pointwise definitions can be clearly seen from the example of a sphere which slides over a plane while spinning about an axis perpendicular to the plane. Every point within the contact is slipping and yet, by the traditional definition of the coefficient of friction, the ratio of tangential and normal forces is smaller than that which would be measured if the sphere was not spinning. The pointwise definition, however, taking account of the local direction of slip, remains consistent.

Although the laws of friction generally describe physical contacts well, there are some significant exceptions. The static coefficient of friction (ie. prior to any slip) is often found to be greater than the kinetic coefficient of friction (ie. during sliding). The coefficient of static friction tends to increase with time and may be due to a combination of the growth in the real contact area due to creep, the strengthening of adhesion points due to atomic diffusion, and the breakdown and penetration of any surface contaminant films. In lubricated contacts the kinetic coefficient of friction tends to vary greatly with the velocity of relative slip, due to viscous effects. However, in dry contacts the variation is much smaller and, over significant ranges of velocity, can be considered constant.

Despite the limitations of the general laws of friction, they are approximately true in many practical situations. They also have the advantage of being easily included in numerical analyses. Hence, when applied to the problems considered in this study, it is assumed that the static and kinetic coefficients of friction have the same, constant value.

Frictional forces are generated at regions of contact when two bodies displace tangentially relative to one another. Hence, a body may be manipulated by pushing it across

the surface of another. Using bodies with discrete points of contact is a convenient way of analyzing the resulting motion. Where the contact is over a distributed area, frictional tractions may arise within the contact area. This occurs, of course, when the bodies slide over each other, but can still happen when the relative displacement is insufficient to cause sliding or in rolling contact. In the last two cases areas of stick and areas of local slip may co-exist within the contact.

1.2 Manipulation

The tendency of frictional forces to oppose the relative motion of two bodies may be exploited by a scheme to manipulate objects. People apply such processes heuristically. For example, a coin may be pushed along the top of a table to the edge, where it can be picked up more easily.

The general requirement to understand how an object, resting on a frictional surface, will move when pushed by another contacting body is important in the field of robotics, where such knowledge is a prerequisite for formulating strategies to grasp an object. There is also a possibility that knowledge of the motion of a body under these conditions might allow orientation of parts by successive sliding operations with the minimum of sensor feedback. Such a capability would be valuable in the area of flexible assembly.

At first sight this would appear to be an elementary problem in mechanics with well known solutions, but although the problem was formulated many years ago, it has only recently been receiving attention when the motivations mentioned above have prompted several investigators to employ numerical methods in the solution of various aspects of the problem. Some notable early work on the mechanics of sliding has been presented by Prescott (1923) and MacMillan (1936). Prescott, in particular, formulated the conditions for rotation of a body about a point of support. He also discussed the case of rotation about any other point, but concluded the problem of finding such a point for a given imposed force "is a difficult one".

The first significant recent contribution was made by Mason (1982; 1986), who studied the mechanics of pushing and devised a means of locating the centre of rotation of a pushed body by numerical means. Other recent contributions were made by Erdmann and Mason (1986) and Peshkin (1986). Peshkin and Sanderson (1988) have considered the limits within which the motion of a pushed body must lie for arbitrary pressure distributions. Goyal (1989) and Goyal, Ruina, and Papadopoulos (1989) have developed the limit surface technique for describing the motion of a body on a frictional surface under the action of a known force. These papers are useful in the case where the direction of the force is known (ie. when there is no friction between a pushing finger and a pushed object) but have less relevance when the force direction is not explicitly specified (e.g. in Mason's work, where the direction of motion of the finger is specified, but there may be friction between finger and pushed body). A similar approach has been adopted in analyzing the sliding of distributed contacts by Liu and Paul (1989). Several authors, e.g. (Mason, 1982; Goyal, 1989), have noted the tendency for an object to rotate about a point of support, although the conditions for this have not been explicitly stated.

In conclusion, there is much to be learned about the manipulation of objects resting on frictional surfaces. Greater knowledge will enable this phenomenon of friction to be exploited more effectively.

1.3 Discrete contacts

A contact may be described as discrete when the bodies involved are rigid and non-conforming. The bodies meet at individual points; the radii of such contacts are infinitesimal compared with the inter-contact dimensions. The simplest example of this is an object resting on a flat surface, making contact at three points of support or "feet". Elementary mechanics provides the solution for the normal reaction at each foot when the weight of the body and its geometry are known. Such an object is an ideal candidate for a manipulation analysis. If an attempt is made to displace the object over the flat

surface, frictional forces will be generated at the feet. Each will act in the plane of the surface in a direction which opposes any actual or potential relative motion at that point. These frictional effects may be exploited to manipulate the object from one position and orientation to another.

Chapters 2 and 3 present analyses of the frictional manipulation of objects with 3 discrete feet over flat surfaces. The extension of the method to encompass distributed contacts is discussed in these Chapters. However, a knowledge of pressure distributions is a prerequisite. In Chapter 5 a methodology is developed which allows the general solution pressure distributions acting over a finite area. The inclusion of this methodology within a scheme to manipulate such objects is beyond the scope of this study because of the often complex interactions of the pushing finger with the pressure distribution. However, the effects of friction in distributed contacts is itself of interest and often difficult to evaluate, especially when the objects in contact have dissimilar elastic properties.

1.4 Pressure distributions and surface displacements

A point contact is a mathematical convenience rather than a common physical occurrence. When an appreciable force is used to push two bodies together, some deformation of one or both of them will occur to generate a contact over a finite area. Simple recourse to the conditions of static equilibrium are no longer sufficient to evaluate the pressure distribution which results. However, the pressure may be found if the compatibility of deformation is considered. This deformation may be elastic or plastic, or a combination of both, but in this study, purely elastic behaviour is considered. If a traction distribution produces relative surface displacements of the bodies which are compatible with the form of the contact, a solution has been found.

In 1882, Hertz (1882) was the first to evaluate a pressure distribution in this way. His analysis applies to the normal contact of two elastic solids with quadratic surface profiles

(for example two spheres) subject to the following constraints:

- The radius of the contact is much smaller than the radii of curvature of the bodies and their characteristic dimensions.

- The bodies are either frictionless or elastically similar.

The first condition implies that the surfaces are non-conforming, that the strains are small and that each solid may be approximated by an elastic half-space. It also implies that a spherical surface (for example) may be represented by a rotated parabola. The second condition ensures that no frictional tractions are generated within the contact.

In its most general form, Hertz's result is the pressure distribution $p(x, y)$ generated over an elliptically shaped contact with major and minor axes a and b, and may be written as

$$p(x, y) = p_0(1 - \frac{x^2}{a^2} - \frac{y^2}{b^2})^{\frac{1}{2}} \tag{1.1}$$

where p_0 is the peak pressure and is given by

$$p_0 = \frac{3P}{2\pi ab} \tag{1.2}$$

where P is the normal load.

In general, normal tractions at the surface of an elastic body produce both normal and, by Poisson's effect, tangential displacements. Similarly tangential tractions tend to produce normal displacements in addition to tangential ones. For elastically similar bodies pressed together by a normal force alone, the tangential displacements in each are identical and so the relative displacement in this plane is zero; hence, no frictional tractions are generated. Even when frictional tractions are generated, through tangential displacement of the bodies, they produce no *relative* normal displacement and hence the

relative curvature of the bodies remains unchanged. As a result, Hertz's solution can be extended to include a tangential as well as normal force provided that the objects in contact have similar elastic properties.

1.5 Elastic Dissimilarity

The degree of coupling between the normal tractions and the resulting tangential deformation and between the frictional tractions and the normal deformation is a function of two properties of each material: Poisson's ratio and the modulus of rigidity. When two elastically dissimilar bodies are pushed together by a normal force, a pressure distribution and normal surface deformation result. In addition, the bodies experience relative tangential deformation, which, if friction is present, will be opposed by frictional tractions. These frictional tractions in turn affect the relative normal deformation. Hence, the pressure distribution and the frictional tractions must be solved simultaneously in the general contact problem.

For certain combinations of materials, and when the coefficient of friction is small, the effect of coupling between frictional tractions and normal displacements is small in comparison with the coupling between the normal tractions and the tangential deformations. Goodman (1962) was the first to analyze a problem ignoring the coupling between tangential tractions and normal displacements. When this approximation is made, the pressure distribution may be evaluated independently of the tangential tractions, which are found subsequently. In this study a distinction will be drawn between "semi-coupled" problems where the so-called Goodman approximation is made and "fully-coupled" ones in which the full effect of tangential tractions upon normal displacements is considered.

1.6 Two dimensional contacts

With the obvious exception of Hertz's analysis, three dimensional contacts are notoriously difficult to analyze. Fortunately a few problems may be reduced to two dimensions which

allow much simpler solutions and offer limited insight into their three dimensional counterparts. For example, when two infinitely long cylinders are pushed together with their axes aligned, all transverse sections through the contact are identical. This is an example of a line contact and mathematically may be evaluated in two dimensions by considering a single section.

1.6.1 Similar elastic properties

If the cylinders have the same elastic properties then the normal pressure distribution is given as a special case of Hertz's theory. Further, the tangential tractions generated when the cylinders are sliding over each other are a constant fraction (the coefficient of friction) of the coincident pressure. The stress field in such a case has been found by Smith and Liu (1953).

Frictional tractions may also be generated, once the cylinders have been pressed together, by the subsequent addition of a tangential load. If this load is insufficient to cause gross sliding the classic Mindlin-Cattaneo (Mindlin, 1949; Cattaneo, 1938) contact results. The distribution of tangential tractions has been shown to have an adhered portion in the middle surrounded by regions of slip at the edges.

When two cylinders are in rolling contact, no frictional tractions result if no tangential force is transmitted between the two rollers (free rolling). However, during tractive rolling, for example if one cylinder is driven or braked, a tangential traction distribution is established. This was first analyzed by Carter (1926).

1.6.2 Dissimilar elastic properties

Several authors have relaxed Hertz's restrictions to consider frictional contact between two cylinders of materials whose properties are elastically dissimilar. The most obvious case—normal indentation—was presented by Spence (1973). He solved the semi-coupled problem in closed form and the fully coupled one numerically. Like the Mindlin-Cattaneo

contact between elastically similar cylinders there is a central stick zone bordered by regions of slip. As a result, the problem is history dependent and so should be solved in an incremental manner. However, Spence showed that the proportion of the contact which falls within the stick zone is independent of the load and hence solved the problem by appealing to self-similarity. When the Goodman approximation is not applicable the fully coupled formulation produces, in addition to tangential tractions, a pressure distribution whose form and extent differs from Hertz's solution.

Nowell, Hills and Sackfield (1988) duplicated Spence's results using a powerful numerical technique (which is also used in parts of this study) and then analyzed the effect of subsequently adding a tangential force, resulting in the dissimilar elastic equivalent of the Mindlin-Cattaneo contact. They formulated the fully coupled problem and like Spence found the solution to be history dependent. Self-similarity arguments could be applied to monotonically increasing loads but not to oscillating ones. Because a nett tangential force is applied, the differences compared to the equivalent elastically similar contact are even more marked than for the purely normal contact and, in addition, the middle of the contact does not necessarily coincide with the line joining the centres of the cylinders.

The steady state sliding contact problem is actually easier to formulate that the normal indentation contact because the tangential tractions take their limiting values and hence are simply a constant fraction of the normal ones. Hills and Sackfield (1985) have presented a closed form solution for the traction distributions from which the stress state within the contacting bodies can be found numerically. The pressure distribution shows the typical differences compared to Hertz's solution and the stress field is also modified; of particular significance is the effect on the largest tensile stress.

Fully coupled rolling contact has been considered by Bentall and Johnson (1967). However, their results focus almost exclusively on free rolling. They showed that even when no tangential force is transmitted, tangential tractions arise due to material dissimilarity. and were able to evaluate the resulting frictional resistance (i.e. energy losses). Tractive

rolling has been analyzed by Kalker (1971) and Nowell and Hills (1988), but in both cases a semi-coupled formulation was employed. Of interest is the observation that for certain combinations of material pairs, the driven roller actually has a greater peripheral velocity than the driver. At first sight, it appears that energy is created by such a system—a clear violation of the first law of thermodynamics. It was postulated that the use of the Goodman approximation resulted in this anomaly. The resolution of this discrepancy is the goal of Chapter 4 of this study where the fully coupled problem is formulated.

1.7 Three dimensional contacts

Far fewer analytic or numerical solutions have been presented for three dimensional contacts than two dimensional ones. The most prominent result is, of course, that by Hertz and a further special case of his analysis is the contact between two spheres. Here the contact area is circular and the form of the contact is axisymmetric rather than strictly varying independently in each of three dimensions. The stress field generated by normal indentation has been found by Hüber (1904) and the one for sliding frictional contact has been found by Hamilton and Goodman (1966) for two elastically similar spheres. Although generally similar, they do show several qualitative differences to the comparable fields generated by the cylinders. For instance, in the axisymmetric case the stress field produced by purely normal indentation has a tensile region whereas the two dimensional field is compressive everywhere.

When the spheres have dissimilar elastic properties normal indentation generates tangential tractions as in the two dimensional equivalent. Goodman (1962) solved this contact problem by assuming that the coefficient of friction was sufficiently high to prevent slip at all points. In addition he made the approximation that the normal tractions were unaffected by the tangential ones. Spence relaxed the former approximation but retained the latter as a first step in solving the fully coupled problem which he achieved numerically (Spence, 1975). The result of both the semi-coupled and fully coupled solution is a

region of stick surrounded by an annulus of slip and, as in two dimensions, self-similarity fixes the slip/stick interface for monotonically increasing loads. Hills and Sackfield (1987) evaluated the stress field produced by the semi-coupled formulation, which shows that the tensile region produced if the spheres are elastically similar is enhanced in the less compliant body and reduced in the more compliant one. Chapter 7 of this study presents a fully coupled solution to the frictional sliding contact of elastically dissimilar spheres.

The Mindlin-Cattaneo solution was formulated for the normal indentation of two spheres followed by the application of a tangential force. The solution may be simplified to model contact between cylinders and it is exactly true provided they are made from similar materials. However, because the original solution assumed that the tangential tractions all act parallel to the applied force, it is only exactly true for elastically similar spheres if their Poisson's ratio is zero. Chapter 8 addresses this type of contact for materials with a non-zero Poisson's ratio and in addition presents a numerical solution to the semi-coupled problem generated by material dissimilarity.

Rolling in three dimensions fully deserves a study on its own. The numerous degrees of freedom of motion tend to make the problems very complex. Kalker has solved several such problems and the results can be found in his recent book (Kalker, 1990).

As discussed earlier, it would be valuable to have a fuller understanding of the manipulation of objects in contact with a plane over an area, rather than a set of discrete points, for application within the field of robotics. In the course of solving some classical contact problems in three dimensions in this study, the tools are developed in Chapter 5 which could be used in a scheme to predict the motion of a pushed body which is in contact with a plane over a finite area. However, there is a degree of coupling between the pushing forces and the traction distributions and hence the solution of the manipulation problem is very complex. Although it is possible to solve such a problem, to generate a locus of instantaneous centres would require a far greater computer resource than that employed to solve the other problems in this study. However, the related problem of loss

of contact is addressed in Chapter 6 as a simple example of the methodology developed in Chapter 5.

Some significant gaps exist in the field of three dimensional non-conforming contacts between materials with dissimilar elastic properties. The most prominent of these, namely frictional sliding and the Mindlin-Cattaneo type contact, are addressed in this study.

1.8 Interactions between cracks and contacts

As alluded to earlier, frictional contacts can generate high tensile stresses. Even an axisymmetric Hertzian-type contact under normal load alone generates a significant annulus of tension if the materials are elastically dissimilar and this has been analyzed by Johnson *et al.* (1973). Roesler (1957) found that a ring crack may result if a very brittle material is indented, and Frank and Lawn (1967) discovered that further loading may produce a crack in the shape of the frustum of a cone.

Sliding frictional contacts generate even greater tensile stresses in the wake of the contact area. Regularly spaced horseshoe shaped cracks have been observed by Lawn (1967) which were produced by this region of tension. This phenomenon is particularly interesting because when one crack is produced, the magnitude of the tensile stress at the trailing edge of the indenter is immediately reduced. Only as the indenter moves away from the initial crack does the stress field recover sufficiently to generate another.

In principle it should be possible to deduce the fracture toughness of a material by using such observations. The first step was made by Gilroy and Hirst (1969) who applied the technique of dimensional analysis to cracks caused by both static and sliding Hertzian loads. Approximate applied stress intensity factors were evaluated by Mouginot (1987) for frictional sliding and Li and Hills (1987) used a finite element method to evaluate stress intensity factors driving the cone crack. In Chapter 9 a method is presented to evaluate more accurately the stress intensity factors at cracks which are propelled by a sliding Hertzian contact.

One phenomenon which has not received much attention is the effect that the crack has on the pressure distribution beneath an indenter. It is common in analyses involving cracks and contacts to assume that the pressure distribution is the same for the flawed body as the flawless one. Such an assumption takes no account of the increased flexibility of the damaged body. Bryant *et al.* (1984) have analyzed the load redistribution affects for a range of crack orientations and positions and found that flaws have an insignificant effect. However, their results are limited to cracks which are only a small fraction of the size of the contact width. Chapter 10 investigates the modification to the pressure distribution and hence the applied stress intensity factor which arises from a larger range of crack sizes.

Chapter 2

The Manipulation of Objects Resting on a Frictional Plane I

2.1 Introduction

Frictional manipulation is the study of the motion of objects which are being pushed over surfaces, when the motion is opposed by frictional forces generated between the object and the surface. As the object is pushed, a displacement is imposed upon it. In quasi-static problems where acceleration forces and hence inertia terms are absent, the pushing force must be in equilibrium with frictional forces which resist the motion.

In the simplest terms, a frictional manipulation problem is solved when the postulated motion of the object is compatible with the imposed displacement, whilst simultaneously satisfying equilibrium between the applied force and the frictional resistance. For simple problems, the solution is always unique except when the points of support of the object are collinear (Goyal *et al.*, 1989) (in which case, of course, like a motorbike, it will not stand up).

One example will suffice to demonstrate how useful, yet complicated, frictional manipulation can be. When a person first picks up a pen, it is extremely unlikely that the pen will be in the ideal orientation within the person's hand for the purpose of writing. By a

---

The work described in this Chapter has been published and can be found in: D. Nowell, D. A. Hills and R. L. Munisamy 1991,"Conditions for translation and rotation of bodies on frictional surfaces" *Proc. Instn. Mech. Engrs.*, Vol 205, pp. 311–316.

process of frictional manipulation, using the fingers as both manipulators and restraining surfaces, the pen can be manoeuvred into the correct position.

Obviously the above example is difficult enough to analyze after the event. It is far more difficult to *predict* how the fingers should move in order to manipulate the pen into the required orientation. This Chapter presents an analysis of a simplified problem which may be used as a first step towards the solution of the more general one. Several simplifying assumptions are made, some of which are relaxed in Chapter 3 as the complexity of the problem is developed.

In the pen manipulation example, the contacts between the pen and the pushing fingers and restraining ones are distributed over finite areas. The resisting surface, which is composed of the other fingers, is three dimensional. Frictional tractions are generated between the pen and all the fingers.

In this Chapter, it is assumed that all contacts are discrete, ie. that the radius of each contact is infinitesimally small compared with the inter-contact dimensions. The frictional surface is a horizontal plane and the object rests on it with three points of support (or "feet"). The "finger" pushes the object in the plane of its feet and the coefficient of friction between the finger and the object is zero. The following questions are addressed:

- Where must the finger push to produce pure translation?

- Where must the finger push to produce rotation about one of the points of support?

- What is the motion if the finger pushes elsewhere?

Several authors, for example (Mason, 1982; Goyal, 1989), have noted the tendency for an object to rotate about a point of support and the aim of question 2 is to elucidate this.

2.2 Formulation

The configuration adopted is shown in Figure 2.1. A body of weight W rests on three feet in contact with a horizontal plane with a coefficient of interfacial friction f. The overall geometry of the body is unimportant, but the locations of the feet are defined relative to the centre of gravity C, located at the origin of coordinates. The body will move as a result of an imposed displacement from the finger which pushes against a surface situated in the plane of the feet, a distance $\bar{y}$ from C. For the case discussed here this surface will be assumed to be frictionless and the direction of the force, P, occurring at the point of contact will therefore be normal to the pushing surface. For such a frictionless surface the relevant parameters are the direction of the force P and its point of application $(\bar{x}, \bar{y})$, but the notion of a pushing surface is helpful in the context of the manipulation simulation discussed in Section 2.4 and for further work in which friction between the finger and the pushed body may be important.

The three feet are inclined at angles ϕ_1, ϕ_2, ϕ_3 to the pushing surface and are situated at distances r_l, r_2, r_3 from C. The pushing force acts at a point a distance $\bar{x}$ along the pushing surface. The configuration of a three–footed body was chosen because the distribution of forces between the surface and the body is statically determinate and no uncertainties exist. The configuration is simple but non-trivial to analyze and the results can be generalised to bodies with more than three points of support, provided that the supporting force (or, in the limit of distributed contact, pressure) distribution is known.

First to be solved is the elementary statics problem of finding the vertical reactions V_i at the feet. Resolving vertically (ie. perpendicular to the frictional plane) gives:

$$\sum_{i=1}^{3} V_i = W. \tag{2.1}$$

Taking moments about a horizontal line through C and parallel to the pushing surface yields:

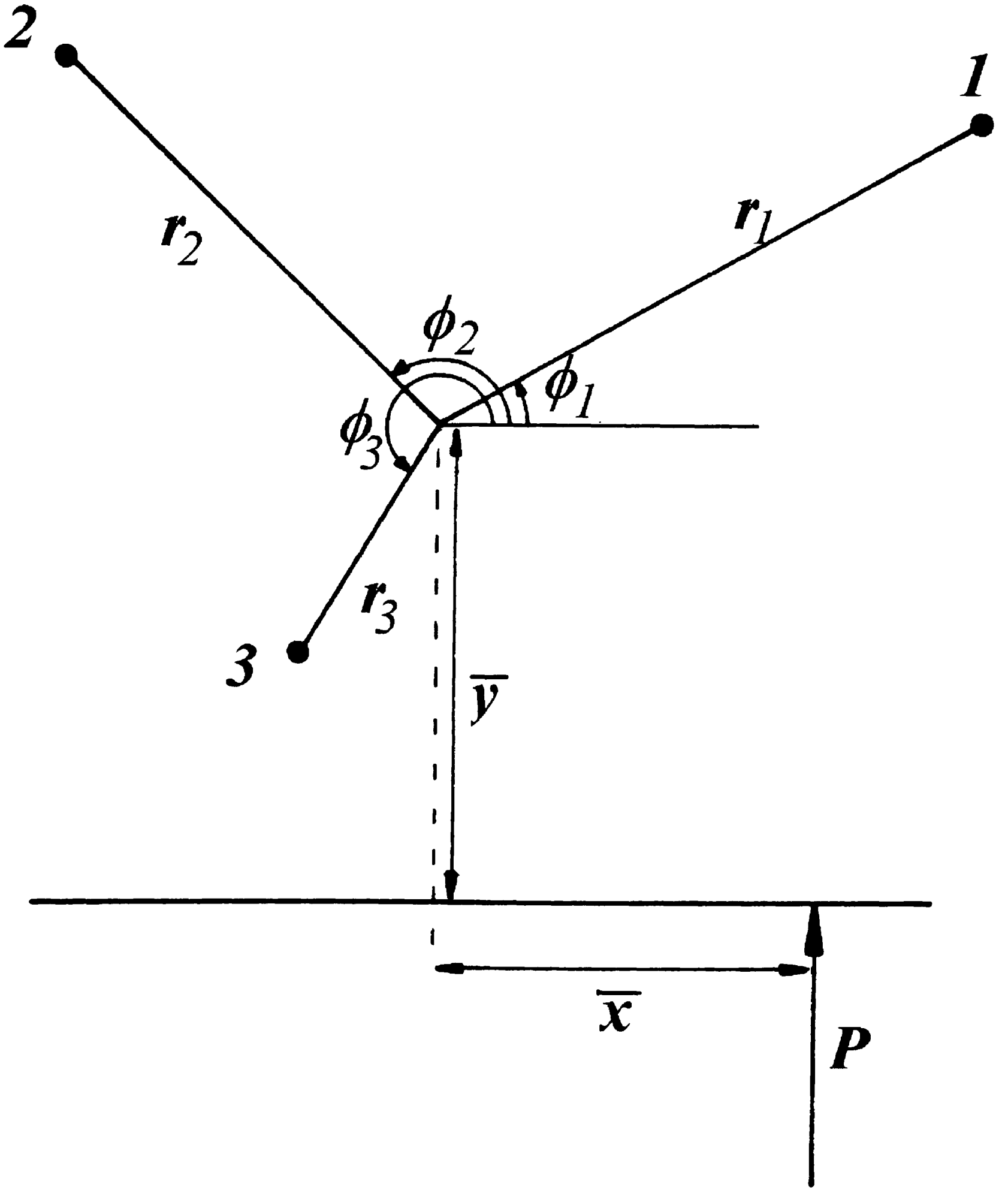

Figure 2.1: Geometry of the pushed body.

$$\sum_{i=1}^{3} V_i r_i \sin \phi_i = 0 \tag{2.2}$$

whereas taking moments about a line through C and perpendicular to the pushing surface gives:

$$\sum_{i=1}^{3} V_i r_i \cos \phi_i = 0. \tag{2.3}$$

These equations are sufficient to solve for the reactions V_i in terms of the weight of the body and its geometry. An exception occurs when the three feet are collinear, in which case the reactions are statically indeterminate and equations 2.1,2,3 are no longer linearly independent.

Next the motion of the body of the body is considered. It is assumed that the problem is quasi-static, so that the pushing force P is just sufficient to move the body (ie. so that inertia forces are small compared with friction: this will be the case in most practical problems where motion is imparted by imposing a displacement, rather than by the application of a controlled force). The motion of the body will be such that an instantaneous centre will exist at some point I, about which the body can be considered to be rotating. The case of pure translation may be catered for by letting the distance of this point from C approach infinity. Figure 2.2 shows the resulting motion. The body is rotating anticlockwise about I and frictional forces H_i arise at each foot, opposing the relative motion. The direction of these forces is therefore specified at each moving foot, whilst their magnitudes are given by

$$H_i = fV_i \qquad i = 1, 2, 3, \tag{2.4}$$

To ensure equilibrium in the plane of sliding it is necessary to resolve the applied and frictional forces parallel and perpendicular to the pushing surface giving respectively:

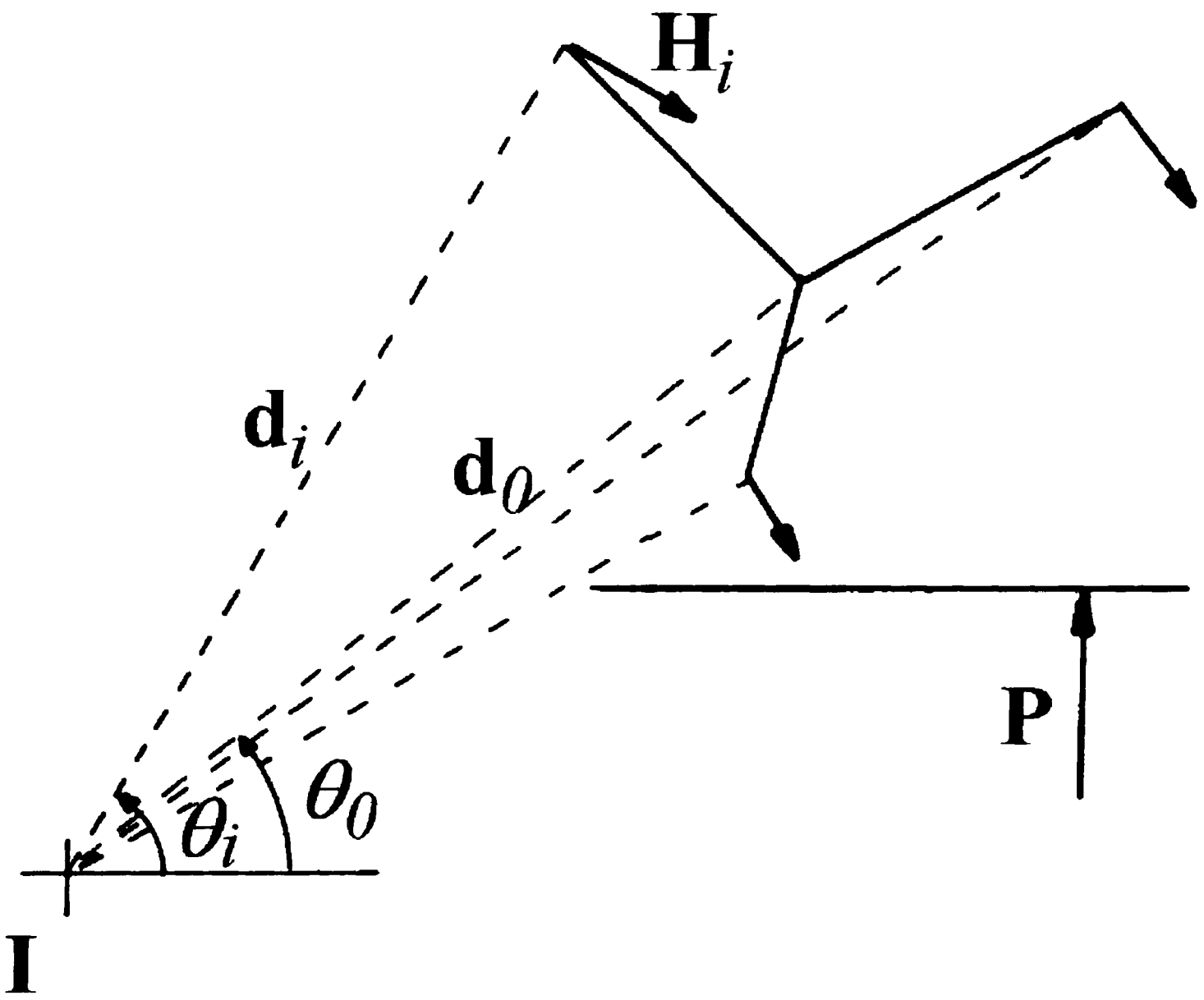

Figure 2.2: Frictional forces acting on the body.

$$\sum_{i=1}^{3} H_i \sin\theta_i = 0 \tag{2.5}$$

$$\sum_{i=1}^{3} H_i \cos\theta_i = P \tag{2.6}$$

whilst taking moments about the instantaneous centre yields

$$\sum_{i=1}^{3} H_i\, d_i = P(d_0 \cos\theta_0 + \bar{x}) \tag{2.7}$$

where d_0 and θ_0 specify the position of I, and d_i, θ_i are given by:

$$d_i \cos\theta_i = d_0 \cos\theta_0 + r_i \cos\phi_i \tag{2.8}$$

$$d_i \sin\theta_i = d_0 \sin\theta_0 + r_i \sin\phi_i \tag{2.9}$$

In this case, when all feet are sliding, H_i are known and the nine equations 2.5–7 are sufficient to solve for the nine unknowns ($d_0, \theta_0, P, \theta_i$, and d_i). In the case where one of the feet sticks, the body must rotate about that foot and the instantaneous centre I must lie there. Since the jth foot is now stationary H_j is no longer equal to the limiting frictional force and now becomes a variable, whereas the position of the instantaneous centre is known and d_j is zero. The direction of the force at j is also unknown so that θ_j remains a variable and the nine equations remain with H_j replacing d_j as an unknown.

Once again, the formulation can be seen to be statically determinate, except in the case of collinearity of the feet which will be discussed more fully later. An outline of a solution procedure will now be developed.

2.3 Solution

In general, three types of motion are possible: pure translation, rotation about a point of support and combined translation and rotation. In order to predict these types of motion,

the three questions posed in the Introduction to this chapter will be addressed in turn. An additional question, viz. "What happens when the points of support are collinear?" will also be considered.

2.3.1 Conditions for pure translation

The conditions for pure translation of a body were first stated explicitly by Macmillan (1936) and repeated by Mason (1982). They are briefly presented here in the current notation as an introduction to later sections. In order for the body to undergo pure translation, the instantaneous centre of the motion must be an infinite distance from the body. Thus:

$$\cos\theta_i = \cos\theta_0 \qquad i = 1,2,3 \tag{2.10}$$

$$\sin\theta_i = \sin\theta_0 \qquad i = 1,2,3. \tag{2.11}$$

Substituting in equation 2.5 gives:

$$\sum_{i=1}^{3} H_i \sin\theta_0 = 0. \tag{2.12}$$

Hence $\sin\theta_0 = 0$, $\cos\theta_0 = \pm 1$.

Substitution of equation 2.6 in equation 2.7 to eliminate P yields:

$$\sum_{i=1}^{3} H_i d_i = (d_0 \cos\theta_0 + \bar{x}) \sum_{i=1}^{3} H_i \cos\theta_i \tag{2.13}$$

and, since $d_i = d_0 \quad (i = 1,2,3)$

$$d_0 = d_0 \cos^2\theta_0 + \bar{x}\cos\theta_0 \tag{2.14}$$

which has the solution $\bar{x} = 0$ when $\cos\theta_0 = \pm 1$.

Therefore, to produce a pure translation of the body, the pushing force needs to be applied at $\bar{x} = 0$, i.e. with the force acting through the centre of gravity of the body. This

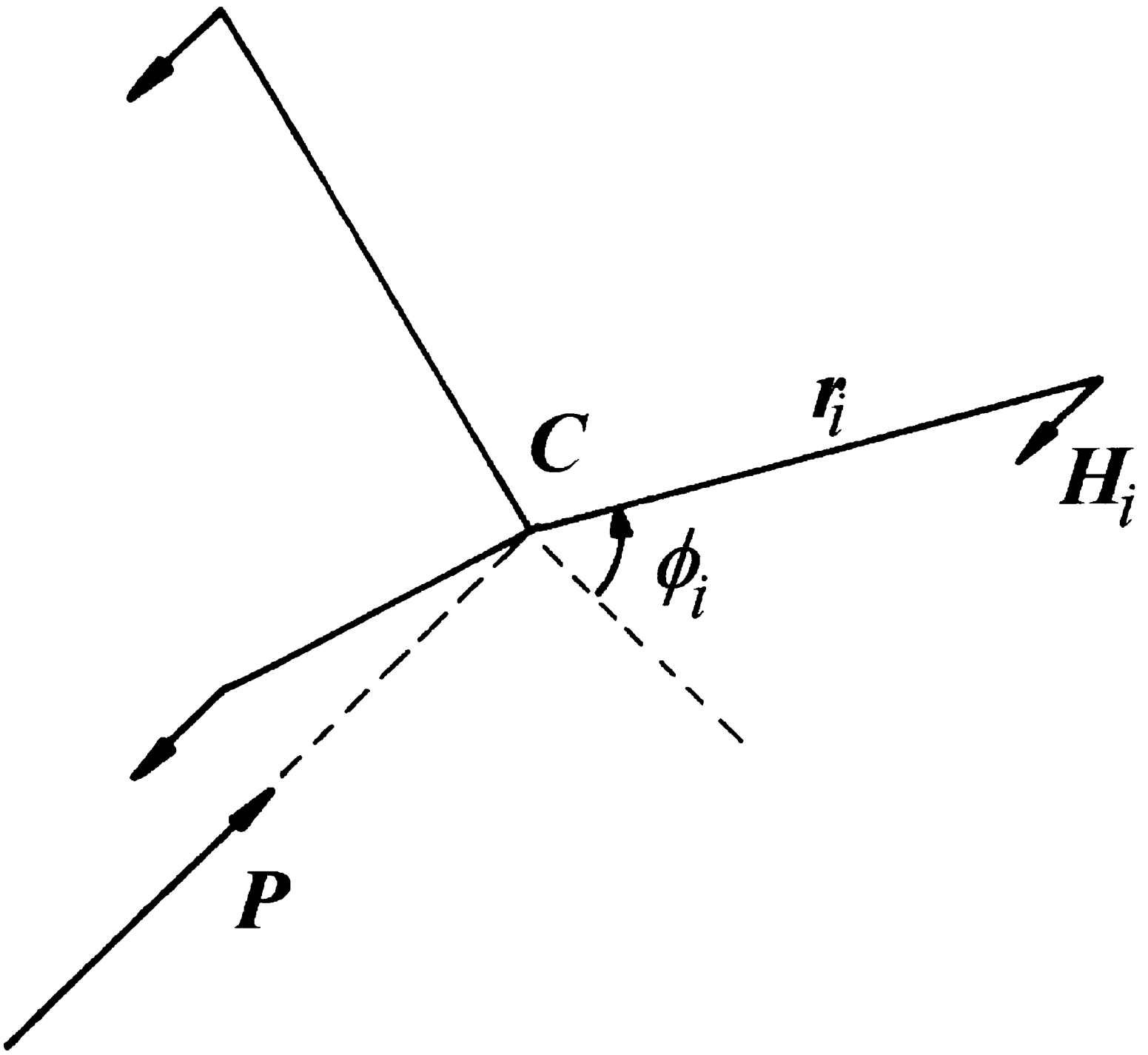

Figure 2.3: Forces acting on body during pure translation.

result may be generalised quite simply for a body with N feet, or in the limit ($N \to \infty$) distributed contact, provided that the pressure distribution is known. Figure 2.3 shows in plan an object with N feet, and with an external, impressed force passing through the centroid C. Taking moments about C gives:

$$\sum_{i=1}^{N} H_i r_i \sin \phi_i = 0. \tag{2.15}$$

Assuming that all the feet are sliding then:

$$f \sum_{i=1}^{N} V_i r_i \sin \phi_i = 0. \tag{2.16}$$

This is automatically satisfied since the expression within the summation sign is a condition for vertical equilibrium (equation 2.2). Therefore, the general result is that a body resting on a surface with constant coefficient of friction can always be translated by pushing through its centre of gravity. In particular, if, instead of discrete feet the contact is continuous, application of the imposed force through the centre of gravity produces pure translation. A corollary of this result is that it is not possible to orientate objects by allowing them to slide down an inclined plane of constant frictional coefficient under the action of gravity. The applied force due to gravity always acts through the centre of gravity and pure translation results.

2.3.2 Conditions for pure rotation

The second problem is to find the conditions for pure rotation of the body about a point of support. Mason (1982) and Goyal (1989) both note that bodies have a tendency to move in this manner and it would be useful to develop closed form expressions for the conditions for such motion. Suppose the body pivots about foot j. All other feet will be sliding and equation 2.5 becomes:

$$H_j \sin \theta_j = -f \sum_{i=1}^{3} \epsilon_{ij} V_i \sin \theta_i = \alpha \tag{2.17}$$

where $\epsilon_{ij} = 0$ for $i = j$ and $\epsilon_{ij} = 1$ for $i \neq j$. Similarly, equation 2.13 becomes:

$$H_j \cos \theta_j = \frac{f \sum_{i=1}^{3} \epsilon_{ij} V_i d_i}{\bar{x} - r_j \cos \theta_j} - f \sum_{i=1}^{3} \epsilon_{ij} V_i \cos \theta_i = \beta \tag{2.18}$$

where d_i and θ_i are given by equations 2.8,9.

Elimination of θ_j leaves:

$$H_j^2 = \alpha^2 + \beta^2 \tag{2.19}$$

i.e.

$$\beta = \sqrt{[H_j^2 - \alpha^2]}. \tag{2.20}$$

For this equation to have real roots, the right hand side must be positive. However, the value of H_j must be strictly less than fV_j if the foot is sticking, and these two requirements mean that

$$V_j^2 \geq \left[\sum_{i=1}^{3} \epsilon_{ij} V_i \sin\theta_i\right]^2. \tag{2.21}$$

The corresponding range of pushing positions $\bar{x}$ for which such rotation is possible may now be determined from equation 2.18, ie.

$$\bar{x} = \frac{f\sum_{i=1}^{3} \epsilon_{ij}\, V_i\, d_i}{\beta + f\sum_{i=1}^{3} \epsilon_{ij}\, V_i \cos\theta_i} + r_j \cos\theta_j. \tag{2.22}$$

Also, the extreme values of the range of $\bar{x}$ over which rotation about foot j is possible are now found by letting β take its extreme values i.e.

$$\beta = \pm f\left[V_j^2 - \left(\sum_{i=1}^{3} \epsilon_{ij}\, V_i \sin\theta_i\right)^2\right]^{\frac{1}{2}}. \tag{2.23}$$

Two interesting features are immediately apparent. As might be expected, the range of finger positions $\bar{x}$ is independent of the distance of the pushing surface from the centre of gravity, i.e. it is purely a function of the orientation of the object. Secondly, the range of $\bar{x}$ is independent of the coefficient of friction. Some typical results are shown in Figure 2.4 for bodies with and without rotational symmetry. There is always a range of $\bar{x}$ for which rotation is possible about one foot and certain configurations allow the possibility of rotation about either of two feet for different ranges of $\bar{x}$. No configuration has been found for which rotation was possible about each point of support, although some configurations (e.g. Figure 2.4c) allow rotation in either direction about a particular foot, with the range of possible values of $\bar{x}$ extending to $\pm\infty$.

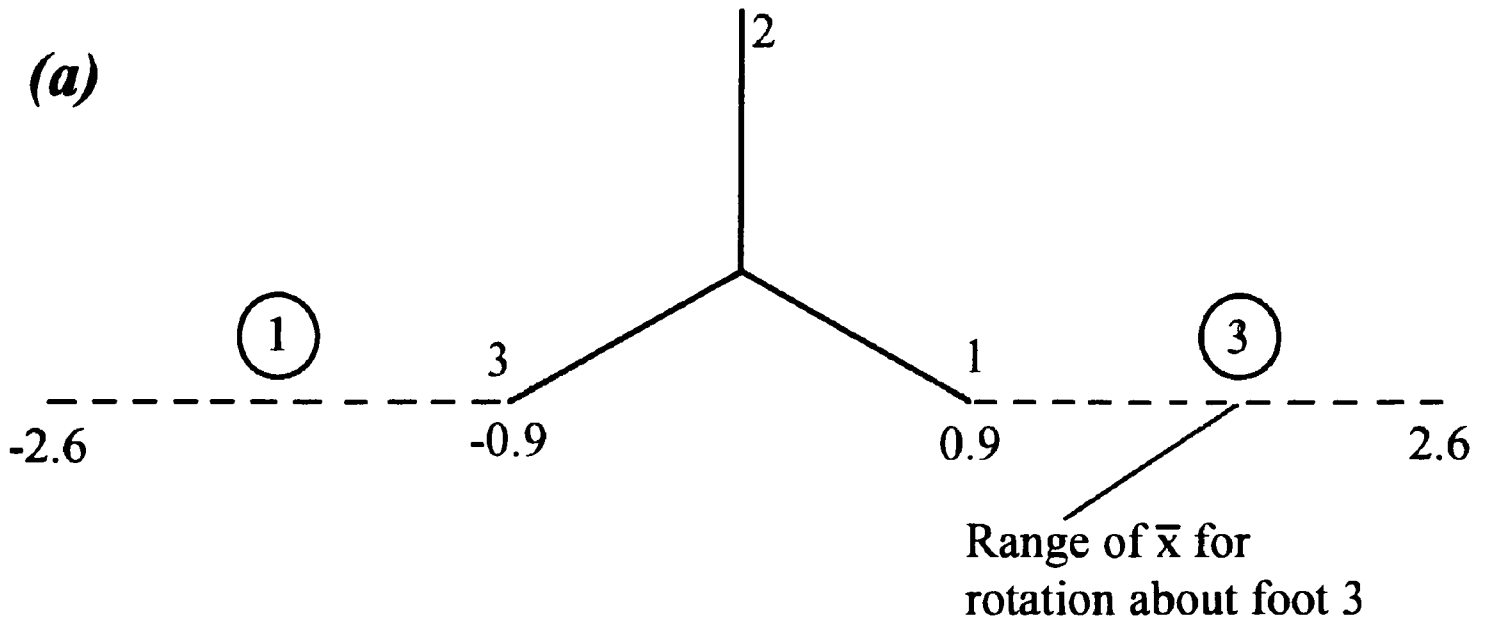

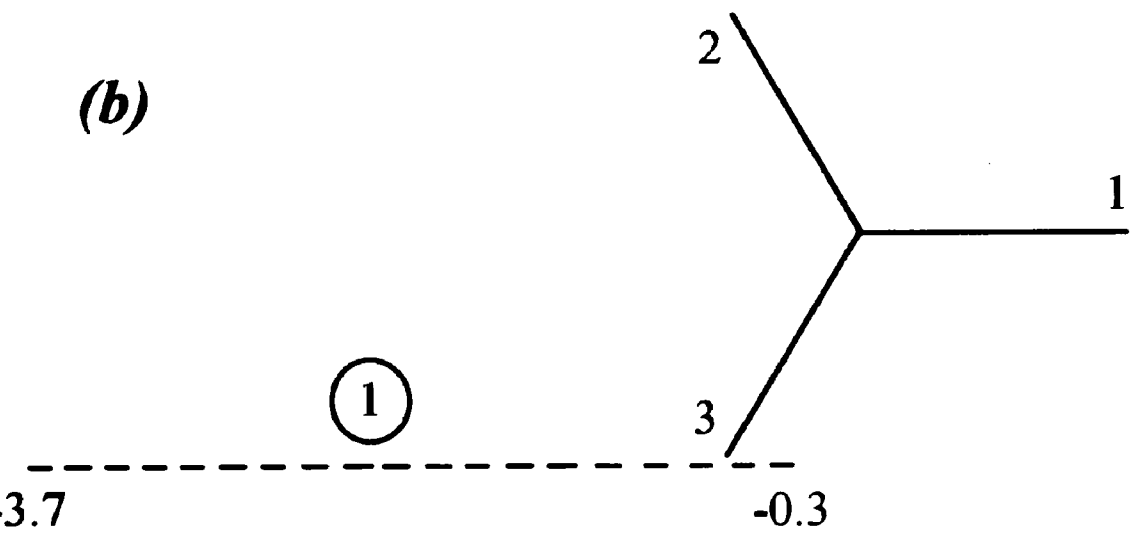

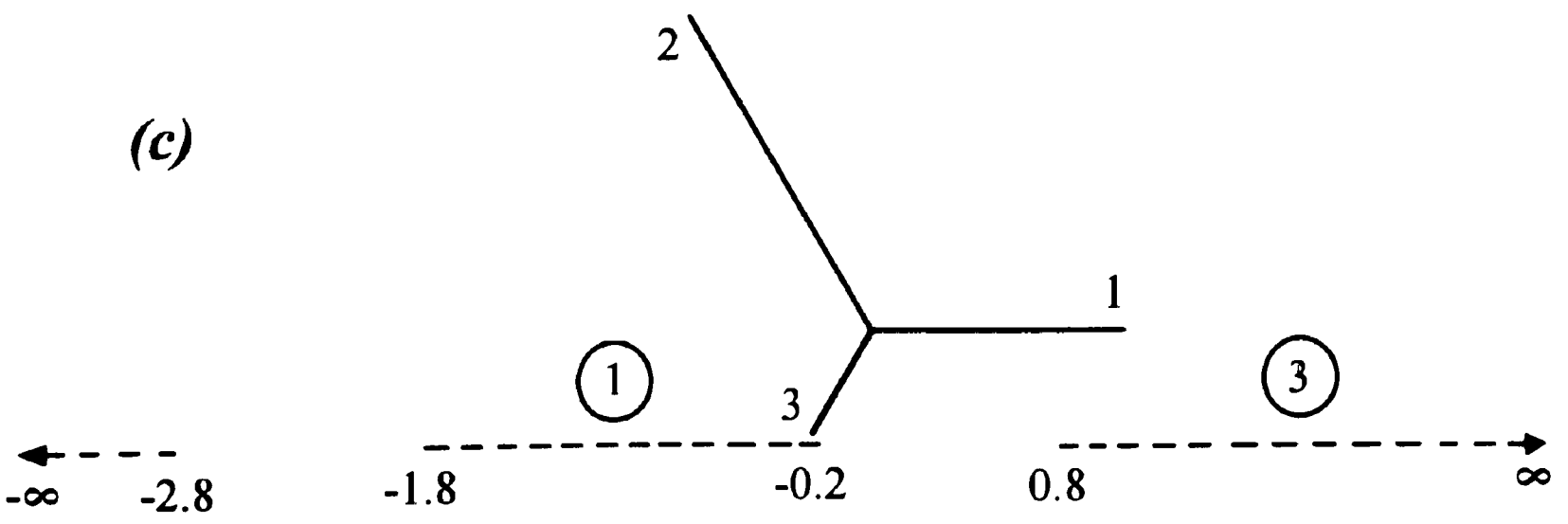

Figure 2.4: Ranges of finger position, $\bar{x}$, which cause rotation about a foot (identified by the number in the circle) for three sample bodies. a) A body symmetric about the y-axis has symmetric ranges. b) Rotating the above body through 30^o permits rotation about one foot only. c) This asymmetric body has one range which extends to $\pm\infty$.

As stated earlier, several authors have noticed that bodies have 'a tendency' to rotate about a point of support. To test this assertion it is useful to determine the range of pushing positions, for any particular object, over which rotation about a foot takes place. This can be done by varying the object's orientation relative to the pushing force and calculating the range of values for $\bar{x}$ over which rotation about a foot occurs. Figure 2.5 shows the results of this calculation for two sample bodies. In Figure 2.5a, the regions of $\bar{x}$ where rotation about a point of support occur are shown for the body with rotational symmetry presented in Figure 2.4a & 2.4b. In this case, the rotational symmetry ensures that the pattern repeats every 120^O because the reaction forces are the same at each foot. Figure 2.5b presents results for a similar body but with the radial position of foot 2, normalised with respect to r_1, increased to 1.5 and that of foot 3 reduced to 0.5. This increases V_3 from $\frac{1}{3}$ to $0.546W$, whilst reducing V_1 and V_2 to $0.272W$ and $0.182W$ respectively. The effect of this change on the motion of the body is quite marked. Compared with the first body, the areas in which rotation about foot 3 occurs have increased markedly in size, whereas those for rotation about the more lightly loaded feet have decreased. It appears, therefore, that a body will indeed rotate about a point of support for a significant proportion of possible pushing motions. This behaviour is particularly marked when the point of support carries a large proportion of the body's weight. This result has practical importance in attempting to apply the theory of pushing to the manipulation of real objects. Rotation about a point is likely to be much more stable under fluctuations in the coefficient of friction at different feet than more general rotation or translation.

2.3.3 Calculation of instantaneous centres

For more general motion, the equations must be solved to find the position of the instantaneous centre. This may be done on a computer using an iterative technique. A value for $d_0 \cos\theta_0$ is selected, together with an estimate for $d_0 \sin\theta_0$. Equation 2.5 is then

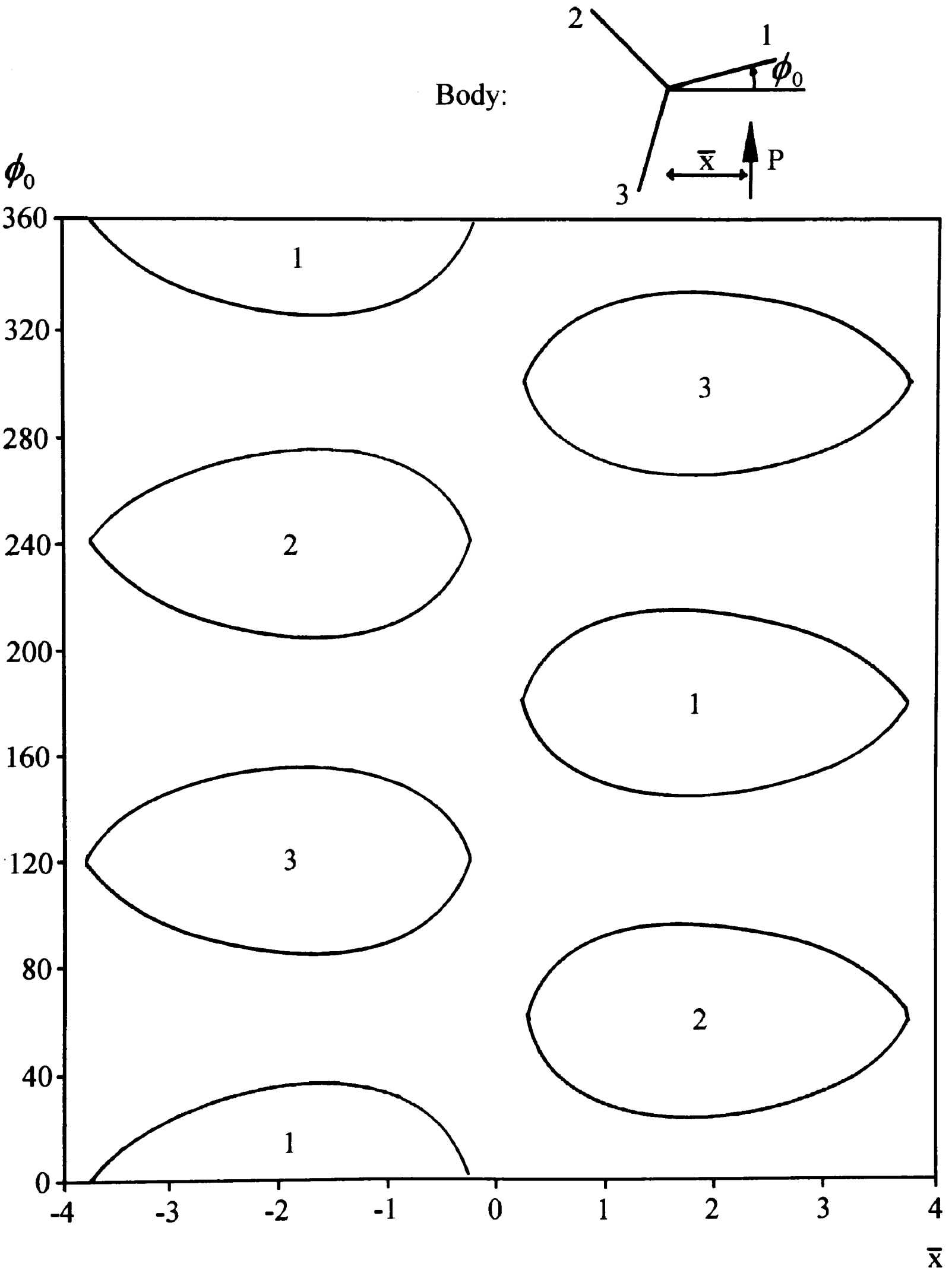

Figure 2.5: Map of pushing configurations which lead to rotation about a point of support. The numbered regions indicate where rotation about a point of support occurs and indentify the foot. Outside these regions, the instantaneous centre is located at an intermediate point. (a) Body with rotational symmetry.

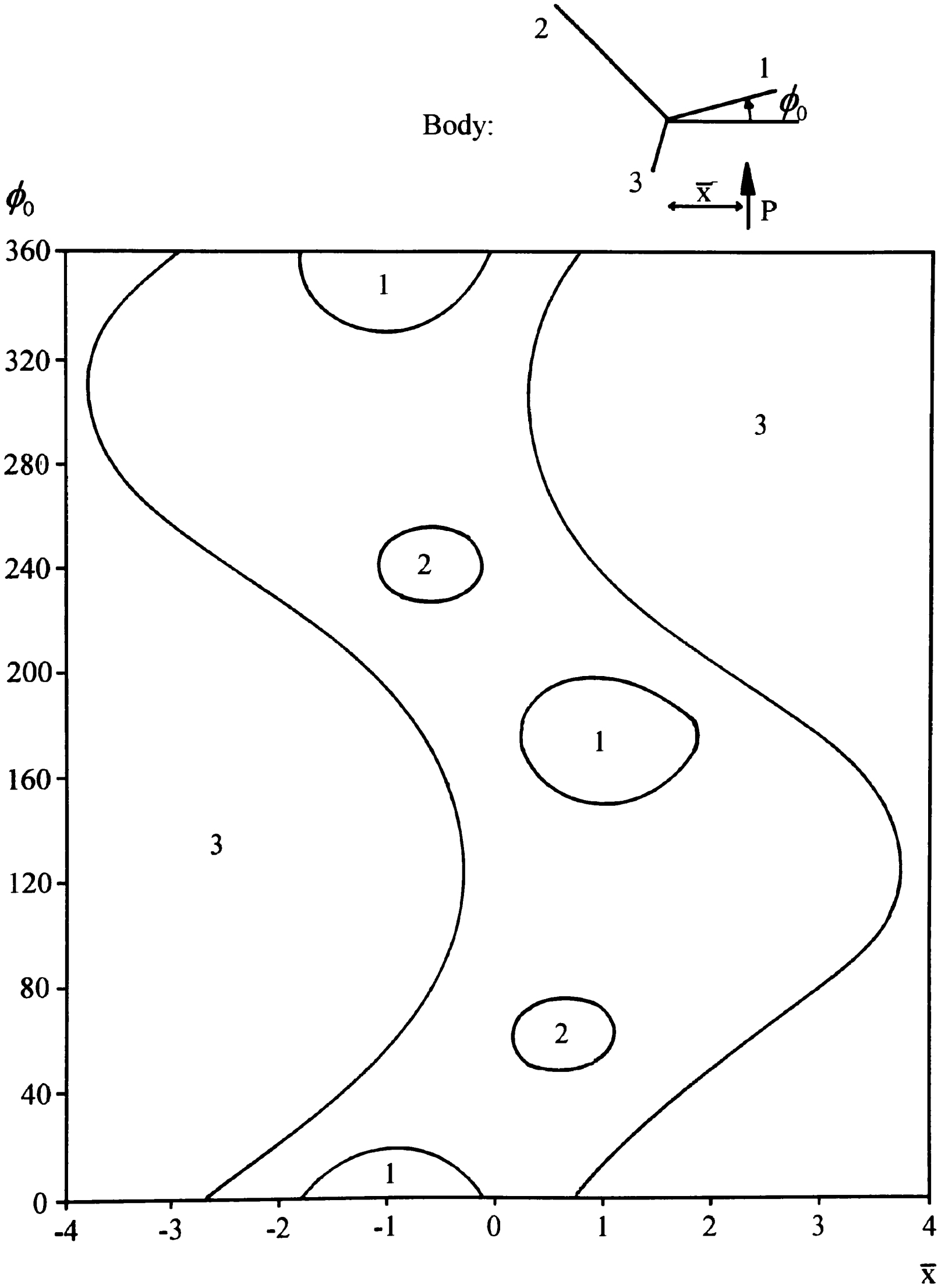

Figure 2.5: (b) Body without rotational symmetry. Note that rotation occurs about foot 3 (which sustains the largest normal reaction) for a wide range of configurations.

used as the basis for a Newton-Raphson technique in conjunction with equations 2.8,9 to obtain a better estimate for $d_0 \sin\theta_0$, and iteration continues until convergence occurs. This method generally produces rapid convergence and few difficulties were experienced with the examples considered. The value of $\bar{x}$ corresponding to the instantaneous centre found may be determined by using equation 2.13.

Some typical loci of instantaneous centres are shown in Figure 2.6. Setting $\bar{x} = 0$ (i.e. pushing through the centroid) locates the instantaneous centre at $y = 0, x = \mp\infty$. Letting $\bar{x}$ approach $\pm\infty$ (i.e. very remote from the centroid) corresponds to applying a pure torque to the body. In this case rotation takes place about a particular centre of rotation I_∞ . For bodies with rotational symmetry this lies at the centre of gravity, although it can lie elsewhere (Figure 2.6c), including at a foot (Figure 2.6b).

2.3.4 Indeterminacy of motion

As first noted by Goyal, Ruina, and Papadopoulos (1989), an indeterminacy in the motion of the body exists when the points of support lie on a straight line and the force is applied perpendicular to this line, through the centre of gravity. This is most simply demonstrated by considering a body with only two points of support, as shown in Figure 2.7. Pushing through the centre of gravity will produce forces at each foot opposing the motion. Any instantaneous centre on the line through the two feet which lies outside AB, results in identical frictional forces. This suggests that pushing through the centre of gravity can produce any motion between rotation about foot A and rotation about foot B, including pure translation.

Such an indeterminacy does not seem physically reasonable since one expects identical response from a body each time it is subjected to a particular force. In practice, however, although such indeterminacy is of academic interest, it does not have a great deal of physical relevance since bodies with collinear point supports cannot be realised in practice, although bodies where the points of support are almost collinear might be expected to

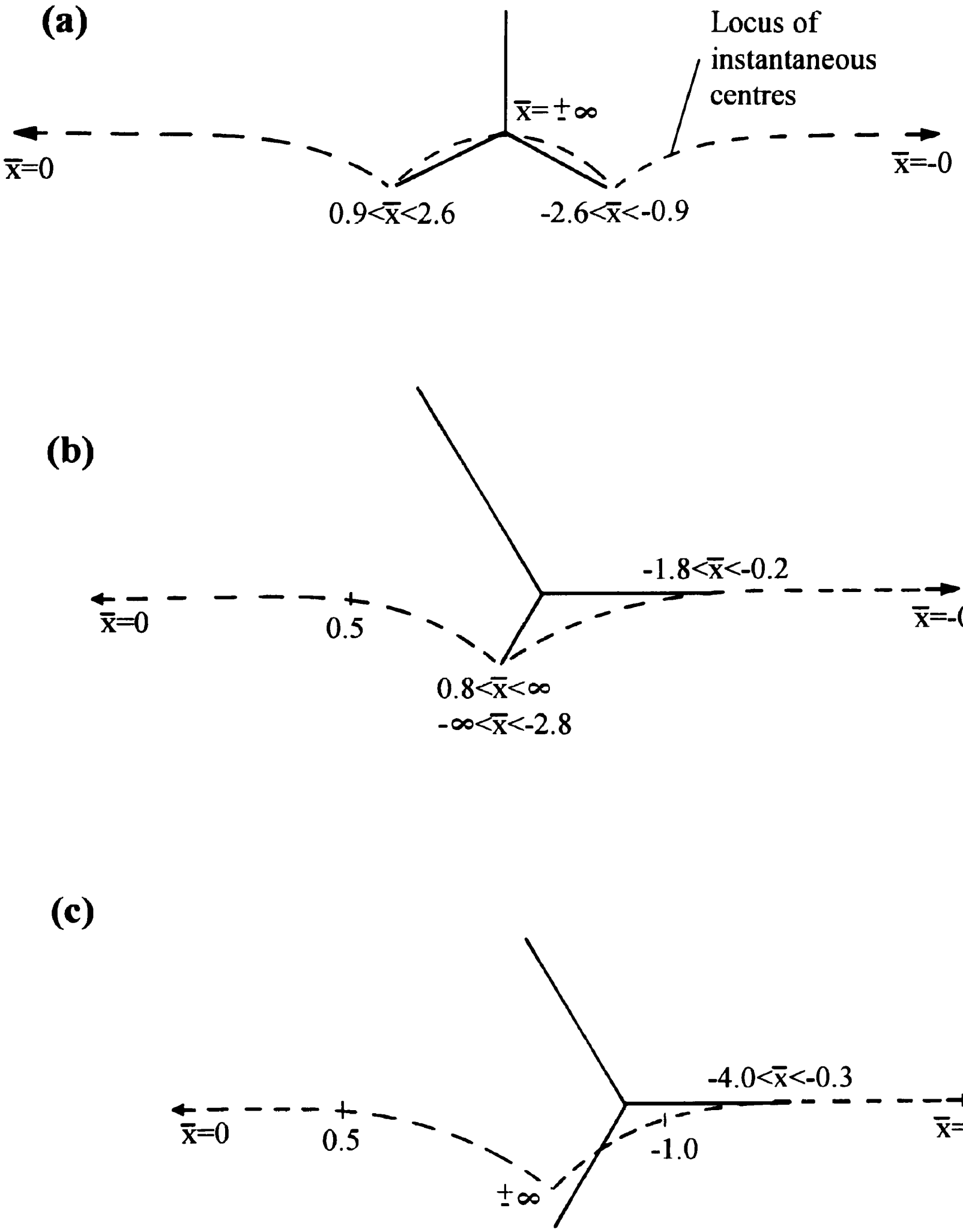

Figure 2.6: Some typical loci of instantaneous centres. Ranges of $\bar{x}$ resulting in rotation about a foot are shown as is the instantaneous centre which results from the application of a pure torque. This can lie (a) at the centre of gravity, (b) at a foot, or (c) at an intermediate point.

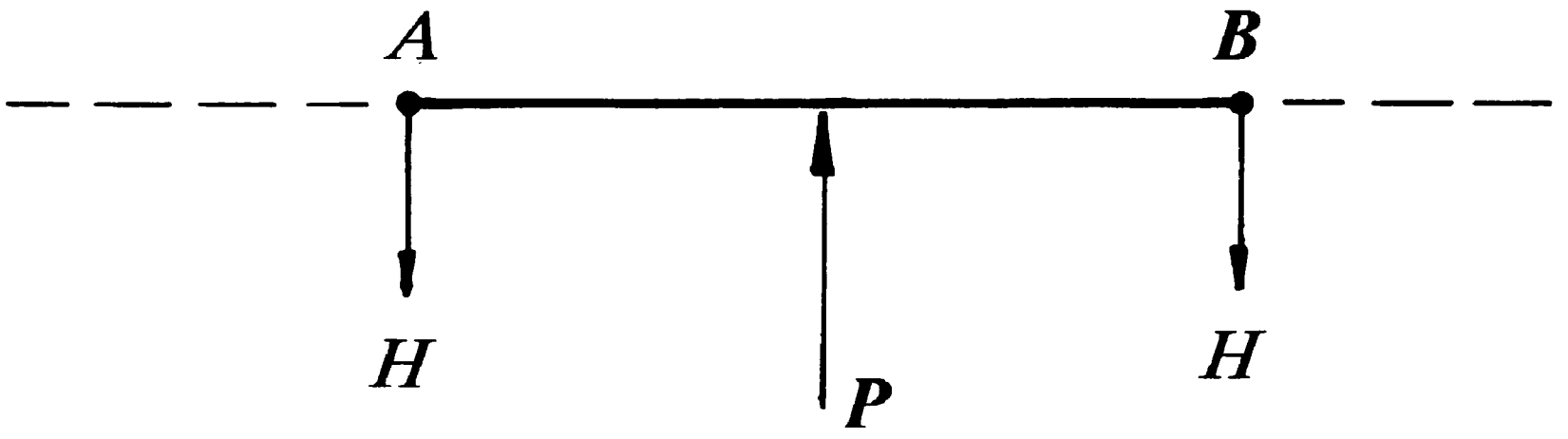

Figure 2.7: A body resting on collinear points of support.

display similar behaviour when subject to small fluctuations in the value of the frictional coefficient. The indeterminacy can be resolved by abandoning the quasi-static nature of the solution and introducing finite mass and moment of inertia. In this respect the indeterminacy may be thought of as due to the simplified quasi-static model adopted.

2.4 Computer simulation

It was a logical progression to produce a computer simulation package capable of predicting the motion of a body on a frictional surface when pushed by an external force in the form of a pushing 'finger'. This has been successfully implemented on a Personal Computer. After the geometry of the body has been entered, the package calculates a look-up table relating the position of the pushing 'finger' to the instantaneous centre of motion of the body. This obviates the need to solve for the instantaneous centre repeatedly, hence reducing processor load during the simulation. The locus of the pushing finger may then be input and graphical output is displayed in real time. A typical output is shown in Figure 2.8. Here a body with feet at the vertices of an equilateral triangle is pushed by a finger which rests against one edge of the triangle. The loci of the finger and the body are clearly displayed and show examples of translation, pure rotation, and the mixed type of motion.

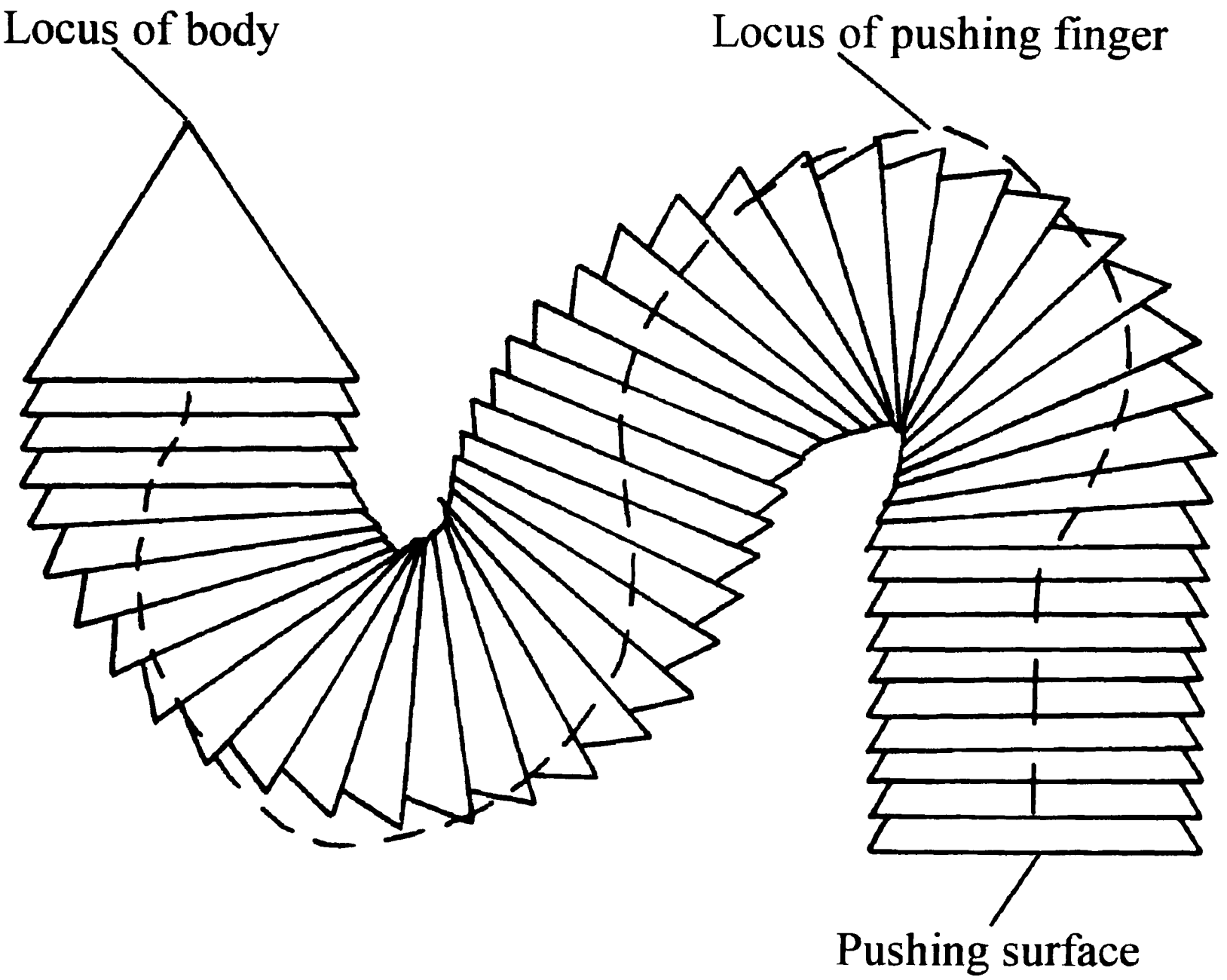

Figure 2.8: Sample trajectory of a pushed body together with the locus of the pushing finger.

2.5 Conclusions

This Chapter has shown how the motion of a three-footed object experiencing Coulomb friction, and subjected to an arbitrary impressed force, may be predicted. Although the analysis carried out is for a statically determinate body the formulation applies in the case of a many-footed body, providing that the vertical reaction at each foot may be determined, and all of the derived equations hold providing the upper limit in the summation sign is replaced by N, the number of feet. In the limit, as $N \rightarrow \infty$ the contact may be considered as a continuous (distributed) one, and again the results found will apply. In particular the conditions for a body to rotate about a point of support have been established in closed form.

The results are the first step towards addressing the more general question of where to push an object in order to attain a particular trajectory. Several problems remain to be addressed before prediction of a body's motion on a frictional surface can be of use in practical orientation problems. The next phase would be to form strategies for the optimum locus of a finger to push an object from its initial position to a given final position and orientation. A suitable object function may be the time taken to achieve this goal, and therefore, for a given finger velocity, the shortest finger path line. However such complex optimisation is beyond the scope of this study.

In practical situations the coefficient of friction on the horizontal plane may vary with position, for example due to spots of grease, and the stability of the solution when subjected to random fluctuations in f needs to be investigated. It is in this area that knowledge of the conditions for rotation about a point of support may be important since it is expected that such motion will be more stable than rotation about a general instantaneous centre. A change in the coefficient of friction at one foot may be modelled instead as a change in the normal reaction at that foot keeping the coefficient of friction uniform. This implies a change in geometry which may be accommodated by moving the

position of the centre of gravity. A locus of the centres of gravity may be found which are equivalent to the possible fluctuations in friction at each foot. This may be used to find points on the pushing surface which generate stable motion.

The effect of friction between the pushing finger and the pushed body needs also to be taken into account if the work is to have wider practical application, although in many situations this will be less important than friction between the body and the supporting surface. This will be analyzed in the next Chapter along with the effect of pushing a three-dimensional body with a finger above the plane of its feet. This makes the problem non-planar and the normal reactions at the feet and the instantaneous centre must be found simultaneously.

Chapter 3

The Manipulation of Objects Resting on a Frictional Plane II

3.1 Introduction

In this Chapter the study of how objects move when pushed over a frictional surface is developed. Some of the simplifying assumptions made in the previous Chapter are relaxed so that the situations found in practice are modelled more realistically.

A smooth contact between the finger and the pushed object can only be realised physically by a frictionless roller. This is unlikely to be present either at the end of a robot finger or on a baffle which is used to orient an object as it moves past on a conveyor. Hence, Coulomb friction between the object and the body which pushes it is introduced.

The objects grasped by robots are three-dimensional so it is extremely restrictive to assume that the pushing force will be co-planar with the surface on which the object lies. Pushing above the plane may also be introduced deliberately to improve the stability of motion induced. However, to allow pushing above the plane introduces several complexities. The normal reactions at the points of support can no longer be determined independently of the pushing force. This increase in the number of unknowns limits the number of feet on which the object may rest to three if a solution is to be found using the method described. In addition, one of the feet may be forced to break contact with the plane; however, this is likely to be dynamically unstable and so is not considered here.

There are not many objects which make discrete contact at only three points with the surfaces on which they rest. This is because they are not perfectly rigid. Elastic and plastic deformation ensures that even non-conforming objects make contact over a finite area. The evaluation of the resulting pressure distribution is difficult enough without the added complication of the pushing force. This problem is discussed further at the end of this Chapter. However, for the present the analysis is restricted to bodies with three feet.

3.2 Pushing in the plane of the feet

3.2.1 Formulation

As before (see Chapter 2) a body, weight W, resting with three feet on a horizontal plane is considered. Its geometry is shown in plan in Figure 3.1.

The three feet are located at $(x_1, y_1), (x_2, y_2), (x_3, y_3)$ with the origin at the centre of mass of the body and the x-axis parallel to the surface against which pushing is to be applied. The feet are assumed to be non-collinear, since, as shown by Goyal (1989), collinearity can produce indeterminacy in the motion. A finger pushes against the body at a point $(\bar{x}, \bar{y})$, with an imposed displacement at an angle ψ to the normal of the pushing surface. The motion of the body is assumed to be quasi-static, which is valid if the frictional forces are much greater than the inertia ones, such that it has an instantaneous centre at (x_0, y_0). The rate of rotation, $\dot{\theta}$, must be compatible with the finger velocity to maintain contact between the finger and the pushing surface.

The planar forces and their directions are shown in Figure 3.2. All feet are assumed to be sliding. The coefficients of friction between the feet and the plane, and between the finger and the pushing surface, are f and f_f respectively. The normal reactions at the feet, V_1, V_2, V_3, produce frictional forces, fV_1, fV_2, fV_3, in the opposite direction to the instantaneous velocity at each foot. The lines joining the instantaneous centre to the feet, perpendicular to the velocities of the feet, make angles, θ_1, θ_2, θ_3, with the x-axis, the direction of the

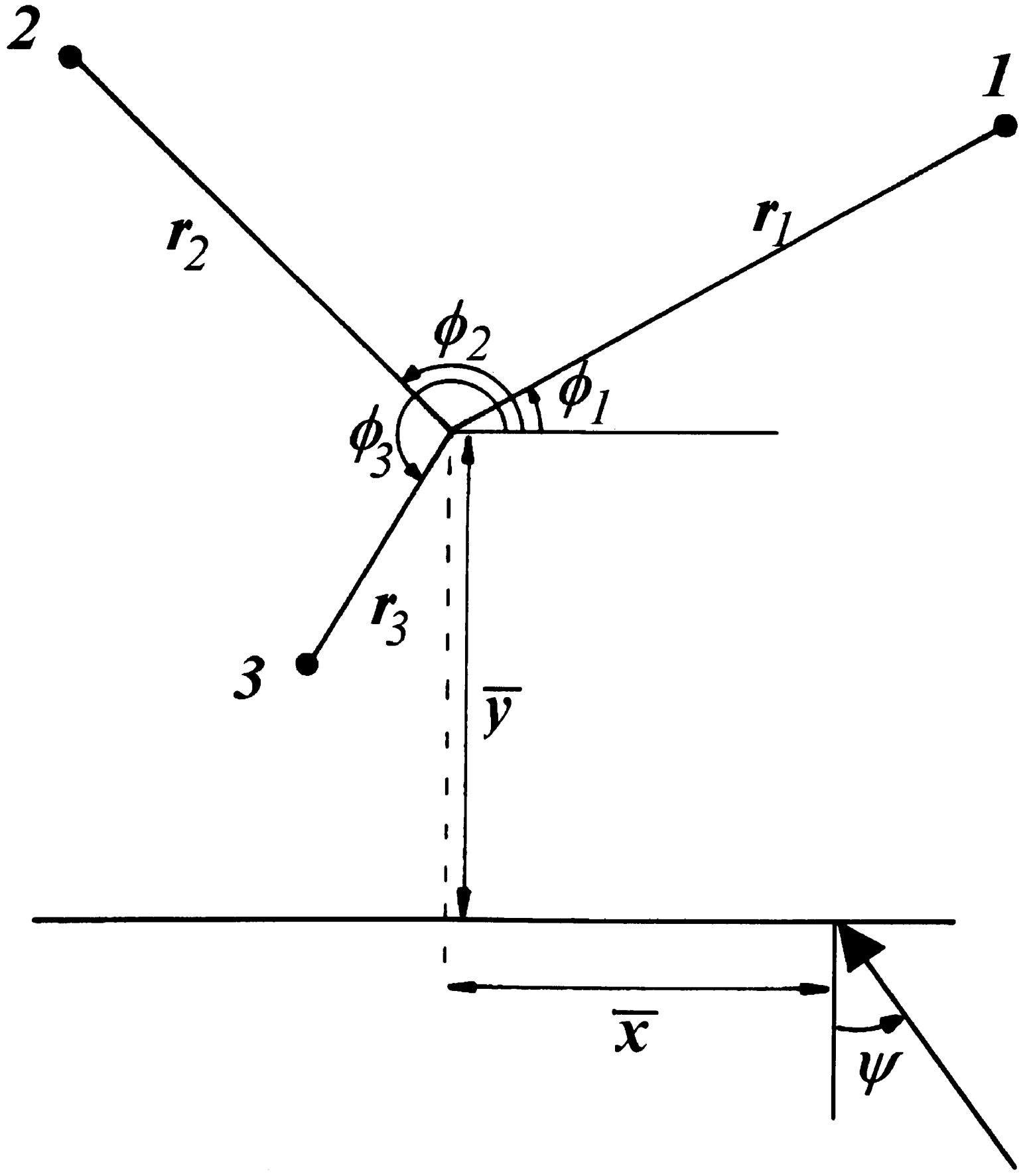

Figure 3.1: Plan of the geometry of the body.

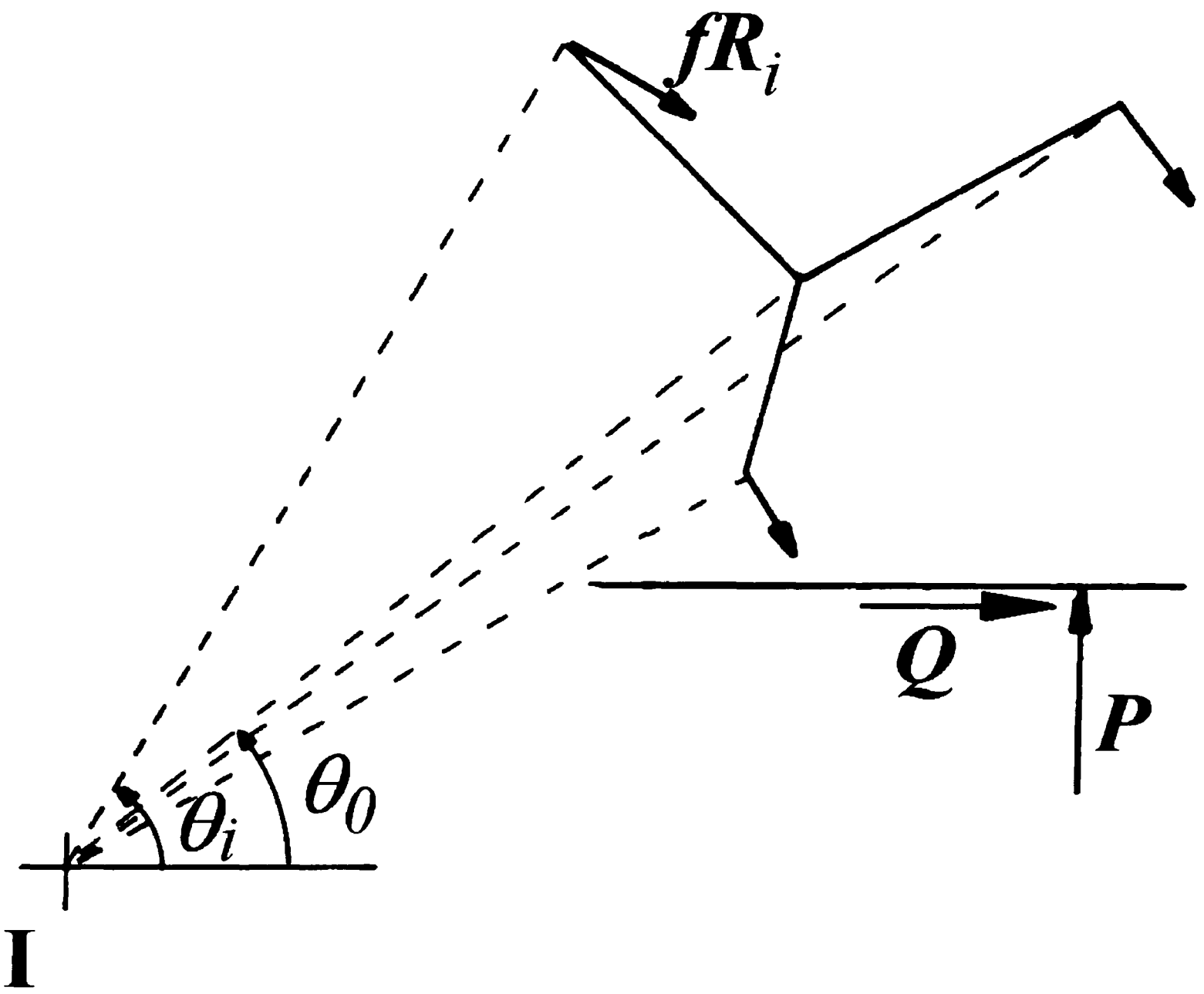

Figure 3.2: Forces acting on the body.

motion depending on the sense of rotation. The forces P and Q are the contact forces exerted by the finger on the body at the contact point.

The three vertical reactions are easily found by taking moments for the body about the x and y-axes, the third equation being that of vertical equilibrium. In the case where the feet are collinear, an indeterminacy is introduced since the two moment equations become linear multiples of each other. However, such a case is clearly not often found in practice.

Next, horizontal equilibrium when the body is undergoing quasi-static motion is considered. Resolving in the x-direction gives:

$$Q + \sum_{i=1}^{3} f\, V_i \operatorname{sgn}(\dot{\theta}) \sin\theta_i = 0. \tag{3.1}$$

Similarly, resolving in the y-direction produces:

$$P + \sum_{i=1}^{3} -f\, V_i \operatorname{sgn}(\dot{\theta}) \cos\theta_i = 0. \tag{3.2}$$

Finally, taking moments about the finger contact $(\bar{x}, \bar{y})$ gives:

$$\sum_{i=1}^{3} [(y_i - \bar{y})\, f\, V_i \operatorname{sgn}(\dot{\theta}) \sin\theta_i - (x_i - \bar{x})\, f V_i \operatorname{sgn}(\dot{\theta}) \cos\theta_i] = 0 \tag{3.3}$$

where

$$\sin\theta_i = \frac{y_i - y}{\sqrt{(x_i - x)^2 + (y_i - y)^2}}$$

$$\cos\theta_i = \frac{x_i - x}{\sqrt{(x_i - x)^2 + (y_i - y)^2}}$$

$$\operatorname{sgn}(x) = \begin{cases} -1 & x \leq 0 \\ 1 & x > 0. \end{cases}$$

The three equations are deficient as there are four unknowns x, y, P, Q. A further equation may be found by considering the possible regimes of motion of the finger, which may either stick to the pushing surface or may slip along it. The possibility of the body rotating about a foot must also be considered, in which case the components of the frictional force at that foot replace the location of the instantaneous centre as unknowns, as they no longer limiting.

3.2.2 Finger sticking to the pushing surface

If the finger is assumed to stick to the pushing surface, the motion of the body is constrained so that the instantaneous centre lies on a line normal to the finger velocity, and passing through the finger contact. Hence, the relationship between y and x:

$$y = \bar{y} + (x - \bar{x}) \tan \psi.$$

Making this substitution for y in equation 3.3, yields a non-linear equation in x, which can be found by numerical means. The Newton-Raphson iterative method proved quite adequate for this purpose.

Once the instantaneous centre has been estimated, equations 3.1 and 3.2 may be used to find the finger forces P and Q. If the ratio $\left|\frac{Q}{P}\right|$ is less than f_f the initial assumption that the finger sticks is correct and the position of the instantaneous centre has been found; otherwise the assumption is wrong, the foot slips and the instantaneous centre must be recalculated.

3.2.3 Finger slipping along the pushing surface

If the finger is sliding along the pushing surface, the pushing forces are related by:

$$Q = n\, f_f\, P,$$

where:

$$n = \begin{cases} 1 & \text{if the finger slides in the } +x \text{ direction } (\tan\psi > \frac{\bar{y}-y}{x-\bar{x}}), \\ -1 & \text{if it slides in the } -x \text{ direction } (\tan\psi < \frac{\bar{y}-y}{x-\bar{x}}) \end{cases}$$

Since the location of the instantaneous centre is unknown at this stage, the direction in which the finger slides cannot be determined. However, it can be *estimated* from the direction of Q, when sticking of the finger was assumed. The compatibility of the direction of slide of the finger with Q must be verified *a posteriori*. Substituting for Q in equation 3.1 and then eliminating P from equation 3.2 yields:

$$\sum_{i=1}^{3} f\, V_i \,\mathrm{sgn}(\dot{\theta})\,(\sin\theta_i + \cos\theta_i) = 0 \tag{3.4}$$

The instantaneous centre may now be found by solving equations 3.3 and 3.4 simultaneously. Since the equations are non-linear, numerical methods are again necessary for their solution. A library routine based upon Powell's hybrid method (Powell, 1970) is employed because of its speed and global convergence. In practice, convergence nearly always occurs rapidly, the exception being when the instantaneous centre is exactly at a foot. Fortunately, the conditions necessary for a foot to stick can be expressed in closed form, so a check can be made to see if a foot is sticking before the iterative solution is sought (see below).

Once a solution for the instantaneous centre is found, it is necessary to verify that it is compatible with the direction of slip of the finger. If it is not compatible, the assumed direction of slip is wrong, the other value of n must be chosen and the solution recalculated.

3.2.4 Rotation about a point of support

If the instantaneous centre lies exactly at a foot, that foot will not slide, so the frictional force will be less than its limiting value. When this is the case, the previous methods will fail to produce an exact solution since they assume that *all* the feet are sliding. To determine the values of $\bar{x}$ and ψ for which a particular foot sticks, it is necessary to formulate the equations again, noting that the location of the instantaneous centre is known but that the pushing forces and the frictional forces at one foot are not.

Suppose, for example, foot j sticks, with the finger sliding. Equations 3.1 and 3.2 become:

$$\alpha\, f\, V_j \sin\theta_j = -n\, f_f\, P - f \sum_{i=1}^{3} e_{ij}\,\mathrm{sgn}(\dot{\theta})\sin\theta_i \tag{3.5}$$

$$\alpha f\, V_j \cos\theta_j = P - f \sum_{i=1}^{3} e_{ij}\,\mathrm{sgn}(\dot{\theta})\cos\theta_i \tag{3.6}$$

where :

$$0 \leq \alpha \leq 1$$

$$e_{ij} = \begin{cases} 0 & \text{if } i = j \\ 1 & \text{otherwise} \end{cases}$$

$$n = \begin{cases} 1 & \text{if the finger slides in the } +x \text{ direction,} \\ -1 & \text{if it slides in the } -x \text{ direction.} \end{cases}$$

It is necessary to consider both directions of finger slide. Eliminating θ_j and solving for P yields:

$$P = \frac{-b \pm \sqrt{b^2 - 4ac}}{2a} \tag{3.7}$$

where

$$a = 1 + f_f^2$$

$$b = -f\,\mathrm{sgn}(\dot{\theta}) \sum_{i=1}^{3} e_{ij}\, r_i\, (\sin\theta_i - n\, f_f\, \cos\theta_i)$$

$$c = \left(f \sum_{i=1}^{3} e_{ij}\, V_i \sin\theta_i \right)^2 + \left(f \sum_{i=1}^{3} e_{ij}\, V_i \cos\theta_i \right)^2 - \alpha^2 f^2 V_j^2$$

When the foot is on the point of sliding, the force there is maximum and α equals 1. Taking the positive and negative root in equation 3.7 gives the upper and lower limits of P. If P has no real, positive solutions, the foot never sticks. Once the bounds for P are established, the range of corresponding locations of the finger can be found.

Taking moments about the instantaneous centre:

$$P\,(\bar{x} - x_j) - n\, f_f\, P\,(\bar{y} - y_j) = f\,\mathrm{sgn}(\ dot\theta) \sum_{i=1}^{3} e_{ij}\, V_i \sqrt{(x_i - x_j)^2 + (y_i - y_j)^2}.$$

Solving for $\bar{x}$, assuming that $\bar{y}$ is constant:

$$\bar{x} = \frac{f\,\mathrm{sgn}(\dot{\theta})}{P} \sum_{i=1}^{3} e_{ij}\, V_i \sqrt{(x_i - x_j)^2 + (y_i - y_j)^2} + n\, f_f\, (\bar{y} - y_j) + x_j \tag{3.8}$$

Substituting the values of P into equation 3.8 yields the range of $\bar{x}$ within which solutions lie. However, not all these solutions are valid since, as has been discussed, there

must be compatibility between the direction in which the finger is sliding and the chosen value of n.

It is of interest to note that the above analysis is applicable even if the number of feet exceeds three, provided that the vertical reactions at the feet are known *a priori* and the summations extended to include all the feet. Additionally, distributed contacts may be considered if the pressure distribution is known, and the summations converted into integrals over the whole contact patch.

3.2.5 Results

The large number of independent variables present prohibits the presentation of a comprehensive set of results, so the results for only one geometry of the body, as shown in Figure 3.3, are presented. The positions of the feet are kept constant relative to the centre of mass, as is the y coordinate of the finger contact. The remaining variables are the x coordinate of the finger contact, the direction of push, ψ, and the coefficients of friction, f and f_f. The results are presented in graphical form, where x and ψ are respectively the x and y coordinates of a "pushing space", showing the conditions that cause the finger to slide along the pushing surface and the body to rotate about a foot. It is immediately apparent from analysis of equations 3.3, 3.4, 3.5 and 3.7 that the location of the instantaneous centre is independent of the coefficient of friction at the feet. The effect of friction at the finger contact can be shown by distinguishing between the two cases: $f_f = 0$ and $f_f > 0$.

No friction ($f_f = 0$)

The case of no friction at the finger contact was studied in the last Chapter. It was shown that the location of the instantaneous centre is independent of the y coordinate of the finger contact, $\bar{y}$ and independent of the direction of push, ψ. The regions of the pushing space where a foot sticks for the geometry chosen for this example is shown in Figure 3.4a.

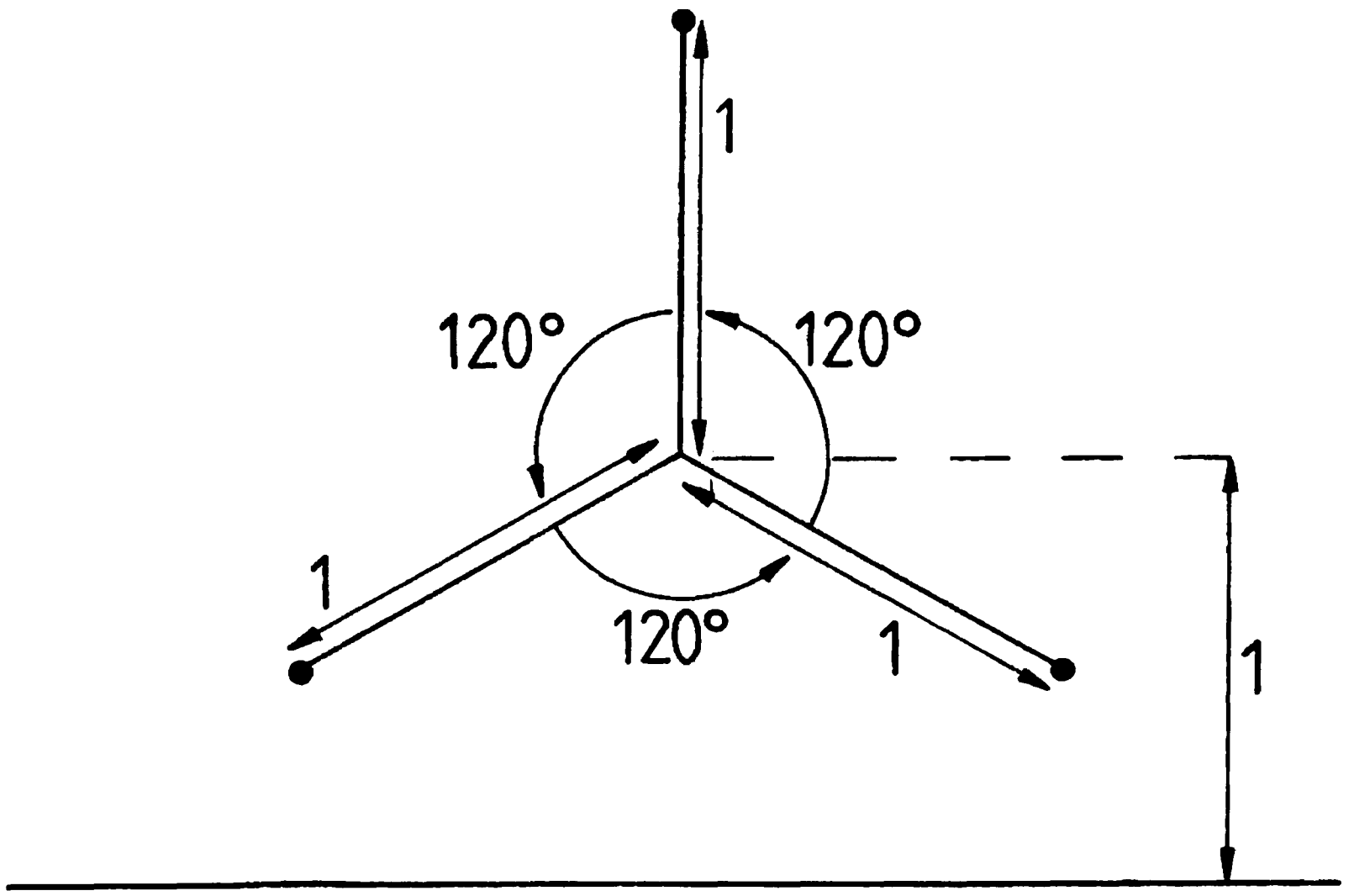

Figure 3.3: Geometry of the body chosen for presentation of results.

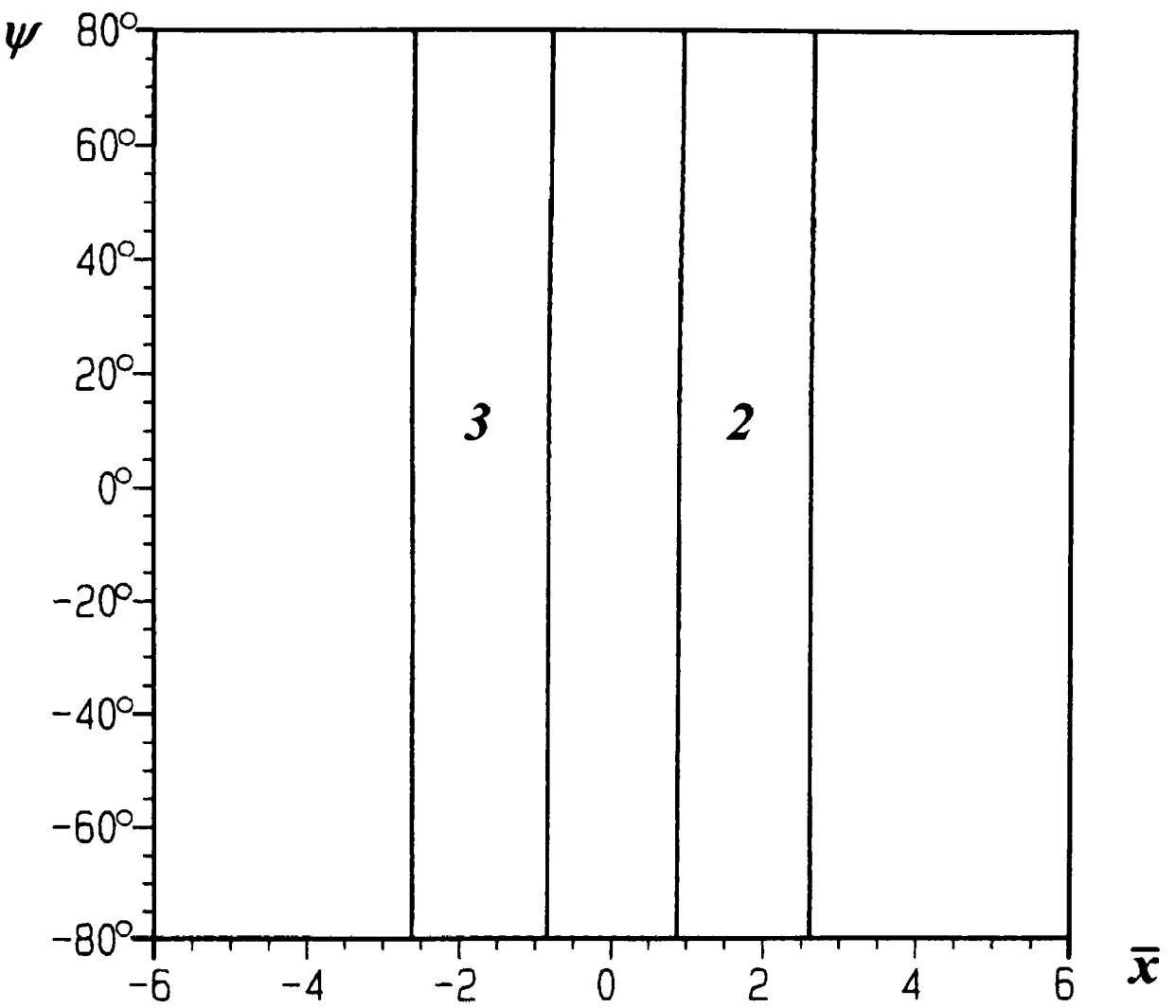

Figure 3.4: Regions where finger sticks (F) and where rotation about a foot occurs, when: (a) $f_f = 0$

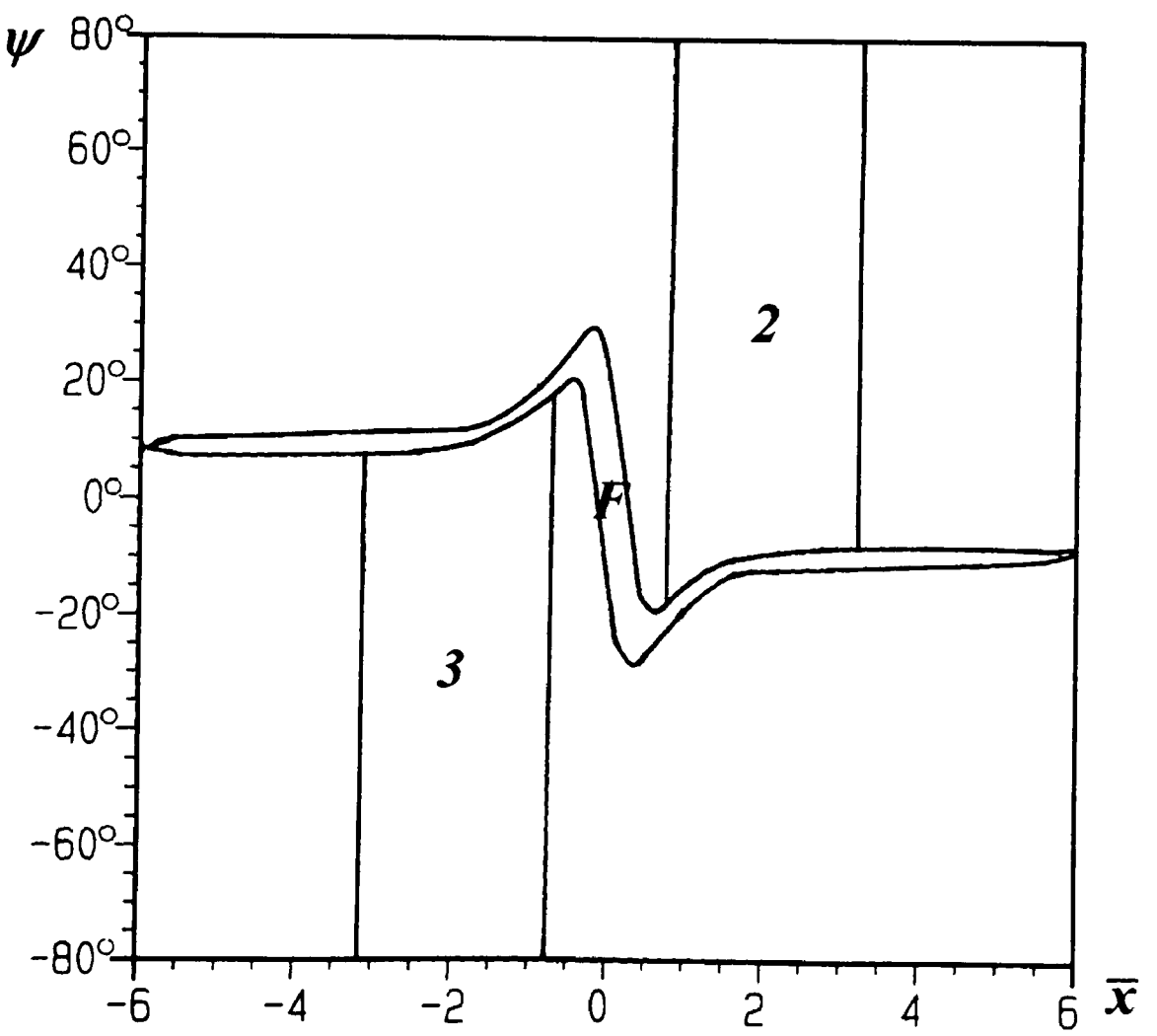

Figure 3.4: (b) $f_f = 0.1$.

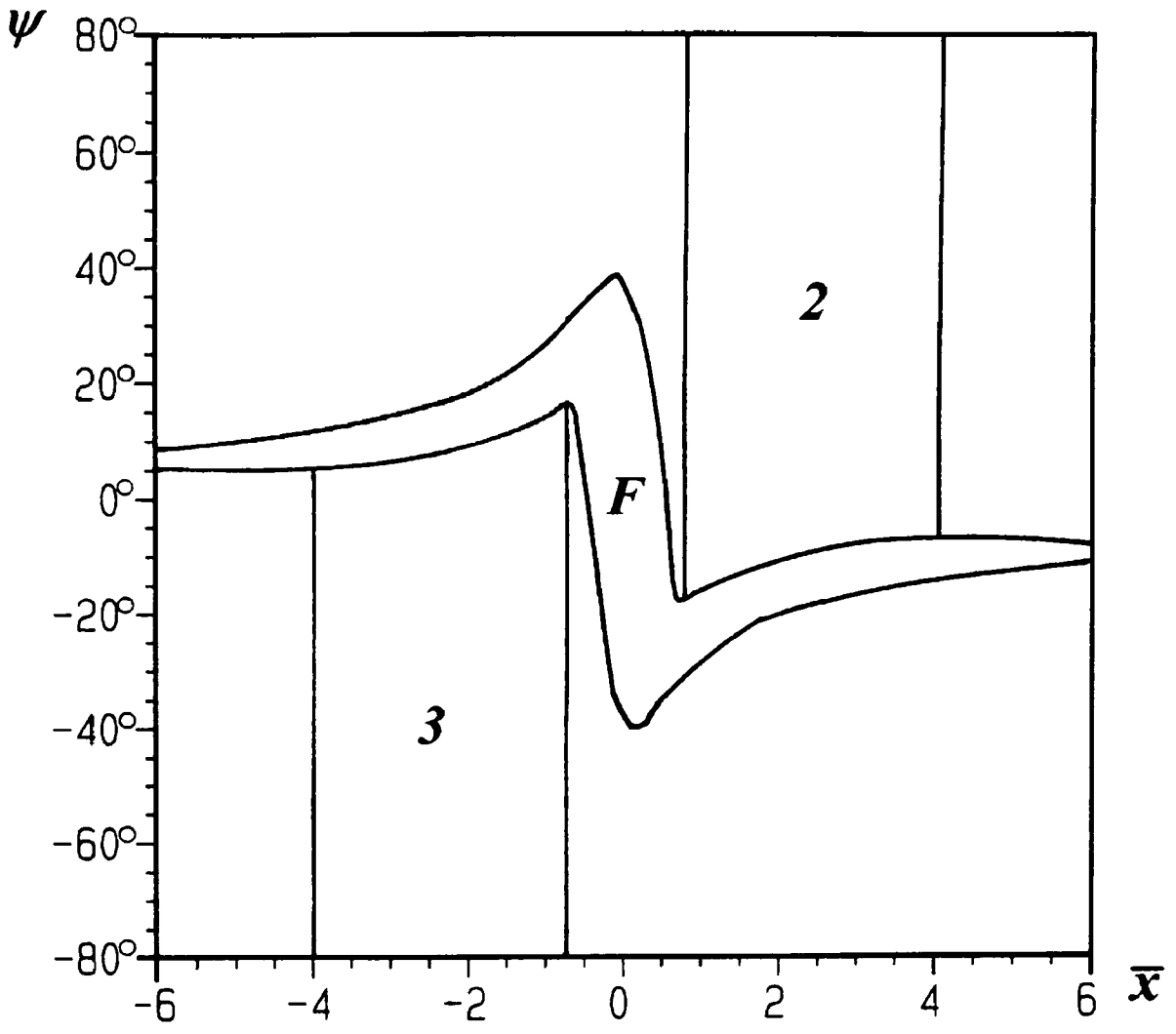

Figure 3.4: (c) $f_f = 0.3$.

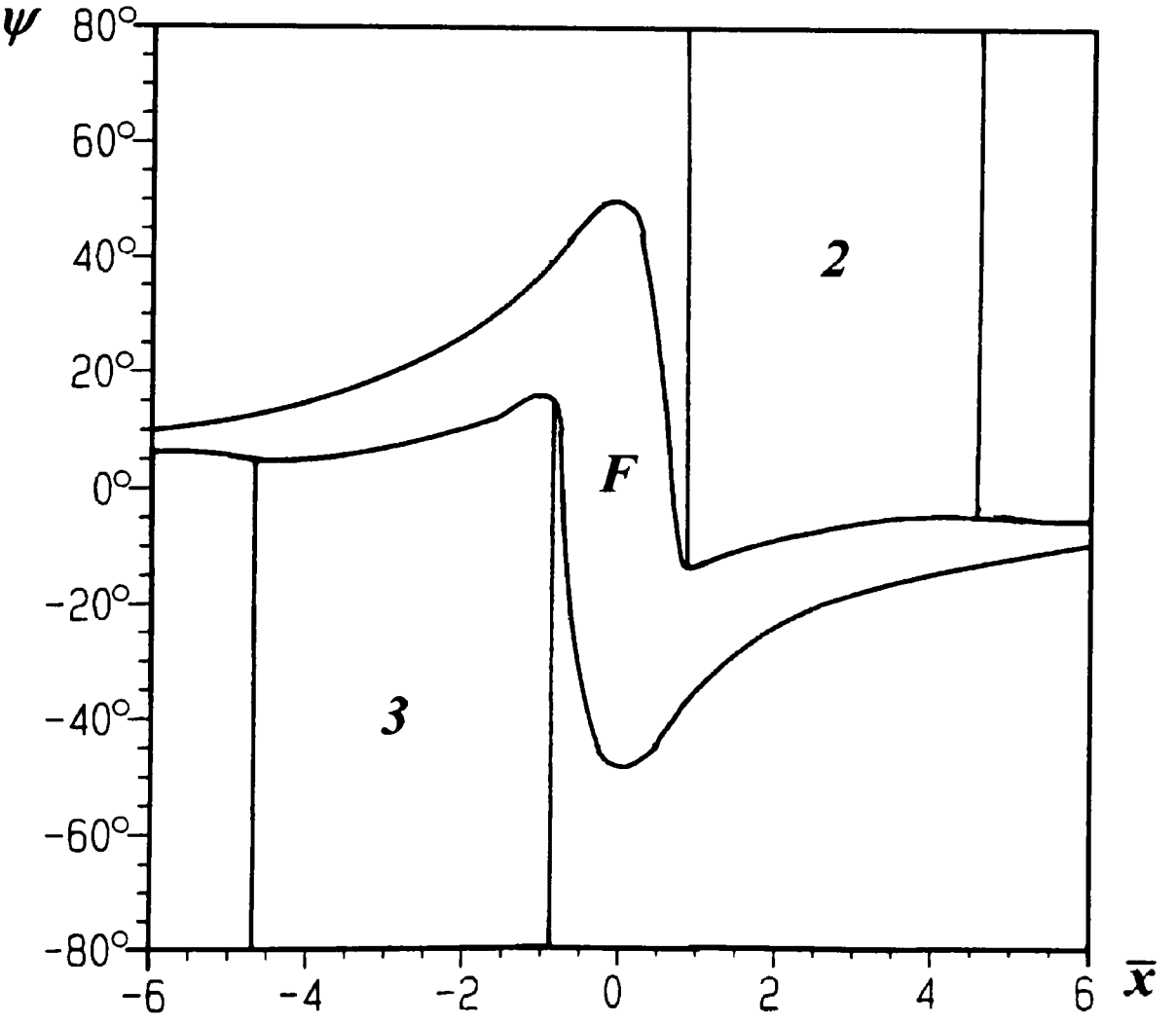

Figure 3.4: (d) $f_f = 0.5$.

Friction at the finger contact ($f_f > 0$)

It can be deduced from equation 3.3 that the introduction of a finite coefficient of friction, f_f, causes the location of the instantaneous centre to become dependent upon both $\bar{y}$ and ψ. Comparing Figure 3.4b, where $f_f = 0.1$, with Figure 3.4a it is perhaps surprising that there is a dramatic reduction in the area of the regions of the pushing space where rotation about a foot occurs; this is due to enforcement of the compatibility condition between the location of the instantaneous centre and the direction of slide. A change in the direction of slide changes the component of the pushing force in the x direction. This tends to move the position of the instantaneous centre, and so, if it is at a foot for one direction of sliding it certainly will not be for the other direction. Of course, if f_f is very small this displacement is also very small and the instantaneous centre is close to the foot.

Figures 3.4b, c, d show the effect of increasing f_f on the regions where the finger sticks. As the coefficient of friction is increased, so does the tendency for the finger to stick, as would be expected. Of interest is the fact that the regions where a foot sticks also become larger.

3.3 Pushing above the plane

3.3.1 Formulation

When the plane of application of the finger lies above the plane of the feet, the contact force,P, produces moments about the x and y axes which must be balanced by the moments of the reactions at the feet, which therefore change from their "at rest" values. Since this contact force is determined by the motion, coupling has been introduced between the location of the instantaneous centre and the reaction forces. In other words, the reactions at the feet have become additional unknowns, and so bodies with no more than three feet can be analyzed by the methodology presented in this Chapter.

Introducing a z coordinate perpendicular to the plane, with the origin at the centroid

of the object, z_c units above the plane, the forces and their locations are now more conveniently represented as vectors.

It is assumed, for simplicity, that the finger does not move in the z direction and so there is no component of force in that direction, ie. the pushing plane is parallel to the plane on which the feet rest.

Six equations may be generated, three by imposing force equilibrium in each of the coordinate directions, and three by imposing moment equilibrium about each of the coordinate axes. Each set of three equations may be combined into a vector equation.

Force equilibrium:

$$\vec{P} - \vec{k}\,W + \sum_{i=1}^{3} \left(-f\,\mathrm{sgn}(\dot{\theta})\,\vec{k} \times \frac{(\vec{x_i} - \vec{x})}{|\,\vec{x_i} - \vec{x}\,|} + \vec{k} \right) V_i = 0. \tag{3.9}$$

Moment equilibrium about centre of mass:

$$\vec{\bar{x}} \times \vec{P} + \sum_{i=1}^{3} \vec{x_i} \times \left(-f\,\mathrm{sgn}(\dot{\theta})\,\vec{k} \times \frac{(\vec{x_i} - \vec{x})}{|\,\vec{x_i} - \vec{x}\,|} + \vec{k} \right) V_i = 0. \tag{3.10}$$

where

$\vec{k}$	unit vector out of plane (along z-axis)
$\vec{x}$	location of the instantaneous centre $(x, y, -z_C)^t$
$\vec{x_i}$	location of foot i $(x_i, y_i, -z_C)^t$
$\vec{\bar{x}}$	point of action of contact force $(\bar{x}, \bar{y}, z_f)^t$
$\vec{P}$	contact force $(P, Q, 0)^t$
$\mathrm{sgn}(\dot{\theta})\,\vec{k} \times \frac{(\vec{x_i}-\vec{x})}{\lvert\vec{x_i}-\vec{x}\rvert}$	unit vector in the direction of motion of foot i $(v_{xi}, v_{yi}, 0)^t$

Equation 3.9 can be rearranged in terms of the reactions to give:

$$\begin{pmatrix} V_1 \\ V_2 \\ V_3 \end{pmatrix} = f \begin{bmatrix} v_{x1} & v_{x2} & v_{x3} \\ v_{y1} & v_{y2} & v_{y3} \\ 1 & 1 & 1 \end{bmatrix}^{-1} \begin{pmatrix} -P \\ -Q \\ W \end{pmatrix} \tag{3.11}$$

The reactions can then be substituted into equation 3.10, and the resulting vector equation may be split into its three component directions. These equations are again deficient by one, the additional equation being formulated, as in the planar case, from the assumed motion of the finger. Once the relevant substitution has been made, the three

simultaneous equations must be solved numerically. As before, a library routine based upon Powell's hybrid method is used.

Unfortunately, it is no longer possible to write down the ranges of the position of the finger where sticking of a foot ensues in closed form, so that, whenever the solution appears to converge towards a foot, a check must be made to determine if rotation about that foot is occurring. In practice the algorithm converges to a solution well, but occasionally it is necessary to restart the iterative process from a different initial estimate of the instantaneous centre.

There are generally two forms of indeterminacy associated with the three feet being collinear: one in determining the vertical reactions at the feet and one associated with particular types of motion. The former, static equilibrium, has been discussed already (see Chapter 2), and the latter can be seen from the following argument: although equation 3.11 is used to find the reactions, it prescribes them from the assumed motion of the body rather than moment equilibrium (which is enforced in equation 3.10). When the body is pushed so that the resulting motion has an instantaneous centre lying along the line of the feet, but not between them, the matrix on the right hand side of equation 3.11 becomes singular and hence has no unique inverse. In this case, an instantaneous centre anywhere along the line, outside the feet, is a solution to the equations; this indeterminacy vanishes if inertial terms are included in the formulation.

3.3.2 Results

Using a body with similar geometry to the planar pushing case, the effect of the height at which the finger pushes on the regions in the pushing space where both the feet and finger stick is shown in Figures 3.5a, b, c. For each height both coefficients of friction (f and f_f) are 0.3. The tendency for the object to rotate about points of support which are on the same side of the centre of mass as the point of application of the pushing force *decreases* as the height at which the finger pushes is increased. Conversely, this tendency

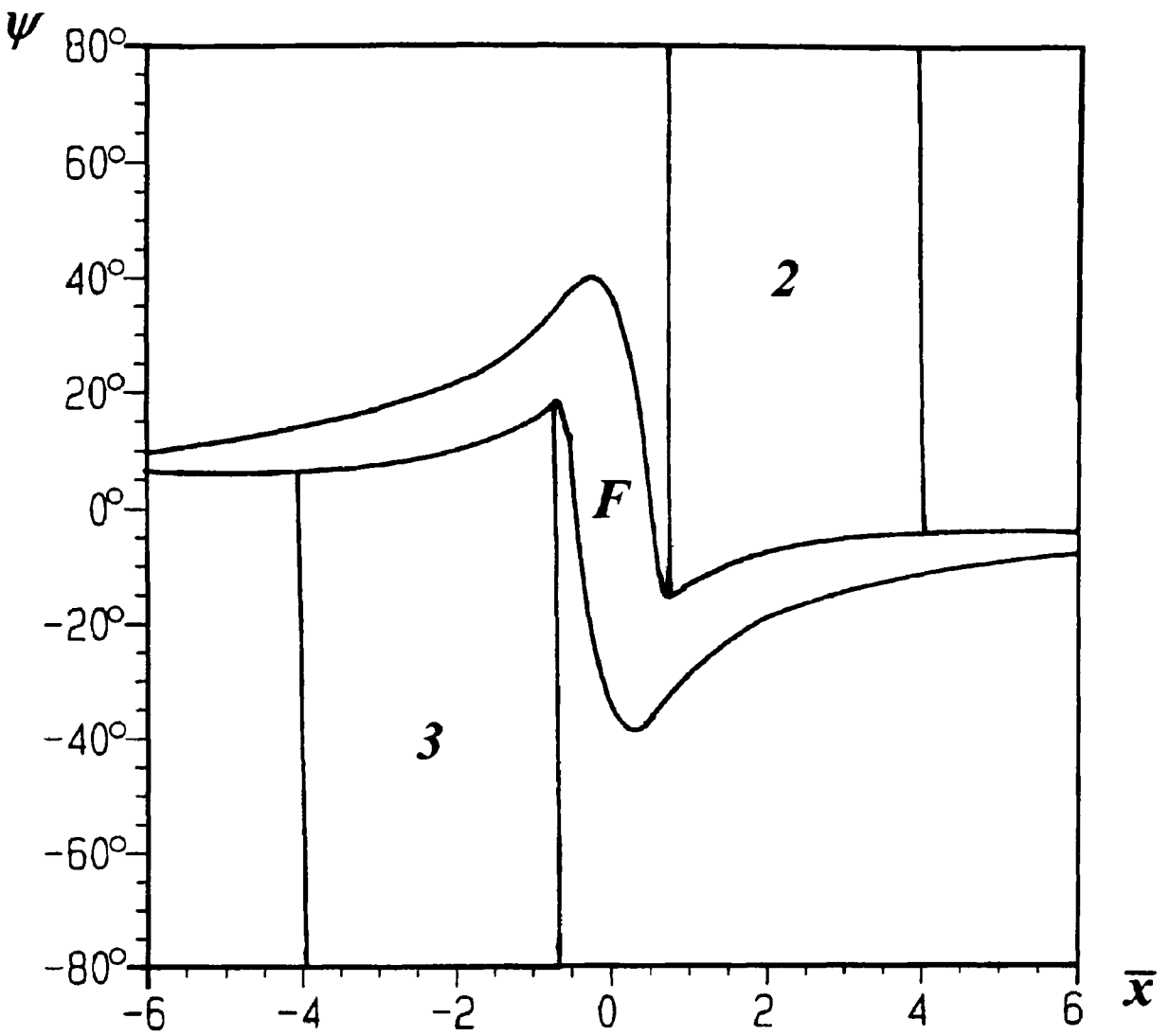

Figure 3.5: Regions where finger sticks (F) and where rotation about a foot occurs ($f = 0.3$, $f_f = 0.3$), when: (a) $z = 0.1$

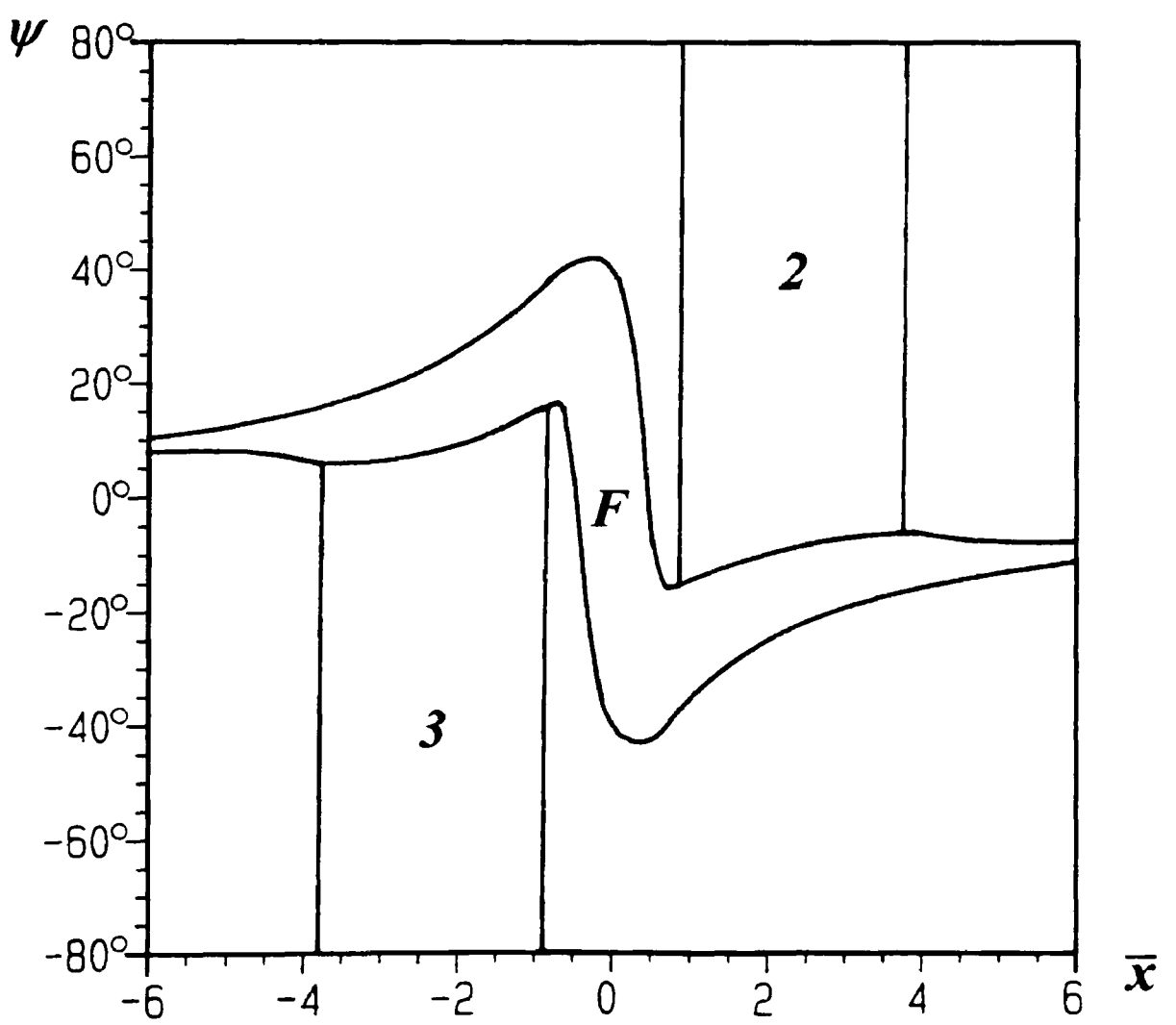

Figure 3.5: (b) $z = 0.5$

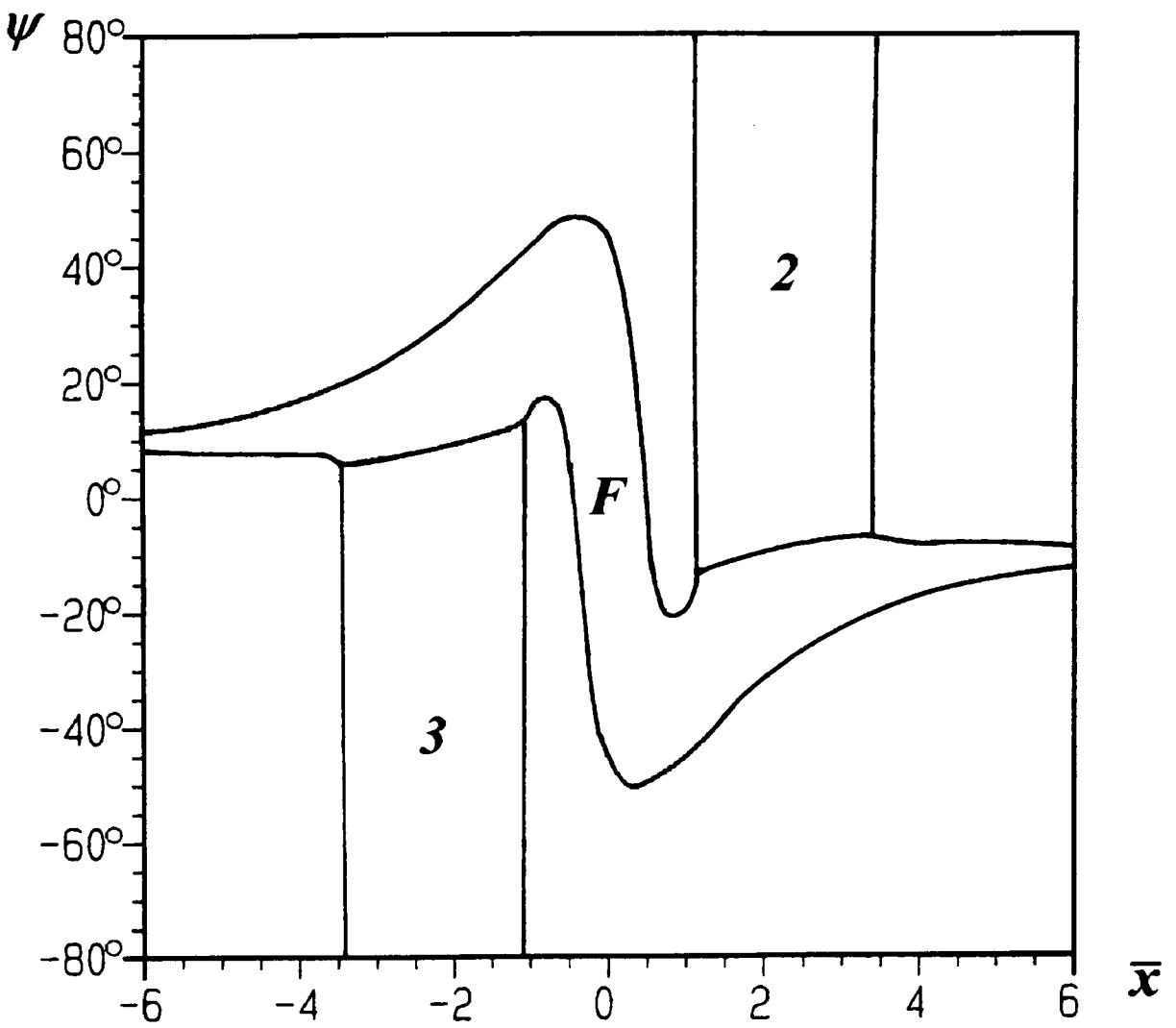

Figure 3.5: (c) $z = 1.0$)

increases for feet which are on the opposite side.

One important consideration is to assess how much the motion of the body changes when only the height of push is varied. The motivation for this is to determine at what heights it is valid to approximate a three dimensional pushing case to the simpler planar one. An easy way to achieve a comparison is to represent the change in motion of the body with the height of push as a scalar. For a unit displacement of the finger, the centre of mass of the body displaces in the x and y directions by amounts d_x and d_y respectively. It also rotates through an angle $\delta\theta$ which, when measured in radians and multiplied by a characteristic length (in this case the mean distance from the centre of mass to a foot), yields a value d_θ. Hence, the motion can be expressed in vector form (d_x, d_y, d_θ). A scalar may be generated by finding the distance between two such normalised vectors at the same location in the pushing space but at different heights of push. Hence, the scalar Δ is defined:

$$\Delta = \sqrt{(\bar{d}_{x2} - \bar{d}_{x1})^2 + (\bar{d}_{y2} - \bar{d}_{y1})^2 + (\bar{d}_{\theta 2} - \bar{d}_{\theta 1})^2},$$

where $(\bar{d}_{xi}, \bar{d}_{yi}, \bar{\theta}_i)$ is the normalised vector describing the motion when the object is pushed at height i.

Figures 3.6a, b show Δ when the body is pushed at heights of 0.1 and 0.5 (normalized with respect to the characteristic length) respectively, relative to pushing in the plane of the feet, again $f = f_f = 0.3$. There is no difference in regions where rotation occurs about a foot at both heights. The difference is small in most of the region where the finger sticks and is largest where the location of the pushing finger, $\bar{x}$, is compatible with foot stick but the direction of finger motion, ψ, is not.

When pushing above the plane, the location of the instantaneous centre is no longer independent of the coefficient of friction at the feet, as shown by equations 3.9,10,11. The effect of changing the coefficient of friction at the feet is shown in Figures 3.7a, b. An increase in the coefficient of friction between the body and the plane, f, increases the effect of the height of push on the location of the instantaneous centre and, as increasing the coefficient of friction tends to increase the force necessary to push the body, the regions of finger stick grow as well.

3.4 Conclusions

This investigation has enabled the motion of any 3-footed object (except ones with collinear feet) to be predicted when pushed by a finger in a plane parallel to the ground. The characteristics of this motion have been presented for one particular geometry of object and could be used to plan a strategy for manipulating it.

Of particular interest are regions of the pushing space where the motion can be accurately predicted despite uncertainty in the values of the coefficients of friction and in the finger position. These regions are the ones where rotation about a foot takes place and

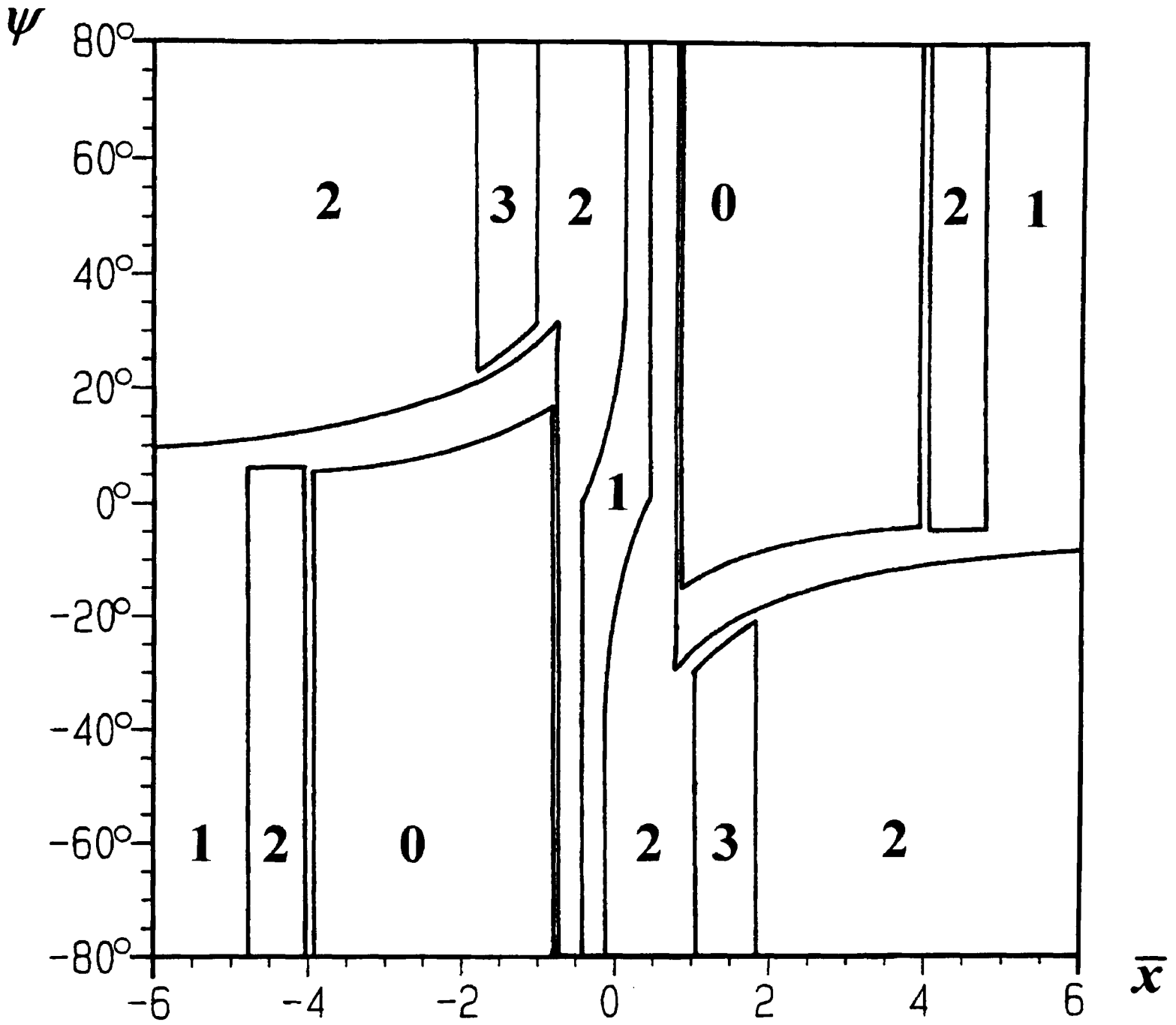

KEY	
0	$\Delta=0$
1	$0.00<\Delta\leq 0.01$
2	$0.01<\Delta\leq 0.05$
3	$0.05<\Delta\leq 0.06$ (max)

Figure 3.6: A measure of the change in motion of the body with height of push compared with pushing in the plane of the feet when: (a) $z = 0.1$

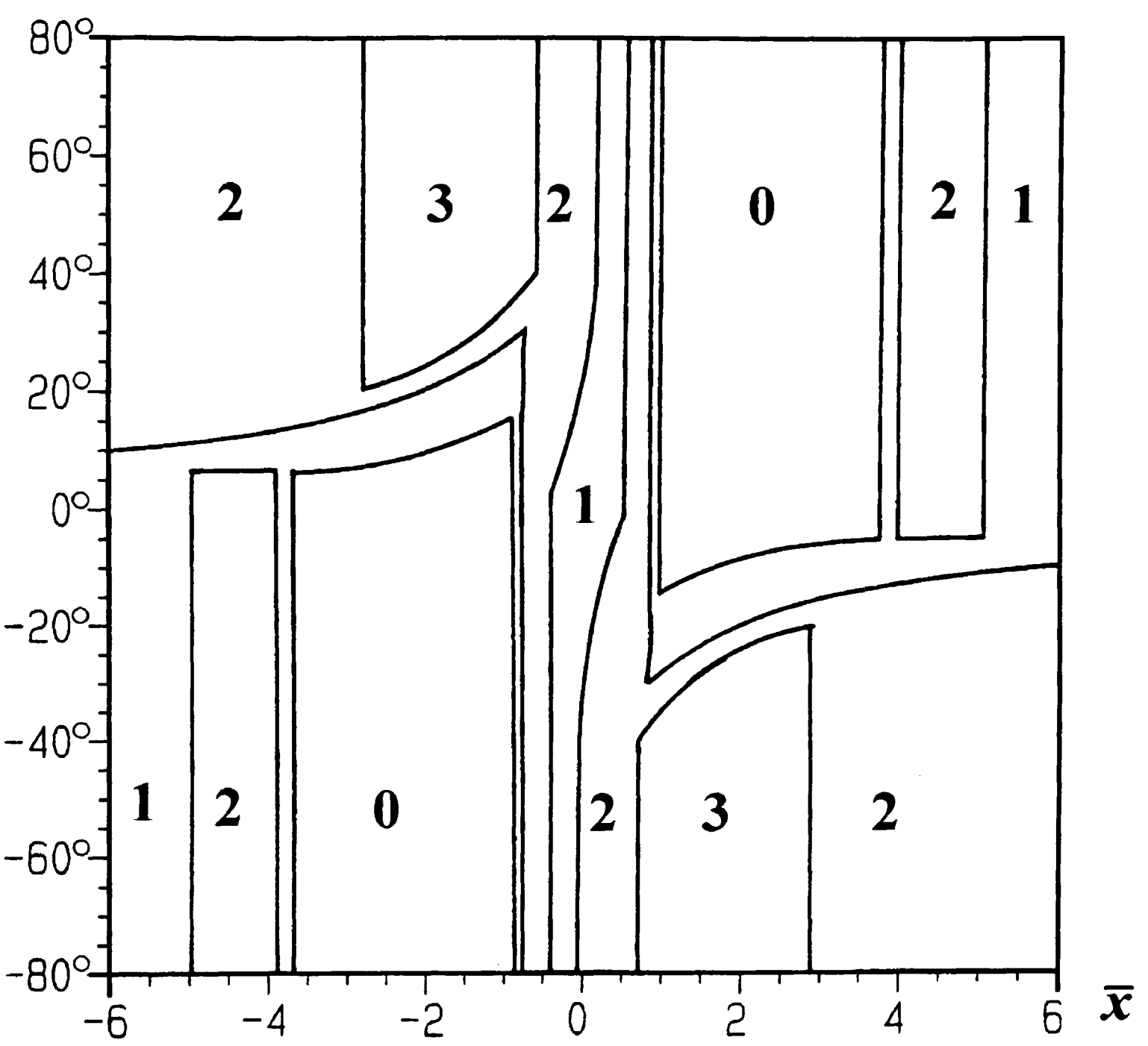

KEY	
0	$\Delta=0$
1	$0.00<\Delta\leq 0.05$
2	$0.05<\Delta\leq 0.20$
3	$0.30<\Delta\leq 0.30$ (max)

Figure 3.6: (b) $z = 0.5$

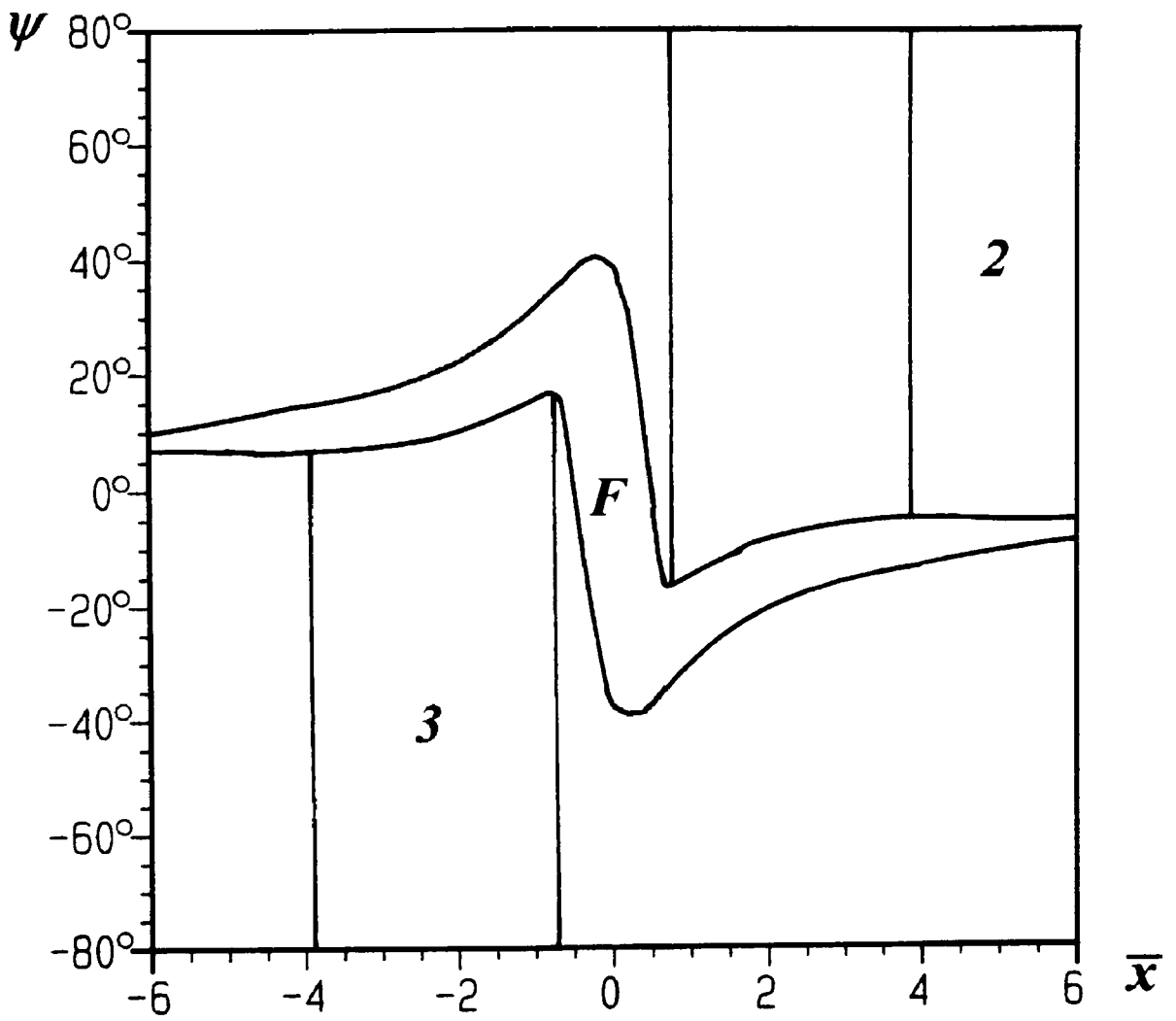

Figure 3.7: Regions where the finger sticks (F) and where rotation about a foot occurs when $f_f = 0.3$, $z = 0.5$ and (a) $f = 0.1$

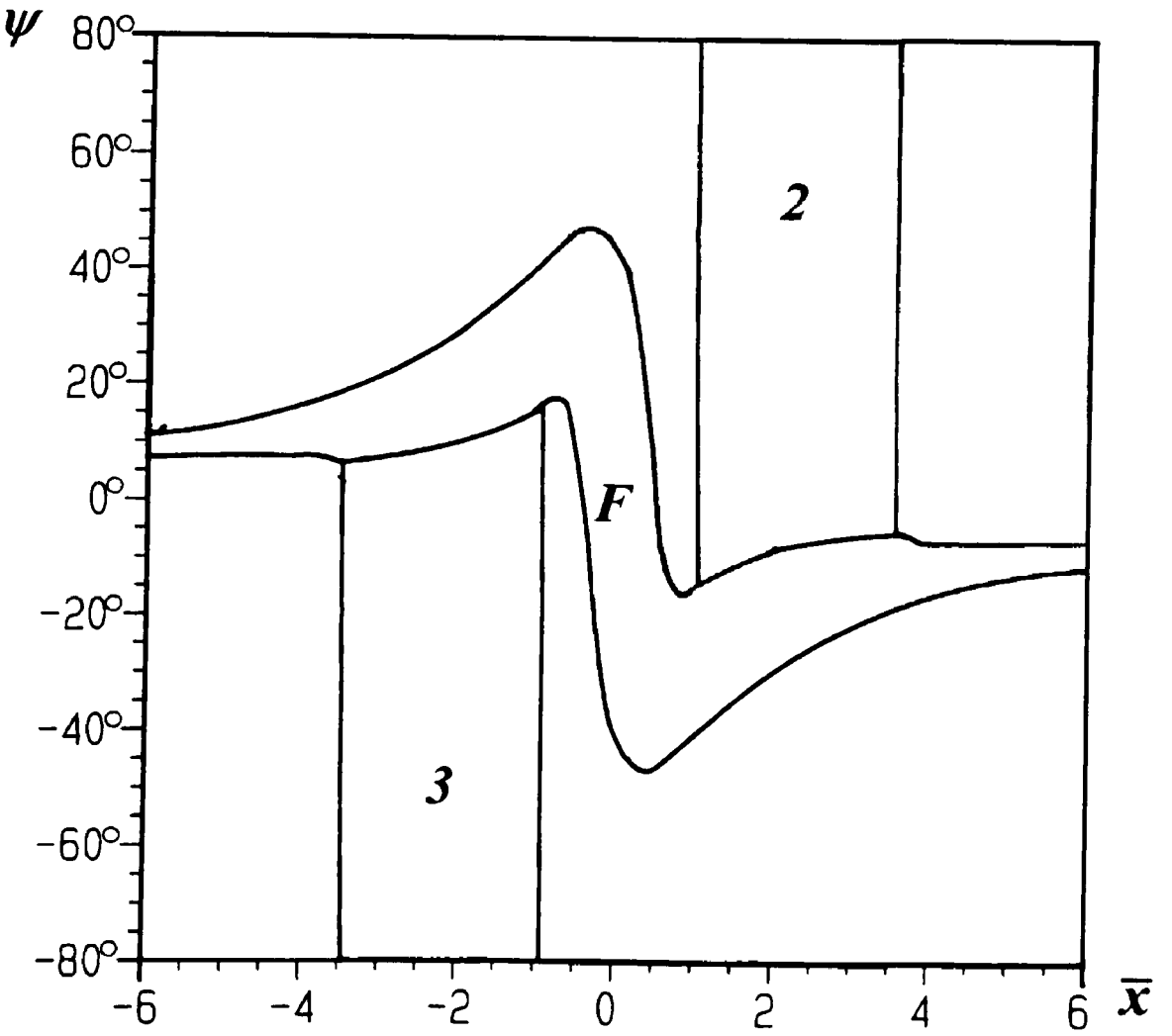

Figure 3.7: (b) $f = 0.5$

ways of increasing the size of these regions have been found. Increasing the coefficient of friction at the finger always expands the stick regions; increasing the friction at the feet and raising the height of push has the *same* effect if the foot is on the opposite side of the centre of mass as the finger and vice versa.

An attempt has been made to show the validity of the results of the previous Chapter, where the pushing force was in the plane of the feet, to the more general 3-dimensional case. No general conclusions can be drawn from this, since the accuracy required depends on the application. For example if a workpiece must be accurately positioned then the height of push must be taken into account; however, the planar approximation does provide a general idea of the regions of rotation about a foot in the pushing space, which do not change significantly over the range of heights considered here.

Extending the analysis further to include contact over a distributed area when pushing above the plane introduces a major complication. The pressure distribution can no longer be found from equilibrium arguments alone and consideration has to be given to the compatibility of deformation of the object and the frictional plane. The development of such tools is the goal of Chapter 5. However, integrating the numerical procedure of locating the instantaneous centre with the numerical procedure for finding the corresponding pressure distribution would require significant computer resource. Although such an analysis is possible it is not pursued in this study.

Chapter 4

Rolling Contact Between Elastically Dissimilar Cylinders

4.1 Introduction

Two cylinders are described as freely rolling when no nett tangential force is transmitted between them. Tractive rolling occurs when a tangential force is transmitted by the driving cylinder to the braking one. For certain combinations of materials the braking cylinder can actually have a greater peripheral velocity than the driver. At first sight energy appears to be generated by such a system; this clearly violates the first law of thermodynamics. In this chapter the mechanism is investigated which explains this apparent anomaly.

Whenever dissimilar bodies are in contact, a change in relative curvature occurs if tangential tractions arise. To determine the interaction of normal and tangential displacements, it is instructive to consider a frame of reference which is fixed with respect to the region of contact. Material in each cylinder is then seen to flow through this region of contact. If the materials have similar elastic properties and the peripheral velocities of the cylinders are equal then the tangential strain of a particle as it moves through the contact is identical if it is in either cylinder. No tangential tractions arise and the normal tractions

The work described in this Chapter has been published and can be found in: R. Munisamy, D. A. Hills and D. Nowell 1991,"Brief note on the tractive rolling of dissimilar elastic cylinders" *Int. J. Mech. Sci.*, Vol. 33, pp. 225–228.

are given by Hertz's solution. If the cylinders roll with different peripheral velocities then material in each cylinder flows into the contact region at different rates. Two extremes may be considered. The first is where the coefficient of friction is sufficiently small and the difference in peripheral speeds is sufficiently large for the cylinders to slide over each other. In this case the tangential tractions take their limiting values. The opposite extreme occurs when the coefficient of friction is infinite causing the contact zone to be an area of complete adhesion. Material in each cylinder must deform tangentially to achieve this. A particle within the faster-moving cylinder experiences compression as it enters the contact and tension as it leaves; a particle within the slower-moving one experiences the opposite. Between these extremes, contacts consist of regions of both adhesion and slip. This kind of solution was first proposed by Reynolds (1875) to explain the phenomenon known as creep where two cylinders, which have different peripheral velocities in the undeformed region, roll over each other without gross sliding.

When tractive rolling occurs between cylinders with similar elastic properties, the tangential tractions induce no relative normal displacements and so Hertz's solution for the normal tractions is again valid. This distribution, in association with the coefficient of friction, limits the absolute local magnitude of the tangential tractions. The task of determining the stick-slip interfaces and finding compatible tangential tractions was first achieved by Carter (1926). If the cylinders have dissimilar elastic properties, coupling between the normal and shear tractions occurs. This results in the generation of frictional tractions and creep even when no nett tangential force is transmitted. Bentall and Johnson (1967) evaluated the tangential tractions for freely rolling cylinders and found the rolling resistance introduced due to energy dissipation in the regions of micro-slip. By splitting the contact region into a series of overlapping triangles of traction they generated a piecewise-linear discretization of the shear traction distribution.

Researchers have often applied the so-called Goodman's approximation (Goodman, 1962) to the solution of these problems wherein Hertz's pressure distribution to represent

the normal tractions is retained. Kalker (1971) has solved the problem of tractive rolling of dissimilar elastic cylinders. He employed a discretization method similar to Bentall and Johnson in conjunction with an optimization routine to find the shear traction distribution and locate the stick-slip interfaces automatically. Nowell and Hills (1988) have also solved the problem for a wide range of material pairs and transmitted forces. However, an anomaly arises from the use of the Goodman approximation by these authors; for some combinations of materials energy appears to be generated by the system. As stated earlier, this in direct contradiction to the first law of thermodynamics. To clear up the discrepancy, an analysis of tractive rolling is presented where full interaction is permitted between the normal and tangential displacements and tractions.

4.2 Formulation

Figure 4.1 shows the essential elements of the geometry. The two cylinders are pressed together by a normal force P to form a contact of semi-width a. As coupling effects between tractions and displacements are to be retained, the problem has no symmetry, and hence the offset of the centre-line of the cylinders to the middle of the contact, ea, is included.

Analysis begins by writing down the integral equations relating the elastic deformations to the distributions of traction at the interface of the two cylinders. It is more convenient to work in terms of displacement gradients rather than actual displacements because constants associated with a fixed point of reference are dispensed with. Treating each body in the vicinity of the contact as an elastic half-plane, the normal displacement gradient of surface particles is given by (Johnson, 1985)

$$\frac{\partial u_{z1}}{\partial x} = -\frac{1-\nu_1}{\pi\,\mu_1}\int_{-a}^{a}\frac{p(\xi)}{x-\xi}\,d\xi + \frac{1-2\nu_1}{2\mu_1}q(x) \tag{4.1}$$

$$\frac{\partial u_{z2}}{\partial x} = +\frac{1-\nu_2}{\pi\,\mu_2}\int_{-a}^{a}\frac{p(\xi)}{x-\xi}\,d\xi + \frac{1-2\nu_2}{2\mu_2}q(x) \tag{4.2}$$

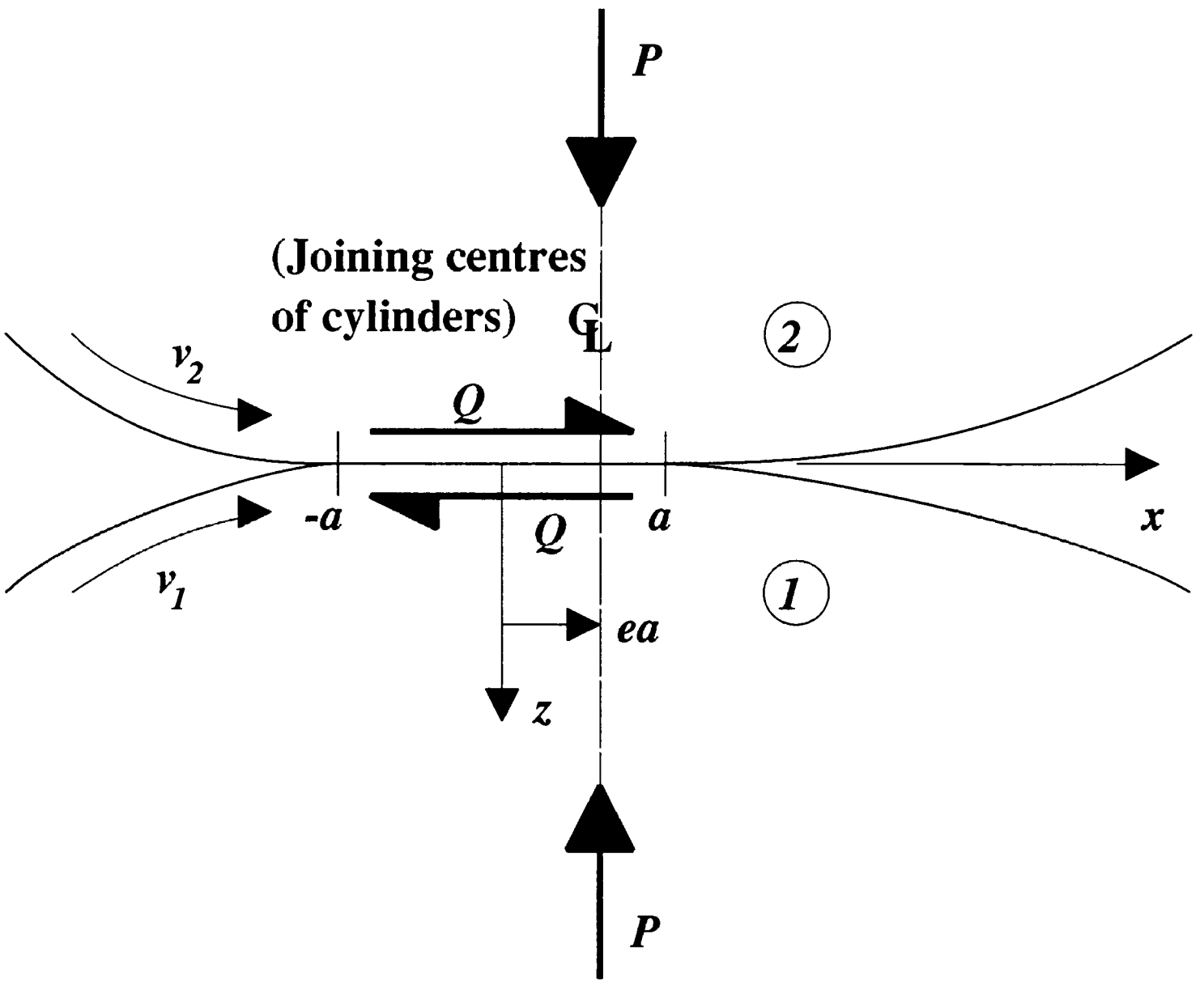

Figure 4.1: Configuration of the contacting bodies.

where ν is Poisson's ratio, μ is the modulus of rigidity and the subscripts 1 and 2 refer to the lower and upper body respectively. Within the contact, compatibility of displacements dictates that relative surface displacement gradient of the bodies must equal the combined gradients of their initial curvature:

$$\frac{\partial u_{z1}}{\partial x} - \frac{\partial u_{z2}}{\partial x} = -k(x - ea) \qquad -a \leq x \leq a \tag{4.3}$$

where

$$k = \frac{1}{R_1} + \frac{1}{R_2} \tag{4.4}$$

and R_1, R_2 are the radii of curvature of the cylinders.

Thus

$$\frac{1}{\pi}\int_{-a} a\frac{p(\xi)}{x-\xi}\,d\xi - \beta q(x) = \frac{k}{A}(x - ea) \qquad -a \leq x \leq a \tag{4.5}$$

where

$$A = \frac{1-\nu_1}{\mu_1} + \frac{1-\nu_2}{\mu_2} \qquad \text{Composite compliance} \tag{4.6}$$

and

$$\beta = \left(\frac{1-2\nu_1}{\mu_1} - \frac{1-2\nu_2}{\mu_2}\right)/2A \qquad \text{Dundurs' constant} \tag{4.7}$$

At this stage it is possible to illustrate the Goodman approximation. It states that the second term in equation 4.5 may be neglected and this is certainly valid if β is small. In such a case a Cauchy integral equation of the first kind results which may be inverted to give Hertz's solution for the traction distribution $p(x)$. In this analysis the simplification will not be made.

An equivalent integral equation may be developed in terms of the gradient of *tangential* displacements. Again Johnson (1985) provides the starting point:

$$\frac{\partial u_{x1}}{\partial x} = -\frac{1-2\nu_1}{2\mu_1}p(x) - \frac{1-\nu_1}{\pi\mu_1}\int_{-a}^{a}\frac{q(\xi)}{x-\xi}d\xi \tag{4.8}$$

$$\frac{\partial u_{x2}}{\partial x} = -\frac{1-2\nu_2}{2\mu_2}p(x) + \frac{1-\nu_2}{\pi\mu_2}\int_{-a}^{a}\frac{q(\xi)}{x-\xi}d\xi \tag{4.9}$$

It is necessary to ensure that the relative slip direction of the two surfaces is compatible with the local shear traction and so a new quantity $h(x)$ is introduced, given by

$$h(x) = \frac{\partial u_{x1}}{\partial x} - \frac{\partial u_{x2}}{\partial x}. \tag{4.10}$$

Hence,

$$\frac{h(x)}{A} = -\frac{1}{\pi}\int_{-a}^{a}\frac{q(\xi)}{x-\xi}d\xi - \beta p(x). \tag{4.11}$$

It is convenient to apply the following normalizations

$$x = as \tag{4.12}$$

$$\xi = ar \tag{4.13}$$

$$\tilde{p}(s) = \frac{ap(s)}{P} \tag{4.14}$$

$$\tilde{q}(s) = \frac{aq(s)}{P} \tag{4.15}$$

to the fundamental integral equations 4.5 & 4.11 to give

$$\frac{1}{\pi}\int_{-1}^{1}\frac{\tilde{p}(r)}{s-r}dr - \beta\tilde{q}(s) = \frac{ka^2}{AP}(s-e) \qquad -1 \le s \le 1 \tag{4.16}$$

$$+\frac{1}{\pi}\int_{-1}^{1}\frac{\tilde{q}(r)}{s-r}dr + \beta\tilde{p}(s) = \frac{ah(s)}{AP} \qquad -1 \le s \le 1. \tag{4.17}$$

The contact has regions of stick and slip within which different conditions apply.

4.2.1 Stick zones

The relative slip velocity of corresponding surface particles within a stick zone must be zero. The velocity of a point on the surface of body i, v_i, is composed of the gross motion of the cylinders and a local effect due to the change in tangential strain. It is given by Johnson (1985), for steady state rolling

$$v_i = V + \delta v_i + V\frac{\partial u_{xi}}{\partial x} \tag{4.18}$$

where V is the mean velocity of the periphery of the two cylinders and δv_i is the creep velocity of cylinder i. Hence, the local slip velocity v_s is given by

$$v_s = v_1 - v_2 = \delta v_1 - \delta v_2 + V\left(\frac{\partial u_{x1}}{\partial x} + \frac{\partial u_{x2}}{\partial x}\right), \tag{4.19}$$

giving

$$\frac{v_s}{V} = \zeta + h(x), \tag{4.20}$$

where

$$\zeta = \frac{\delta u_{x1} - \delta u_{x2}}{V} \qquad \text{Creep ratio.} \tag{4.21}$$

Enforcing $v_s = 0$ within a stick zone requires that $h(x) = -\zeta$. Moreover, if there is more than one stick zone continuity demands that $h(x)$ is the same in all stick zones. In addition the shear traction must be less than the limiting value, i.e.

$$|q(x)| < fp(x) \tag{4.22}$$

where f is the coefficient of friction.

4.2.2 Slip zones

Within a slip zone the magnitude of the shear traction must take its limiting value, hence

$$|q(x)| = fp(x), \tag{4.23}$$

whilst its sense should be consistent with the relative slip velocity of the corresponding surface particles, ie. that tangential tractions should oppose relative slip. This is expressed by

$$\mathrm{sgn}(v_s) = -\mathrm{sgn}[q(x)], \tag{4.24}$$

ie.

$$\mathrm{sgn}[h(x) + \zeta] = -\mathrm{sgn}[q(x)]. \tag{4.25}$$

These conditions are necessary to define the tractions within the slip and stick zones but are insufficient to define the actual transition points between the zones. Kalker's variational approach, which finds the transition points automatically, cannot be applied in this case since two distributions, the normal and shear tractions, must be found. Fortunately, the form of the shear tractions is quite well known and this may be exploited.

Carter's (1926) solution of tractive rolling contact for elastically *similar* cylinders showed that there is always a single stick zone followed by a single zone of slip, provided that the transmitted shear force is less than the limiting value. Bentall and Johnson (1967) present an example of tractive rolling of *dissimilar* elastic cylinders where there is an additional slip zone at the front of the contact. This slip zone may be the same or opposite in sense to the one at the rear. When the cylinders roll freely the situation is somewhat more complex. There may be as many as five regions starting with a slip zone and exhibiting alternating zones of stick and slip. The first and last slip zones are of the same sense and of opposite sense to the one in the middle. The second stick zone is nearly always vanishingly small. Nowell and Hills (1988) have confirmed that all forms of tractive rolling between dissimilar elastic cylinders (ie. $-1 < Q/fP < 1$ and $-0.5 < \beta < 0.5$) is described by one of the above distributions. These results form the basis of a numerical procedure.

Unfortunately it is not possible to evaluate the normal and tangential tractions simultaneously, so an iterative scheme is developed. Initially the normal traction distribution is assumed to be Hertzian. The tangential and normal tractions are then found by sequential iteration; the process is repeated until convergence is achieved.

4.3 Numerical solution

The first case to be considered is when there are two slip zones of the same sense bordering a single stick zone as shown in Figure 4.2a. As an initial approximation, the normal traction distribution is assumed to be Hertzian. Since the shear traction takes its limiting value within the slip zones, it is sensible to find the perturbation to this value within the stick zone. Hence, $\tilde{q}(s)$ is written as

$$\tilde{q}(s) = f\tilde{p}(s) + q'(s) \qquad q'(s) = 0 \quad s < b_1, s > b_2 \tag{4.26}$$

where b_1 and b_2 define the limits of the stick zone. Substituting this into equation 4.17 and enforcing the no slip condition within the stick zone gives

$$\frac{f}{\pi}\int_{-1}^{1}\frac{\tilde{p}(r)}{s-r}dr + \frac{1}{\pi}\int_{b_1}^{b_2}\frac{q'(r)}{s-r}dr + \beta\tilde{p}(s) = \frac{a\zeta}{AP} \qquad b_1 \leq s \leq b_2. \tag{4.27}$$

The first integral is evaluated numerically. The second may be evaluated by a quadrature described by Erdogan *et al.* (1973) if $q'(s)$ is approximated by a truncated series of Chebyshev polynomials. To facilitate this procedure, a further transformation of coordinates is required:

$$t = \frac{2r - (b_1 + b_2)}{b_2 - b_1} \tag{4.28}$$

$$w = \frac{2s - (b_1 + b_2)}{b_2 - b_1}. \tag{4.29}$$

Equation 4.27 then becomes

$$\frac{1}{\pi}\int_{-1}^{1}\frac{q'(t)}{w-t}dt = -\beta\tilde{p}(s) - \frac{f}{\pi}\int_{-1}^{1}\frac{\tilde{p}(r)}{s-r}dr + \frac{a\zeta}{AP} \qquad -1 \leq w \leq 1. \tag{4.30}$$

Following the method of Erdogan *et al.*, $q'(w)$ is written as the product of a fundamental function $\sqrt{1-w^2}$ and an unknown function $\phi(w)$. The Gaussian quadrature may now be

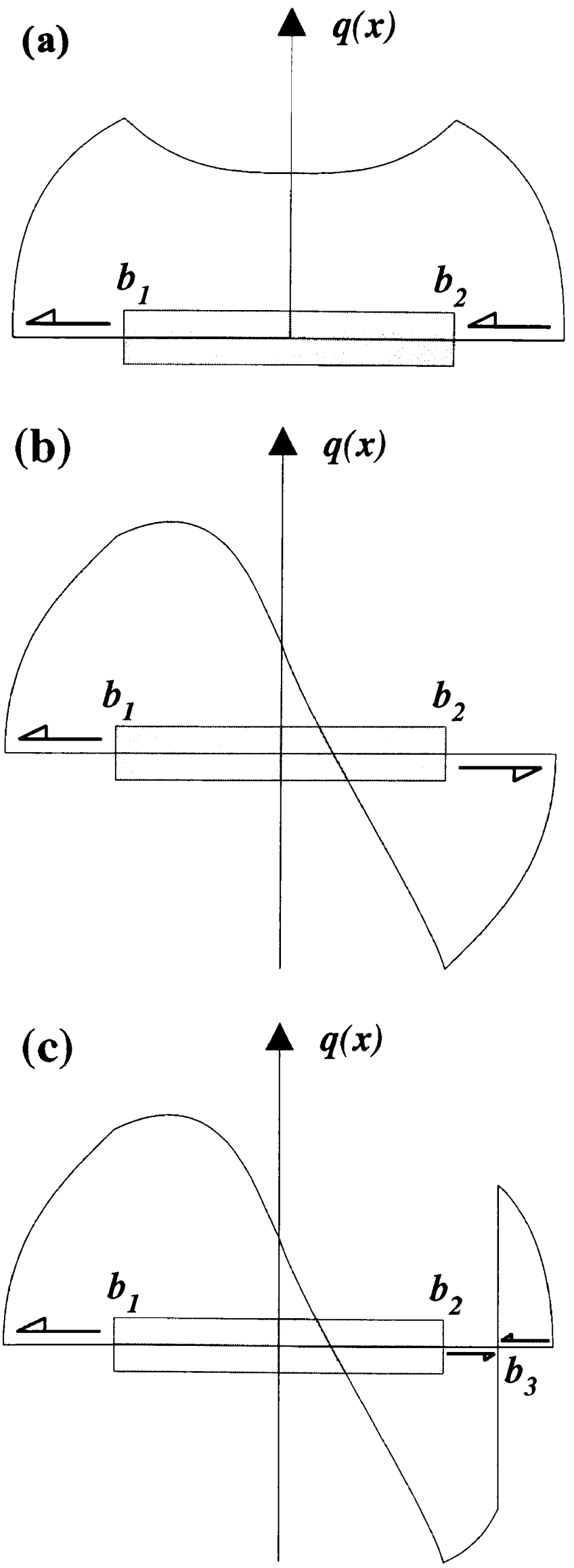

Figure 4.2: Variation of shear traction and slip velocity. (a) Two slip zones of the same sign. (b) Two slip zones of opposite sign. (c) Three slip zones.

applied and equation 4.30 discretized:

$$\sum_{i=1}^{m} \frac{(1-t_i^2)\phi(t_i)}{(m+1)(w_k - t_i)} = -\beta\tilde{p}(s_k) - \frac{f}{\pi}\int_{-1}^{1} \frac{\tilde{p}(r)}{s_k - r}dr + \frac{a\zeta}{AP} \tag{4.31}$$

where

$$t_i = \cos\left(\frac{\pi i}{m+1}\right) \qquad i = 1, m \tag{4.32}$$

$$w_k = \cos\left(\frac{\pi(k-\frac{1}{2})}{m+1}\right) \qquad k = 1, m+1 \tag{4.33}$$

and s_k is given by equation 4.29.

The material properties f and β are input variables. In practice, the position of the stick-slip transition points b_1 and b_2 are estimated *a priori* and input as well. The result is a determinate set of $n+1$ linear equations which are inverted simultaneously to give the n values of $\phi(t_i)$ and the normalised creep ratio $a\zeta/AP$. However, the solution must be shown to be consistent with condition 4.25, i.e. the direction of relative slip outside the stick zone must be the consistent with the local shear tractions. Hence, $h(x)$ is evaluated from equation 4.17 making the substitution of equation 4.26, and normalising to give

$$\frac{ah(s)}{AP} = -\frac{f}{\pi}\int_{-1}^{1} \frac{\tilde{p}(r)}{s-r}dr - \frac{1}{\pi}\int_{b_1}^{b_2} \frac{q'(r)}{s-r}dr + \beta\tilde{p}(s). \tag{4.34}$$

Since $h(s)$ needs to be evaluated within the slip zones only, where the second integral is non-Cauchy, the quadrature described above may be employed. Hence,

$$\frac{ah(s)}{AP} = -\sum_{i=1}^{n} \frac{(1-t_i^2)\phi(t_i)}{(m+1)(w - t_i)} + \beta\tilde{p}(s) - \frac{f}{\pi}\int_{-1}^{1} \frac{\tilde{p}(r)}{s-r}dr \tag{4.35}$$

A solution that is wholly consistent with the conditions 4.22 and 4.25 may be found by adjusting the position of b_2 while maintaining b_1 fixed. However, the effect of the tangential tractions on the normal ones must be evaluated first.

The normal tractions are approximated by a series of Chebyshev polynomials in an analogous manner to the representation of the tangential ones. Hence $\tilde{p}(s)$ is written as

the product of $\sqrt{1-s^2}$ and the unknown function $\psi(s)$. The same quadrature is employed to evaluate the integral on the left hand side of equation 4.16, which becomes

$$\sum_{i=2}^{n} \frac{(1-r_i^2)\psi(r_i)}{(n+1)(s_k-r_i)} = \beta\tilde{q}(s_k) + \frac{ka^2}{AP}s_k - \frac{ka^2e}{AP} \tag{4.36}$$

where

$$r_i = \cos\frac{\pi i}{n+1} \qquad i = 1, n \tag{4.37}$$

$$s_k = \cos\frac{\pi(k-\frac{1}{2})}{n+1} \qquad k = 1, n+1. \tag{4.38}$$

The tangential tractions have been evaluated only at the integration points t_i. A variation of Krenk's formula (1975) is required to find them at the collocation points s_k. The interpolation formula is

$$\phi(t) = \sum_{j=1} mU_{j-1}(t)\frac{2}{m+1}\left[\sum_{i=1} m\sin\left(\frac{\pi i}{m+1}\right)\sin\left(\frac{\pi ij}{m+1}\phi(t_i)\right)\right] \tag{4.39}$$

where U_j is the jth Chebyshev function.

This results in a set of $n+1$ equations in the n values of $\psi(r_i)$, the contact law (ka^2/AP) and the eccentricity (ka^2e/AP). A further equation may be generated by considering normal equilibrium:

$$\int_{-a}^{a} p(\xi)d\xi = P \tag{4.40}$$

which may be written in normalised and discretized form as

$$\frac{\pi}{n+1}\sum_{i=1}^{n}(1-r_i^2)\psi(r_i) = 1 \tag{4.41}$$

The normal tractions, once found by solving the equations simultaneously, are used in equation 4.31 to re-evaluate the tangential tractions (an interpolation formula analogous to 4.39 is used to find the normal tractions at the points w_k). The alternate solution of equations 4.31 and 4.36 is repeated until the tractions converge. The location of the

stick-slip interface then is adjusted to satisfy the relevant conditions for the magnitude and direction of the shear tractions within the stick and slip zones.

Of course, for some regimes of stick and slip, a different form of tangential tractions is required. The two others considered here are: two slip zones of opposite sign and three slip zones (as shown in Figures 4.2b and 4.2c).

The only modification to the above method required when there are two slip zones of opposite sign is a redefinition of the tangential traction distribution. This is achieved by recasting equation 4.26 as

$$\begin{aligned} \tilde{q}(s) &= f\tilde{p}(s) && -1 < s < b_1 \\ &= q'(s) + f\tilde{p}(b_1) - f(\tilde{p}(b_2) + \tilde{p}(b_1)) && \frac{s-b_1}{b_2-b_1}b_1 < s < b_2 \\ &= -f\tilde{p}(s) && b_2 < s < 1 \end{aligned} \tag{4.42}$$

The only difference this makes to the subsequent equations is in the integrals which need to be evaluated numerically. For example equation 4.30 becomes

$$\begin{aligned} \frac{1}{\pi}\int_{-1}^{1}\frac{q'(t)}{w-t}dt &= -\beta\tilde{p}(s) - \frac{f}{\pi}\int_{-1}^{b_1}\frac{\tilde{p}(r)}{s-r}dr - \frac{f}{\pi}\int_{b_1}^{b_2}\frac{\tilde{p}(b_1)(b_2-r)-\tilde{p}(b_2)(r-b_1)}{(s-r)(b_2-b_1)}dr \\ &\quad + \frac{f}{\pi}\int_{b_2}^{1}\frac{\tilde{p}(r)}{s-r}dr + \frac{a\zeta}{AP} \qquad -1 \le w \le 1 \end{aligned} \tag{4.43}$$

The integral on the left hand side is discretized by the method of Erdogan *et al.* as before and the three integrals on the right hand side are evaluated numerically.

Accommodating three slip zones is only slightly more complicated. Let b_1 and b_2 define the limits of the first stick zone as in the previous cases; since the subsequent slip zone is vanishingly small, b_3 is used to define the transition from reverse to forward slip. The tangential tractions are then recast as

$$\tilde{q}(s) = f\tilde{p}(s) \qquad -1 < s < b_1$$

$$
\begin{aligned}
&= q'(s) + f\tilde{p}(b_1) - f(\tilde{p}(b_2) + \tilde{p}(b_1))\frac{s - b_1}{b_2 - b_1} \qquad b_1 < s < b_2 \\
&= -f\tilde{p}(s) \qquad b_2 < s < b_3 \\
&= f\tilde{p}(s) \qquad b_3 < s < 1.
\end{aligned} \tag{4.44}
$$

Again, the numerical integrals are slightly modified compared with the original formulation. As with the variables b_1 and b_2, the location of the transition point b_3 is estimated *a priori*. Hence the set of equations remains determinate. The condition that the slip velocity is zero at this point (i.e. that $h(s) = -\zeta$) is used to adjust the position of b_3 on subsequent iterations.

Whatever the form of the tangential tractions, the resultant tangential force is found by integrating tractions over the contact:

$$
Q = \int_{-a}^{a} q(x)dx \tag{4.45}
$$

which in normalised form is

$$
\frac{Q}{P} = \int_{-1}^{1} \tilde{q}(s)ds \tag{4.46}
$$

The integral on the right hand side must be evaluated numerically. However, use may be made of the quadrature to find the component of force Q' due to $q'(s)$:

$$
\frac{Q'}{P} = \frac{(b_2 - b_1)\pi}{2(n+1)} \sum_{i=1}^{n} (1 - t_i^2)\phi(t_i). \tag{4.47}
$$

4.3.1 Energy dissipated

The law of the conservation of energy demands that the power put into the system must equal the sum of the power out and the power dissipated. The energy expended by friction within the regions of slip is the source of all power dissipation and may be written as

$$
W_{loss} = -\int_{-a}^{a} v_s(x)q(x)dx \tag{4.48}
$$

or in non-dimensional terms and substituting for $v_s(x)$,

$$\frac{W_{loss}a}{VP^2A} = -\int_{-1}^{1} \tilde{q}(s)\left(\frac{ah(s)}{AP} + \frac{\zeta a}{AP}\right) ds. \tag{4.49}$$

The difference between power in and out of the system may be obtained by an external balance:

$$\text{power in} = Qv_1 + e'aPv_1/R_1 \qquad \text{and} \tag{4.50}$$

$$\text{power out} = Qv_2 - e'aPv_2/R_2 \tag{4.51}$$

where $e' = e + \tilde{x}$ and $\tilde{x}$ is the location of the centroid of pressure with respect to the mid-point of the contact. This eccentricity arises only because coupling between the tangential displacements and the normal tractions has been taken into account. If the Goodman approximation were made, this important term would be missing from the nett power delivered to the system resulting in a non-zero power audit.

The nett power supplied to the system is then

$$W_{nett} = QV\zeta + e'aPVk \tag{4.52}$$

which may be written in dimensionless form as

$$\frac{W_{nett}a}{VP^2A} = \frac{a\zeta}{AP}\int_{-1}^{1} \tilde{q}(s)ds + \frac{ka^2e'}{AP} \tag{4.53}$$

4.3.2 Convergence of solution

Once formulated, the problem was coded into FORTRAN and run on a VAX mainframe computer. Matrix inversion and numerical integration were performed by the appropriate routines in the Numerical Algorithms Group library. It was found that increasing the value of m and n above 20 gave no significant improvement in the accuracy of the tangential and normal tractions. After four cycles of iteration the solution had converged sufficiently for the calculated values to be accurate to at least 3 significant figures.

4.4 Results

The large number of independent variables associated with this problem prohibit the presentation of a comprehensive set of results. Since the effect of coupling increases roughly with the product $f\beta$ (as can be inferred from equation 4.16), it is informative to maximize this product. Dundurs' constant β must lie between the extremes of ± 0.5 and the coefficient of friction rarely exceeds 0.5 in engineering practice. Hence the results presented here are for $\beta = 0.5$ and $f = 0.5$. Figure 4.3 shows the regimes of stick and slip for the full range of transmitted shear force. It should be noted that on the horizontal axis x is defined relative to the centre of the contact and *not* to the line joining the centres of the cylinders, and that the contact half-width a varies with Q/fP. The creep ratio $a\zeta/AP$, eccentricity ka^2e/AP and the contact law ka^2/AP are shown in Figure 4.4. An example of the tangential tractions for each form of stick and slip zone regime are shown in Figures 4.5a,b,c. These relate to problems where there are two slip zones of the same sign, two of opposite sign and three slip zones respectively. The normal traction distribution for each is plotted for comparison with the Hertzian distribution in Figure 4.6. The axes are normalised with respect to the Hertzian half-width a_0 and centred. It is clear that, apart from the offsets of the contact, the actual shapes of the distributions are reasonably similar.

Of particular interest is the nett power supplied to the system. This is shown in Table 4.1 for case where cylinder 1 is driving cylinder 2. For comparison, the values obtained when the Goodman approximation is made are also shown and the anomalous results when the creep velocity is negative (i.e. cylinder 2 is faster than cylinder 1). It can be seen by comparing the nett power supplied with the frictional losses that the law of conservation of energy is satisfied.

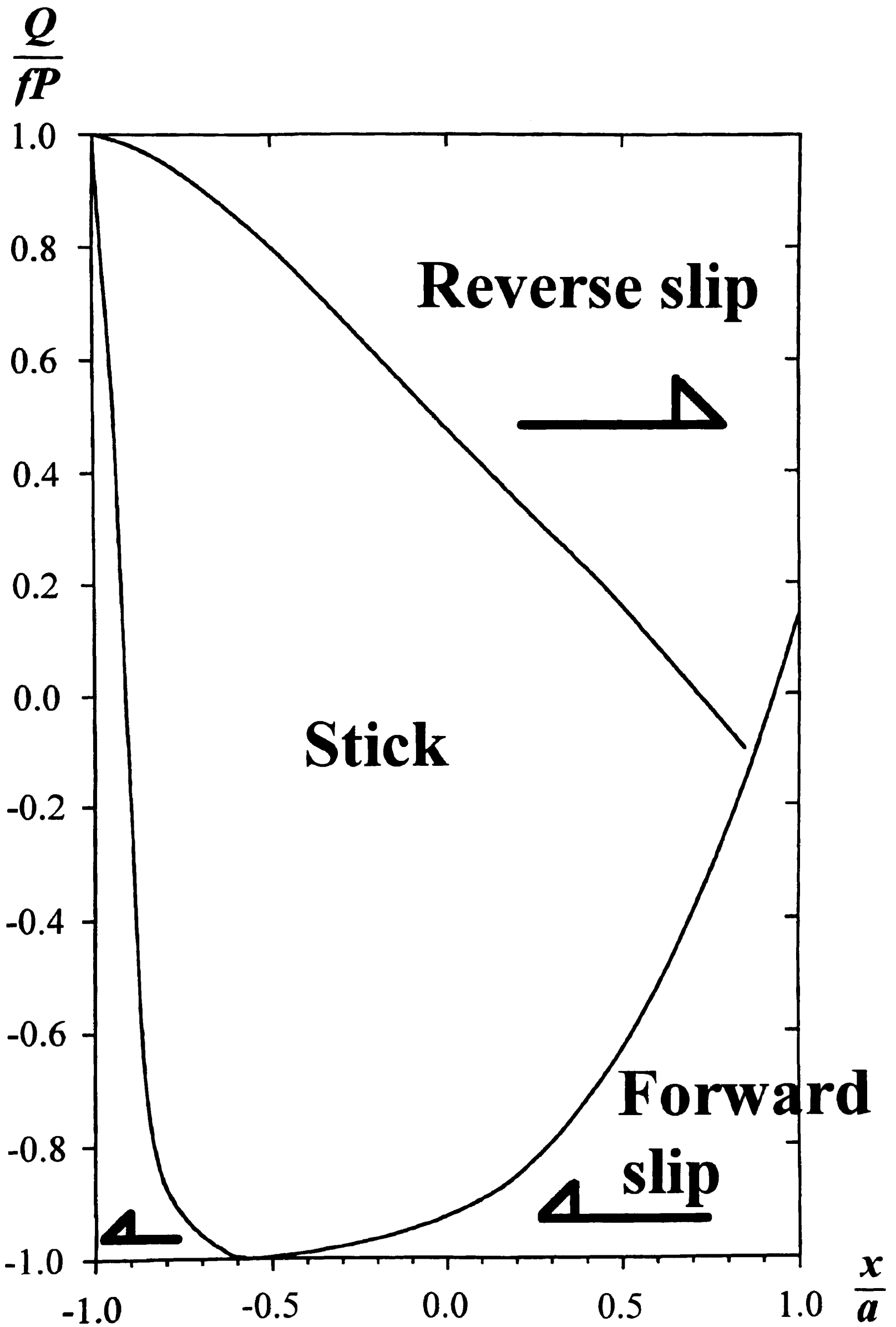

Figure 4.3: Regimes of stick and slip for $\beta = 0.5$ and $f = 0.5$.

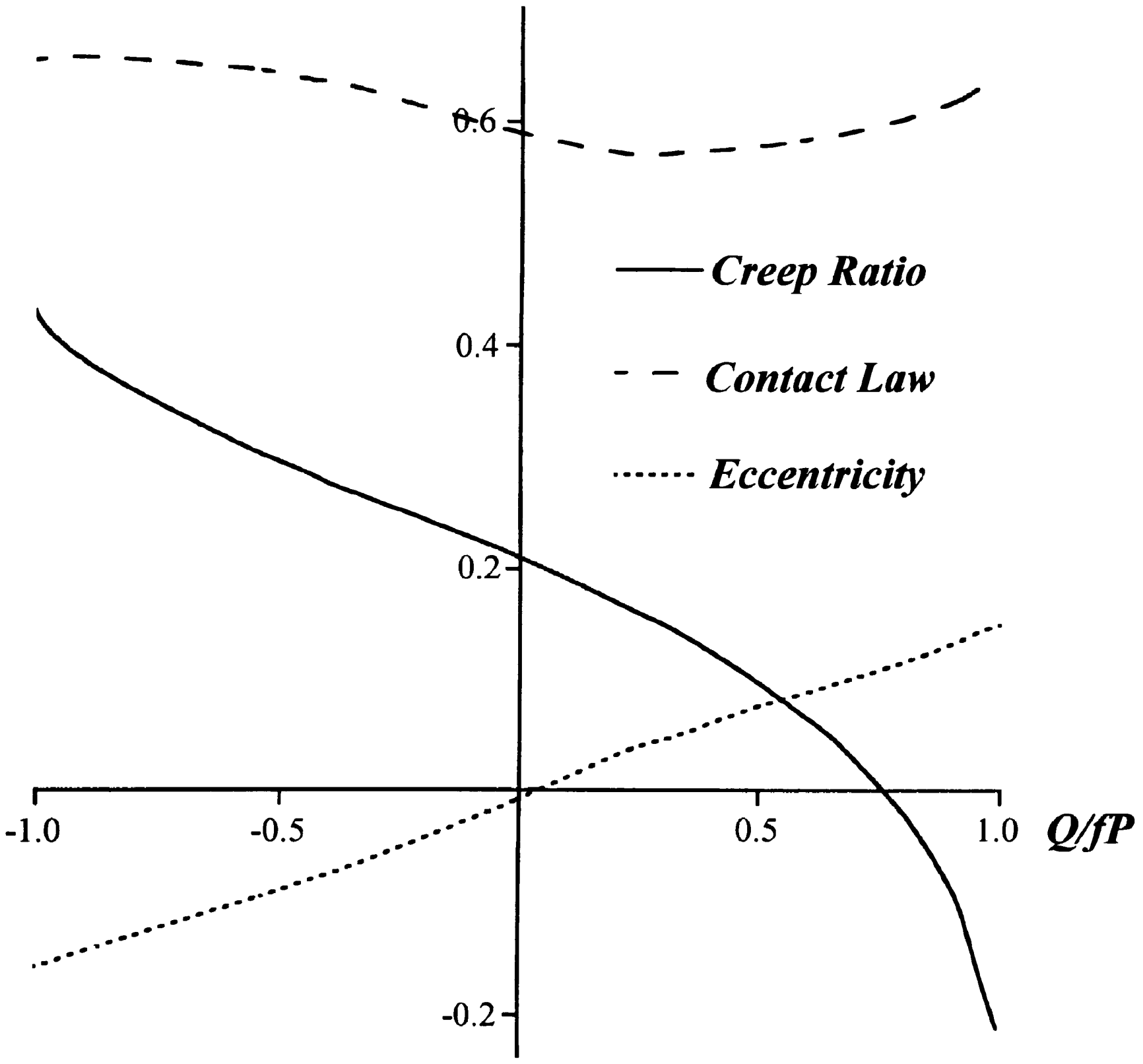

Figure 4.4: Variation of creep ratio, eccentricity and contact law with transmitted tangential force.

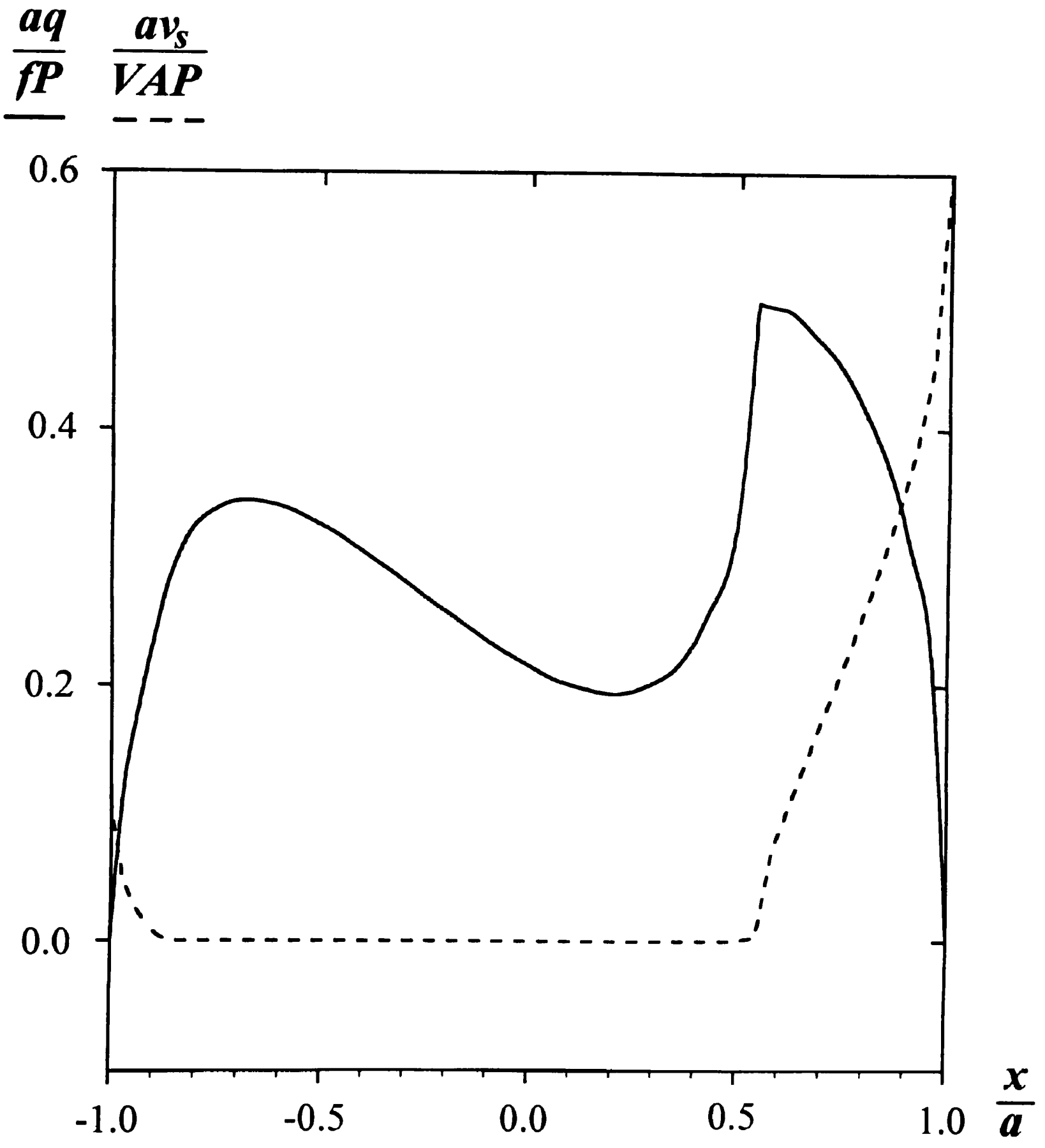

Figure 4.5: Tangetial traction distribution and slip velocity distributions for sample solutions. (a) Two slip zones of the same sign.

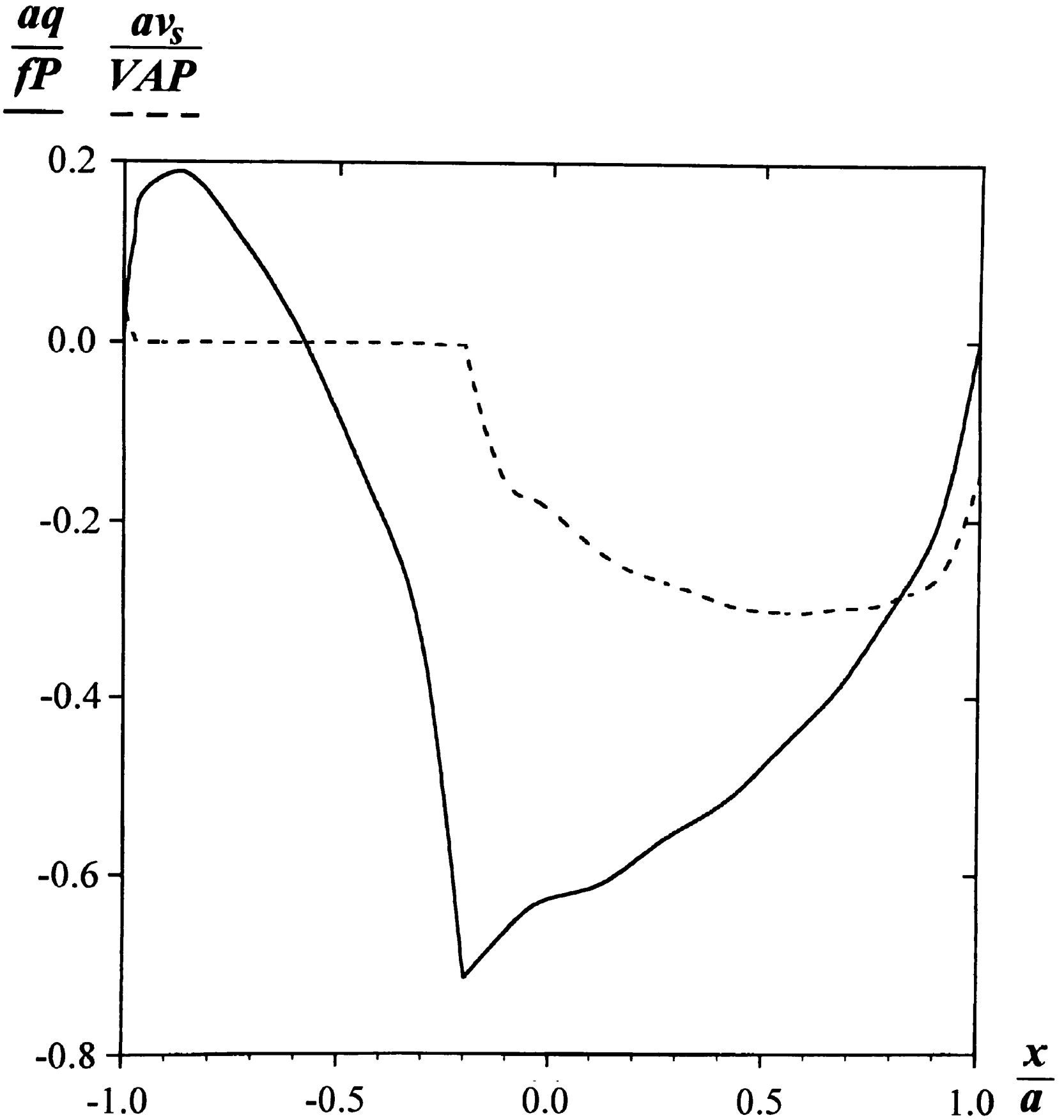

Figure 4.5: (b) Two slip zones of opposite sign.

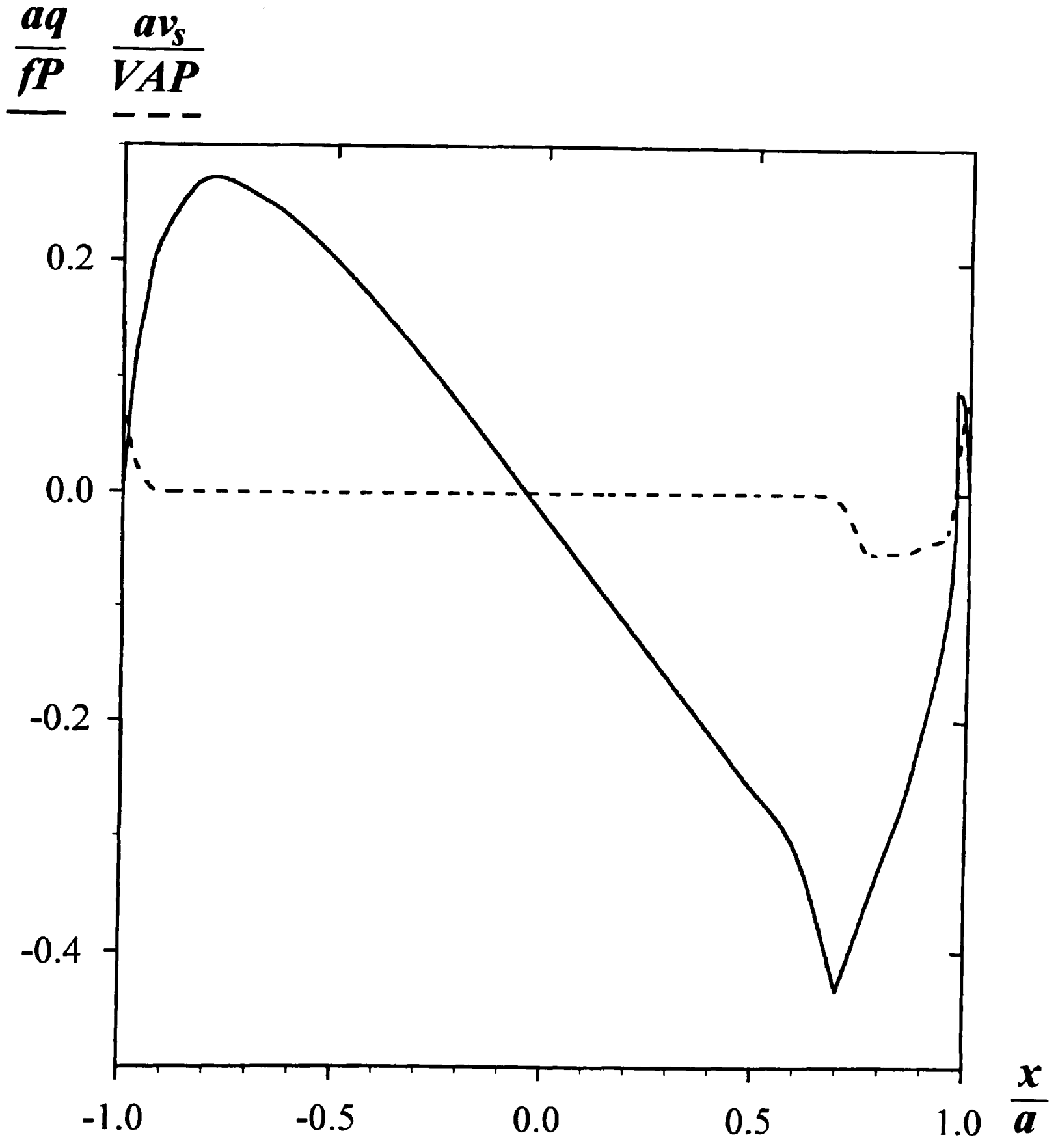

Figure 4.5: (c) Three slip zones.

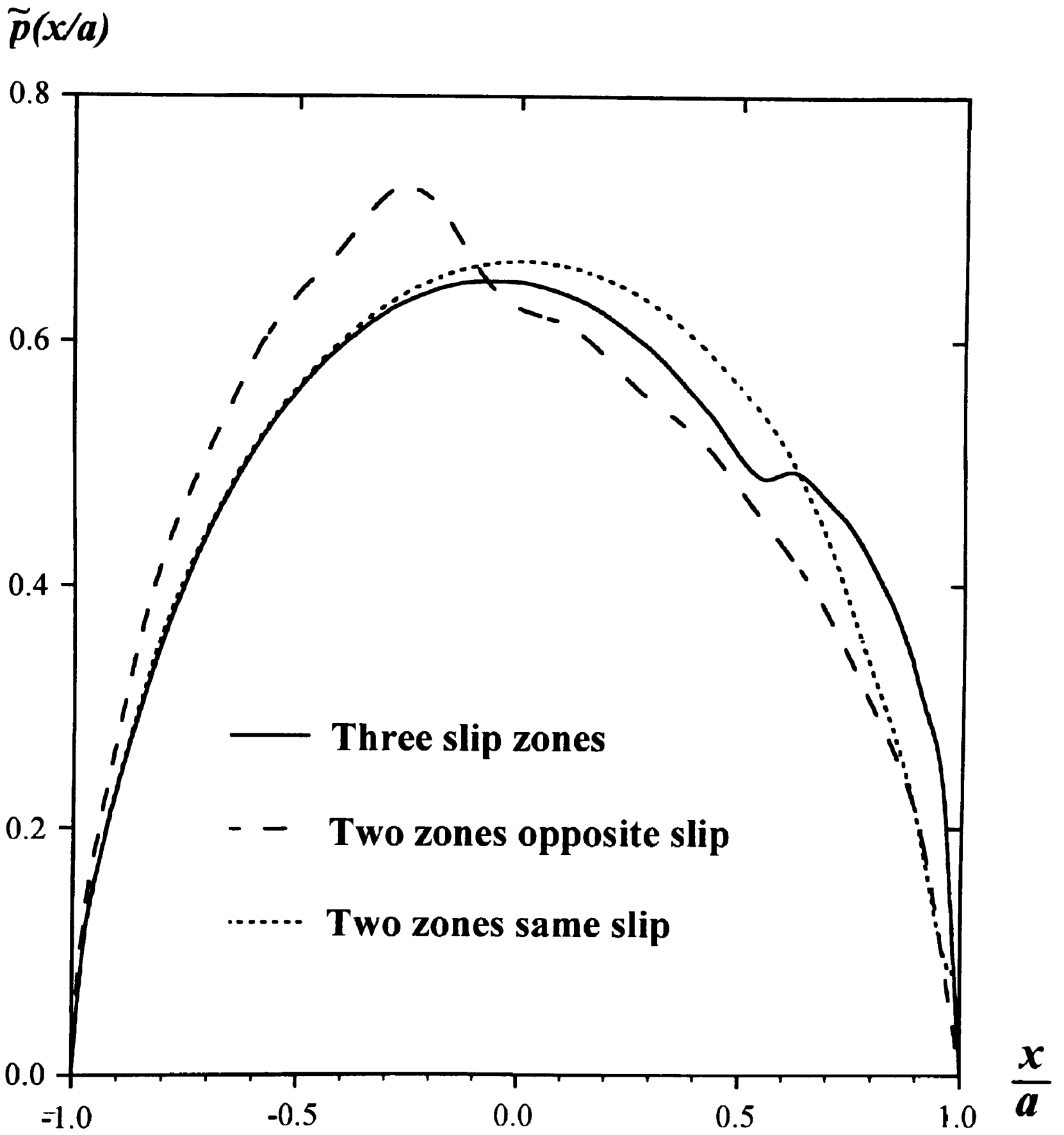

Figure 4.6: Sample normal traction distributions.

Table 4.1:

$\frac{Q}{fP}$	Coupled Solution				Uncoupled Solution
	$\frac{ka^2}{AP}$	$\frac{ka^2e}{AP}$	$\frac{Wa}{VP^2A}$ (eqn 4.49)	$\frac{Wa}{VP^2A}$ (eqn 4.53)	$\frac{Wa}{VP^2A}$ †
	Contact Law	Contact Offset	Frictional Losses	External Balance	External Balance
1.0000	0.6525‡	0.1018‡	–	–	–
0.9963	0.6398	0.0944	0.2412	0.2445	0.1359
0.9453	0.6314	0.0891	0.1978	0.1996	0.0685
0.8542	0.6135	0.0767	0.1420	0.1432	0.0029
0.7419	0.5982	0.0642	0.1017	0.1015	−0.0013
0.6101	0.5859	0.0522	0.0683	0.0688	−0.0168
0.4664	0.5768	0.0408	0.0417	0.0443	−0.0247
0.3450	0.5720	0.0292	0.0255	0.0252	−0.0237
0.2087	0.5698	0.0182	0.0117	0.0124	−0.0179
0.1522	0.5705	0.0132	0.0075	0.0074	−0.0135

† Uncoupled results based upon the method of Nowell and Hills (Nowell & Hills, 1988).
‡ Values for coupled sliding cylinders from closed form solution (Hills & Nowell, 1989).

4.5 Conclusions

The Goodman approximation is often made in the solution of two dimensional contact problems. In the case of contacting cylinders, ignoring the influence of tangential tractions on normal displacements simplifies the normal traction distribution to a Hertzian one: elliptical and centred on the line joining the centres of the cylinders. In this chapter the traction distributions for rolling cylinders have been found using both the approximation and the full formulation. It has been shown that the form of the traction distributions and the locations of the stick/slip transitions differ little. However, the eccentricity of the contact zone can be quite considerable (up to 15% of the contact half-width) and generates a significant resisting moment which balances the nett power supplied and the frictional losses.

Chapter 5

Tools For Solving Three Dimensional Contact Problems

5.1 Comparison of two and three dimensional contact problems

In Chapter 4 the two dimensional problem of tractive rolling between elastically dissimilar cylinders was solved using a one dimensional integral equation method. This permits an elegant solution described by Erdogan *et al.* (1973). Once the fully coupled integral equations were formulated, the unknown traction distributions were represented, to a good approximation, by a truncated series of continuous functions which allowed integration by a Gaussian quadrature. The result was a determinate set of simultaneous equations which was inverted in a straightforward manner. This method provided very accurate results in comparison with computing effort. Unfortunately there is no equivalent procedure for three dimensional contacts and it is instructive to consider why this is so. In the two dimensional case, neither the limits of the contact nor the points of transition between stick and slip were known *a priori*. However, each edge of both the contact and the stick zones was defined as a single variable and so was easily integrated into the solution process. In contrast, the boundary of a three dimensional contact must be defined as a *continuous function* of one variable. A similar complication presents itself in the type of integral equation that must be used actually to define the contact. In the two dimensional

contact a one dimensional integral equation sufficed: for the general three dimensional contact a two dimensional integral equation is necessary. Even if the tractions are defined in a discretized manner, such as a truncated series of continuous functions, direct inversion of this integral equation is not possible since there are no quadrature rules available for integrating over arbitrary areas. Hence, a different methodology for solving three dimensional contact problems must be developed.

Valuable insights may be gained, however, by applying the process used for the initial formulation of problems in two dimensions to their three dimensional counterparts. In two dimensions, the normalised integral equations revealed that the problems are dependent solely on: geometry, the combination of material constants known as Dundurs' constant β, and the coefficient of friction f. In the case of fully coupled problems, the three quantities are independent whereas in semi-coupled ones, the latter two combine to form the ratio β/f. This large reduction in the apparent number of variables required uniquely to define the problems simplified their solution and enabled results to be presented in a concise form. A similar approach would clearly be valuable for three dimensional problems. In the following section, the salient quantities in three dimensional contacts are examined.

5.2 Formulation of a general three dimensional problem

The object of this section is to determine which material properties, or combinations of them, affect the general contact problem. As in the case of two dimensional problems, this is best achieved by formulating the full integral equations which describe the general problem.

Consider two bodies (1 and 2) with arbitrary, non-conforming surface profiles, pressed into contact over the area S as shown in Figure 5.1. Since the tractions act with equal magnitude but in the opposite sense on each body, the relationship between relative surface displacements at a general point $(x, y, 0)$ and contact traction distributions may

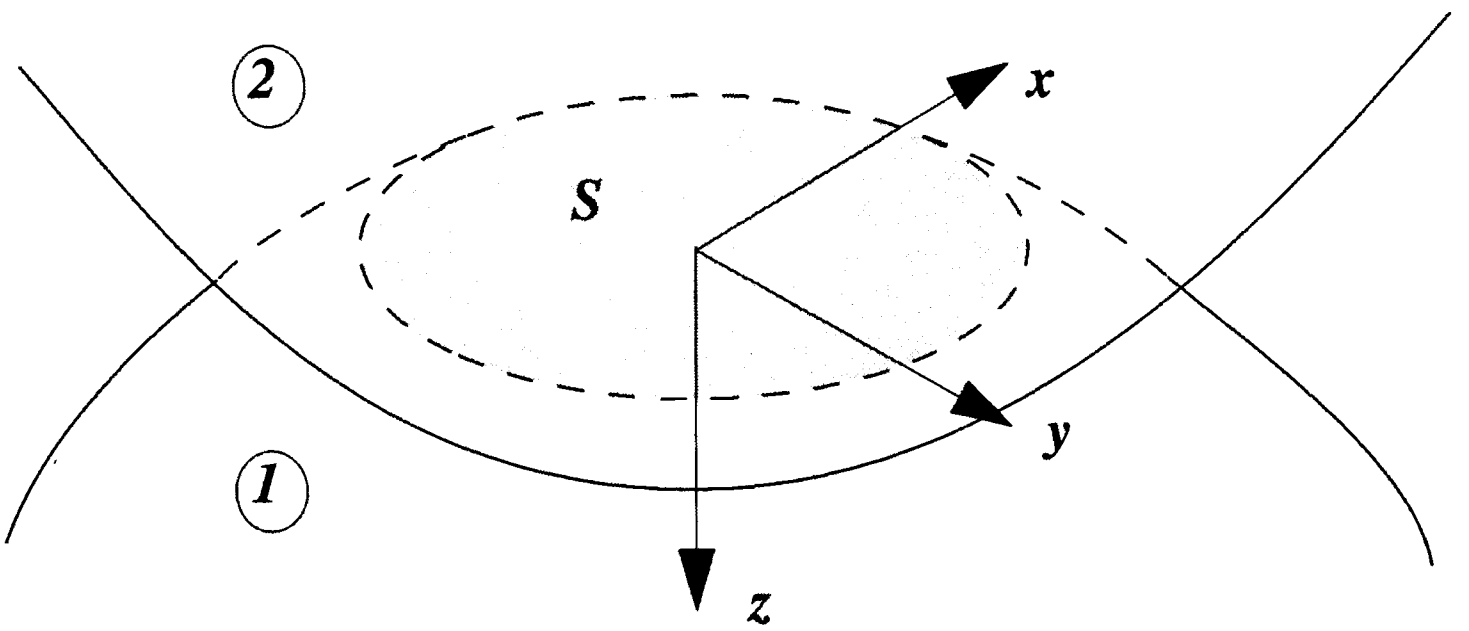

Figure 5.1: Configuration of two contacting bodies.

be written as (Johnson, 1985)

$$
\begin{aligned}
u_x(x,y) &= \frac{1}{4\pi}\int\int_S \left[\left(\frac{1-\nu_1}{\mu_1}+\frac{1-\nu_2}{\mu_2}\right)\frac{2}{\rho}q_x(\zeta,\eta)\right. \\
&\quad +\left(\frac{\nu_1}{\mu_1}+\frac{\nu_2}{\mu_2}\right)\left\{\frac{2(\zeta-x)^2}{\rho^3}q_x(\zeta,\eta)-\frac{2(\zeta-x)(\eta-y)}{\rho^3}q_y(\zeta,\eta)\right\} \\
&\quad \left.-\left(\frac{1-2\nu_1}{\mu_1}-\frac{1-2\nu_2}{\mu_2}\right)\frac{\zeta-x}{\rho^2}p(\zeta,\eta)\right]d\zeta d\eta \qquad (5.1)\\
u_y(x,y) &= \frac{1}{4\pi}\int\int_S \left[\left(\frac{1-\nu_1}{\mu_1}+\frac{1-\nu_2}{\mu_2}\right)\frac{2}{\rho}q_y(\zeta,\eta)\right. \\
&\quad +\left(\frac{\nu_1}{\mu_1}+\frac{\nu_2}{\mu_2}\right)\left\{\frac{2(\eta-y)^2}{\rho^3}q_y(\zeta,\eta)+\frac{2(\zeta-x)(\eta-y)}{\rho^3}q_x(\zeta,\eta)\right\} \\
&\quad \left.-\left(\frac{1-2\nu_1}{\mu_1}-\frac{1-2\nu_2}{\mu_2}\right)\frac{\eta-y}{\rho^2}p(\zeta,\eta)\right]d\zeta d\eta \qquad (5.2)\\
u_z(x,y) &= \frac{1}{4\pi}\int\int_S \left[\left(\frac{1-\nu_1}{\mu_1}+\frac{1-\nu_2}{\mu_2}\right)\frac{2}{\rho}p(\zeta,\eta)\right. \\
&\quad \left.-\left(\frac{1-2\nu_1}{\mu_1}-\frac{1-2\nu_2}{\mu_2}\right)\left\{\frac{\zeta-x}{\rho^2}q_x(\zeta,\eta)+\frac{\eta-y}{\rho^2}q_y(\zeta,\eta)\right\}\right]d\zeta d\eta \\
&\qquad (5.3)
\end{aligned}
$$

where ν is Poisson's ratio, μ is the modulus of rigidity and the subscripts 1 and 2 denote

the body to which the material property refers. These may be normalised by dividing both sides by $p_o a A$ to obtain:

$$\frac{u_x(x,y)}{p_o a A} = \frac{1}{2\pi p_0 a}\int\int_S \left[\frac{1}{\rho}q_x(\zeta,\eta) + \lambda\left\{\frac{(\zeta-x)^2}{\rho^3}q_x(\zeta,\eta) - \frac{(\zeta-x)(\eta-y)}{\rho^3}q_y(\zeta,\eta)\right\} - \beta\frac{\zeta-x}{\rho^2}p(\zeta,\eta)\right] d\zeta d\eta \tag{5.4}$$

$$\frac{u_y(x,y)}{p_o a A} = \frac{1}{2\pi p_0 a}\int\int_S \left[\frac{1}{\rho}q_y(\zeta,\eta) + \lambda\left\{\frac{(\eta-y)^2}{\rho^3}q_y(\zeta,\eta) + \frac{(\zeta-x)(\eta-y)}{\rho^3}q_x(\zeta,\eta)\right\} - \beta\frac{\eta-y}{\rho^2}p(\zeta,\eta)\right] d\zeta d\eta \tag{5.5}$$

$$\frac{u_z(x,y)}{p_0 a A} = \frac{1}{2\pi p_0 a}\int\int_S \left[\frac{1}{\rho}p(\zeta,\eta) - \beta\left\{\frac{\zeta-x}{\rho^2}q_x(\zeta,\eta) + \frac{\eta-y}{\rho^2}q_y(\zeta,\eta)\right\}\right] d\zeta d\eta \tag{5.6}$$

where a is the size of the contact, p_0 is a characteristic value of the contact pressure and

$$A = \frac{1-\nu_1}{\mu_1} + \frac{1-\nu_2}{\mu_2} \tag{5.7}$$

$$\beta = \left(\frac{1-2\nu_1}{2\mu_1} - \frac{1-2\nu_2}{2\mu_2}\right)/A \tag{5.8}$$

$$\lambda = \left(\frac{\nu_1}{\mu_1} + \frac{\nu_2}{\mu_2}\right)/A \tag{5.9}$$

These equations reveal that the normalised, fully coupled problem is uniquely defined by the geometry of the contacting bodies, the *two* material parameters β and λ, and the friction law relating the shearing tractions to the normal ones (eg a ratio whose limiting coefficient is f). In semi-coupled problems where the tangential tractions are assumed to have no effect upon the normal displacements, the second and third terms disappear from equation 5.6 and so the normal tractions depend only upon the geometry of the problem. In addition, if a coefficient of Coulomb friction f is assumed and the frictional tractions are themselves normalised by the peak shear traction fp_o, then the problem is uniquely defined, in terms of material parameters, by λ and the ratio β/f.

This discovery which describes the dependency of fully coupled and semi-coupled contact solutions is invaluable in simplifying the presentation of results. The number of

variables has been reduced from five ($\nu_1, \nu_2, \mu_1, \mu_2$ and f) to three independent ones (β, λ and f) in fully coupled problems and from five to two (β/f and λ) in semi-coupled problems.

The integral equations have been formulated in their most general form. The next task is to discretize the problem in some way such that their solution becomes possible.

5.3 Methods of discretization

It has already been stated that no elegant discretization of the unknown traction distribution may readily be contrived for three dimensional problems. Before considering cruder means of discretising the traction distributions, it should be noted that a completely different approach may be followed.

The Finite Element Method (FEM) now enjoys universal acceptance as a tool for solving a wide range of solids and structures problems including those involving contact. In this numerical method, the volume of the contacting bodies are generally modelled by a contiguous mesh of elements within which the displacement variation takes a prescribed form. Unfortunately, the cost of solution (in terms of computing effort) of the three-dimensional contact problems considered in this study, with comparable accuracy, would be prohibitive. Even using the simplest constant strain brick elements, which have twenty-four degrees of freedom, the number of variables generated by a sufficiently refined mesh of the contacting solids would be immense. As a result, few complex three dimensional contact problems have been solved by FEM; however, there are some notable exceptions (for example Klarbring (1986)).

There is an alternative to the discretization of a significant volume of solid, as is necessary in the Finite Element Method. It is possible to generate a mesh which discretizes only the *surface* of the solids in the region of the contact. If it is assumed that this mesh does not distort during contact loading, far fewer elements are required for the same resolution of the traction distribution. However, in order to solve the contact problem,

it is necessary to find the influence of each element in this surface mesh upon the stress and strain fields within the solid, which is generally assumed to be approximated by an elastic half-space. Once the influence functions of a single surface element have been determined, the effect of many such elements may be added by linear superposition (in elastic problems) to obtain a solution which is compatible with the displacements imposed on the contacting bodies. This approach is known as the Influence Function Method.

5.3.1 Choice of discretization element

An important choice which must be made is the form of the traction distribution which acts over the area of a single element. Four candidate element types for discretising a pressure distribution are shown in Figure 5.2. The simplest (Figure 5.2a) is a concentrated force acting at the centre of a rectangular element. The next element (Figure 5.2b) is a rectangular area over which the pressure is constant (piecewise constant elements). A piecewise linear traction distribution may be constructed from a surface mesh of triangles where the tractions are defined at each apex and vary linearly between them (Figure 5.2c). Finally a knowledge of the form of the overall traction distribution at the edges of the contact may be exploited to produce elements which emulate this parallel to one axis in the form of strips (Figure 5.2d shows an element that might be used for a Hertzian-type problem). The use of concentrated forces may be ruled out immediately because the surface displacement and stress field at the point of action of the force is undefined. This makes it necessary to enforce the equations of compatibility of deformation at intermediate points and so the problem becomes ill conditioned. The thin strips of elliptical tractions seem to offer the benefit of accurately modelling the traction distribution especially at the edges, however, because each strip is not exactly aligned with the contact boundary this advantage is lost. In addition these elements are not particularly suited to modelling discontinuous traction gradients such those found in partial slip problems.

The choice is then between piecewise constant and piecewise linear elements. Neither

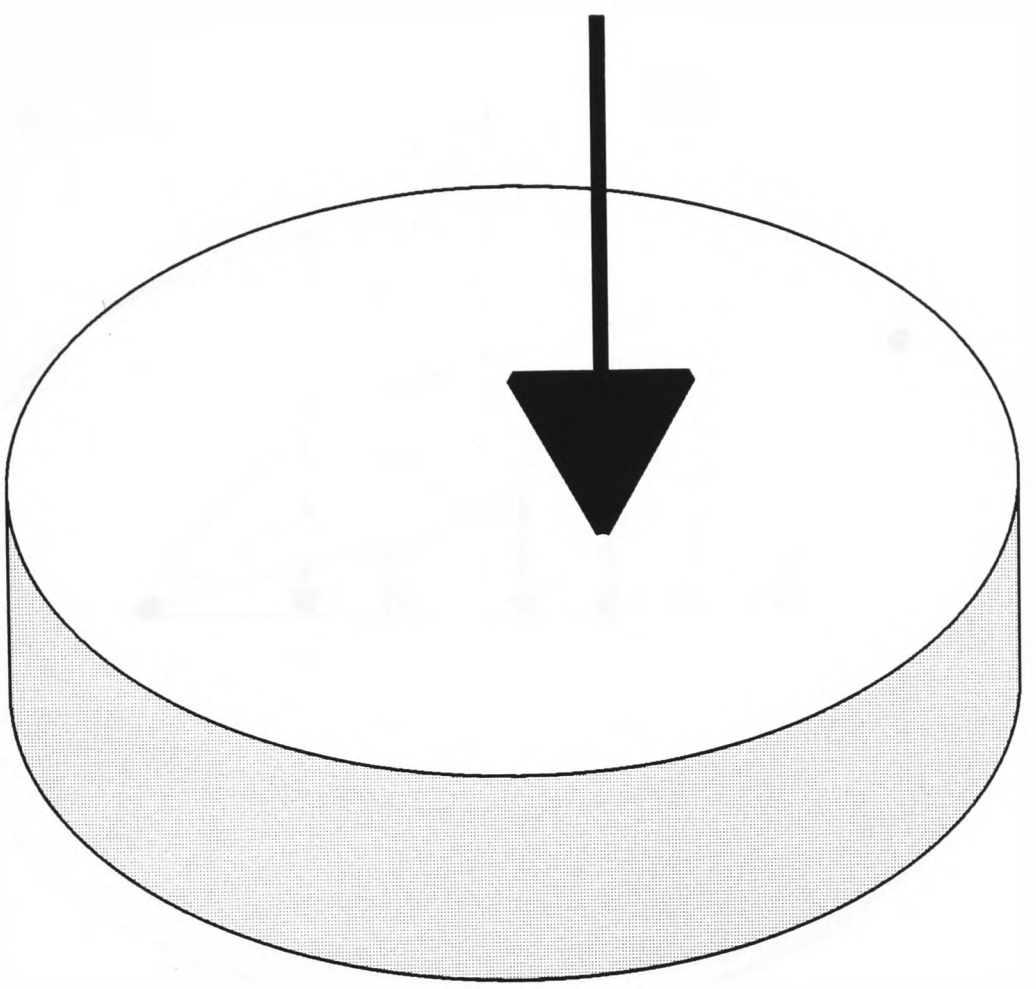

Figure 5.2: Candidate discretization elements. (a) Discrete forces.

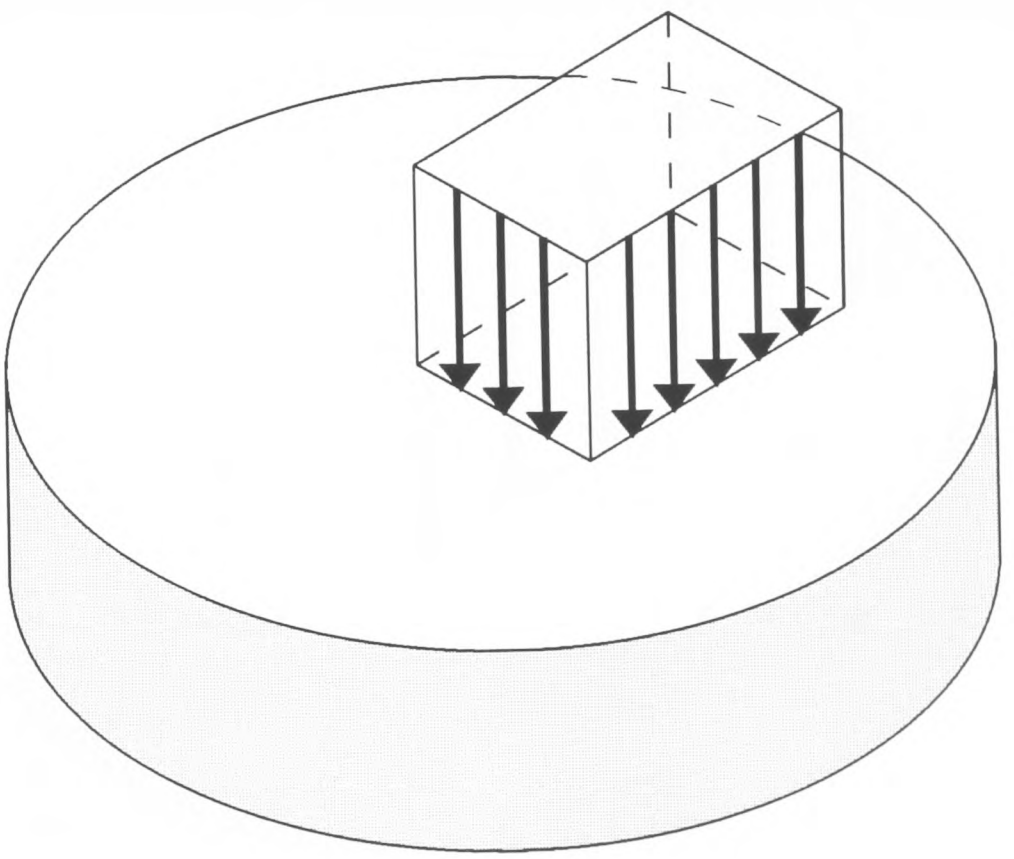

Figure 5.2: (b) Uniform traction element.

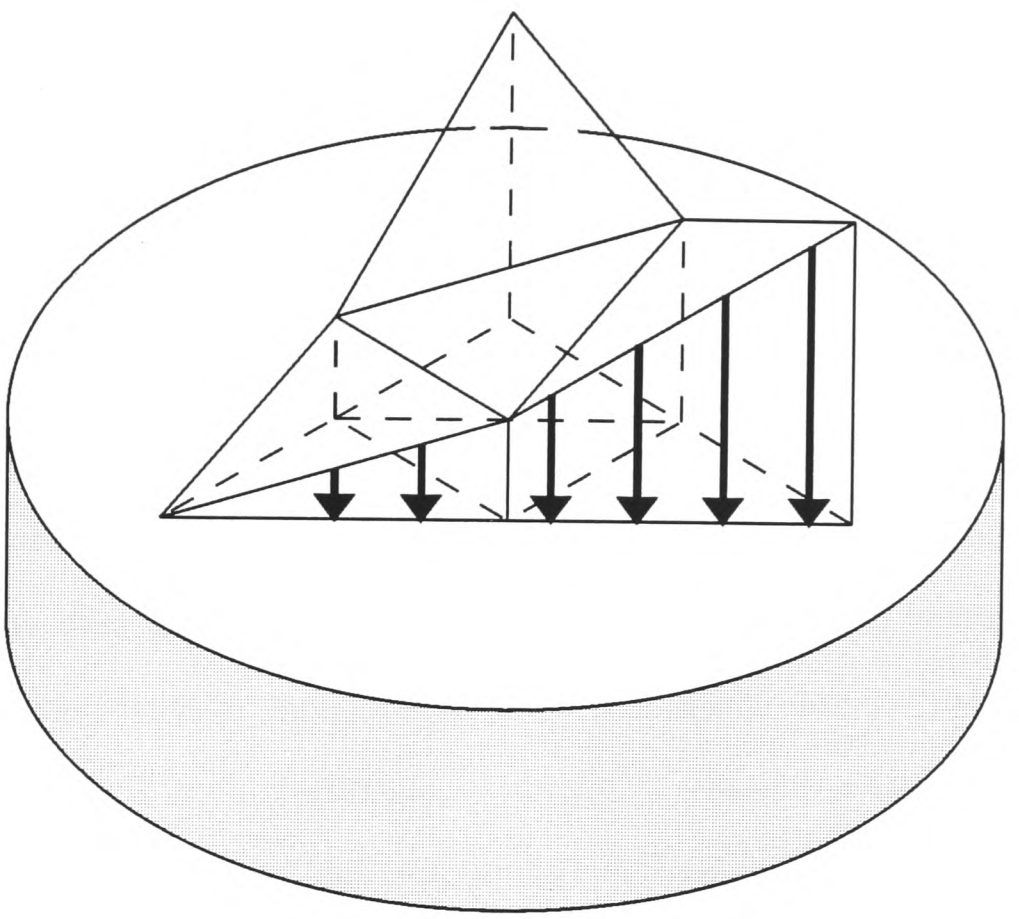

Figure 5.2: (c) Linear traction element.

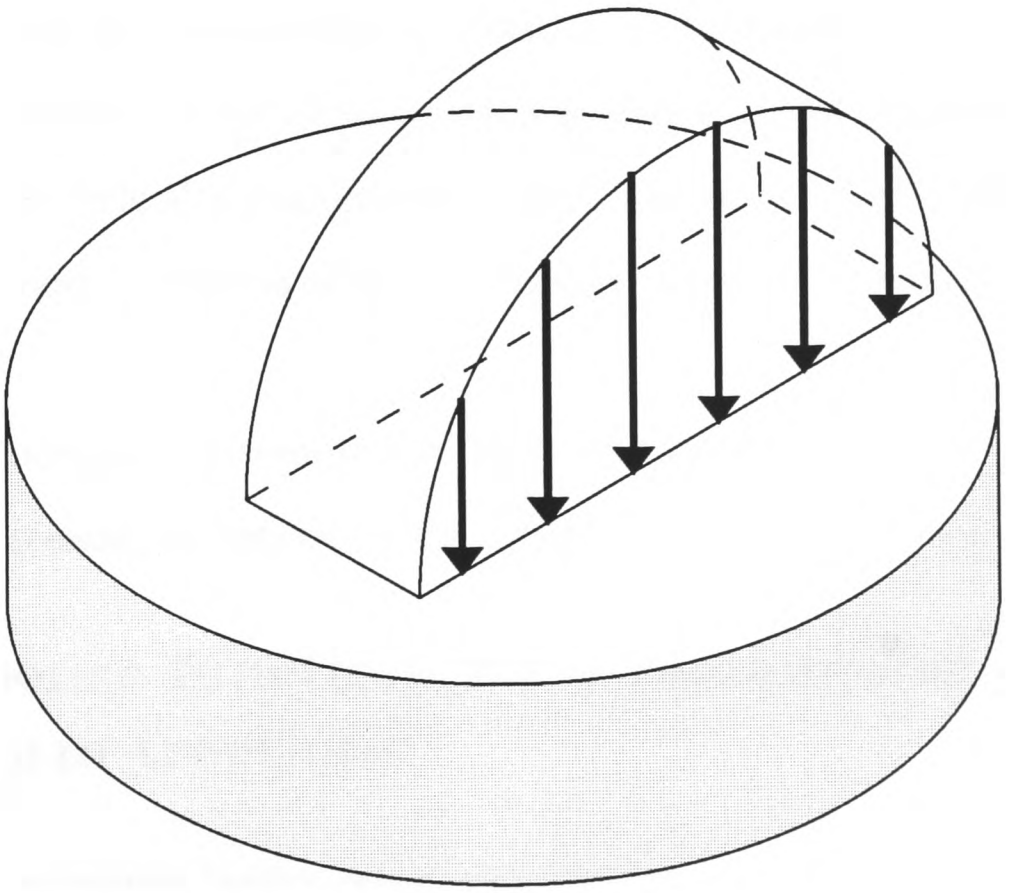

Figure 5.2: (d) Herztian traction element.

is very accurate in regions where the traction gradient changes rapidly (such as at the contact boundaries) but due to Saint Venant's principle this will not have an adverse effect on the results a small distance away. The former generates a traction distribution which is discontinuous and so the stress and strain fields are undefined along the edges of the elements. However, Kalker (1990) has shown that both types have the same accuracy when used to evaluate displacements at the centre of an element and it is there that the compatibility equations are most conveniently satisfied. Piecewise linear elements have the advantage that they generate defined displacement and stress fields. However, each element requires three times as many variables to specify the tractions acting over it as a piecewise constant one. This is important since the boundary of the contact and regions within it can only be observed at the *junction* of two elements and computer time limits the number of *variables* which may be employed.

The above reasoning seems to favour piecewise constant elements and the choice is settled by the fact that working out the influence functions for piecewise linear elements is formidable. There are disadvantages involved in using constant traction elements type, such as the inaccurate representation of steep gradients in the traction distribution and the undefined stress field along the element edges. The former may be offset by increasing the density of elements in regions of rapidly changing tractions; the latter will be addressed in Chapter 7.

It is straightforward to discretize the region of contact, but before any problems can be solved, it is necessary to determine the influence functions of a single element.

5.4 Influence functions for a rectangular element of uniform tractions

When two non-conforming bodies, which obey the linear small strain theory of elasticity, are pressed together, the actual size of the contact is small compared with their characteristic dimensions. This results in a state of stress in each which is the superposition of two

independent components. One is the highly concentrated stress field at the contact which decays rapidly with distance from it. The other is the bulk stress field due to the overall shape of each body and the means by which it is supported. This study is concerned with evaluating the former whose limited extent permits that part of the body local to the contact to be approximated by a half-space. This section develops the influence functions of rectangles of uniform normal and shear tractions acting over the surface of an elastic half-space.

It is possible to take Equations 5.1, 5.2 and 5.3 and to integrate them over the area of a rectangle for a uniform traction distribution to obtain the influence functions for surface displacements. However, it is more efficient to look back to the source of these equations. Boussinesq (1885) and Cerruti (1882) employed potential functions to relate displacements and stresses to surface tractions acting on an elastic half-space. Their work has been presented by Love (1929), who applied it to the rectangle of uniform tractions considered here. His results will be summarised and extended as necessary. Consider the loaded region of Figure 5.3. Normal tractions $p(\zeta,\eta)$ and shearing tractions $q_x(\zeta,\eta)$ and $q_y(\zeta,\eta)$ act over area S. The starting point is the definition of the following potential functions, each satisfying Laplace's equation:

$$F_1 = \int_S \int q_x(\zeta,\eta)\Omega d\zeta d\eta \tag{5.10}$$

$$G_1 = \int_S \int q_y(\zeta,\eta)\Omega d\zeta d\eta \tag{5.11}$$

$$H_1 = \int_S \int p(\zeta,\eta)\Omega d\zeta d\eta \tag{5.12}$$

where

$$\Omega = z\ln(\rho+z)-\rho \tag{5.13}$$

$$\rho^2 = (x-\zeta)^2+(y-\eta)^2+z^2. \tag{5.14}$$

The following may then be derived:

$$F = \frac{\partial F_1}{\partial z} = \int\int_S q_x(\zeta,\eta)\xi d\zeta d\eta \tag{5.15}$$

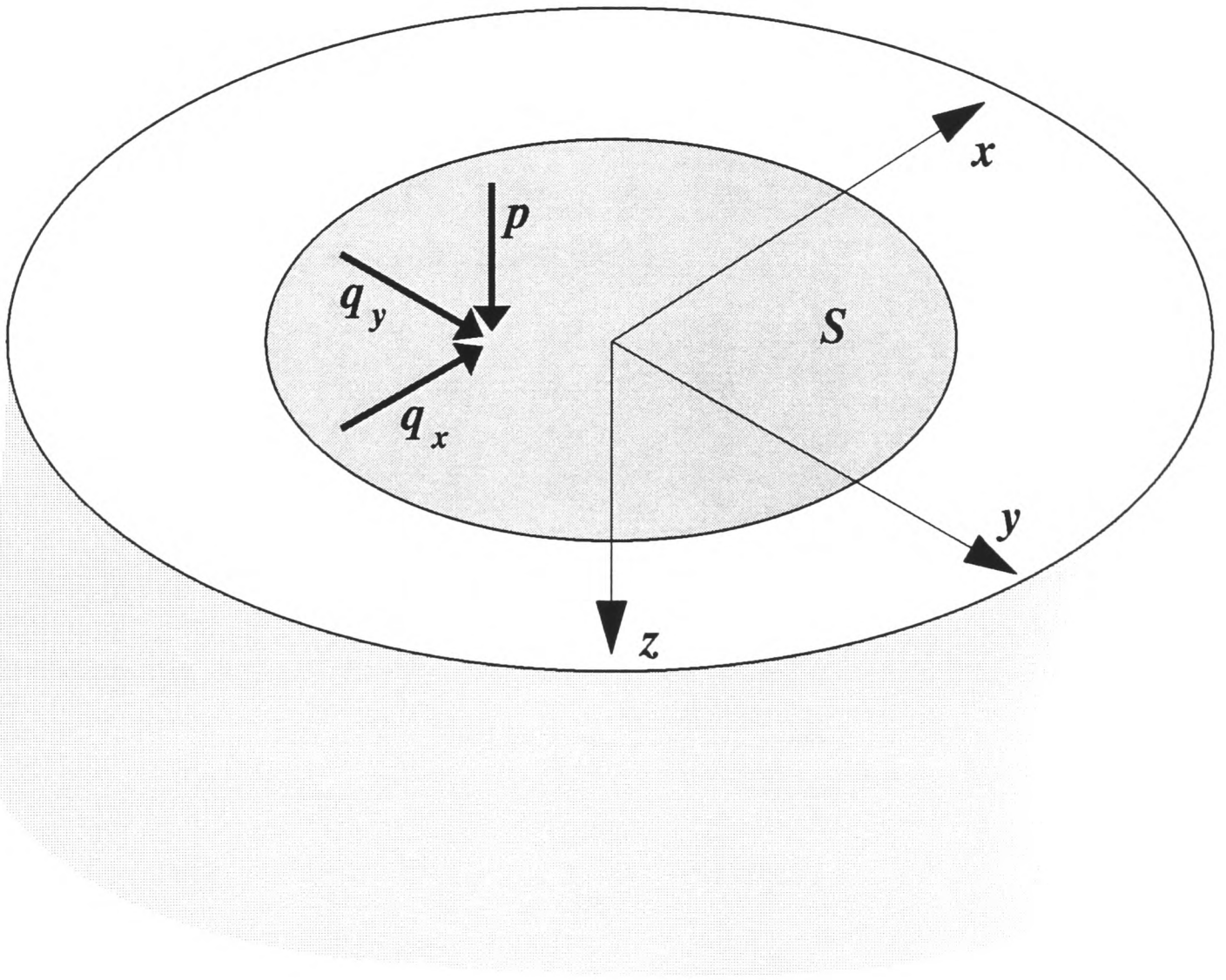

Figure 5.3: Representation of the loaded region.

$$G = \frac{\partial G_1}{\partial z} = \int\int_S q_x(\zeta,\eta)\xi d\zeta d\eta \tag{5.16}$$

$$H = \frac{\partial H_1}{\partial z} = \int\int_S q_x(\zeta,\eta)\xi d\zeta d\eta \tag{5.17}$$

where

$$\xi = \frac{\partial \Omega}{\partial z} = \ln(\rho + z) \tag{5.18}$$

and finally

$$\Psi_1 = \frac{\partial F_1}{\partial x} + \frac{\partial G_1}{\partial y} + \frac{\partial H_1}{\partial z} \tag{5.19}$$

$$\Psi = \frac{\partial \Psi_1}{\partial z} = \frac{\partial F}{\partial x} + \frac{\partial G}{\partial y} + \frac{\partial H}{\partial z}. \tag{5.20}$$

The displacements at (x, y, z) can now be written as

$$u_x = \frac{1}{4\pi\mu}\left\{2\frac{\partial F}{\partial z} - \frac{\partial H}{\partial x} + 2\nu\frac{\partial \Psi_1}{\partial x} - z\frac{\partial \Psi}{\partial x}\right\} \tag{5.21}$$

$$u_y = \frac{1}{4\pi\mu}\left\{2\frac{\partial G}{\partial z} - \frac{\partial H}{\partial y} + 2\nu\frac{\partial \Psi_1}{\partial y} - z\frac{\partial \Psi}{\partial y}\right\} \tag{5.22}$$

$$u_z = \frac{1}{4\pi\mu}\left\{\frac{\partial H}{\partial z} + (1-2\nu)\Psi - z\frac{\partial \Psi}{\partial z}\right\} \tag{5.23}$$

and the corresponding state of stress is found from the application of Hooke's law

$$\sigma_{xx} = \frac{1}{2\pi}\left\{2\nu\frac{\partial \Psi}{\partial z} - z\frac{\partial^2 \Psi}{\partial x^2} - (1-2\nu)\frac{\partial^2 \Psi_1}{\partial x^2}\right\} \tag{5.24}$$

$$\sigma_{yy} = \frac{1}{2\pi}\left\{2\nu\frac{\partial \Psi}{\partial z} - z\frac{\partial^2 \Psi}{\partial y^2} - (1-2\nu)\frac{\partial^2 \Psi_1}{\partial y^2}\right\} \tag{5.25}$$

$$\sigma_{zz} = \frac{1}{2\pi}\left\{\frac{\partial \Psi}{\partial z} - z\frac{\partial^2 \Psi}{\partial z^2}\right\} \tag{5.26}$$

$$\tau_{xy} = -\frac{1}{2\pi}\left\{(1-2\nu)\frac{\partial^2 \Psi_1}{\partial x \partial y} + z\frac{\partial^2 \Psi}{\partial x \partial y}\right\} \tag{5.27}$$

$$\tau_{yz} = -\frac{1}{2\pi}z\frac{\partial^2 \Psi}{\partial y \partial z} \tag{5.28}$$

$$\tau_{xz} = -\frac{1}{2\pi}z\frac{\partial^2 \Psi}{\partial x \partial z} \tag{5.29}$$

By reducing the area over which the tractions act to an infinitesimal size, while maintaining the magnitude of the integrals of the components of force, it is possible to derive the influence functions for a point load (see for example Johnson (1985)). The contact

problem could be discretized using this as the fundamental loading element; however, as stated earlier, both the displacement field and the state of stress are undefined at the point where the force is applied. A rectangle of uniform tractions lends itself far more readily to the solution of contact problems. The evaluation of the integrals to find the influence functions of such an element is somewhat involved and the results for the surface displacement and internal stress field are recorded in Appendix A.

5.5 The solution process

The methodology employed so far has enabled the contact problem to be cast into its most general form, the combination of material properties that characterise the problem to be determined, and the contact area to be discretized into a mesh of uniform traction elements. The influence of each element on the surface displacements and internal stress field can be evaluated using the influence functions developed in the previous section. However, the magnitudes of the tractions are still unknown and in this section various approaches are considered which allow them to be evaluated efficiently. It is convenient to consider the example of two frictionless bodies pressed together to form a contact of unknown area (and, in general, shape). Hence, it is necessary to produce a mesh that is larger than the actual contact. At the centre of each traction element an equation of compatibility may be written between the original underformed shape of the bodies, the distance they are pushed together and the elastic deformation induced by the surface tractions. If such an equation is formulated for each element the result is a determinate set of simultaneous equations in terms of the unknown tractions. However, not all the elements fall within the actual contact. Two different approaches have been used to solve such a set of equations. The variational method has been applied with great success by Kalker to various contact problems especially those involving rolling (see for example (Kalker, 1979)). Its application to contact mechanics was facilitated by the work of Fichera (1984) and Duvaut & Lions (1972) who developed various uniqueness theorems.

As applied to the current problem, a functional would be developed, perhaps based upon a product of surface separation and contact pressure, which is valid both inside and outside the contact. This functional would then be minimised by a quadratic programming procedure to find both the traction distribution and the contact boundary. In other types of problems a similar procedure has been applied to find, for example, stick-slip interfaces in rolling contact problems. A comprehensive collection of variational analyses can be found in Kalker's recent book (Kalker, 1990).

The other approach relies on some iterative procedure in which the simultaneous equations are inverted. The first difficulty to address is that a large number of elements results in a very ill-conditioned set of equations and therefore direct inversion of the full set of equations is impossible. Hartnett (1980) overcame this by grouping equations and elements together to reduce the number of equations inverted at any one time. Each group of equations was then inverted in turn and the process repeated until convergence was achieved. Ahmadi *et al* (1983) extended this approach by reducing the number of parameters that should be checked after each iteration. In their scheme, all the equations are included in the inversion scheme for the first iteration, assuming every element is in contact and so sustains a finite traction. Every element which sustains negative pressure is then known to be outside the true contact area and its corresponding equation is removed from the next iteration. An additional equation is used which equates the sum of the elemental tractions to a fixed applied load and allows the distance of approach to become an unknown. This ensures that at each iteration the contact lies within the area covered by the remaining elements. Convergence is achieved when none of the remaining elements sustain negative tractions. Unfortunately, such an approach cannot be applied to problems involving tangential tractions to locate stick-slip interfaces.

In this study a different approach is used which is called the "Sequential Release Method". It requires a general experience of contact problems so that a first guess may be made of the normal and shear traction distributions. For the example of normal contact

between two bodies with similar elastic properties where the size and shape of the contact is unknown, the procedure would be as follows:

1. Estimate the pressure distribution.
2. Set the magnitude of the normal traction at each element to the value at the corresponding location in the estimated pressure distribution.
3. Select an element.
4. Solve the equation of compatibility at the centre of that element to find the local contact pressure assuming the bodies are in contact at that point.
5. If the result is positive, set the magnitude of the traction at the element to that value.
6. If the result is negative, the assumption that the bodies were in contact at that point must have been incorrect. Reset the traction to zero.
7. Repeat steps 3 to 6 for each element in the mesh.
8. Repeat step 7 until convergence has been achieved.

An analogous approach may be used if there is shear loading. For example, in a partial slip problem where the normal traction distribution is already known the following procedure would be used:

1. Estimate the shear traction distribution.
2. Set the magnitude of the shear traction at each element to the value at the corresponding location in the estimated traction distribution.
3. Select an element.

4. Solve the equation of compatibility at the centre of that element to find the magnitude and direction of the local shear traction assuming that the bodies are adhered at that point.

5. If the result satisfies the friction law at that point, set the magnitude of the traction at the element to that value.

6. If the result does not satisfy the friction law at that point, the assumption that the bodies were locally adhered must have been incorrect. Recalculate the direction of the shear traction at that point assuming that it is a region of micro-slip and set the magnitude at that element to the limiting value and the direction as calculated.

7. Repeat steps 3 to 6 for each element in the mesh.

8. Repeat step 7 until convergence has been achieved.

In the sequential release scheme, every element of the mesh is released. This is repeated until a convergence criterion is reached, for example that the change in traction at any element after release is below an arbitrarily chosen cut-off value which indicates the residual error. Although it is beyond the scope of this study to prove mathematically the conditions under which convergence will occur, several points may be noted:

1. The influence function of an element of normal traction on normal surface displacement and the influence function of tangential tractions on tangential displacements is greatest at the centre of the element and reduces rapidly with distance from it. Hence, each individual compatibility equation is very well conditioned in terms of the traction acting over the element where the equation is satisfied.

2. The rate of convergence decreases, in terms of the number of times each element must be released to achieve the same residual error, at a greater rate than the rate at which the density of the elements is increased. However, lack of convergence is

not a concern for problems with up to 1000 elements, which is more than enough to determine accurately a traction distribution.

A final choice remains between a fixed mesh and one that is modified to fit the contact. Paul and Hashemi (1981) opted for an adaptive mesh. In their scheme the mesh is optimised so that it is a best fit to the shape of the contact at each iterative step. However, in doing so the great advantage of the fixed mesh is lost, i.e. that the influence functions for each element need only be evaluated once. The computer time involved in re-evaluating the influence functions far out-weighs the small increase in accuracy of the contact boundary, so fixed meshes are employed in this study.

5.6 Conclusions

A full methodology has been developed for the solution of three-dimensional contact problems. The combination of material properties which characterises each problem has been found. Methods of discretization have been considered and the Influence Function Method has been selected. A rectangle of uniform traction has been selected as the optimum element and its influence functions have been developed. Finally a method of solution has been devised which can locate the contact boundary and accommodate different regions within the contact such as stick/slip interfaces. In subsequent chapters this methodology will be applied to progressively more complex contact problems. First it will be applied to a relatively simple case where frictional forces are ignored but the contact will be incomplete and so the actual traction boundary must be determined as part of the solution Next the methodology will be applied to solve the contact between a sphere sliding over a half-space which has dissimilar elastic properties. In this problem frictional tractions will be included and it will be assumed that they act in the direction of gross sliding. However, their effect on normal displacements will be considered (i.e. the problem is fully coupled) and so the traction boundary must again be determined

as part of the solution. Finally two partial slip problems will be considered. The first will be to solve the Mindlin problem and evaluate the traction distribution generated when two elastically similar spheres are pressed together and then displaced slightly by a tangential force. There will be a stick/slip interface which will be located. The second will extend the analysis to include elastically dissimilar spheres. However, the influence of shear tractions on normal displacements will be ignored and so the normal tractions for both cases will remain Hertzian.

Chapter 6

Incomplete Contact

6.1 Introduction

This Chapter addresses a simple problem in order to demonstrate the sequential release method of establishing the size of the contact patch developed in Chapter 5. The problem to be solved may be posed as: "What is the area of contact and what is the pressure distribution when a flat, rigid punch is inclined and pressed into an elastic half-space?". Although the problem of incomplete contact between a rigid punch and an elastic half-space does not involve friction it is nevertheless included here as an excellent illustration of the influence function method. The model could have included friction effects, for instance if the punch were sliding as well as tilting. However, this is somewhat contrived and indeed the method is best presented initially with normal tractions alone. A single plan for the cross-section of the punch is considered, viz. circular.

6.2 Formulation

In Figure 6.1 a rigid punch is shown pressed by a normal force P into an elastic half-space. The angle that the flat end of the punch makes with the undeformed surface of the half-space is constrained to indent at an angle θ by an unknown moment M. For simplicity, the region of potential contact S_p is assumed to be limited to the bottom face of the punch alone and the small area of interaction at the deepest edge is ignored. The

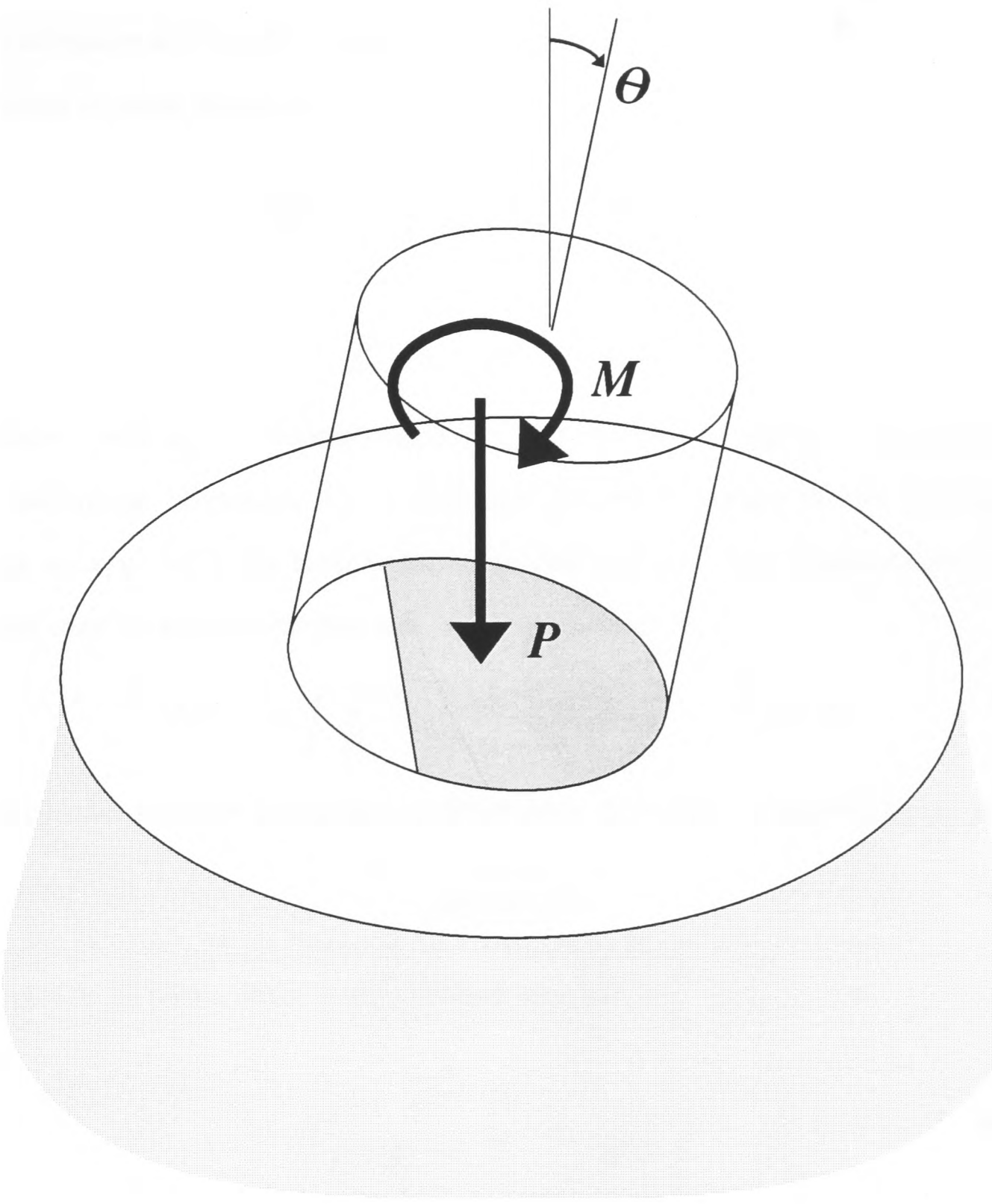

Figure 6.1: Configuration of the inclined indentation problem.

boundary conditions of the problem are that the normal pressure $p(x, y)$ is always positive (i.e. no adhesion is permitted) and that the normal displacements of the half-space are compatible with the indentation profile of the punch. The displacement of the surface of the half-space at $(x, y, 0)$ is first written, assuming that the pressure is a continuous distribution of point forces, as

$$u_z(x, y) = \int\int_{S_p} \frac{2(1-\nu)}{4\pi\mu} \frac{p(\zeta, \eta)}{\rho} d\zeta \, d\eta \tag{6.1}$$

where

$$\rho^2 = (\zeta - x)^2 + (\eta - y)^2 \tag{6.2}$$

and where ν and μ are Poisson's ratio and the modulus of rigidity respectively of the elastic half-space. Equation 6.1 is valid over the whole surface of the half-space. By equating $u_z(x, y)$ with the local indentation depth $\delta(x, y)$, the displacement boundary condition may be stated over the area of actual contact S:

$$\delta(x, y) = \int\int_{S_p} \frac{2(1-\nu)}{4\pi\mu} \frac{p(\zeta, \eta)}{\rho} d\zeta \, d\eta \qquad x, y \subset S. \tag{6.3}$$

The contact pressure boundary condition may be written in general terms as:

$$p(x, y) \geq 0 \tag{6.4}$$

or specifically in terms of the actual contact area as:

$$p(x, y) = 0 \qquad x, y \not\subset S \tag{6.5}$$

$$p(x, y) > 0 \qquad x, y \subset S. \tag{6.6}$$

It remains to be determined, of course, what the area of actual contact S and the pressure distribution $p(x, y)$ are. Further equations may be established by considering static equilibrium in the direction normal to the surface of the half-space and moment equilibrium about the x and y-axes. It is assumed that the origin of the coordinate set lies at the

middle of the face of the indenter and that the line of action of the normal force P is through this. The inclination of the punch is maintained by the application of moments about the x and y axes of M_x and M_y respectively. Considering vertical equilibrium then,

$$P = \int \int_S p(\zeta, \eta) d\zeta d\eta \tag{6.7}$$

and moment equilibrium about axes in the plane of the contact gives:

$$M_x = \int \int_S p(\zeta, \eta) \eta d\zeta d\eta \tag{6.8}$$

and

$$M_y = \int \int_S p(\zeta, \eta) \zeta d\zeta d\eta \tag{6.9}$$

Rather than determine the pressure distribution and region of contact subject to the generalised forces above, it is more convenient to consider the forces and moments as unknowns and to prescribe the depth of indentation at the centre of the punch as α and the angles of inclination of the base of the punch with respect to the x and y-axes as θ_x and θ_y. Hence, the indentation profile for a flat punch is written as:

$$\delta(x, y) = \alpha + \theta_x y + \theta_y x \qquad x, y \subset S \tag{6.10}$$

In this way a single integral equation must be solved to find the pressure distribution that is compatible with the imposed displacements. The force and moments required to produce the indentation geometry can be easily evaluated using equations 6.7, 6.8 and 6.9 *a posteriori*.

6.3 Discretization

Before discretizing the problem, it is convenient to normalize the variables using characteristic parameters. Johnson (1985) lists the pressure distribution $p(r)$ and indentation depth α_0 for a flat ended circular punch of radius a pressed by a normal force P into an

elastic half-space:

$$p(r) = p_0 \left(1 - \frac{r^2}{a^2}\right)^{-\frac{1}{2}} \tag{6.11}$$

$$\alpha_0 = \frac{\pi(1-\nu)}{2\mu} p_0 a \tag{6.12}$$

where

$$p_0 = \frac{P}{2\pi a^2} \tag{6.13}$$

and $r^2 = x^2 + y^2$.

Using the substitutions $p = p_0\tilde{p}$ and $x = a\tilde{x}$, etc. equation 6.3 may be written as:

$$\tilde{\delta}(\tilde{x},\tilde{y}) = \int\int_{\tilde{S}} \frac{\tilde{p}(\tilde{\zeta},\tilde{\eta})}{\pi^2\rho} d\tilde{\zeta}\, d\tilde{\eta} \qquad \tilde{x},\tilde{y} \subset \tilde{S} \tag{6.14}$$

where

$$\tilde{\delta}(\tilde{x},\tilde{y}) = \frac{\delta(x,y)}{\alpha_0} = \tilde{\alpha} + \tilde{\theta}_x\tilde{y} + \tilde{\theta}_y\tilde{x} \tag{6.15}$$

and $\alpha = \alpha_0\tilde{\alpha}$, $\theta_x = \tilde{\theta}_x\alpha_0/a$, $\theta_y = \tilde{\theta}_y\alpha_0/a$. Following the sequential release method of Chapter 5, the region S_p is discretized into a mesh of m square elements of uniform pressure. In Chapter 5, the influence functions for a traction element were developed and so by combining equations 6.14 and 6.15 and discretizing the result, a set of simultaneous linear equations may be written:

$$\sum_{j=1}^{m} \tilde{p}_j D_{ij}^N = \tilde{\alpha} + \tilde{\theta}_x\tilde{y}_i + \tilde{\theta}_y\tilde{x}_i \qquad i = 1,m \tag{6.16}$$

where $\tilde{p}_j$ is the normalized, uniform pressure acting over square j and $\tilde{x},\tilde{y}$ is the location of square j with respect to the centre of the indenter's face. D_{ij}^N is the influence function relating the normalized displacement at the centre of square i due to unit pressure acting on square j and can be found in Appendix A. It is noteworthy that the normalized problem is independent of both μ and ν. It is not possible to solve the problem directly by inverting the set equations since the condition of non-negative pressures (equation 6.4) must be satisfied concurrently. However, a solution may be obtained by the sequential

release method of Chapter 5. First, the magnitude of uniform pressure over each element is set to some approximate distribution. For present purposes, a constant value over the whole potential contact area is a sufficient starting point. Next an element is selected and the pressure acting over it is found assuming that the indenter is in contact with the elastic half-space at the element's centre and that the tractions acting at every other element are correct. To evaluate this pressure, at element i say, equation 6.16 must be rearranged:

$$\tilde{p}_i = \frac{1}{D^N_{ii}} \left(\tilde{\alpha} + \tilde{\theta}_x \tilde{y}_i + \tilde{\theta}_y \tilde{x}_i - \sum_{j=1}^{m} \tilde{p}_j D^N_{ij} \right) \qquad j \neq i \tag{6.17}$$

If the result is negative, implying that an adhesive local traction is required to maintain contact, then the assumption was wrong, there is no local contact and so the traction over that element is set to zero. However, if the pressure evaluated is strictly greater than zero, the value of the traction at the element is set to this new value. By repeating this process for each element in turn, a progressively more accurate approximation to the actual pressure distribution is found. This procedure may, of course, be repeated indefinitely and so some measure of the current error is necessary. Since the actual traction distribution is unknown, it is not possible to define an absolute error. However, the amount that the traction distribution changed since the last time that the entire mesh was swept may be monitored. Once this relative error falls below some threshold value for all squares (which depends on the accuracy required, the form of the traction distribution and the number of contributing elements) the solution process may be terminated. The accuracy of the traction distribution at the boundary of the contact (i.e. where contact is just lost and at the edge of the indenter) depends on the density of the traction elements at these locations. Once the "loss of contact" boundary has been found approximately, the mesh in that region may be refined and the process repeated to determine its position and form more accurately. Likewise at the edge of the contact where the pressure gradient is large, a greater density of elements may be employed.

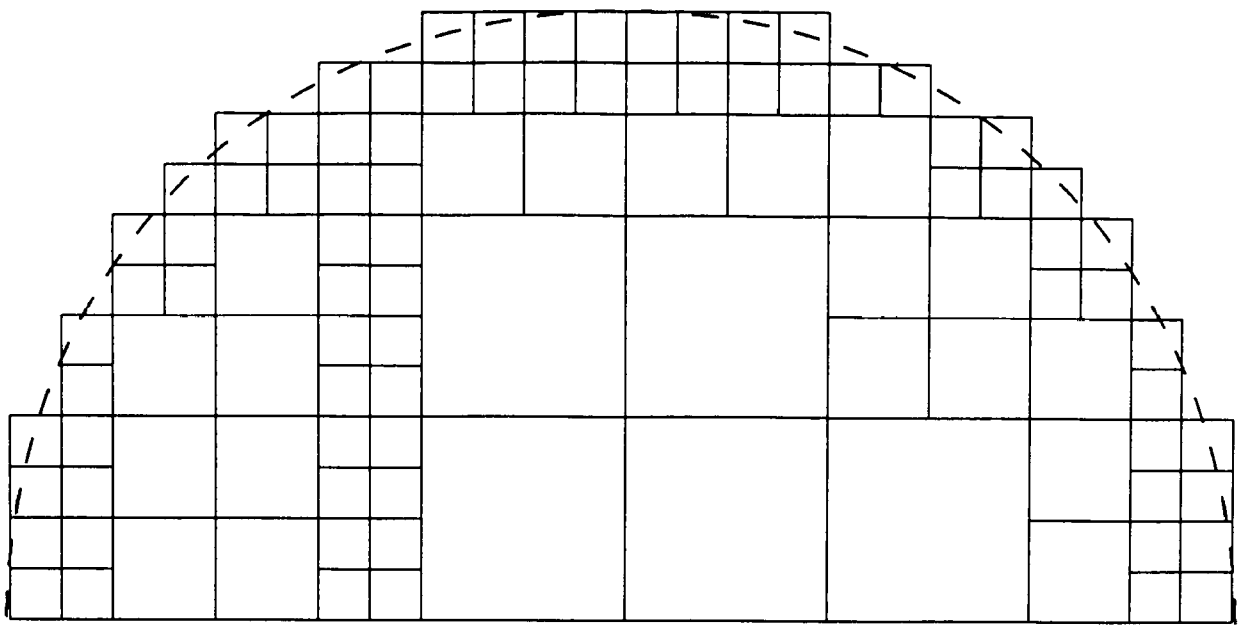

Figure 6.2: A typical unrefined mesh.

6.4 Results

The geometry of an indenter with a circular face is such that the traction distribution always has one plane of symmetry. Hence, it is efficient to model just half of the contact by assuming that the $y = 0$ is the symmetry plane and hence $\theta_x = 0$. Equation 6.17 is still valid provided that the influence functions include the effect of an traction element of equal magnitude on the opposite side of the x-axis. Figure 6.2 shows a typical unrefined mesh used for the analysis. Note the higher density of elements at the edge of the indenter, where the gradient of the pressure distribution is expected to be large; and in the region where loss of contact is predicted. Figure 6.3 shows how the loss of contact boundary changes as the angle of inclination is increased with fixed indentation depth. The corresponding normal loads and bending moments are shown in Figure 6.4. The change in gradient of both curves coincides with point at which loss of contact first occurs when $\tilde{\theta} \approx 0.5$. For each analysis, the refined mesh contained around 800 elements. Figure 6.5 shows the reduction in relative error as the solution proceeds. This measure of error is actually the *sum* of the absolute change in traction at each element for a single cycle of release of pressure at every element. It is clear that even for the large number of elements involved,

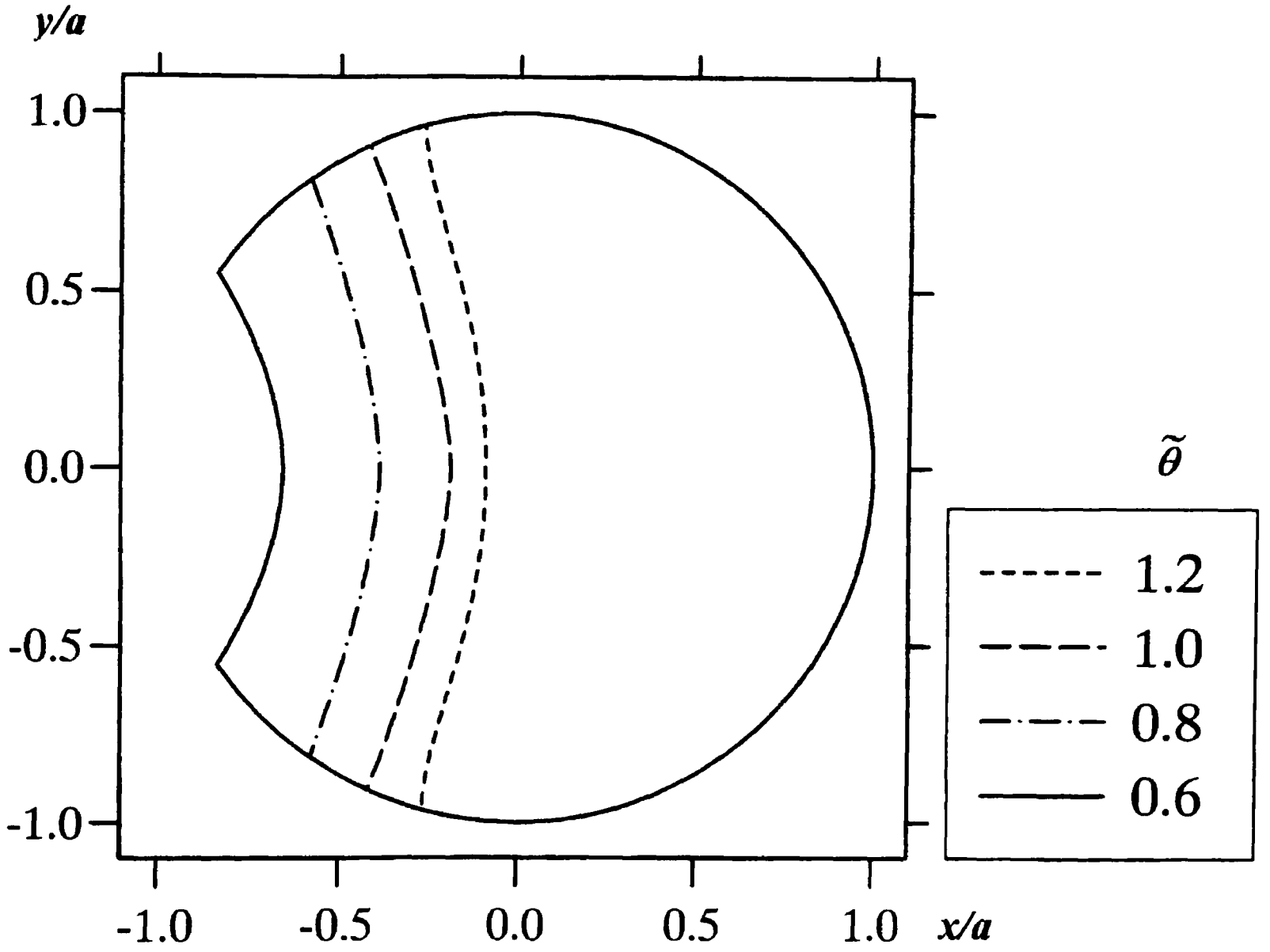

Figure 6.3: Evolution of the region of contact as the angle of inclination is increased.

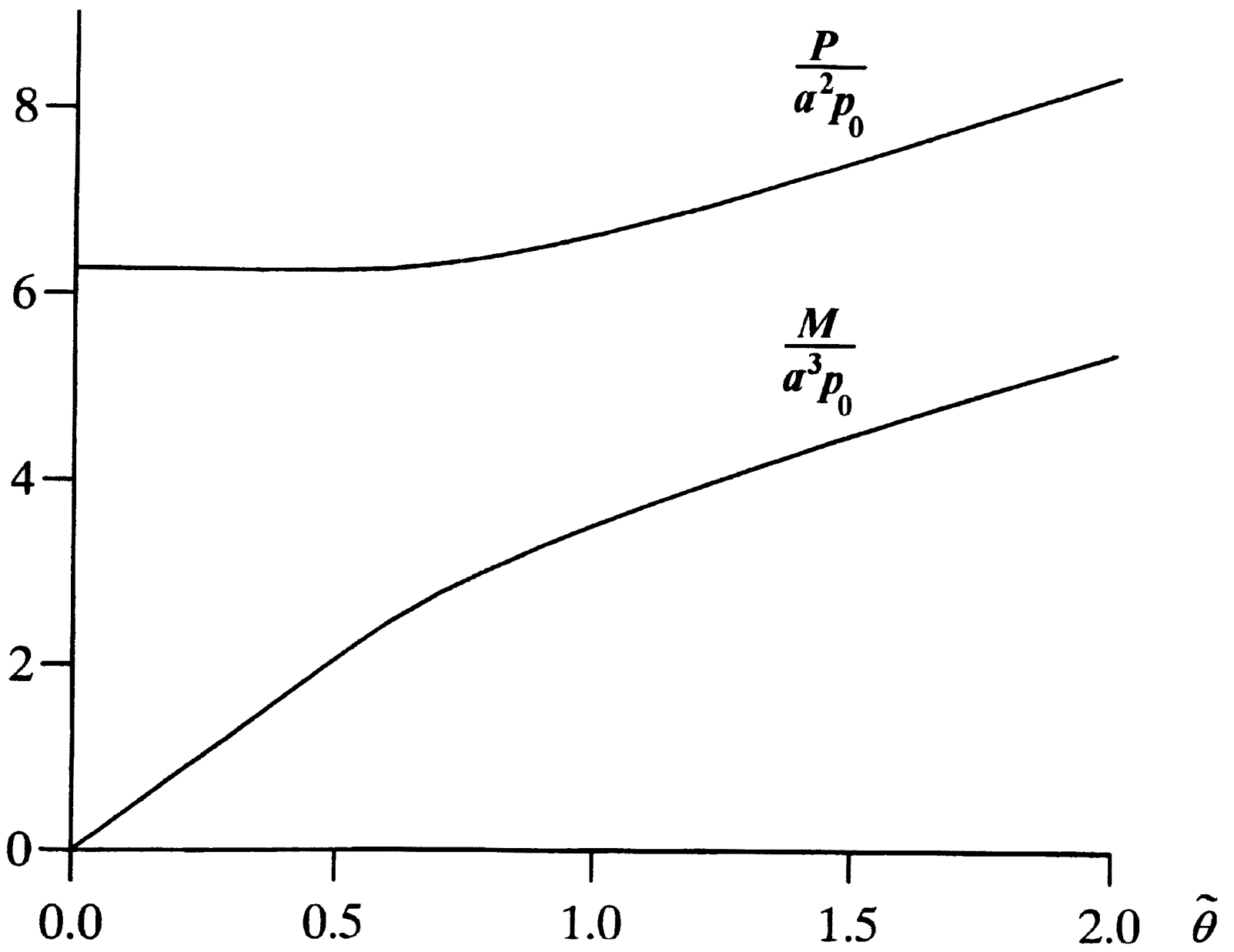

Figure 6.4: Variation of force and moment with angle of indentation.

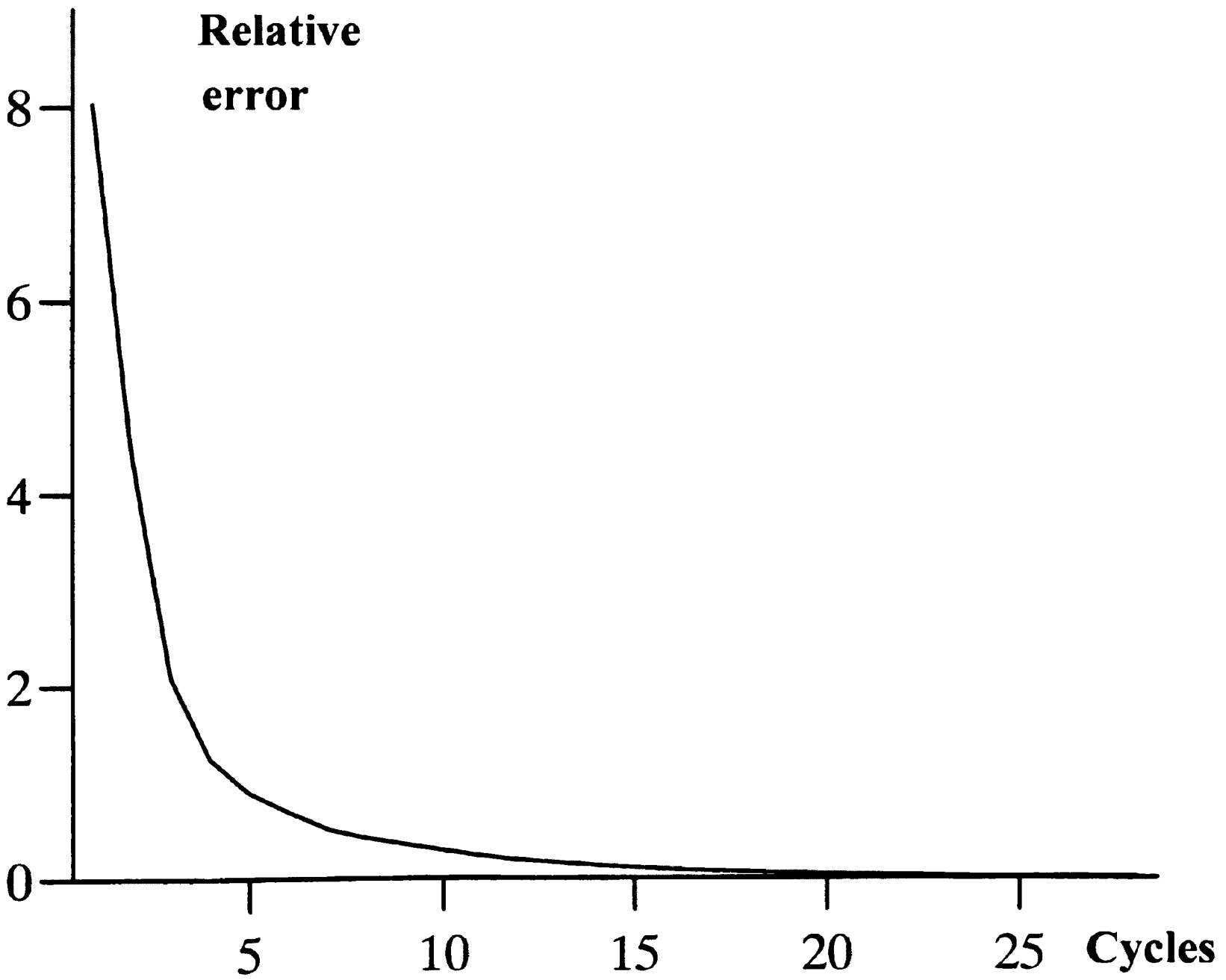

Figure 6.5: Reduction in relative error with sweeps through the mesh.

convergence is rapid.

6.5 Conclusions

The sequential release method developed in Chapter 5 has been applied to a sample problem of indentation of an elastic half-space by a flat-ended cylindrical punch. The problem was normalized and discretized and then solved by the sequential release method. Traction distributions and loss of contact boundaries were found and relative errors monitored. The problem could be developed to study the stability of inclined indenters to small perturbations to discover the point of equilibrium. Such analyses may be useful in understanding the stability of rigid containers resting on flexible ground and subject to transverse fluid loading, but this is beyond the scope of the present study.

Chapter 7

Sliding Sphere with Dissimilar Elastic Properties

7.1 Introduction

The solution for a sliding contact problem is arguably the most useful one to obtain, after normal indentation, as it is also the limiting case of both rolling contact and Mindlin type contact. In any contact where there is relative tangential displacement between two bodies, even if the resulting area of slip does not encompass the whole contact, there is the potential for wear damage. In the case of a Mindlin type contact in particular, fretting damage is a cause for concern. The stress fields for such partial slip problems, which may be used to quantify such damage, are particularly difficult to evaluate and so the stress field generated by sliding contact provides an extremely useful upper-bound.

In 1882, Hertz (1882) presented his classical analysis of contact between two non-conforming, elastic bodies with quadratic surface profiles. The results of that analysis may, in particular, be applied to the following configurations, viz. the contact of two cylinders having their axes parallel and the contact of two spheres. The pressure distribution Hertz found is valid for both normal and sliding contact provided, in each case, that the bodies have either similar elastic properties or that the coefficient of friction is zero.

The work described in this Chapter has been published and can be found in: R. L. Munisamy, D. A. Hills and D. Nowell 1991,"A numerical analysis of an elastically dissimilar three-dimensional sliding contact" *Proc. Instn. Mech. Engrs.*, Vol. 206, pp. 203–211.

The stress fields resulting from the contact of two cylinders have been found by M'Ewen (1949), Poritsky (1950), and Smith and Liu (1953), for both normal and frictional sliding contact. The corresponding fields for the contact of two spheres have been found by Hüber (1904) for normal contact and by Hamilton and Goodman (1966) for frictional sliding. A comparison of the fields produced by each geometry reveals a qualitative difference in addition to their respective two and three dimensional natures. This is most apparent for the case of normal contact: a region of tensile stress develops around the edge of the contact area of the spheres, whereas the state of stress for the cylindrical case is everywhere compressive.

A Hertzian (i.e. elliptical) pressure distribution is no longer valid when the contacting bodies are elastically dissimilar and frictional tractions are present. This is because coupling effects, which occur between the normal tractions and any shear tractions, are not included in Hertz's formulation. Hills and Sackfield (1985) have analyzed sliding frictional contact between two elastically dissimilar cylinders taking full account of coupling between the normal and shearing tractions. There are several quantitative differences between their solution and the corresponding Hertzian (uncoupled) one. First, the position of the region of contact is fractionally displaced and secondly the pressure distribution takes a slightly modified form. The resulting state of stress well within the bodies is not altered, but there is a significant variation at the surface.

A summary of the work presented on the subject of frictional sliding of elastic cylinders and spheres is shown in the table below.

	Cylinders (2-D)	Spheres (3-D)
Uncoupled	M'Ewen (1949)	Hamilton & Goodman (1966)
Coupled	Hills & Sackfield (1985)	This Chapter

Recently, Hamilton and Goodman's solution (presented in a more tractable form by Hamilton (1983)) has been used to study deformation and fracture in sliding indentation experiments. Van Groenou and Kadijk (1988) used a ruby sphere to indent polycrystalline

ceramics and Atkins (1991) a steel ball on glass. Since the materials have dissimilar elastic properties and friction is not negligible, the appropriateness of the Hertzian solution must be called into question. Brittle fracture was found to initiate near the trailing edge of the contact where one would expect the effect of coupling upon the stress fields to be greatest.

In this Chapter the sliding contact between a sphere and a half-space with dissimilar elastic properties is considered. The solution that is developed includes the effect of coupling between the normal tractions and tangential displacements and between tangential tractions and normal displacements. Thus the differences between the uncoupled and the fully coupled solutions will be quantified.

First, the pressure distribution is evaluated using the sequential release method developed in Chapter 5. This requires that both the normal and tangential tractions, and the extent of the contact are found as part of the solution. The assumption that the tangential tractions all act parallel to the direction of slide is made and justified. Then the resulting state of stress in the bodies is found. Particular emphasis is devoted to the regions of the stress fields which are likely to produce failure.

7.2 The pressure distribution

The geometry of the problem is shown in Figure 7.1. A sphere (body 2) is sliding across a half-space (body 1) along the positive x-axis, at a sufficiently slow rate for inertia effects to be ignored. If the bodies have similar elastic properties the solution for the normal pressure $p(x, y)$ is given by Hertz (1882) as

$$p(x,y) = p_0 \left\{ 1 - \left(\frac{r}{a} \right)^2 \right\}^{\frac{1}{2}} \tag{7.1}$$

where $r^2 = x^2 + y^2$, p_o is the peak Hertzian pressure, and a the Hertzian contact radius. It is convenient to use this traction distribution to prove that the frictional tractions act in the direction of slide. Assuming this hypothesis to be true the shear tractions are given

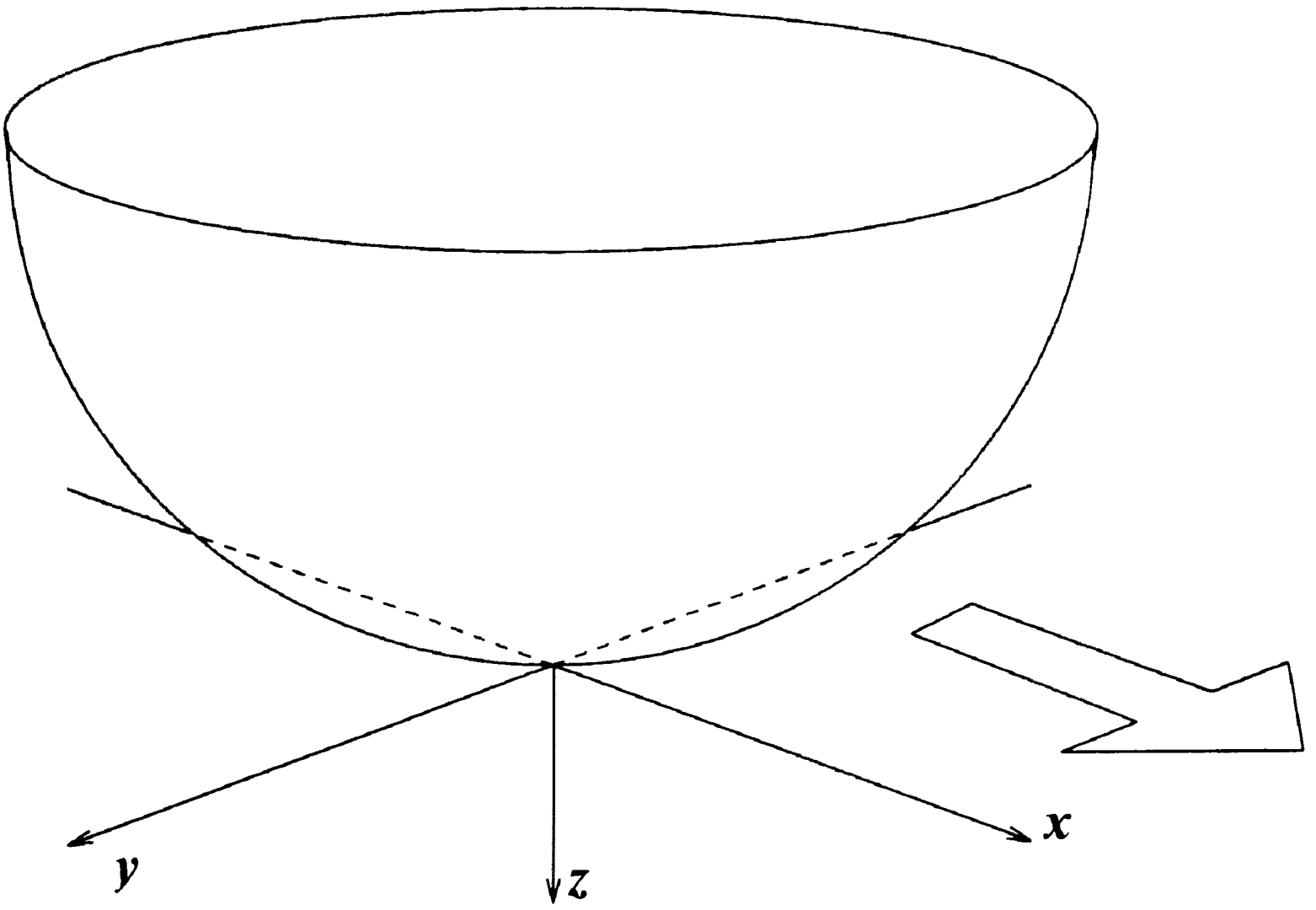

Figure 7.1: Configuration of the sliding conact.

by:

$$q_x(x,y) = fp(x,y) \tag{7.2}$$

$$q_y(x,y) = 0. \tag{7.3}$$

In the steady state, particles in the sphere experience a constant traction distribution and so do not move relative to each other. Hence, it is convenient to consider the sphere to be fixed. However, particles in the half-space experience changing tractions as they pass through the contact. Within the contact interface, elastic displacement in the transverse direction due to normal tractions only is

$$u_y^N = \frac{(1-2\nu)}{6\mu}\frac{a^2 y}{r^2}p_0\left\{1-\left(1-\frac{r^2}{a^2}\right)^{\frac{3}{2}}\right\} \tag{7.4}$$

where ν and μ are Poisson's ratio and the modulus of rigidity respectively. This must be added to the gross relative motion of the sphere and half-space. The actual direction of motion of particles can then be found by differentiating with respect to x to obtain the trajectory of the displacement increment:

$$\frac{\partial u_y^N}{\partial x} = \frac{(1-2\nu)}{6\mu}\frac{xy}{r^2}p_0\left[\frac{2a^2}{r^2}\left\{1-\left(1-\frac{r^2}{a^2}\right)^{\frac{3}{2}}\right\}+\frac{3}{2}\left(1-\frac{r^2}{a^2}\right)^{\frac{1}{2}}\right]. \tag{7.5}$$

This has an order of magnitude of a/R (where R is the radius of curvature of the sphere) and Hertz's analysis assumes this ratio to be very small. Similarly, the transverse displacement due to the shear tractions alone (again assuming they act in the direction of slide) is given by

$$u_y^S = \frac{\pi\nu xyfp_0}{32\mu a} \tag{7.6}$$

whose derivative has the same very small order of magnitude. Therefore, the assumption made has been shown to be valid for a Hertzian contact; it should also hold true for an elastically dissimilar one since even a large change in traction distribution can have little effect on the direction of slide of a particle within the contact zone. The effect of normal

tractions on tangential displacements should be of a similar, small magnitude. Indeed, if the problem is solved in this manner and the direction of relative slip found *a priori*, the initial assumption is confirmed.

When the sphere and half-space have dissimilar elastic properties, the problem must be re-formulated. The normal surface displacements u_z of each body may be written (making use of Johnson (1985)):

$$u_{z1}(x,y) = \int\int_S \left(\frac{2(1-\nu_1)}{4\pi\,\mu_1} \frac{p(\zeta,\eta)}{\rho} - \frac{1-2\nu_1}{4\pi\,\mu_1} q_x(\zeta,\eta) \frac{\zeta - x}{\rho^2} \right) d\zeta\, d\eta \qquad (7.7)$$

$$u_{z2}(x,y) = \int\int_S \left(-\frac{2(1-\nu_2)}{4\pi\,\mu_2} \frac{p(\zeta,\eta)}{\rho} - \frac{1-2\nu_2}{4\pi\,\mu_2} q_x(\zeta,\eta) \frac{\zeta - x}{\rho^2} \right) d\zeta\, d\eta \qquad (7.8)$$

where

$$\rho^2 = (\zeta - x)^2 + (\eta - y)^2, \qquad (7.9)$$

$p(x,y)$ is the normal pressure, $q_x(x,y)$ is the shearing traction in the x-direction, $\mu_{1,2}$ and $\nu_{1,2}$ are the moduli of rigidity and Poisson's ratio respectively of the bodies and the region of integration S is the area of contact, which is unknown *a priori*. The shearing traction is related to the normal pressure by Coulomb friction:

$$q_x(x,y) = f\,p(x,y) \qquad (7.10)$$

where f is the coefficient of friction between the two surfaces. It is assumed, subsequent to an initial point contact, that a rigid body displacement is imposed upon the bodies such that two suitably distant points within each move a distance α closer together in the z-direction. The normal displacements within the region of contact may be written:

$$u_{z1}(x,y) - u_{z2}(x,y) = \alpha + \delta(x,y) \qquad x,y \subset S \qquad (7.11)$$

where $\delta(x,y)$ is the undeformed surface profile of the sphere. In keeping with Hertz's analysis, this profile may be approximated by a paraboloid and written as:

$$\delta(x,y) = -\frac{r^2}{2R}. \qquad (7.12)$$

Substituting equations 7.7 and 7.8 into 7.11, making use of 7.10 and 7.12 produces:

$$\int\int_S p(\zeta,\eta)\left[\frac{1}{\rho}-\beta\, f\frac{\zeta-x}{\rho^2}\right]d\zeta\, d\eta=\frac{2\pi}{A}\left(\alpha-\frac{r^2}{2R}\right) \tag{7.13}$$

where

$$A=\frac{1-\nu_1}{\mu_1}+\frac{1-\nu_2}{\mu_2} \tag{7.14}$$

which is the composite compliance, and

$$\beta=\left(\frac{1-2\nu_1}{2\mu_1}-\frac{1-2\nu_2}{2\mu_2}\right)/A \tag{7.15}$$

the Dundurs' constant for the material pair. The pressure distribution must satisfy equation 7.13 and two further conditions, viz. it must never be tensile

$$p(x,y)\geq 0, \tag{7.16}$$

and the normal displacements which result must not give rise to interpenetration of the two bodies outside the region of contact, i.e.

$$u_{z1}(x,y)-u_{z2}(x,y)<\alpha+\delta(x,y)\qquad x,y\notin S. \tag{7.17}$$

It is convenient to normalize the contact pressure with respect to the peak *Hertzian* pressure which would result if the contact were frictionless

$$p_0=\frac{4}{\pi\, A}\sqrt{\frac{\alpha}{R}} \tag{7.18}$$

and the dimensions with respect to the corresponding *Hertzian* contact radius

$$a_0=\sqrt{\alpha\, R}. \tag{7.19}$$

Using the substitutions $p=p_0\tilde{p}$ and $x=a_0\tilde{x}$, etc. equation 7.13 may be re-written as

$$\int\int_S \tilde{p}(\tilde{\zeta},\tilde{\eta})\left[\frac{1}{\tilde{\rho}}-\beta\, f\frac{\tilde{\zeta}-\tilde{x}}{\tilde{\rho}^2}\right]d\tilde{\zeta}\, d\tilde{\eta}=\frac{\pi^2}{2}(1-\frac{1}{2}\tilde{r}^2) \tag{7.20}$$

revealing that the pressure distribution is solely a function of the combined parameter βf.

Equation 7.20 may be solved using the procedure developed in Chapter 5. A region of the surface containing the contact area $\tilde{S}$ is discretized into a mesh of $2m$ squares, each one being a uniform traction element of unknown pressure p_i and tangential traction fp_i. This permits equation 7.20 to be satisfied at the centre of each element resulting in a set of simultaneous equations:

$$\sum_{j=1}^{2m} \tilde{p}_i (D_{ij}^N - \beta f D_{ij}^S) = \frac{\pi^2}{2}(1 - \frac{1}{2}\tilde{r}_i^2) \quad i = 1, 2m \tag{7.21}$$

where D_{ij}^N, D_{ij}^S are the influence functions relating the normalized displacement at the centre of square i to unit normal and shearing tractions respectively acting on square j (and which are stated explicitly in Appendix A), and $\tilde{r}_i$ is the normalised distance of square i to the origin of coordinates. It is not possible to invert this set of equations directly because of the nature of the additional inequalities 7.16 and 7.17, which must be simultaneously satisfied. As a first approximation, a Hertzian pressure distribution is applied over the mesh. This approximation is improved iteratively by the sequential release of the pressure elements. The pressure at square i is found which satisfies equation 7.21 assuming the current approximation for the rest of the pressure elements. If the local pressure is found to be tensile it is set to zero; otherwise it becomes part of a refined approximation. This process is carried out for each square of the mesh, and repeated until the pressure distribution converges to a solution. Convergence is assumed when the greatest change in magnitude of any element of the mesh is less than a certain fraction (1%) of the peak Hertzian pressure. Once the approximate location of the boundary of the contact area is found, it may be used to generate a refined mesh with a greater density of elements near the boundary and the whole technique repeated. Displacements exterior to the contact patch may be evaluated to check that there is no interpenetration of the

two bodies. This is verified if the left hand side of equation 7.21 is less than the right hand side, which is equivalent to satisfying inequality 7.17 and confirms the appropriateness of the solution. It is worth noting that the problem is symmetrical about the $y = 0$ plane and this may be exploited to make the solution process more efficient. The tractions at points (x, y) and $(x, -y)$ are identical, so it is convenient to use a mesh which is also symmetrical about the x-axis. If the first m elements of the mesh all have positive y-coordinates, and the second m elements are reflections of them in the x-axis, the equation at the heart of the iterative algorithm is:

$$\tilde{p}_i = \frac{1}{D^N_{ii} + D^N_{ik} - \beta f(D^S_{ii} + D^S_{ik})} \left[\frac{\pi^2}{2} \tilde{r}^2_{ij} - \sum_{j=1}^{m} \tilde{p}_j (D^N_{ij} + D^N_{il} - \beta f(D^S_{ij} + D^S_{il})) \right] \quad j \neq i \tag{7.22}$$

where $k = i + m$ and $l = j + m$.

7.2.1 Results

Pressure distributions were found for a range of values of βf using a refined mesh of 800 squares of which at least 500 elements sustained finite tractions when the solution had converged (a maximum of 30 passes over the mesh was required when $\beta f = 0.3$). Figure 7.2 shows a much coarser mesh but illustrates how a larger density of squares near the expected boundary of the contact can be used to find it accurately. To test the method, the pressure distribution was found for $\beta f = 0$, starting from a uniform pressure distribution, and compared with the Hertzian solution: the correlation was excellent.

Figure 7.3 shows an interpolated contour plot of the pressure distribution for $\beta f = 0.3$. The dashed circle shows the area of the equivalent Hertzian contact and the cross-hairs show the location of the peak Hertzian pressure. The total normal load was found to be 8% greater than the equivalent Hertzian one required to produce the same approach of distant points, α. For positive values of β(i.e. when the half-space is more complaint than the sphere), both the contact region and the peak pressure were displaced along the

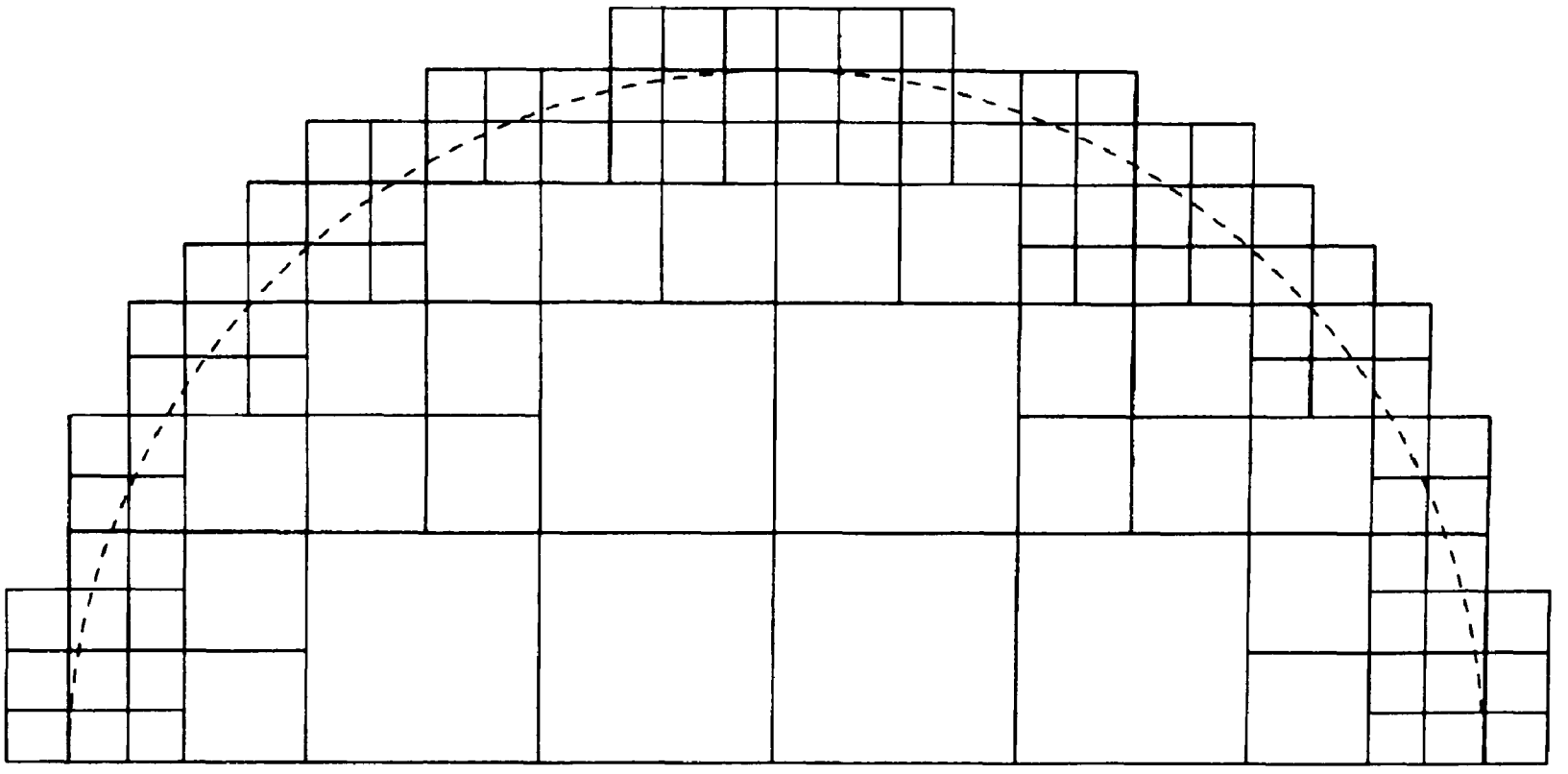

Figure 7.2: Schematic of the type of mesh used to solve the problem.

negative x-axis; for negative β the displacement was in the direction of slide of the sphere.

Figure 7.4 shows the close correspondence between the pressure found along the x-axis and a pressure distribution of the form:

$$p(s) = p_1(1+s)^B(1-s)^{1-B} \tag{7.23}$$

which is that produced by sliding dissimilar elastic cylinders (Hills & Sackfield, 1985), where $B = 1/\pi \tan^{-1} \beta f$, and s and p_1 are chosen to match the distributions at the end points and in the middle.

7.3 The stress field

Once the traction distribution has been found, it is relatively straightforward to derive the state of stress which results. The stress field generated in an elastic half-space by a rectangle of uniform normal and tangential tractions was discussed in Chapter 5 and its components are recorded in a convenient form in Appendix A.

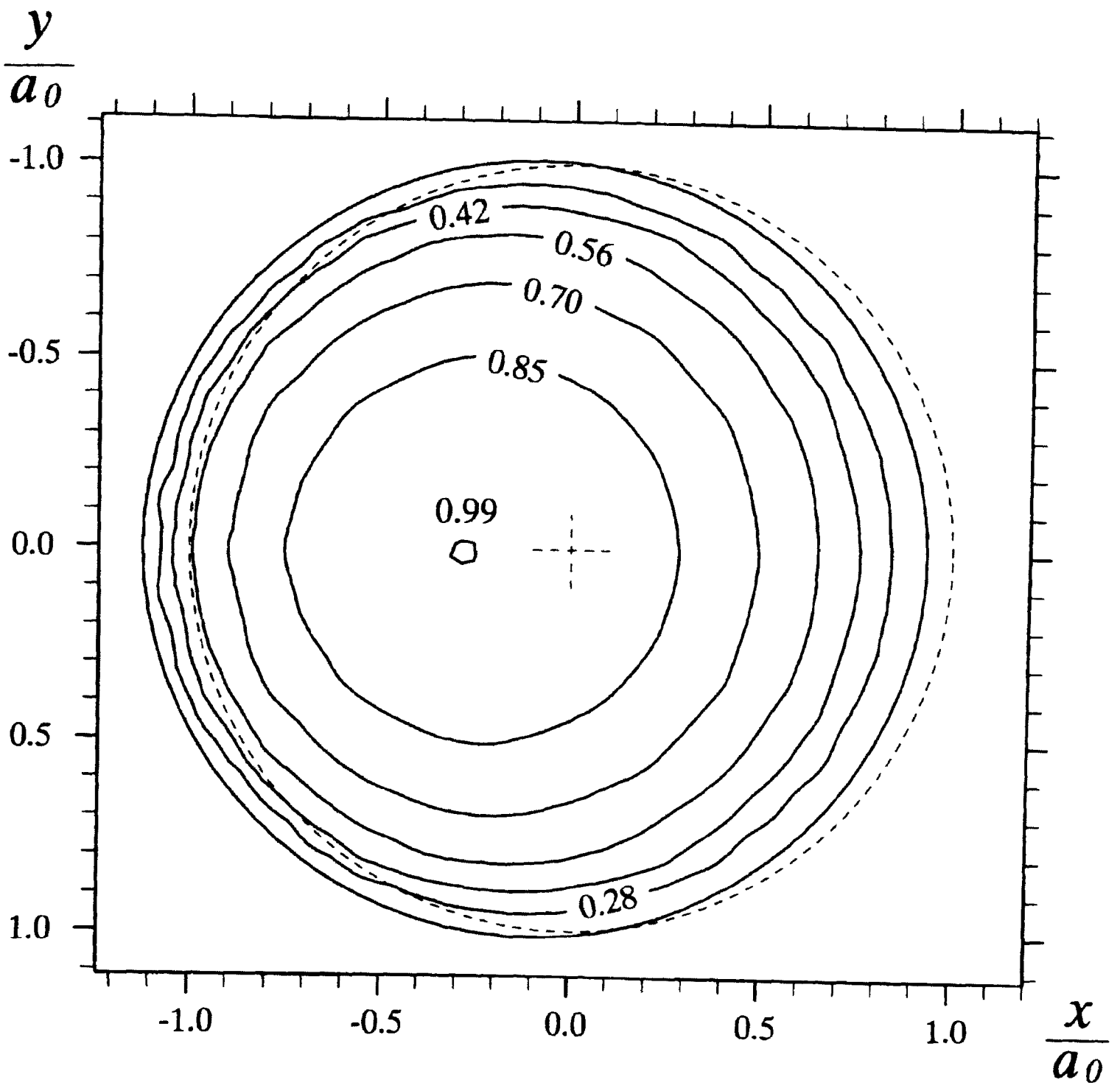

Figure 7.3: Interpolated contour plot of the normalized traction distribution for $\beta f = 0.3$. Comparison with the equivalent Hertzian traction distribution (whose extent and peak is shown by the dashed circle and cross-hairs) reveals that the centre of pressure has displaced along the negative x-axis.

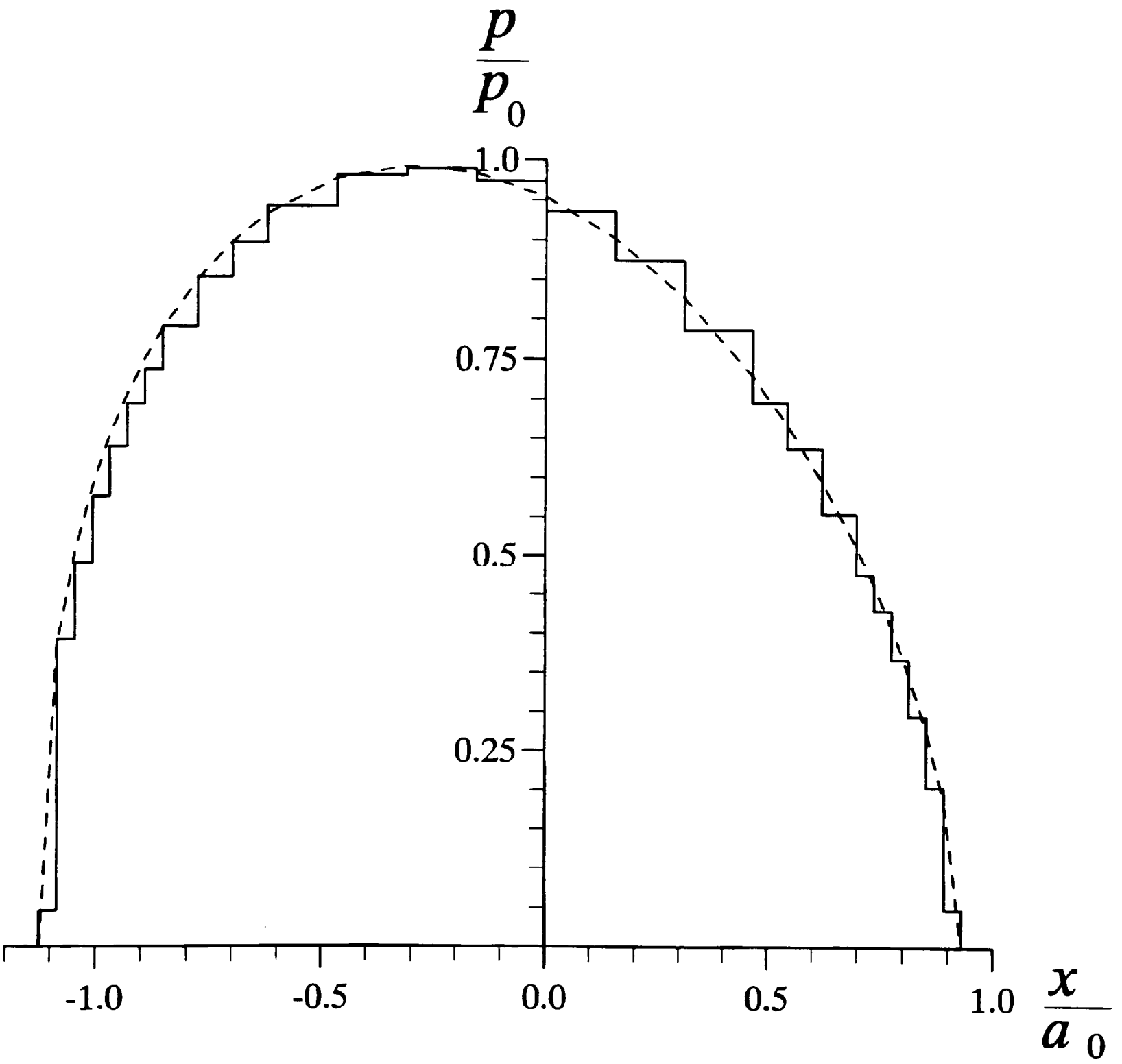

Figure 7.4: Normal traction distribution along the x axis ($\beta f = 0.3$). Solid line shows values from mesh, dashed line shows the equivalent tractions for cylinders in sliding contact.

The components of the stress field, for example σ_{xx}, produced by the sliding sphere can easily be found by superimposing the contributions of each element in the mesh:

$$\sigma_{xx}(x,y,z) = \sum_{i=1}^{2m} p_i \left(G^N_{xxi}(x,y,z) + f\, G^S_{xxi}(x,y,z) \right) \tag{7.24}$$

where G^N_{xxi}, G^S_{xxi}, etc. are the components of the stress field generated by unit normal and shearing traction respectively over element i. The pressure distribution was found to depend solely on the product β and f; equation 7.24 shows that the stress components depend on the pressure distribution, the coefficient of friction and Poisson's ratio for the body in which they are evaluated. There is no difficulty in evaluating the state of stress well within the elastic half-space. However, the singular nature of some of the components of the stress field causes problems when evaluating them at the edge of an element. Hamilton (1983) found that failure was likely to occur at the trailing edge of sliding Hertzian contacts and it is necessary to employ some modifications to the mesh to find the stresses there.

The problem of the singularity produced by a step change in pressure resulting from the use of uniform pressure elements can be overcome by replacing strips of the mesh with single "slice" elements over which the pressure varies continuously and smoothly. To find the stress field at the trailing edge of the contact it is appropriate to use a strip laid along the x-axis, as shown in Figure 7.5, which has a pressure which depends on x only and takes the form of the pressure distribution produced by sliding cylinders (equation 7.23). The components of the stress field along the x-axis, for example σ_{xx}, produced by such an element can be found from the following equation:

$$\sigma_{xx}(x) = \int_{te}^{le} p_1 (1-s)^B (1+s)^B [H^N_{xx}(x,a) + f\, H^S_{xx}(x,a)] da \tag{7.25}$$

where H^N_{xx}, H^S_{xx}, etc. are the derivatives with respect to a of the components of the stress fields of a rectangle of uniform normal and shearing traction which has the same width as the strip and which extends from 0 to a; these are recorded in Appendix A. The leading

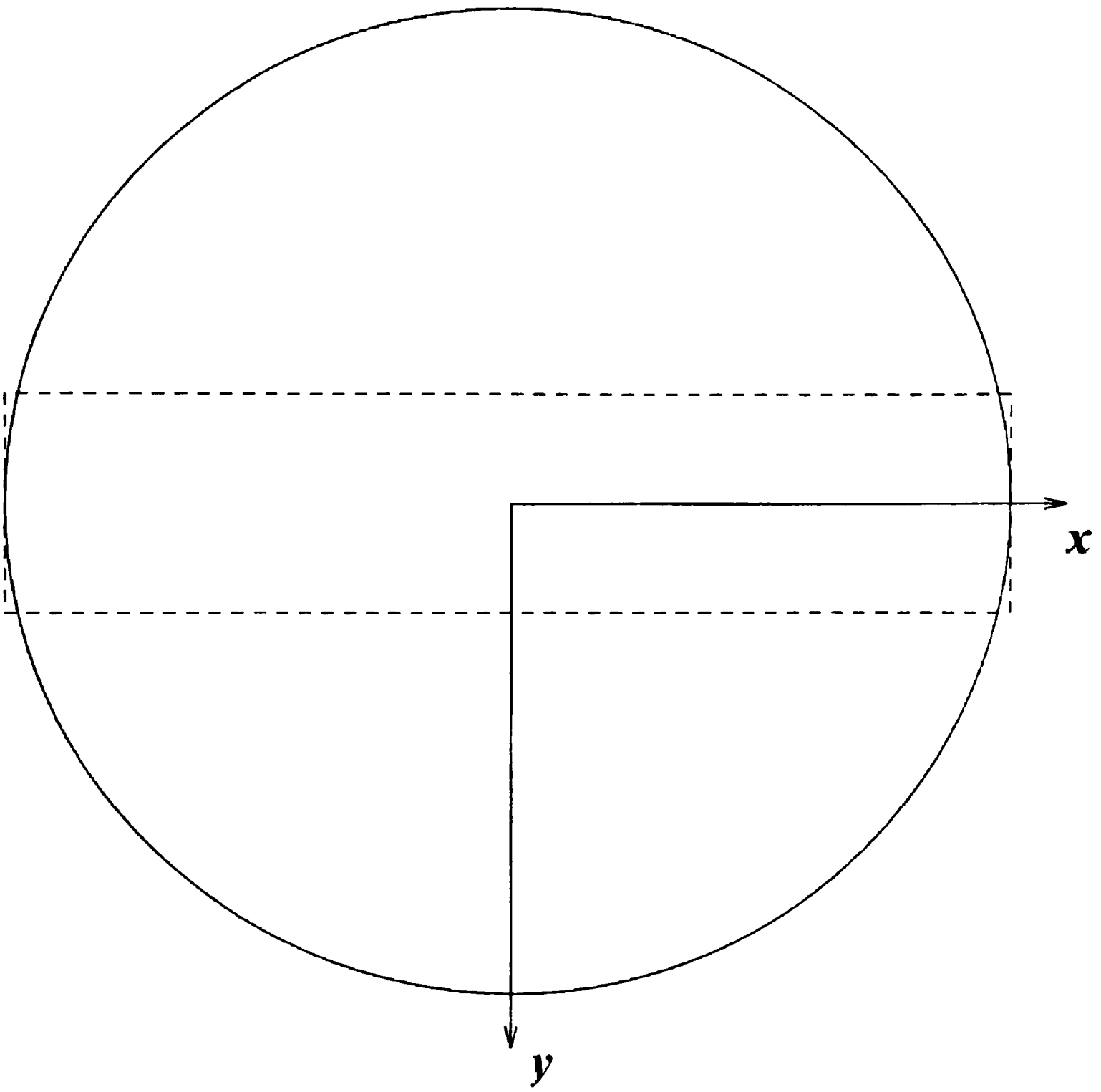

Figure 7.5: Location of the continuous traction element.

and trailing edges of the contact on the x-axis are located at le and te respectively, so that $s = -1 + 2(\zeta - te)/(le - te)$ and p_1 is the pressure at $s = 0$. Hence, the stress field can be found at every point below the surface of the half-space and, by a special procedure, along the x-axis for $y = z = 0$.

7.3.1 Results

The stress fields were found within the elastic half-space for a range of values of β and f. Of particular interest are the maximum tensile stress, which was always found to be σ_{xx} at the trailing edge of the contact and is associated with brittle fracture, and the maximum of the second invariant of the stress deviator tensor

$$J_2 = \frac{1}{6}[(\sigma_1 - \sigma_2)^2 + (\sigma_2 - \sigma_3)^2 + (\sigma_3 - \sigma_1)^2] \tag{7.26}$$

(where $\sigma_{1,2,3}$ are the principal stresses) which controls ductile yielding according to von Mises' yield criterion. To allow a meaningful display of how these two maxima vary with β and f, the value of Poisson's ratio of the half-space ν_1 was kept at 0.25 (which is its value for glass). It should be noted from equation 7.15 that this limits β to a maximum positive value of $\frac{1}{3}$. Figure 7.6 shows the maximum tensile stress in the half-space for different values of β and f. As β is increased positively from zero, the tensile stress is augmented; for negative β it is reduced. This is amplified as the coefficient of friction increases. The effect of material dissimilarity can obviously be significant, and when $\beta = 0.21$ (corresponding to a steel ball sliding over glass), shown in Figure 7.6 by the dashed line, the maximum tensile stress is 12% greater than a Hertzian analysis would predict for $f = 0.6$.

The maximum values of von Mises' yield parameter $J_2^{\frac{1}{2}}$ are shown in Figure 7.7 for a range of positive values of β and f, when $\nu_1 = 0.25$. For frictionless contacts, the maximum is located below the surface and as f increases, it moves slightly nearer to the surface. In addition, another region of likely yielding develops at the trailing edge which

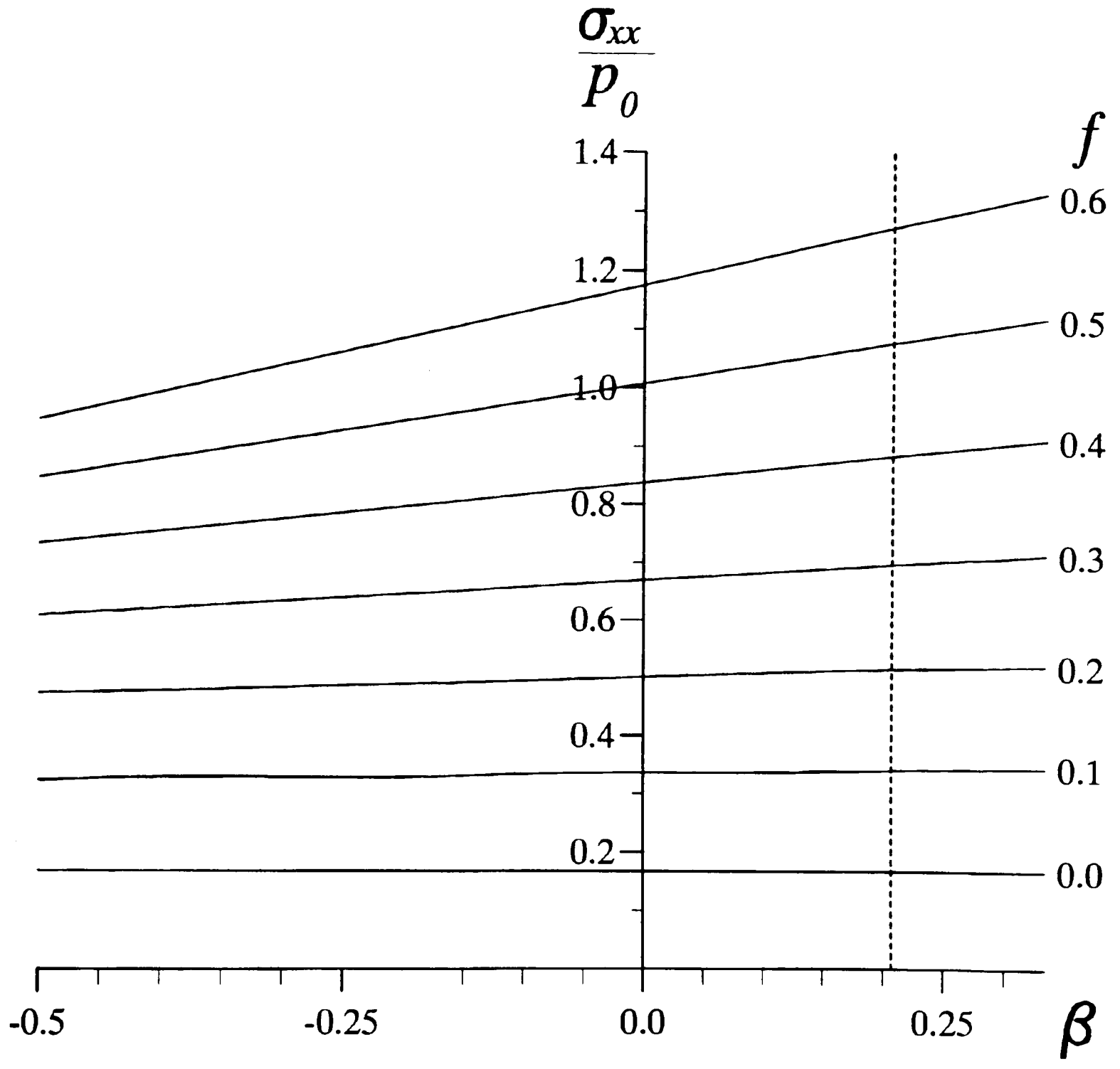

Figure 7.6: Maximum tensile stress (located at trailing edge) for a range of values of β and f ($\nu_1 = 0.25$). Dashed line indicates steel on glass.

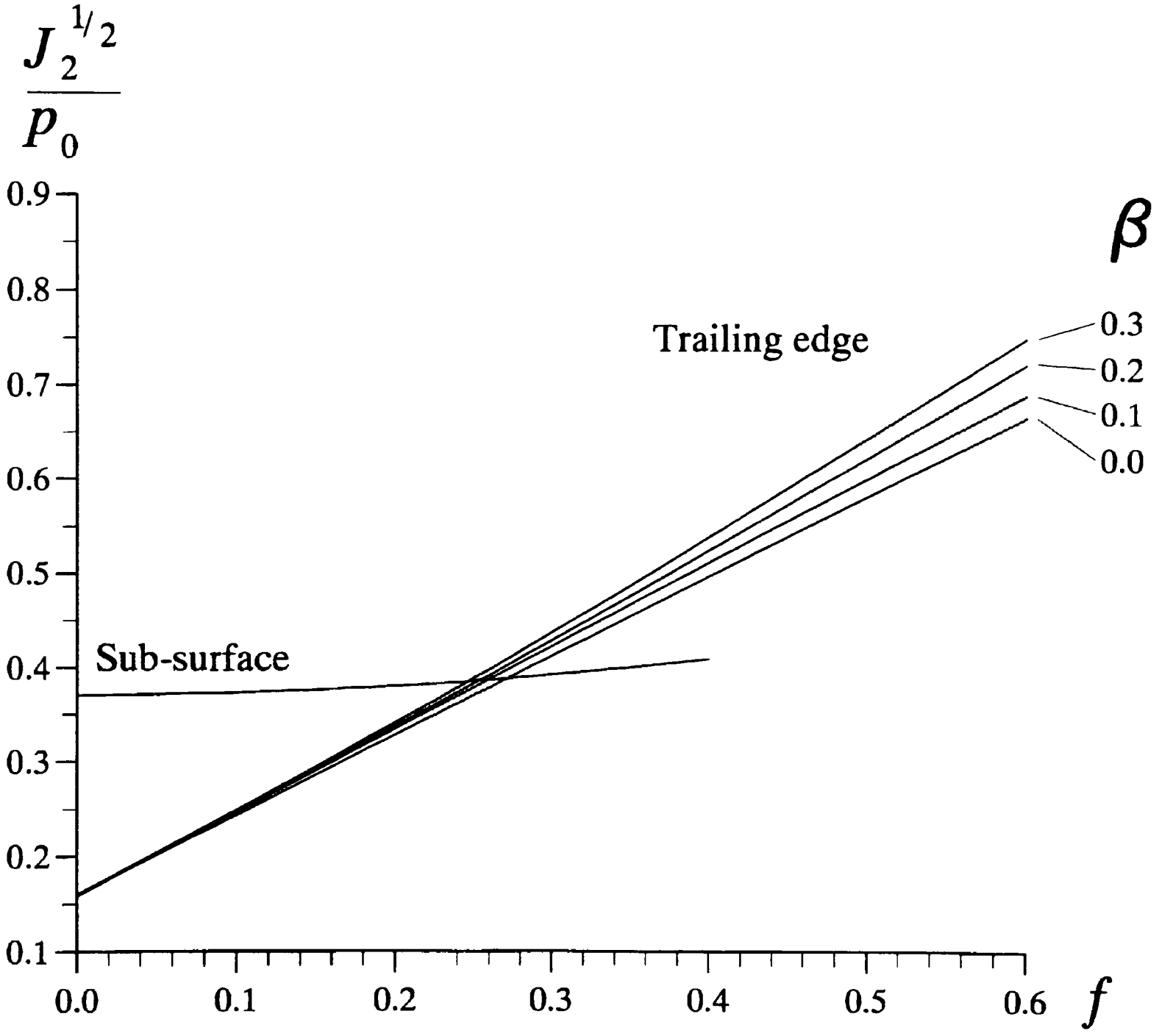

Figure 7.7: Maximum values of yield parameter in the plane $y = 0$ for a range of values of f and β ($\nu_1 = 0.25$).

is dominant for large values of f. The position of the sub-surface maximum varies greatly with β but its magnitude does not; the value at the trailing edge does depend on the dissimilarity of the materials.

When β is negative, the location of the maximum value of the yield parameter at the surface does not necessarily coincide with the trailing edge. To illustrate this, Figure 7.8 shows $J_2^{\frac{1}{2}}$ at the surface along the x-axis for various values of β and a constant coefficient of friction of 0.6. Compared to the Hertzian case, when $\beta = 0$, increasing β causes the yield parameter to take a greater value at the trailing edge. As β becomes more negative, however, the peak at the trailing edge decreases, a plateau forms and the maximum moves towards the leading edge.

7.4 Conclusions

The sequential release method developed in Chapter 5 has been successfully applied to solve the fully coupled formulation of sliding contact between a sphere and a half-space with dissimilar elastic properties. Numerical results have been found for the pressure distribution and hence the tangential tractions; the actual region of contact was found as part of the solution process. These have been used to find the stress field within the half-space. A comparison with the corresponding uncoupled analysis reveals that material dissimilarity can have a significant effect upon both the maximum tensile stress and von Mises' yield parameter, but only for large values of coefficient of friction.

For the purpose of discussion, it is convenient to consider the compliance $(1 - 2\nu)/\mu$ of each body, the difference between which is responsible for coupling between the shear tractions and the normal displacements. In the Hertz case, the compliances are identical and the normal relative surface displacement is zero. However, if the half-space in which the state of stress is evaluated is more compliant than the contacting sphere sliding in the x-direction (i.e. $\beta > 0$), the resulting difference in normal displacements moves the contact region off centre, in the negative x-direction. In addition, the peak pressure is displaced

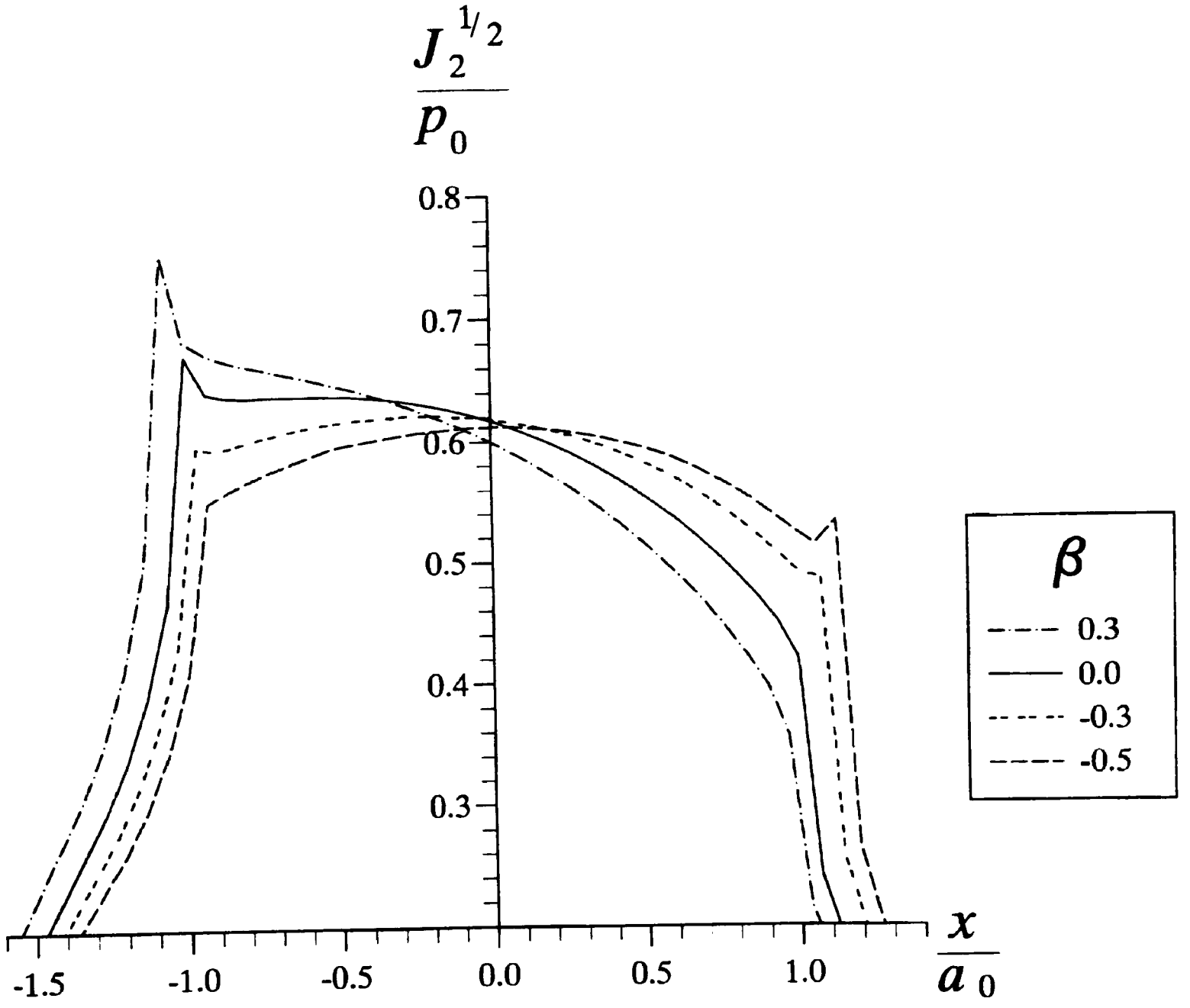

Figure 7.8: Yield parameter evaluated along the x axis for representative values of β ($f = 0.5, \nu_1 = 0.25$).

towards the trailing edge. This increases the gradient of the pressure distribution at the rear of the contact, augmenting the tensile stress within the half-space and making it more prone to failure. The reverse occurs when the sphere is the more compliant body. However, since in this case the concentration is near the leading edge, where all the stress components in the half-space are compressive, it is of less significance.

A complicated non-linear calculation has been conducted. It is of note, therefore, that the final results shown in Figure 7.6 are a series of straight lines. This suggests that it may be possible to simplify the theory of the problem. However, this is beyond the scope of the present study.

Chapter 8

Static Axisymmetric Hertzian Contacts Subject to Shearing Forces

8.1 Introduction

When two convex bodies are pressed together by a normal force and then displaced tangentially by a force which is insufficient to cause sliding, a central stick zone remains but the periphery of the contact experiences slip. If the tangential force is applied in an oscillating manner then energy is expended within the slip zones. Such a situation is called fretting, and wear and crack initiation can result within the region of frictional energy expenditure.

The first solutions to the problem of pressing together two bodies to form a Hertzian contact and then applying a shearing force in the plane of the contact, but less than that needed to cause sliding, were published independently in the first half of this century by Cattaneo (1938) and by Mindlin (1949). These solutions are both developed in a way appropriate to a general elliptical Hertzian contact, and rely on a superposition of the solutions for the surface displacements induced under *sliding* conditions, a concise explanation of which is provided by Johnson (1985). However, although the Cattaneo-Mindlin solution is exact for the contact of cylinders, it has long been recognised that for

The work described in this Chapter has been published and can be found in: R. L. Munisamy, D. A. Hills and D. Nowell 1994, "Static Axisymmetric Hertzian contacts subject to shearing forces" *AMSE Journal of Applied Mechanics*, Vol. 61(2), pp. 278–283.

a general elliptical or circular contact the relative displacement of surface particles within the slip zone has a component perpendicular to the direction of the applied tangential force. This violates the requirement that within a slip zone the frictional tractions must be directed so as to oppose an increment of relative displacement. This discrepancy seems particularly marked in the case of an applied shearing force acting at an angle to the axes of the contact ellipse (Szalwinski, 1985).

The intention of this Chapter is first to re-evaluate the partial slip problem for the case of a circular contact formed between two elastically similar bodies, and in particular to examine the regions of maximum frictional energy expenditure to throw more light on the question of how fretting contacts induce crack initiation. The methodology developed in Chapter 5 will be employed to locate the stick/slip interfaces and the detailed distribution of tangential tractions in terms of both magnitude and direction. The results will then be compared with those using Mindlin's formulation. From this preliminary calculation, the partial slip problem for elastic contact between elastically *dissimilar* bodies will be considered. Both the transitory and steady state solutions will be found, the two dimensional equivalents of which are already known (Nowell *et al.*, 1988). For the contact of elastically dissimilar bodies, it will be assumed that the relative normal displacements of the bodies are not affected by the tangential tractions; i.e. the formulation will be semi-coupled. Thus only the tangential tractions need be found. This assumption is, of course, exactly true for elastically similar contacts and is known as the Goodman approximation for elastically dissimilar ones. It is also exactly true for bodies with dissimilar elastic properties when the Dundurs' constant for the material combination is zero.

8.2 Formulation: Similar materials

First, attention is restricted to the case of contact between elastically similar bodies. Two spheres are pressed into contact by normal load P (see Figure 8.1), giving rise to a

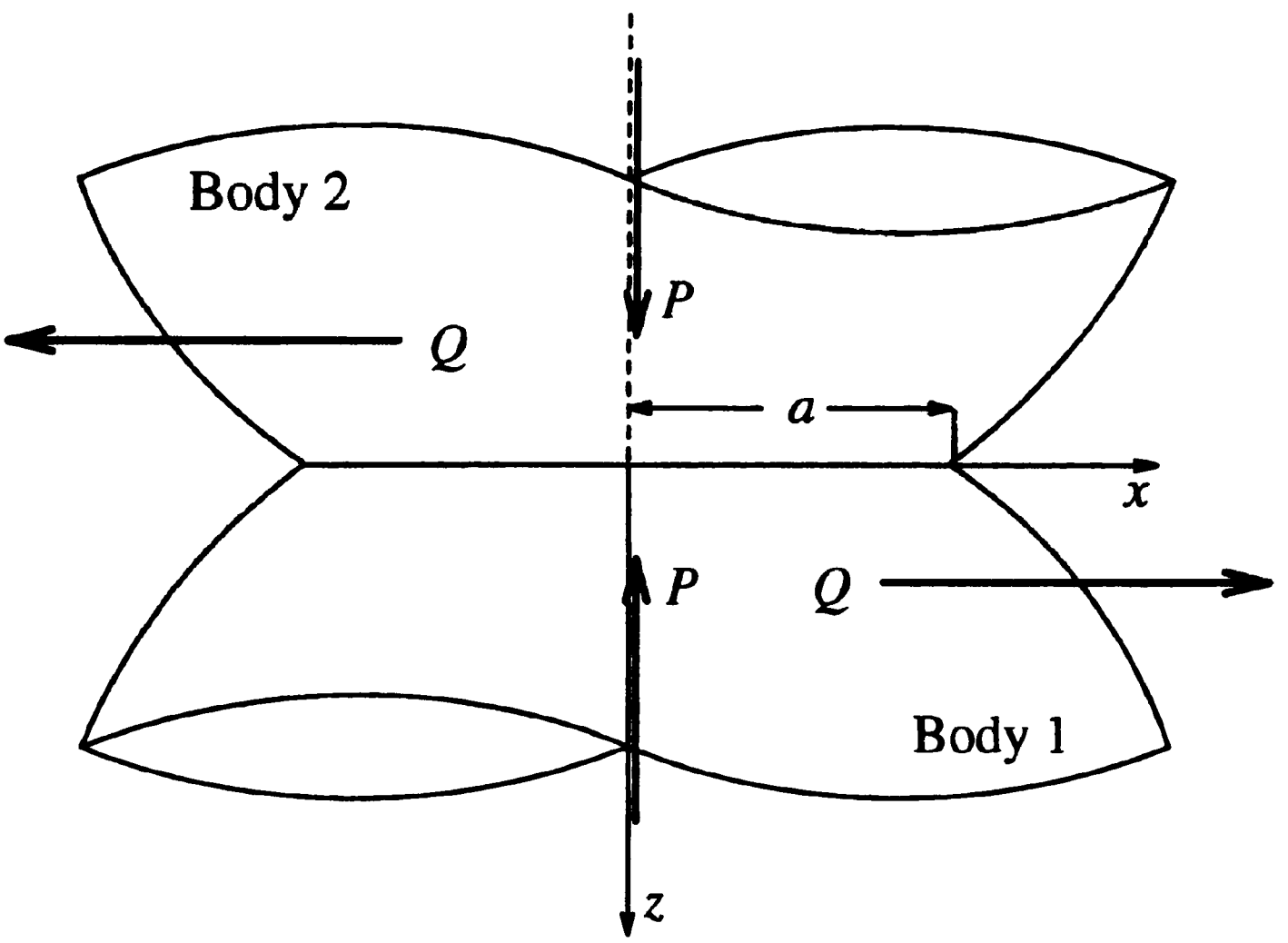

Figure 8.1: Overall geometry of the problem: two spheres pressed together by a normal force P followed by a tangential force Q.

Hertzian pressure distribution:

$$p(x,y) = p_0\sqrt{1-\left(\frac{r}{a}\right)^2} \qquad r^2 = x^2 + y^2 \leq a^2 \tag{8.1}$$

where

$$p_0 = \frac{3P}{2\pi a^2} \tag{8.2}$$

and a is the contact radius. Subsequently, a tangential force Q, whose magnitude is insufficient to cause gross sliding, is applied incrementally to the bodies parallel to the x-axis. A distant point in the undeformed region of one body is thus displaced relative to one in the other by δ_x (symmetry dictates that the relative transverse displacement is zero), whilst at the surface of the lower body, tangential elastic displacements due to the

shearing tractions alone are (Johnson, 1985)

$$u_{x1}(x,y) = \frac{1}{4\pi\mu_1}\int\int_S \left[q_x(\zeta,\eta)\left\{\frac{2(1-\nu_1)}{\rho}+\frac{2\nu_1(\zeta-x)^2}{\rho^3}\right\}-q_y(\zeta,\eta)\frac{2\nu_1(\zeta-x)(\eta-y)}{\rho^3}\right]d\zeta d\eta \tag{8.3}$$

$$u_{y1}(x,y) = \frac{1}{4\pi\mu_1}\int\int_S \left[q_y(\zeta,\eta)\left\{\frac{2(1-\nu_1)}{\rho}+\frac{2\nu_1(\eta-y)^2}{\rho^3}\right\}+q_x(\zeta,\eta)\frac{2\nu_1(\zeta-x)(\eta-y)}{\rho^3}\right]d\zeta d\eta \tag{8.4}$$

where

$$\rho^2 = (\zeta-x)^2+(\eta-y)^2, \tag{8.5}$$

$q_x(x,y)$ and $q_y(x,y)$ are the x and y-components of tangential traction $\mathbf{q}(x,y)$, μ_1 and ν_1 are the modulus of rigidity and Poisson's ratio respectively of body 1, and the region of integration S is the area of contact. Since body 2 has the same elastic properties as body 1 but the tangential tractions act on it in the opposite sense, u_{x2} and u_{y2} are equal in magnitude but of opposite sign to u_{x1} and u_{y1}. Hence, the components of *relative* displacement $\mathbf{s}(x,y)$ within the contact are

$$s_x(x,y) = \delta_x - (u_{x1}-u_{x2}) = \delta_x - 2u_{x1} \tag{8.6}$$

$$s_y(x,y) = -(u_{y1}-u_{y2}) = -2u_{y1} \tag{8.7}$$

It is noted that the contribution to relative tangential displacements resulting from the normal tractions is zero as the bodies are elastically similar. For the same reason, the shearing tractions have no effect upon the pressure distribution and the problem is "uncoupled".

The contact is composed of regions of stick and micro-slip. Within a stick zone the shear tractions cannot exceed the limiting frictional value:

$$|\mathbf{q}(x,y)| \leq fp(x,y), \tag{8.8}$$

where f is the coefficient of Coulomb friction, and for a monotonically increasing shear

force, Q, the relative incremental displacements are zero:

$$\frac{d}{dQ}s_x = 0 \tag{8.9}$$

$$\frac{d}{dQ}s_y = 0. \tag{8.10}$$

Hence, from equations 8.6 and 8.7

$$2\frac{d}{dQ}u_{x1} = \frac{d}{dQ}\delta_x \tag{8.11}$$

$$2\frac{d}{dQ}u_{y1} = 0. \tag{8.12}$$

Within a slip zone the shearing traction takes its limiting value

$$|\mathbf{q}(x,y)| = fp(x,y), \tag{8.13}$$

and opposes the relative incremental displacement, giving the requirement

$$\frac{\mathbf{q}(x,y)}{|\mathbf{q}(x,y)|} = -\frac{d}{dQ}\frac{\mathbf{s}(x,y)}{|\mathbf{s}(x,y)|}. \tag{8.14}$$

This is met when the ratios of the x and y components of the two vectors are equal, which after cross multiplying may be written as:

$$q_x\frac{d}{dQ}s_y - q_y\frac{d}{dQ}s_x = 0, \tag{8.15}$$

and the corresponding components of each vector act in opposite directions, i.e.

$$q_x\frac{d}{dQ}s_x \leq 0 \tag{8.16}$$

$$q_y\frac{d}{dQ}s_y \leq 0. \tag{8.17}$$

It is necessary to find a solution for the tangential tractions subject to the constraints of either 8.8, 8.11 and 8.12 or 8.13, 8.15, 8.16 and 8.17. To achieve this the sequential release method developed in Chapter 5 is employed. First, it is convenient to discretize the contact into a mesh of m square, uniform traction elements of unknown magnitudes

q_{xj}, q_{yj}. The relative displacements at the centre of square i, located at (x_i, y_i), may now be written in discretized form:

$$s_{xi} = \delta_x - \sum_{j=1}^{m} (2I_{ij}^{x1} q_{xj} - 2I_{ij}^{t1} q_{yj}) \tag{8.18}$$

$$s_{yi} = -\sum_{j=1}^{m} (2I_{ij}^{y1} q_{yj} + 2I_{ij}^{t1} q_{xj}) \tag{8.19}$$

where

$$I_{ij}^{x1} = \frac{1}{4\pi\mu_1} \int\int_{\text{square } j} \left(\frac{2(1-\nu_1)}{\rho} + \frac{2\nu_1(\zeta - x_i)^2}{\rho^3} \right) d\zeta d\eta \tag{8.20}$$

$$I_{ij}^{t1} = \frac{1}{4\pi\mu_1} \int\int_{\text{square } j} \frac{2\nu_1(\zeta - x_i)(\eta - y_i)}{\rho^2} d\zeta d\eta \tag{8.21}$$

$$I_{ij}^{y1} = \frac{1}{4\pi\mu_1} \int\int_{\text{square } j} \left(\frac{2(1-\nu_1)}{\rho} + \frac{2\nu_1(\eta - y_i)^2}{\rho^3} \right) d\zeta d\eta. \tag{8.22}$$

These influence functions are recorded in Appendix A.

As the tangential tractions are history-dependent, it is proposed to solve the incremental problem by increasing the load in small finite steps and recording the relative displacements s_{xi}, s_{yi} at the end of each. In fact, the displacement δ_x (whose increments are δ_x^{inc}) is taken as the independent variable; Q_x may be found by integrating over the contact *a posteriori*. At the starting point $\delta_x = 0$, the tangential tractions and hence relative displacements are also zero. Solution proceeds as follows. Each square of the mesh is considered in turn and is initially assumed to be within the stick zone. The tangential tractions are found assuming that discretized versions of equations 8.11 and 8.12 alone are satisfied, i.e.

$$\sum_{j=1}^{m} 2(I_{ij}^{x1} q_{xj} - I_{ij}^{t1} q_{yj}) - s_{xi} = \delta_x^{inc} \tag{8.23}$$

$$\sum_{j=1}^{m} 2(I_{ij}^{y1} q_{yj} + I_{ij}^{t1} q_{xj}) - s_{yi} = 0 \tag{8.24}$$

where s_{xi}, s_{yi} are the relative displacements recorded after the *previous* increment of load.

Noting that $I_{ii}^{t1} = 0$ (the traction acting over a square has no effect on the transverse displacement at its centre) permits these to be rewritten as

$$q_{xi} = \frac{1}{2I_{ii}^{x1}}(\delta_x^{inc} + s_{xi} - \bar{u}_{xi}) \tag{8.25}$$

$$q_{yi} = \frac{1}{2I_{ii}^{y1}}(s_{yi} - \bar{u}_{yi}) \tag{8.26}$$

where

$$\bar{u}_{xi} = \sum_{j=1}^{m\ j\neq i} 2(I_{ij}^{x1} q_{xj} - I_{ij}^{t1} q_{yj}) \tag{8.27}$$

$$\bar{u}_{yi} = \sum_{j=1}^{m\ j\neq i} 2(I_{ij}^{y1} q_{yj} + I_{ij}^{t1} q_{xj}). \tag{8.28}$$

A check is then made to determine whether these tractions meet condition 8.8. If they do they are used to update the current approximation of the traction distribution and the next square is considered; otherwise the assumption was wrong and the square cannot lie within the stick zone. If the square is not stuck, relative slip must occur, so that equation 8.15 must be satisfied, which may written in discretized form as

$$q_{yi}\{\delta_x^{inc} + s_{xi} - (\bar{u}_{xi} + 2I_{ii}^{x1} q_{xi} - 2I_{ii}^{t1} q_{yi})\} - q_{xi}\{s_{yi} - (\bar{u}_{yi} + 2I_{ii}^{y1} q_{yi} + 2I_{ii}^{t1} q_{xi})\} = 0. \tag{8.29}$$

The advantage of using square elements is again evident: shear tractions acting over a square in the x and y-directions have the same influence function for parallel displacements at its centre, i.e. $I_{ii}^{x1} = I_{ii}^{y1}$. Hence, equation 8.28 simplifies to

$$q_{yi} = \left(\frac{s_{yi} - \bar{u}_{yi}}{\delta_x^{inc} + s_{xi} - \bar{u}_{xi}}\right) q_{xi} \tag{8.30}$$

and can be substituted into equation 8.13 with the result

$$q_{xi} = \sqrt{f^2 p_i^2 \left\{1 + \left(\frac{s_{yi} - \bar{u}_{yi}}{\delta_x^{inc} + s_{xi} - \bar{u}_{xi}}\right)^2\right\}^{-1}}. \tag{8.31}$$

The sign of q_{xi} is chosen such that

$$q_{xi}(\delta_x^{inc} + s_{xi} - \bar{u}_{xi}) \leq 0 \tag{8.32}$$

and q_{yi} is found from equation 8.30.

Since the square is experiencing relative slip, the inequalities 8.16 and 8.17 are implied by 8.32 so the solution for the tractions is a valid one. In this way the tractions within each square are evaluated, whether the square is within the stick zone or the region of relative slip, and used to update the current approximation of the complete distribution.

The process is repeated for the whole mesh until convergence is achieved. This can be judged by finding the largest change in magnitude of the shearing traction components after each complete pass. When the solution has been found the relative elastic displacements are recorded at each square, and the method repeated for the next increment of displacement. At any stage, the loads required for the imposed displacement may be found by summing the forces acting on each element. The cumulative density of energy dissipated within the contact may be found by summing the products of the components of relative displacement and tangential tractions at each square within the slip zone: they must be collinear by virtue of equation 8.14.

The efficiency of the procedure may be improved by making use of symmetry. It is obvious that the contact is symmetrical about the x-axis, so $q_x(x,-y) = q_x(x,y)$ and $q_y(x,-y) = -q_y(x,y)$. However, the y-axis provides another line of symmetry. This may be illustrated by defining a set of axes $(\hat{x},\hat{y},\hat{z})$ for body 2 which are in the $(-x,y,-z)$ directions respectively (see Figure 8.2). As the centre of contact is the origin, the spheres may be considered separately as identical problems in the two coordinate sets. Shown in Figure 8.2 are the components of traction acting at (x,y) upon each sphere, revealing that $q_x(-x,y) = q_x(x,y)$ and $q_y(-x,y) = -q_y(x,y)$. Hence, it is necessary to find the tangential tractions for only one quadrant of the mesh and to use these to update the tractions in the other three.

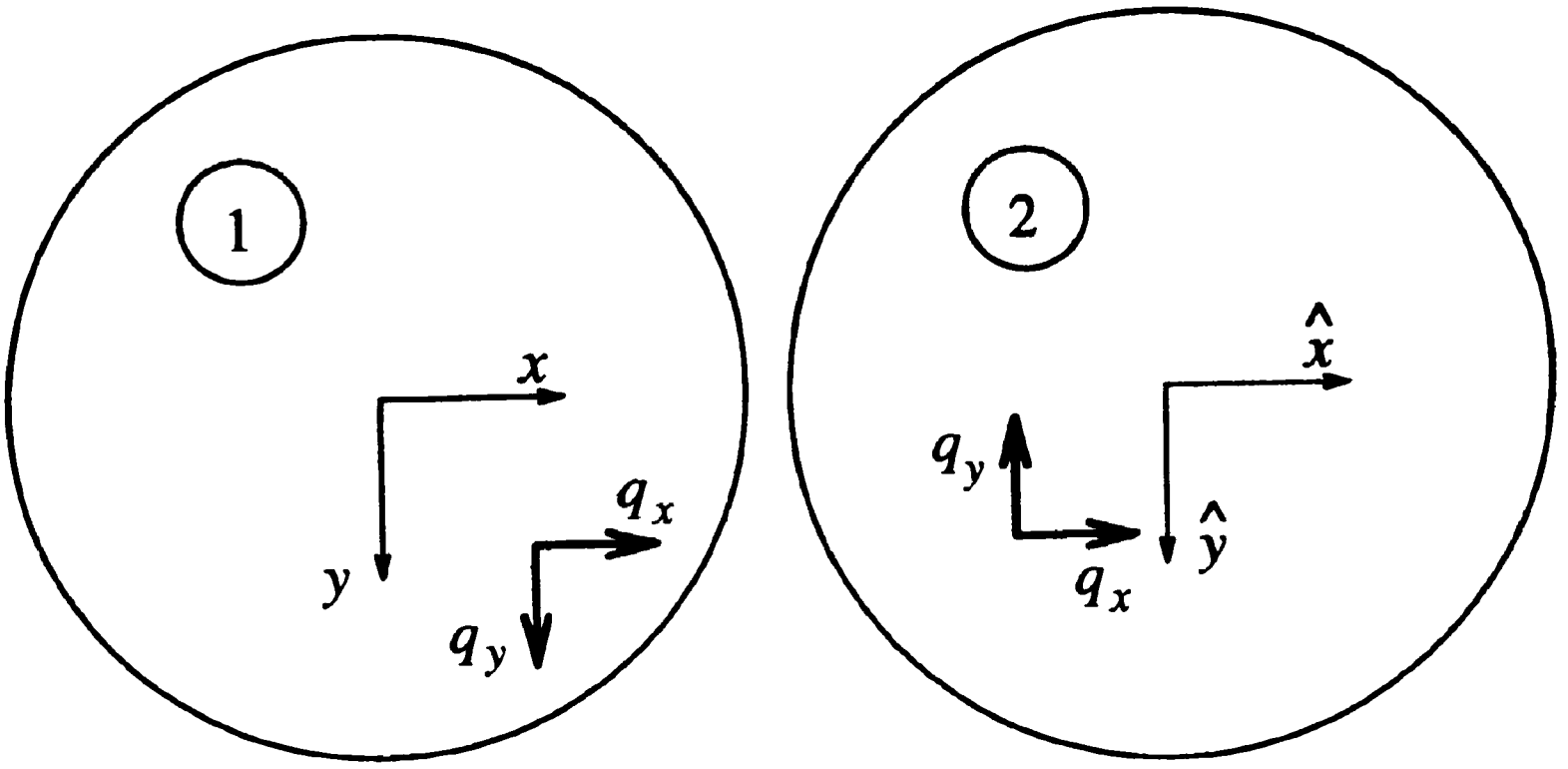

Body 1. Looking along the z-axis.

Body 2. Looking along the -z (or $\hat{z}$)-axis.

Figure 8.2: Plan view of the contact disc of both spheres. Two set of coordinates may be used to exploit symmetry.

8.3 Formulation: Dissimilar materials

The situation is somewhat more complex when two spheres which have dissimilar elastic properties are pressed into contact. In general, there is coupling between the normal and shearing tractions. Any normal tractions within the contact give rise to tangential displacements at the surface of each body in proportion to the combination of material constants $(1-2\nu)/\mu$. If friction is present, shearing tractions are generated at the interface which tend to oppose any relative tangential displacement. These shearing tractions in turn produce normal displacements proportional to the same parameter $(1-2\nu)/\mu$. For two dimensional and axisymmetric contacts *only*, the magnitude of the coupling phenomenon caused by Poisson's effect and difference in the direct compliance, $2(1-\nu)/\mu$, of each body is conveniently quantified by Dundurs' constant

$$\beta = \frac{(1-2\nu_1)/\mu_1 - (1-2\nu_2)/\mu_2}{2(1-\nu_1)/\mu_1 + 2(1-\nu_2)/\mu_2}. \tag{8.33}$$

The present problem falls into neither of these categories and Dundurs' contraction of dissimilar elastic constants cannot immediately be made. This will be discussed more fully later, but first the initial problem of normal loading, which *is* axisymmetric, is considered, as a prelude to the full problem.

It is noted that the limiting value of the shearing tractions is the fraction f of the normal pressure. Hence, when the coefficient of friction is small, the coupling effect of the normal tractions on the tangential ones is much greater than vice-versa. This trend is compounded in normal loading because the tangential tractions are self equilibrating, i.e. have no resultant. This fact may be exploited to make the approximation, first used by Goodman (1962), that the pressure distribution is little different from that given by the Hertz theory. This contact problem has been solved by Spence (1975) and Hills and Sackfield (1987) who found the distribution of shearing tractions, ignoring their effect on the normal pressure, in closed form:

$$\frac{q_r(r)}{fp_0}\mathrm{sgn}\beta = \sqrt{1-r^2} - rH(c-r)\int_r^c \frac{\Psi(t,c)}{t^2\sqrt{1-t^2}}dt \quad 0<r<1 \tag{8.34}$$

where $H(r)$ is Heaviside's step function,

$$\Psi(r,c) = \frac{2wr}{\pi}\Pi(n,\frac{\pi}{2},c'^2) - \frac{2cK(c')}{\pi r}\left\{\frac{w}{c'} - \frac{\ln\frac{1+w}{1-w}}{\ln\frac{1+c}{1-c}}\right\} \tag{8.35}$$

$$w^2 = \frac{c^2-r^2}{1-r^2} \tag{8.36}$$

$$c'^2 = 1-c^2 \tag{8.37}$$

$$n = \frac{1-c^2}{1-w^2} \tag{8.38}$$

and $K(c)$ and $\Pi(n,\frac{\pi}{2},c)$ are the complete elliptic integrals of the first and third kinds respectively. Near the centre of the contact the tangential tractions are below their limiting value and prevent relative slip to radius c, which is related to the material properties by

$$\frac{\beta}{f} = \frac{cK(c')}{\ln\frac{1+c}{1-c}}. \tag{8.39}$$

To determine whether Goodman's approximation can be justifiably made when the tangential load is applied, it is instructive to consider the extreme case of gross sliding between two elastically dissimilar spheres. In Chapter 7 the traction distribution was presented for the case when the product βf is 0.3. Although the difference between this and uncoupled analysis is quite marked, a similar comparison for βf less than 0.1 results in significantly less difference. Hence, for the latter it would be valid to approximate the traction distribution by Hertz's solution, and throughout the cycle of tangential loading, it will be assumed that the normal tractions are given by equation 8.1.

After the normal load has been applied, but prior to any tangential loading, in contrast to the elastically similar problem, a degree of relative prestraining is produced. However, the direction of subsequent shearing tractions depends on the *incremental* change in surface displacements alone, and since the tangential displacements caused by the normal

tractions remain constant, they may be ignored in the subsequent analysis. The tangential tractions do, of course, vary and the initial relative displacements they cause may be found by distributing them over the full mesh and using modified versions of equations 8.18 & 8.19

$$s_{xi} = \delta_x - \sum_{j=1}^{m}\{(I_{ij}^{x1} + I_{ij}^{x2})q_{xj} - (I_{ij}^{t1} + I_{ij}^{t2})q_{yj}\} \tag{8.40}$$

$$s_{yi} = \delta_y - \sum_{j=1}^{m}\{(I_{ij}^{y1} + I_{ij}^{y2})q_{yj} + (I_{ij}^{t1} + I_{ij}^{t2})q_{xj}\} \tag{8.41}$$

where $I_{ij}^{x2}, I_{ij}^{y2}, I_{ij}^{t2}$ are the influence functions associated with body 2.

It is now possible to use the method of solution employed for the previous problem. The only modifications necessary are the inclusion of the effects of the second body; and so the following equations replace 8.25 and 8.26:

$$q_{xi} = \frac{1}{I_{ii}^{x1} + I_{ii}^{x2}}(\delta_x^{inc} + s_{xi} - \bar{u}_{xi}) \tag{8.42}$$

$$q_{yi} = \frac{1}{I_{ii}^{y1} + I_{ii}^{y2}}(s_{yi} - \bar{u}_{yi}) \tag{8.43}$$

where

$$\bar{u}_{xi} = \sum_{j=1}^{m\ j\neq i}\{(I_{ij}^{x1} + I_{ij}^{y2})q_{xj} - (I_{ij}^{t1} + I_{ij}^{t2})q_{yj}\} \tag{8.44}$$

$$\bar{u}_{yi} = \sum_{j=1}^{m\ j\neq i}\{(I_{ij}^{y1} + I_{ij}^{y2})q_{yj} + (I_{ij}^{t1} + I_{ij}^{t2})q_{xj}\}. \tag{8.45}$$

Because the two bodies have elastically dissimilar properties, the y-axis is no longer a line of symmetry, although, the x-axis remains one. In this way the tangential tractions need be evaluated for only one half of the mesh.

8.4 Results: the Mindlin Problem

First, the technique is applied to a re-evaluation of the Mindlin problem for elastically similar bodies. In Mindlin's analysis (Mindlin, 1949), an approximate solution was found by

a superposition of the stress field associated with a sliding Hertzian contact. Specifically, the traction distribution is taken as

$$\tau_{zx}(x,y) = fp_0 \left[\sqrt{1-\left(\frac{r}{a}\right)^2} - \left(\frac{\bar{c}}{a}\right) \sqrt{1-\left(\frac{r}{\bar{c}}\right)^2} \right] \tag{8.46}$$

where $\bar{c}$ is the radius of the stick zone and p_0 the peak Hertzian contact pressure. The stick zone size, $\bar{c}$, is found by imposing equilibrium in the x-direction giving

$$\left(\frac{\bar{c}}{a}\right)^3 = 1 - \frac{Q}{fP}. \tag{8.47}$$

The surface strains and hence displacements within the slip zone corresponding to tractions (8.46) may be found by using the solutions for the state of stress produced by a sliding Hertzian contact (see for example Hamilton and Goodman (1966)). These reveal an inconsistency in that, for non-zero Poisson's ratio, there is a finite relative displacement in the y direction. Johnson (1985) notes that this may be neglected in comparison with the component of relative displacement in the x direction which he approximates as:

$$s_x(r) \approx \frac{3fP}{32a} \left(\frac{2-\nu_1}{\mu_1} + \frac{2-\nu_2}{\mu_2} \right) \left\{ \left(1 - \frac{2}{\pi} \sin^{-1} \frac{\bar{c}}{r}\right) \left(1 - 2\frac{\bar{c}^2}{r^2}\right) + \frac{2}{\pi} \frac{\bar{c}}{r} \left(1 - \frac{\bar{c}^2}{r^2}\right)^{1/2} \right\} \frac{r^2}{a^2} \tag{8.48}$$

This displacement is, of course, independent of θ, and is included in Figure 8.3 which is a comparison of slip, s_x, for two cases of loading: first, for the case when there is incipient sliding, and secondly when the imposed tangential displacement is about 70% of the value at the onset of sliding, which corresponds to a Q/fP value of 0.8. It is exact for components exhibiting no Poisson's effect, i.e. $\nu = 0$. Also shown in Figure 8.3 are the corresponding results using the present numerical method, for the cases when Poisson's ratio is 0.25 and 0.5. The larger value of ν, representing incompressibility, gives rise to the greatest discrepancy between the numerical and Mindlin's solutions. For non-zero values of Poisson's ratio, relative *transverse* displacements result within the slip zone and are maximum along the lines $y = \pm x$. An example is included in Figure 8.3 for incipient

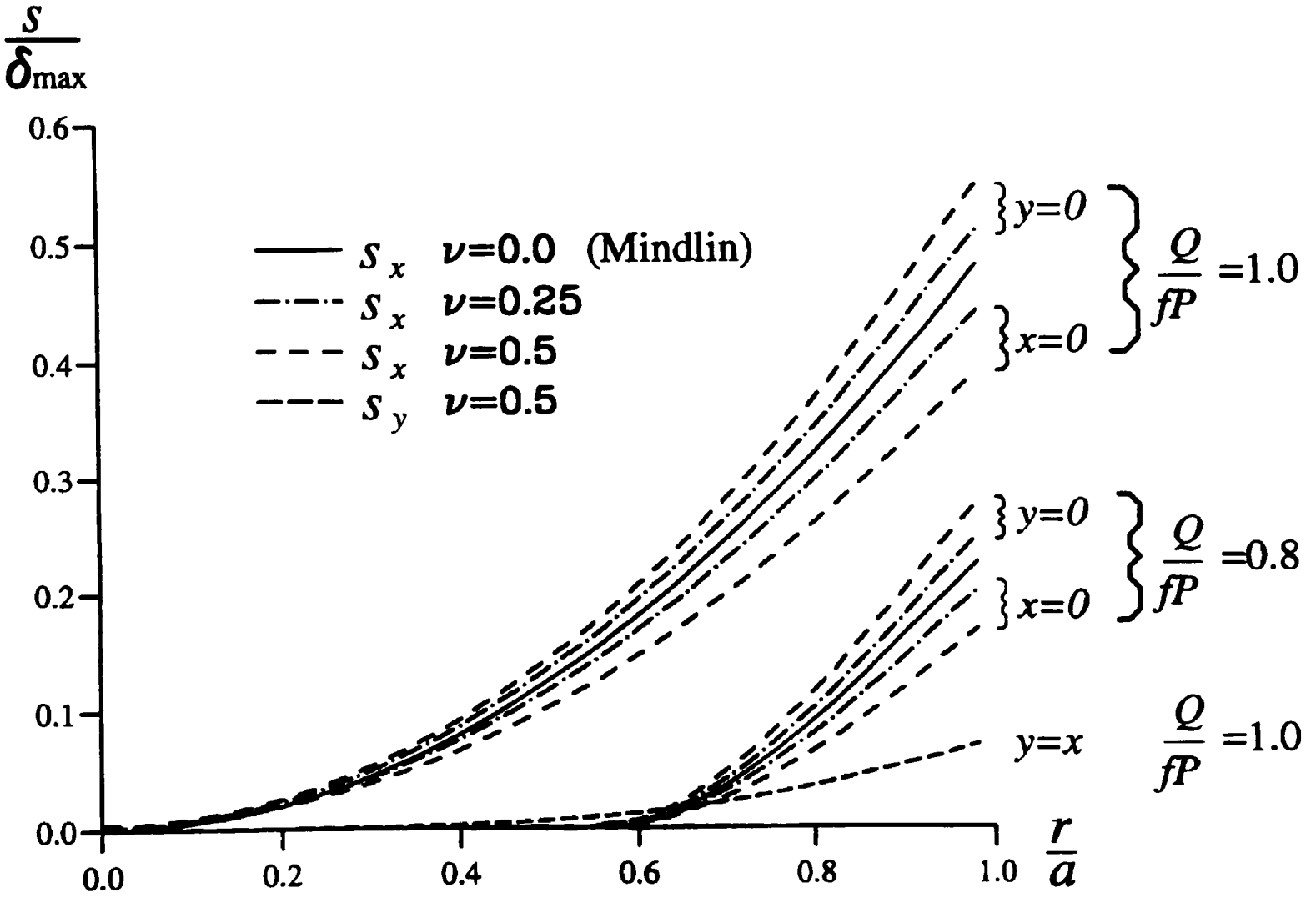

Figure 8.3: Components of relative slip for Mindlin type contact.

sliding with $\nu = 0.5$. The magnitude of the y-displacement at the edge of the contact is 15% of the magnitude of the x-displacement predicted by equation 8.48. Mindlin gave the bulk relative tangential displacement of the two bodies as

$$\delta_{mind} = \frac{3fP}{16a}\left(\frac{2-\nu_1}{\mu_1} + \frac{2-\nu_2}{\mu_2}\right)\left\{1 - \left(1 - \frac{Q}{fP}\right)^{2/3}\right\} \tag{8.49}$$

and the displacements in the Figures are normalised by δ_{max}, which corresponds to δ_{mind} when $Q/fP = 1.0$.

Of course there are no transverse shear tractions in the Mindlin solution, but significant values do arise in the numerical scheme. These are shown, again for an incompressible material, in Figure 8.4, first for incipient sliding (Figure 8.4a) and secondly for the case of $Q/fP = 0.8$ (Figure 8.4b). It will be noted that the maximum transverse tractions occur on the lines $y = \pm x$, and that they are larger in the partial slip case than under incipient sliding conditions.

The overall force-displacement history for a full cycle of shear loading is shown in Figure 8.5. For any value of Poisson's ratio the numerical results are imperceptibly different from the Mindlin approximation. The total energy dissipated during a cycle—equivalent to the area of hysteresis in the Figure—is therefore independent of ν. However, of much greater practical interest in the application of these data to the study of fretting fatigue is the localized density of the frictional energy expenditure $e(x, y)$. In the Mindlin case, because the solution is axisymmetric, the work expended per unit area is also the same along all radial lines. Figure 8.6 shows the frictional work expenditure per cycle in the steady state predicted by the Mindlin solution, for oscillations where Q/fP just reaches unity and $Q/fP = 0.8$. Also shown on the Figure are the values obtained numerically for the two cases along the lines $x = 0$ and $y = 0$. A plot of the energy density over the contact area per cycle for $Q/fP = 1.0$ is given in Figure 8.7. It will be noted that the amount of work dissipated per unit area is about 50% higher in the crescent shaped areas on "either side" of the plane of symmetry compared with the line $x = 0$ itself.

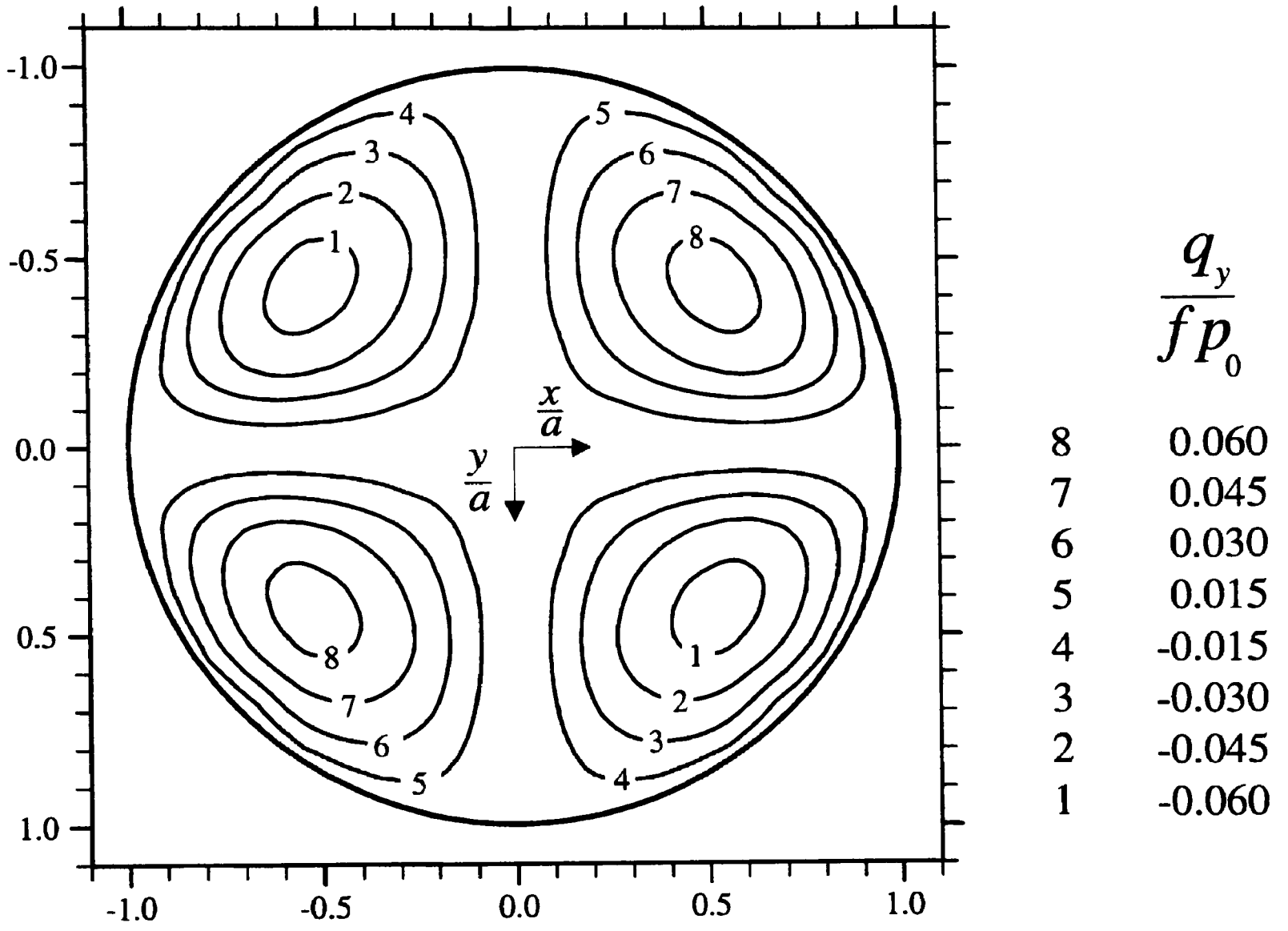

Figure 8.4: Transverse shearing tractions in the contact for two incompressible bodies ($\nu = 0.5$): (a) Incipient sliding.

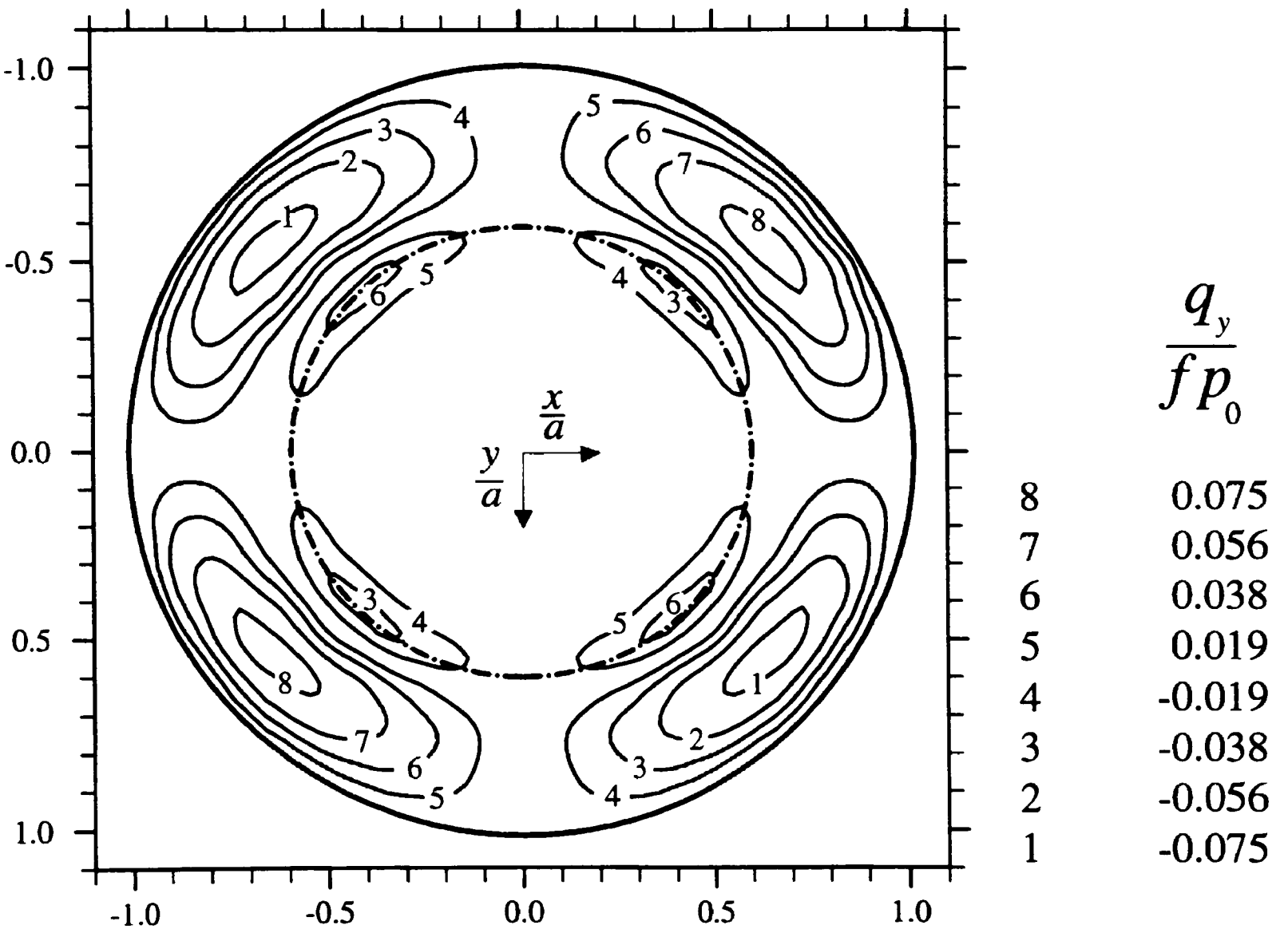

Figure 8.4: (b) $Q/fP = 0.8$. Chain line encloses the stick zone.

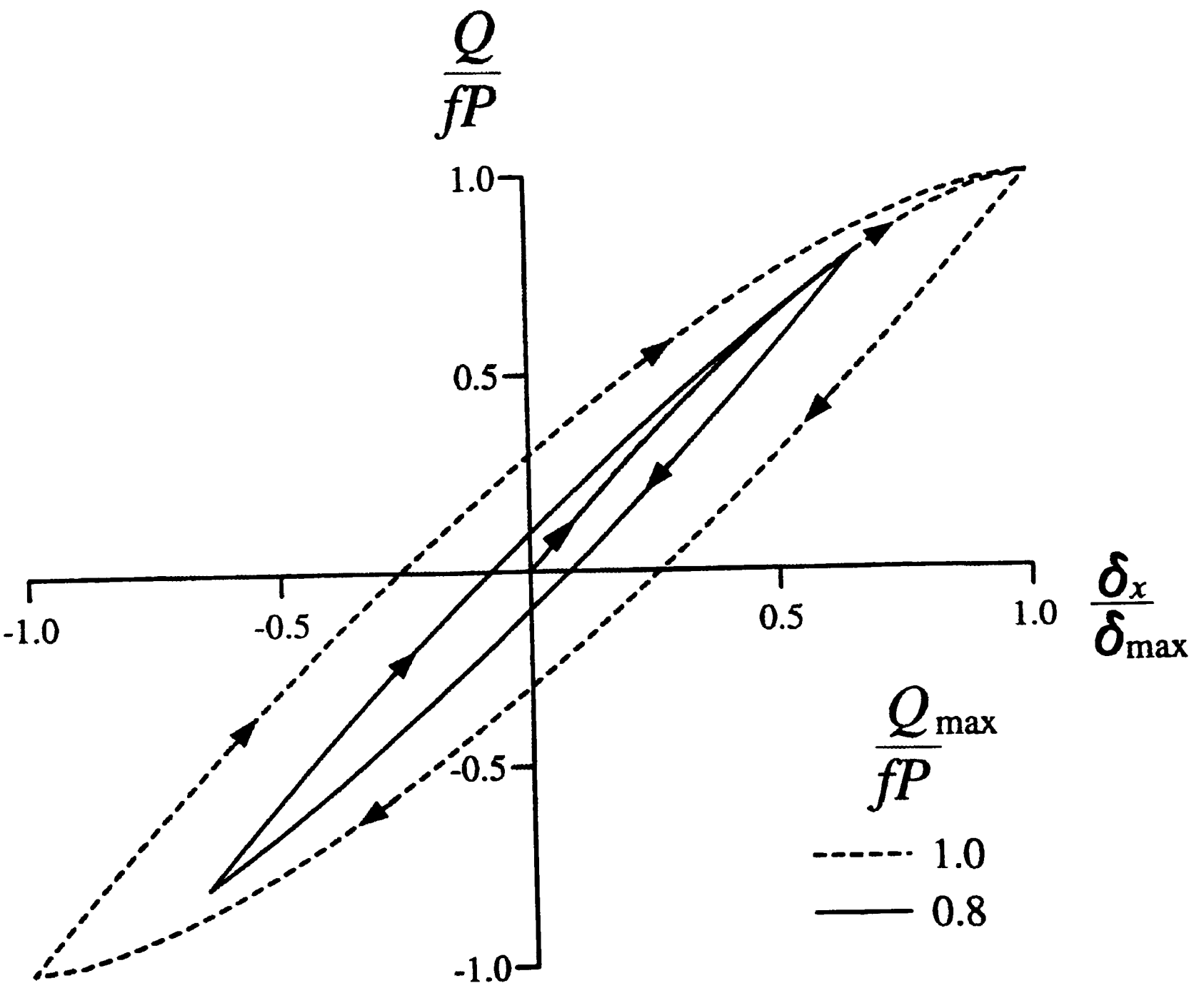

Figure 8.5: Force-displacement history for cyclic loading.

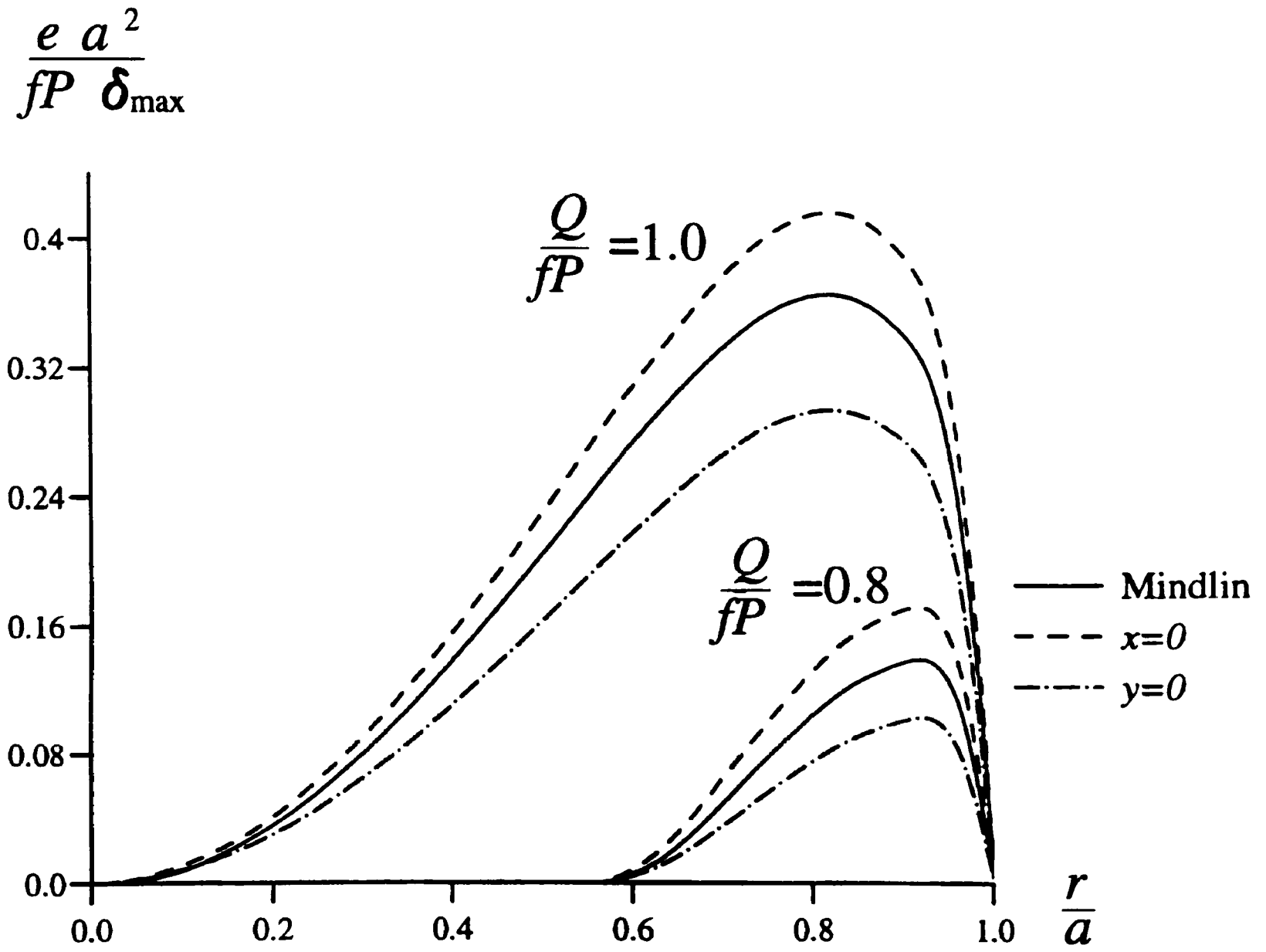

Figure 8.6: Dissipation of energy per cycle along $x = 0$ and $y = 0$ ($\nu = 0.5$).

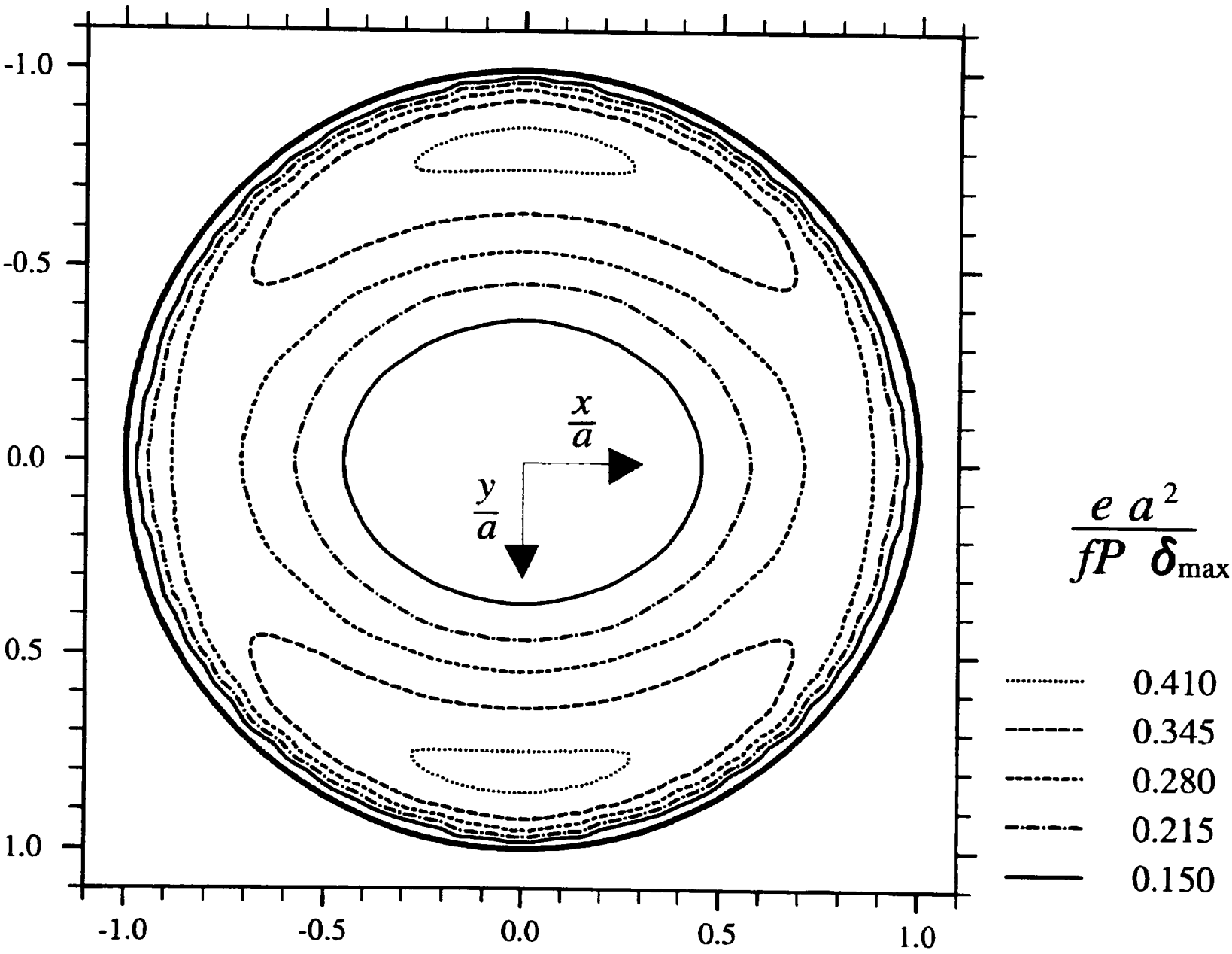

Figure 8.7: Plan of frictional work dissipation for $Q/fP = 1.0$ and $\nu = 0.5$.

Consideration will now be briefly given to the direction of the resultant surface shearing tractions. Although the magnitude of the transverse shear is small, it is not infinitesimal. Figure 8.8 is a plan of the contact disk for $Q/fP = 0.8$ with arrows indicating both the magnitude of the shearing tractions (by the size of the arrow) and their orientation. The most noticeable deviation from the x-direction is within the slip band, approximately along the lines $y = \pm x$.

It may be remarked that a similar phenomenon is observed under sliding conditions: thus whenever two spheres are slid one over the other, the shear traction is oriented exactly opposite the sliding direction *only* if both bodies have a Poisson's ratio of zero. However, a consideration of the factors affecting the direction of slip reveals that the effect is not as great as that in the Mindlin problem (see Chapter 7). If a particle is followed as it passes through the contact in the sliding case, it experiences varying local tractions, which give rise to elastic displacements U_x, U_y that must be added to the gross relative motion of the two bodies. However, these displacements are small and the gradient of relative slip is given by $\partial U_y/\partial x$, which has an order of magnitude of a/R where R is the relative radius of curvature of the contacting bodies and Hertz theory assumes this to be small. In the Mindlin case, it is assumed that the change in position of each particle within the contact is sufficiently small for it to experience no change in normal pressure. This can be justified because, even on the verge of sliding, the normalised rigid body displacement, δ_x/a is of the order of magnitude of a/R. Any relative transverse displacement results from the change in the frictional tractions as the tangential load is increased. Hence, the gradient of relative slip is $(\partial U_y/\partial Q)/(\partial U_x/\partial Q)$, which, in contrast to sliding, is not a second order effect.

8.5 Results: Partial Slip of Dissimilar Bodies

Attention is now turned to the problem of two elastically dissimilar bodies pressed together to form a Hertzian contact and with a subsequent shearing force imposed parallel to the

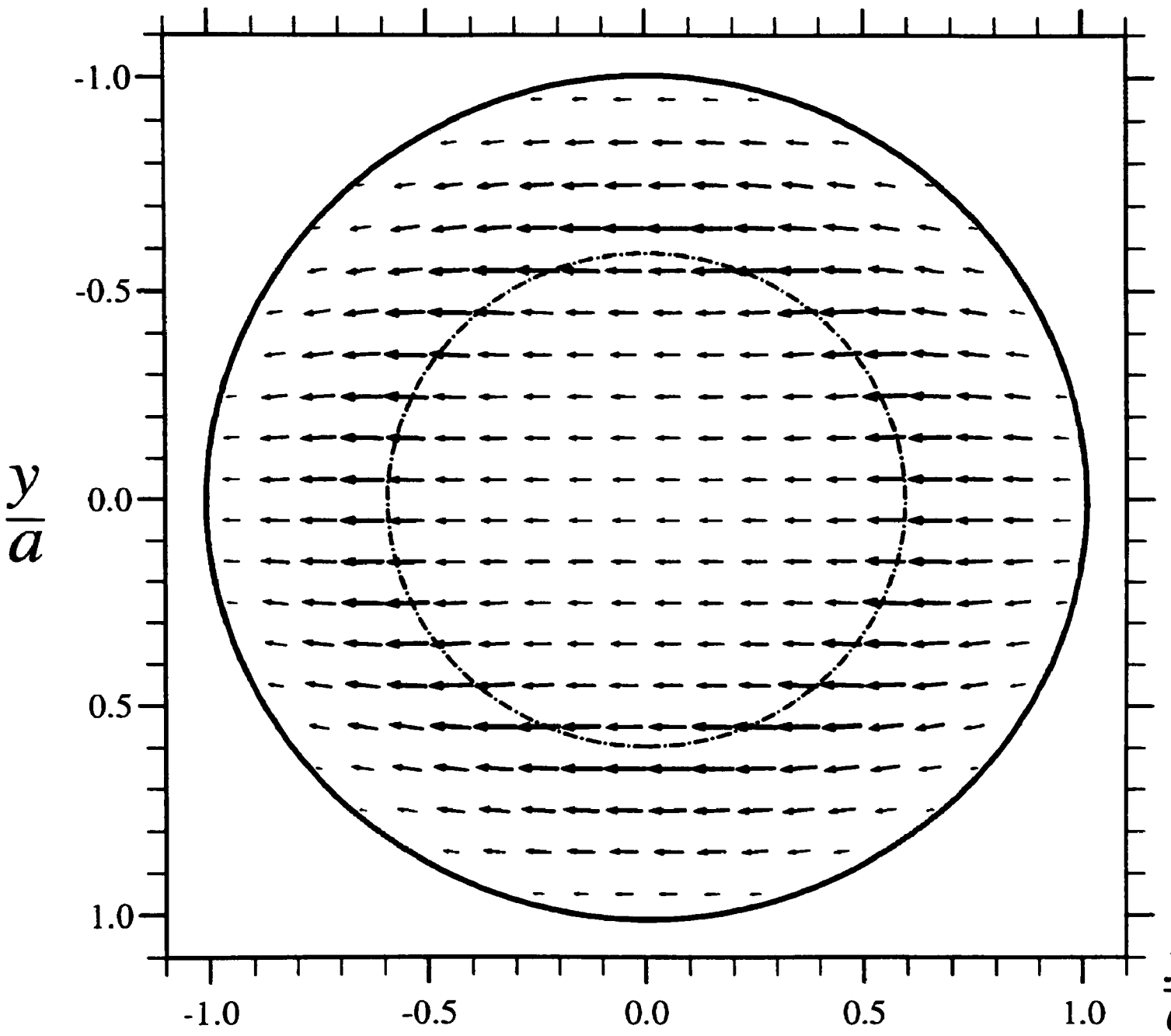

Figure 8.8: Orientation and magnitude of surface shearing tractions under partial slip conditions for $Q/fP = 0.8$ and $\nu = 0.5$.

plane of contact. A previous solution to this problem has been found for the case of plane contact (Nowell *et al.*, 1988) and hence these results concentrate on a nominally axisymmetric contact (although the presence of the shearing tractions may render the actual contact slightly non-circular as was shown in Chapter 7, Figure 7.3). As was stated in the formulation it is assumed that $\beta f < 0.1$ which allows the influence of the shearing tractions on the normal surface displacement to be ignored; hence, the contact pressure remains Hertzian (Goodman, 1962).

The first step in the solution to the problem is to determine the surface traction distribution when the normal contact force only is applied. This is given in equation 8.34 and is associated with an annular region of slip surrounding a circular region of stick. Its radius is $0.485a$ when $\beta/f = 1.0$ and is shown in Figure 8.9 by the broken line. An infinitesimal shear force is then imposed, which gives rise to the stick zone shown by the chain line in Figure 8.9. At the points which were initially outside this new stick zone, the limiting frictional tractions had a component in the *same* direction as the increment of displacement; superimposing an infinitesimal traction opposing the displacement produces a resultant frictional traction which is no longer limiting. As a finite shear force is imposed, the stick zone recedes as indicated.

In order to present a comprehensive set of results, it is essential to consider how the material properties affect the contact problem. To do this it is necessary to write down the full integral equations expressing the relationship between the tractions and relative surface displacements. If, for the time being, *all* the terms are included it can be seen (Johnson, 1985) that

$$\begin{aligned} u_z(x,y) \;=\; & \frac{1}{4\pi}\int\int_S \left[\left(\frac{1-\nu_1}{\mu_1}+\frac{1-\nu_2}{\mu_2}\right)\frac{2}{\rho}p(\zeta,\eta)\right. \\ & \left.-\left(\frac{1-2\nu_1}{\mu_1}-\frac{1-2\nu_2}{\mu_2}\right)\left\{\frac{\zeta-x}{\rho^2}q_x(\zeta,\eta)+\frac{\eta-y}{\rho^2}q_y(\zeta,\eta)\right\}\right] d\zeta\, d\eta \end{aligned} \tag{8.50}$$

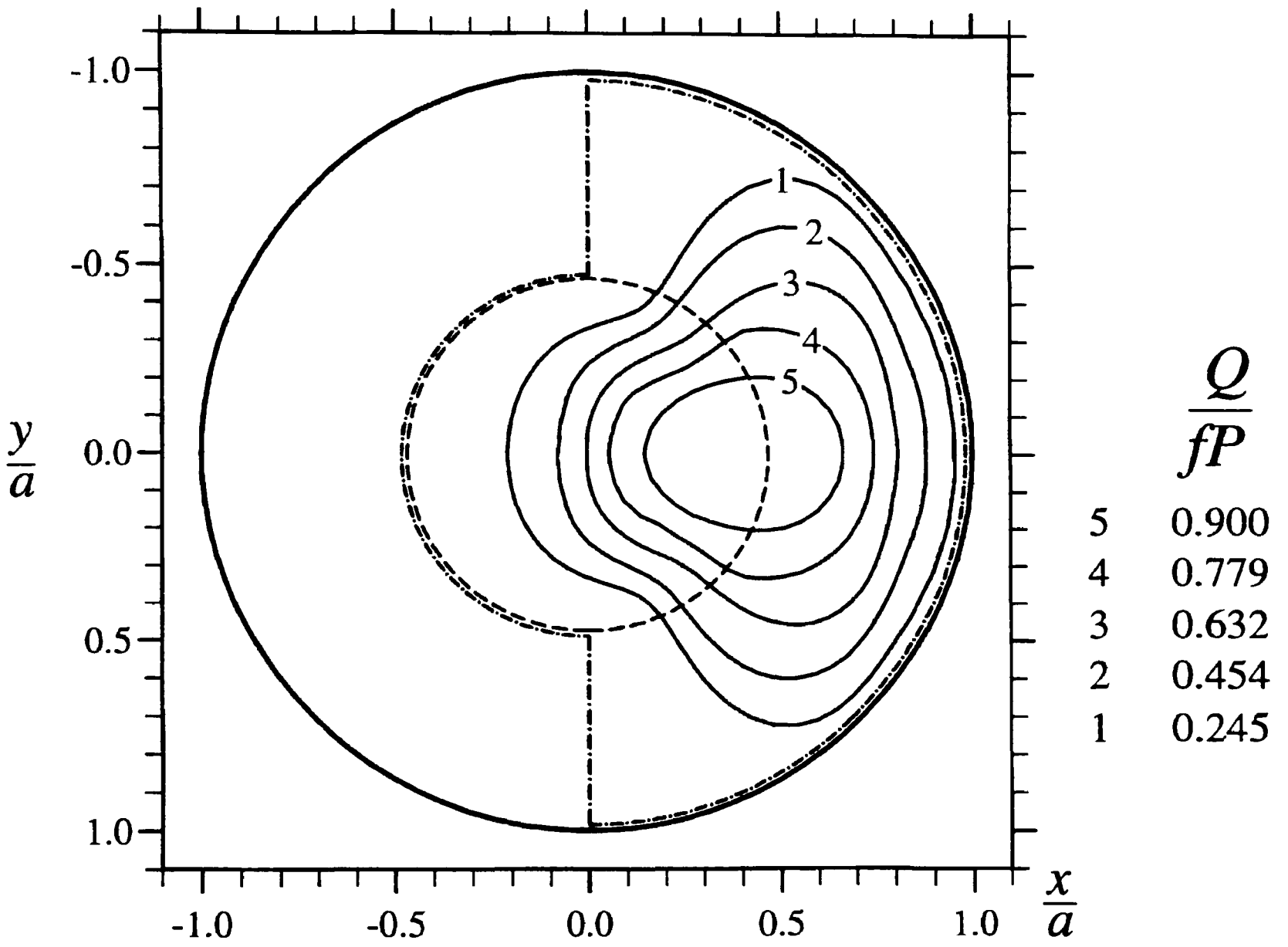

Figure 8.9: Evolution of stick zone for contact between dissimilar elastic materials. Broken line corresponds to normal loading alone and chain line to a subsequent infinitesimal tangential force.

$$u_x(x,y) = \frac{1}{4\pi}\int\int_S \left[\left(\frac{1-\nu_1}{\mu_1}+\frac{1-\nu_2}{\mu_2}\right)\frac{2}{\rho}q_x(\zeta,\eta) + \left(\frac{\nu_1}{\mu_1}+\frac{\nu_2}{\mu_2}\right)\left\{\frac{2(\zeta-x)^2}{\rho^3}q_x(\zeta,\eta) - \frac{2(\zeta-x)(\eta-y)}{\rho^3}q_y(\zeta,\eta)\right\} - \left(\frac{1-2\nu_1}{\mu_1}-\frac{1-2\nu_2}{\mu_2}\right)\frac{\zeta-x}{\rho^2}p(\zeta,\eta)\right] d\zeta d\eta \quad (8.51)$$

$$u_y(x,y) = \frac{1}{4\pi}\int\int_S \left[\left(\frac{1-\nu_1}{\mu_1}+\frac{1-\nu_2}{\mu_2}\right)\frac{2}{\rho}q_y(\zeta,\eta) + \left(\frac{\nu_1}{\mu_1}+\frac{\nu_2}{\mu_2}\right)\left\{\frac{2(\eta-y)^2}{\rho^3}q_y(\zeta,\eta) + \frac{2(\zeta-x)(\eta-y)}{\rho^3}q_x(\zeta,\eta)\right\} - \left(\frac{1-2\nu_1}{\mu_1}-\frac{1-2\nu_2}{\mu_2}\right)\frac{\eta-y}{\rho^2}p(\zeta,\eta)\right] d\zeta d\eta \quad (8.52)$$

These may be normalized by dividing both sides by $p_o aA$ to obtain:

$$\frac{u_z(x,y)}{p_0 aA} = \frac{1}{2\pi p_0 a}\int\int_S \left[\frac{1}{\rho}p(\zeta,\eta) - \beta\left\{\frac{\zeta-x}{\rho^2}q_x(\zeta,\eta)+\frac{\eta-y}{\rho^2}q_y(\zeta,\eta)\right\}\right] d\zeta d\eta \quad (8.53)$$

$$\frac{u_x(x,y)}{p_o aA} = \frac{1}{2\pi p_0 a}\int\int_S \left[\frac{1}{\rho}q_x(\zeta,\eta) + \lambda\left\{\frac{(\zeta-x)^2}{\rho^3}q_x(\zeta,\eta) - \frac{(\zeta-x)(\eta-y)}{\rho^3}q_y(\zeta,\eta)\right\} - \beta\frac{\zeta-x}{\rho^2}p(\zeta,\eta)\right] d\zeta d\eta \quad (8.54)$$

$$\frac{u_y(x,y)}{p_o aA} = \frac{1}{2\pi p_0 a}\int\int_S \left[\frac{1}{\rho}q_y(\zeta,\eta) + \lambda\left\{\frac{(\eta-y)^2}{\rho^3}q_y(\zeta,\eta) + \frac{(\zeta-x)(\eta-y)}{\rho^3}q_x(\zeta,\eta)\right\} - \beta\frac{\eta-y}{\rho^2}p(\zeta,\eta)\right] d\zeta d\eta \quad (8.55)$$

where

$$A = \frac{1-\nu_1}{\mu_1}+\frac{1-\nu_2}{\mu_2} \quad (8.56)$$

$$\lambda = \left(\frac{\nu_1}{\mu_1}+\frac{\nu_2}{\mu_2}\right)/A. \quad (8.57)$$

These equations reveal that the normalised problem is uniquely defined by the two material parameters β and λ, and the friction law relating the shearing tractions to the normal ones (for example a ratio whose limiting coefficient is f).

The present formulation is somewhat more specific than the general one outlined above. In particular, the shearing tractions are assumed to have no influence upon the

normal tractions, which eliminates all but the first term from the integral of equation 8.53 and determines that the frictional tractions (normalised by fp_0) after normal loading depend upon the ratio β/f alone. In addition, the subsequent displacements are evaluated incrementally, which removes the constant normal tractions from equations 8.54 and 8.55, and so the normalised shearing tractions are dependent only upon their previous values and the material parameter λ.

As can be seen from equation 8.49, Mindlin's prediction of the gross relative displacement of the two bodies attempts, in a simple way, to account for material dissimilarity. In order to facilitate the comparison of our results with his, δ_{max} (Mindlin's approximation when $Q/fP = 1.0$) is used as the normalizing length. Quite fortuitously the ratio of $(2-\nu_1)/\mu_1 + (2-\nu_2)/\mu_2$ to A is a linear function of λ, so no further normalization is necessary. The first observed difference of the numerical scheme is a reduction in the stiffness of the contact when the tangential load is applied in a monotonically increasing manner. This property depends critically upon β/f but is unaffected by changing λ. Figure 8.10 shows the displacement resulting from the numerical analysis compared with that given by equation 8.49 as Q/fP is increased for representative values of β/f. When elastically dissimilar spheres are loaded normally and then tangentially, the shear tractions, which are initially radial, retain a radial component as the tangential load is increased; the result is that the bodies experience gross sliding before $Q/fP = 1.0$ and this is responsible for the apparent dramatic reduction in tangential stiffness as sliding is approached. When the tangential load is applied in a cyclic manner the *global* force-displacement characteristic appears to "shakedown" after the first cycle; however, a study of the *local* shear tractions reveals that an actual steady state is not achieved until several more cycles are completed. An example of this is shown in Figure 8.11 where $\beta/f = 1.0$ and

$|Q_{max}/fP| = 0.8$. In every case the modification of the displacement history compared with Mindlin's results (see Figure 8.5 for an example) is independent of λ and depends on the ratio β/f and the magnitude of the tangential force alone. After the first cycle

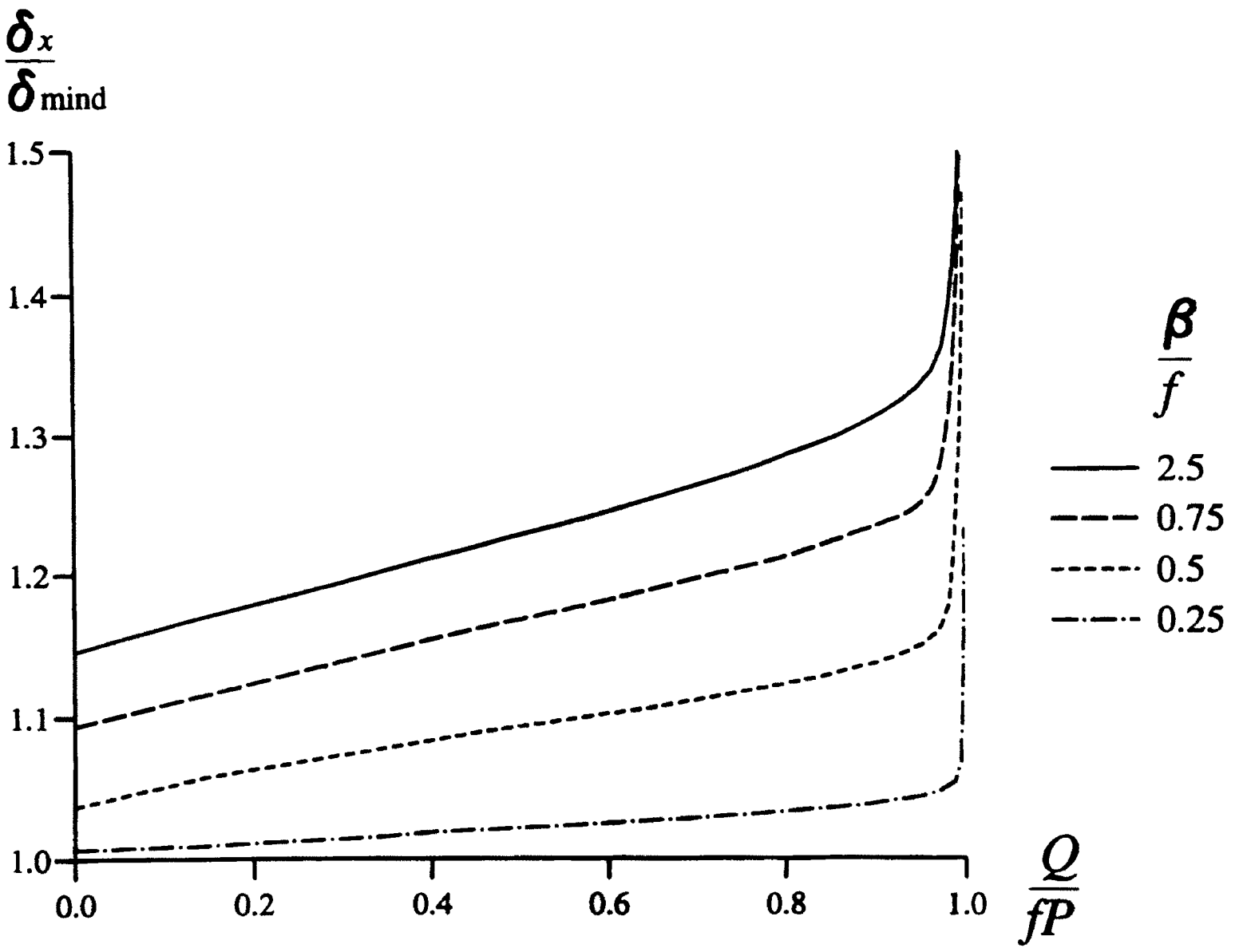

Figure 8.10: Initial tangential compliance of the numerical scheme compared with Mindlin's approximation.

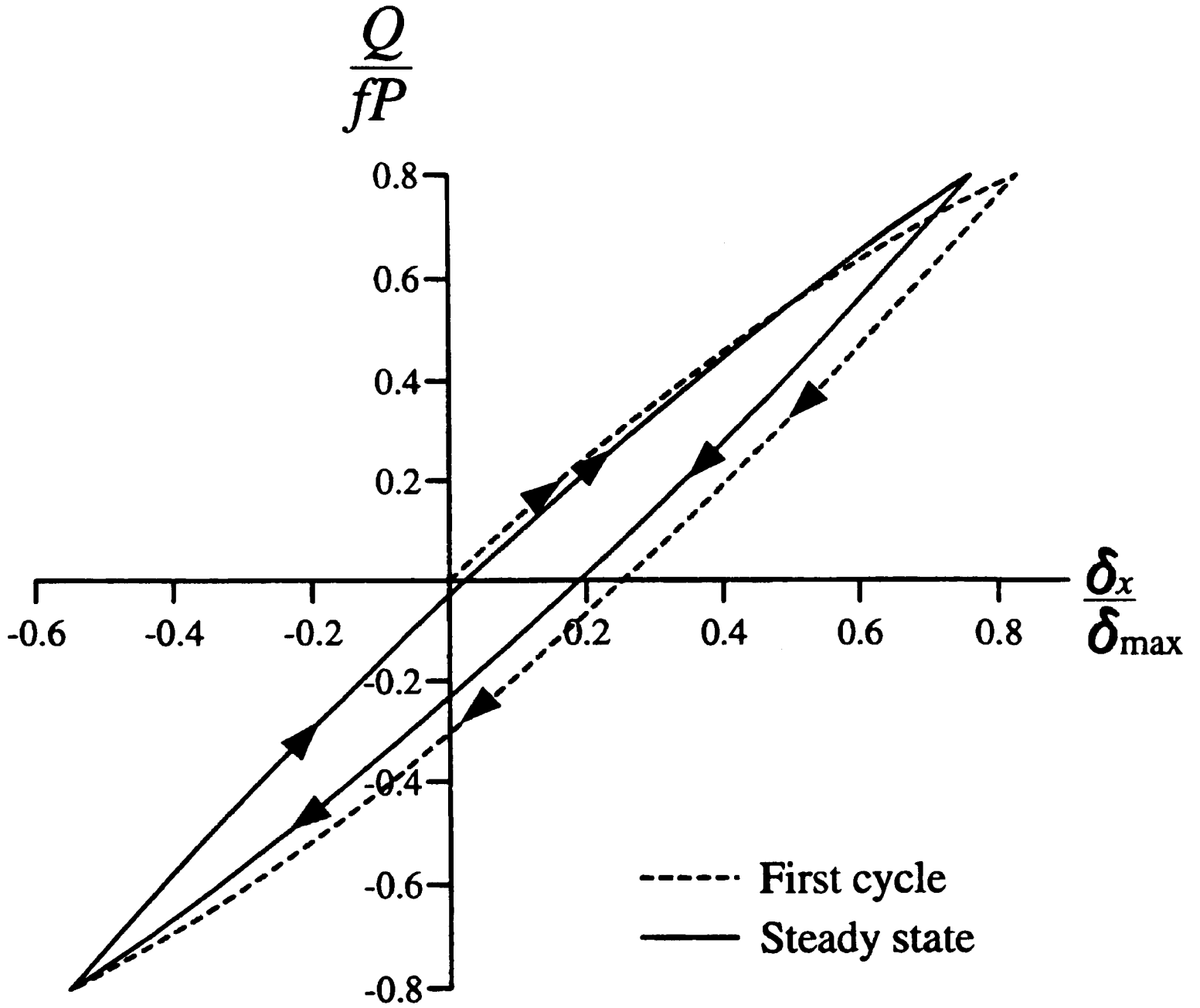

Figure 8.11: Force-displacement history for dissimilar spheres under cyclic tangential loading for $\beta/f = 1.0$ and $|Q_{max}/fP| = 0.8$.

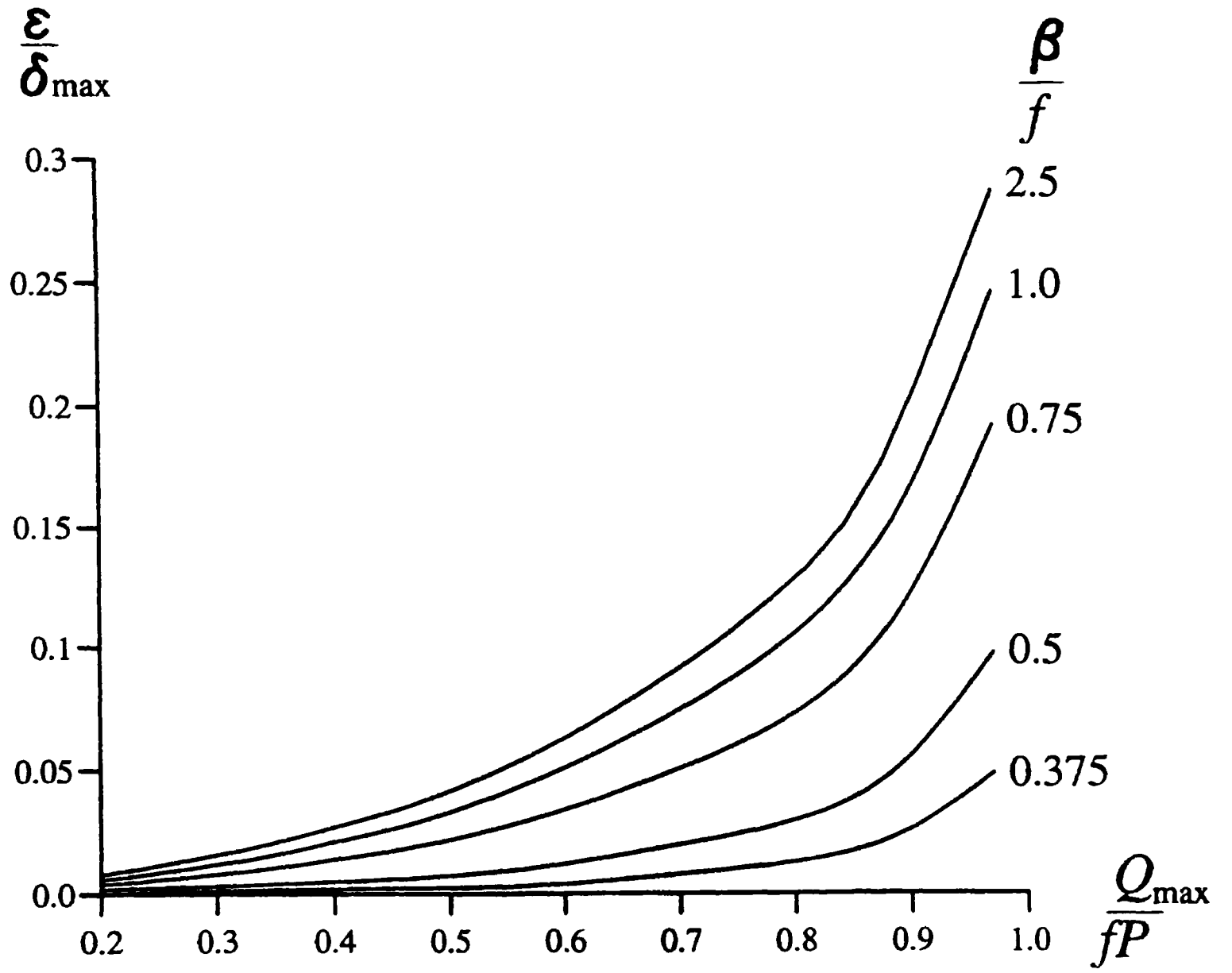

Figure 8.12: Offset of oscillations for cyclic loading after shakedown.

the shearing tractions within the slip zone gradually take up an orientation parallel to the applied load. During this process the magnitude of the oscillations is the same as that predicted by Mindlin. However, the *mid-point* of these oscillations is displaced from the original centre of the contact. In Figure 8.11 this offset ϵ would be defined as the average of δ_x when $Q_{max}/fP = \pm 0.8$. The value of ϵ is shown in Figure 8.12 for a range of values of Q/fP and β/f. After frictional shakedown, the area of the force-displacement hysteresis is identical to Mindlin's approximation. This implies that the normalised total energy dissipated, as in the case of similar materials, is independent of the material properties.

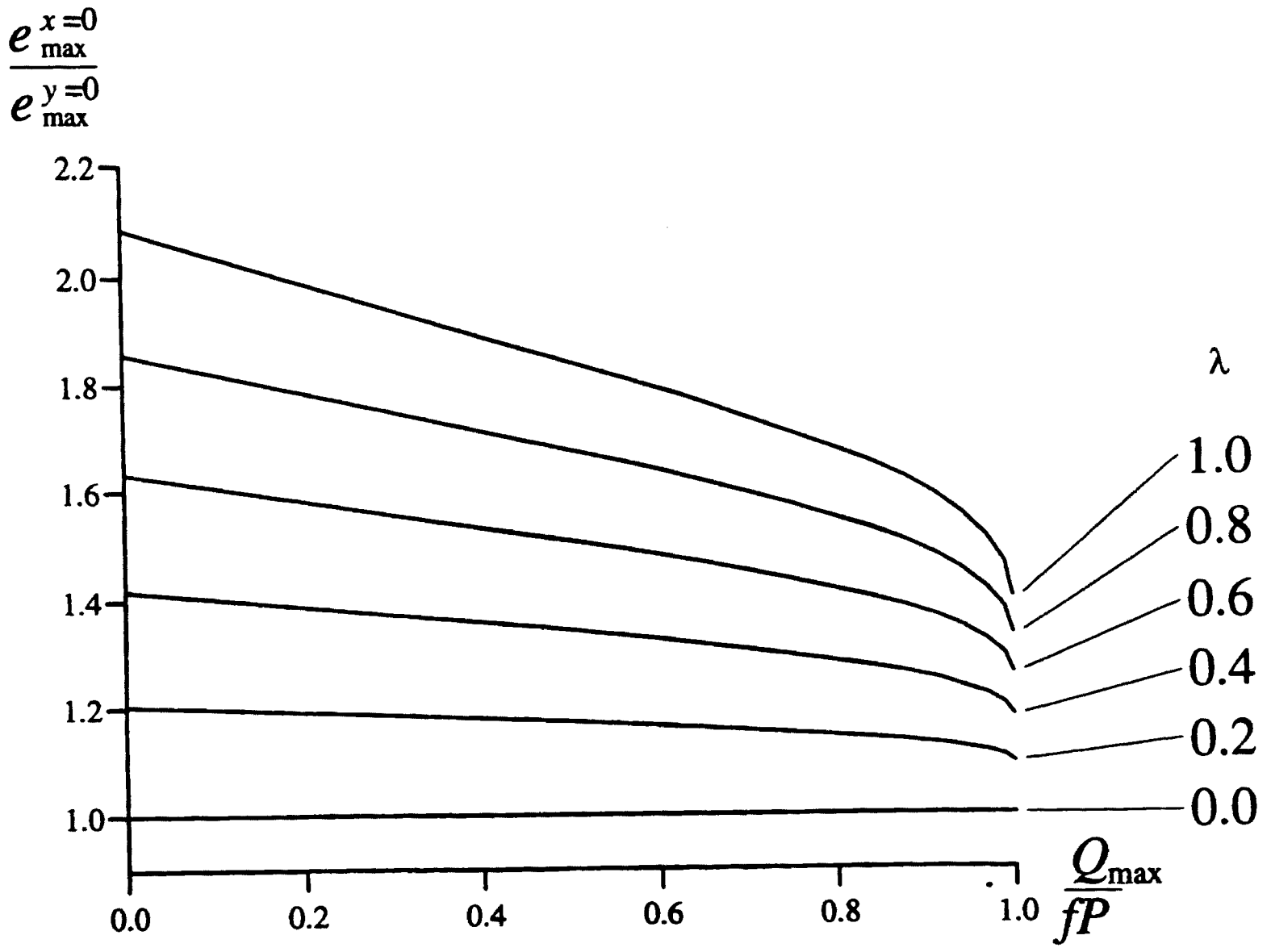

Figure 8.13: Ratio of maximum energy density dissipated per cycle along $x = 0$ and $y = 0$.

However, the *localised* energy density is affected by the material parameter λ, but not β. The ratio of the maxima along the lines $x = 0$ and $y = 0$ is plotted in Figure 8.13 which shows how it increases with λ and decreases with Q_{max}/fP. As this property is not dependent on β, the graph is valid for similar materials.

Finally, Figure 8.14 shows a typical distribution of shear tractions (magnitude and direction) for $\beta/f = 1.0$ and $|Q_{max}/fP| = 0.8$ after 2 complete cycles. This is part of the transition stage between the initial force-displacement response and the steady state. The shape of the stick zone, shown by the chain line, merits further discussion. With each oscillation of the tangential force, the transverse component of tractions within the slip zone is reduced. Initially, this slip zone includes two areas at its edge on each

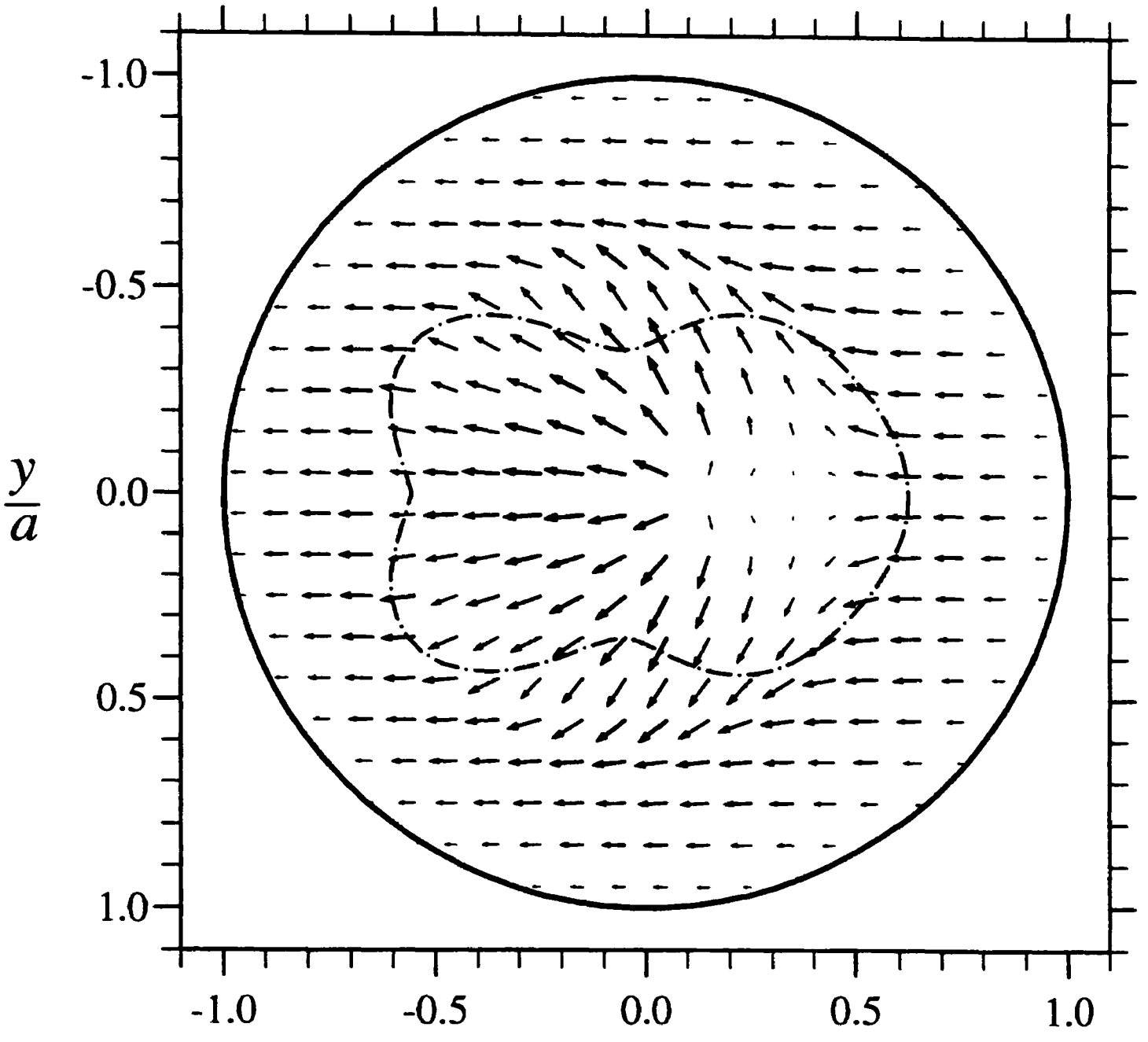

Figure 8.14: Orientation and magnitude of surface shearing tractions after 2 cycles for $\beta/f = 1.0$, $\lambda = 0.0$ and $Q/fP = 0.8$.

side of the axis of symmetry. Within these regions, the remaining radial component of traction is just sufficient to produce minute micro-slip, but insufficient to affect the local energy dissipation or the force-displacement characteristic. Eventually, the tractions there align more closely to the applied tangential load, they no longer experience relative displacement, and the stick zone expands to include them. After about 10 complete cycles, the stick zone adopts the circle predicted by Mindlin. Within the stick zone the shearing tractions retain a radial component, but outside it they are aligned with the tangential force. At this stage the material dissimilarity is in evidence only by the offset of the mid-point of the oscillations; the other properties depend upon λ alone.

8.6 Conclusion

The methodology developed in Chapter 5 has been applied successfully to re-solve the Mindlin type contact. Both the directions and magnitudes of the tangential tractions have been found and the stick/slip interfaces located. Considering, first, the re-evaluation of contact between elastically similar bodies, it is clear that the transverse shear tractions and displacements are not insignificant, and may not safely be ignored in a study of surface damage. The density of frictional energy dissipation is considerably localised either side of the plane of symmetry, in contrast to the Mindlin solution which predicts an axisymmetric dissipation. The tangential compliance is not significantly affected.

Turning to the corresponding problem for contact between dissimilar materials, it is clear that the pre-existing tractions, present after normal indentation, have a profound effect on the stick zone size and location during the first cycle of loading. This ultimately gives rise to an offset force-displacement history. It is noteworthy, however that the ratio β/f has an insignificant effect on the distribution of energy dissipated after the first cycle. In the present formulation of the problem, in which the influence of shearing tractions on surface normal displacements is neglected, the contact pressure remains Hertzian, and it is shown that the solution is characterised by the two dimensionless ratios β/f and

λ. This reduced dependence on the elastic constants permits comprehensive results to be displayed.

Chapter 9

Interactions Between Cracks and Contacts

9.1 Introduction

Many surface controlled failure mechanisms such as wear, rolling contact fatigue and fretting involve the propagation of cracks under the influence of a stress field imposed as a result of contact loading. Such situations have been the subject of much research in recent years as various analytical models have been developed in an attempt to extend the predictions of fracture mechanics to the more complex situations described where severe stress gradients exist in the neighbourhood of the contact loading. Typical of such analyses have been those by Bower (1988) (rolling contact fatigue), Nowell, Hills and O'Connor (1987) (fretting fatigue) and Dubourg (1989) (failure under sliding load). In Chapter 10 a similar analysis will be attempted. Such analyses are concerned with determining the stress intensity factors for a crack under the influence of a stress field resulting from indentation of an elastic half-plane by an indenter of known geometry. A common simplifying assumption made is to split the problem into two distinct halves: first the contact problem itself is solved by considering contact between the indenter and an uncracked half-plane. This permits the use of standard techniques such as those available for Hertzian contact (e.g. (Timoshenko & Goodier, 1970; Sackfield & Hills, 1983)). The stress field resulting from the surface tractions just determined may then be evaluated

by determining the unsatisfied tractions on the crack faces and applying an additional loading to cancel these, thus making use of Beuckner's superposition theorem (1970).

Implicit in the analyses described above is the assumption that the compliance of the half-plane remains unaffected by the presence of the crack so that the surface tractions determined from the analysis of an undamaged half-plane remain valid. This assumption is clearly acceptable when the crack is some distance from the contact but must be called into question when the crack and contact are close, as would be the case in many practical configurations. An important analysis in this area was carried out by Bryant, Miller and Keer (1984) who employed a technique using Muskhelishvili potentials to examine the case of a crack loaded by a rigid cylinder passing over the surface of a half-plane. The analysis included coupling between the crack and the contact so that the increased compliance of the half-plane was taken into account and the pressure distribution modified from that predicted by Hertz (1882). The conclusion of these workers was that the stress intensity factors were little different from those calculated using the uncoupled approximation, the difference never exceeding 10% in the configurations studied by them. These conclusions have been cited by many subsequent authors to support the use of the uncoupled approximation for a range of different geometries.

Recently, however, a number of analyses have been carried out involving a considerable degree of sophistication in the modelling of the crack. Dubourg (1989) has examined the effects of crack closure carefully, and Goshima and Keer (1990) have included thermoelastic effects together with coupling between crack and contact problems, although the frictional heating was taken to be that due to a Hertzian distribution. Such careful modelling is clearly valuable but the case for neglecting the coupling effects must be re-examined when incorporating such a degree of sophistication. In addition a number of experimental investigations (Mouwakeh, 1989; Atkins, 1991) have examined interesting examples of surface failure in which coupling could be significant. In the light of these developments it is appropriate to determine where the effect of coupling is most signifi-

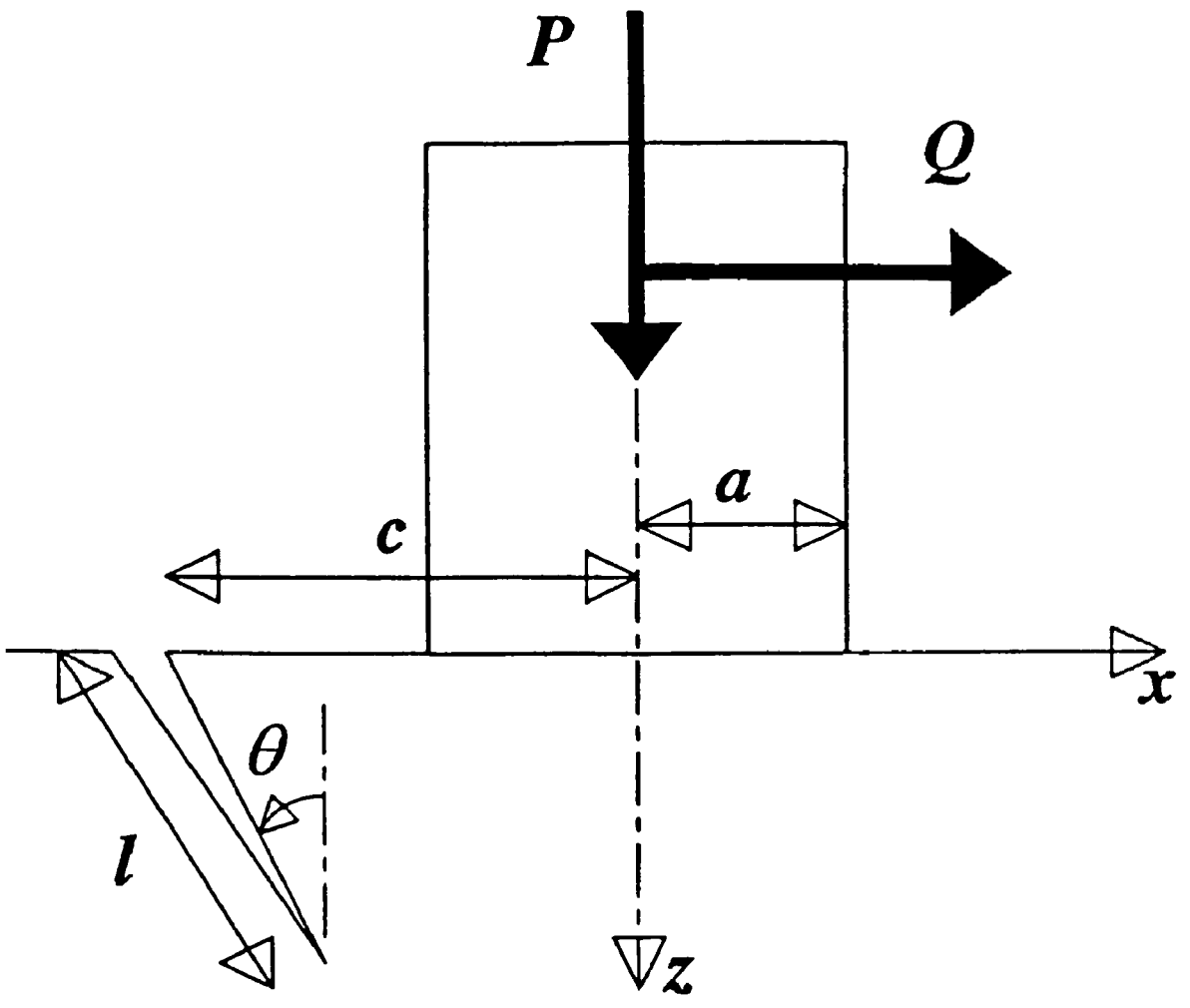

Figure 9.1: Configuration of the problem.

cant and to investigate whether any simple method of approximating the coupling can be determined.

In contrast to Chapter 10, where the contact considered will be Hertzian, a flat ended indenter is used in this Chapter. The main reason for this is that the contact region is well defined and does not depend on the material properties or any change in compliance of the half-space due to the presence of a crack. To avoid any problems associated with the Cauchy nature of the integral equations and the discontinuity at the point of contact between the indenter and each edge of the crack mouth, a finite distance is maintained between them.

9.2 Formulation.

The geometry of the problem to be analyzed is shown in Figure 9.1. A rigid punch, of half-

width a, is sliding in the positive x-direction along an elastic half-plane containing a crack of length l, assumed to be fully open, inclined at an angle θ to the surface normal, with the mouth of the crack located at a distance c from the centre of the indenter. Two co-ordinate sets have been defined: (x, z) with its origin at the centre of the contact interface and a rotated set $(\hat{x}, \hat{z})$ with the $\hat{z}$-axis lying along the crack and an origin located at the mouth of the crack at $(-c, 0)$ expressed in terms of the former axis set. The problem is solved by simultaneously satisfying the boundary conditions at the contact and the crack. The first requires that the surface displacement matches the profile of the indenter; the second requires that the normal and shear tractions at the crack faces vanish. A convenient method of solution is to model the problem by the superposition of two stress fields: the first is due to a continuous distribution of surface tractions at the contact, the second is due to a continuous distribution of displacement discontinuities, or dislocations, along the line of the crack. The resulting integral equations will be discretized using the method of Erdogan et al. (1973) to produce two sets of simultaneous algebraic equations which may be inverted using a computer library routine.

9.2.1 Surface displacements

The first task is to determine the displacement of the surface of an unflawed half-plane by the contact tractions. The effect of the dislocations may then be added by linear superposition. To remove the arbitrary constant of displacement present in any half-plane problem the analysis is formulated in terms of the displacement gradient, and hence the surface displacement gradient $(\partial z/\partial x)_{contact}$ due to a due to a distribution of line tractions between $x = -a$ and $x = a$ may be written for plane strain as (Johnson, 1985):

$$\left(\frac{\partial z}{\partial x}\right)_{contact} = -\frac{1-\nu}{\pi\,\mu}\int_{-a}^{a}\frac{p(\xi)}{x-\xi}\,d\xi + \frac{1-2\nu}{2\mu}q(x) \tag{9.1}$$

where μ and ν are the modulus of rigidity and Poisson's ratio respectively of the elastic half-plane and plane strain is assumed. As the punch is sliding, the shear tractions $q(x)$,

are related to the direct tractions $p(x)$, assuming Coulomb friction, by

$$q(x) = f\, p(x) \tag{9.2}$$

where f is the coefficient of friction between the half-space and the indenter.

For the case of the unflawed half-plane, $(\partial z/\partial x)_{contact}$ is set to the gradient of the indenter, i.e. $(\partial z/\partial x)_{contact} = 0\ |x| \leq 0$, and equation 9.1 may be inverted analytically to give the familiar Boussinesq solution (1885); the introduction of a crack, however, alters the compliance of the half-plane, which may be modelled in the following way; the contact stress field will induce unsatisfied tractions along the line of the crack. These may be cancelled by distributing dislocations along the line of the crack, and, in a solution where interaction between the crack and contact was not permitted, the problem would now be considered solved. However, the displacement field induced by the dislocations modifies the profile of the surface of the half-plane, and this is the manifestation of the change in compliance.

The Airy stress function for a single dislocation of magnitude (b_x, b_z) near the interface of 2 bonded isotropic half-planes with dissimilar elastic properties has been given by Dundurs and Sendeckyj (1965). It is straightforward to deduce the displacement field from this using the stress function-displacement relations given by Dundurs and Mura (1964). The interface may be simplified to a free surface to model the half-plane of the present problem with the dislocation at (x_d, z_d) in terms of the global coordinate set. The displacement gradient at the surface $(\partial z/\partial x)$ is then written as:

$$\left(\frac{\partial z}{\partial x}\right) = D_x(x, x_d, z_d)\, b_x + D_z(x, x_d, z_d)\, b_z \tag{9.3}$$

where

$$D_x = \frac{2(x - x_d)\, z_d^2}{\pi((x - x_d)^2 + z_d^2)^2} \tag{9.4}$$

$$D_z = -\frac{2z_d}{\pi((x-x_d)^2+z_d^2)}\left(1-\frac{(x-x_d)^2}{(x-x_d)^2+z_d^2}\right). \tag{9.5}$$

As the crack is being modelled by distributing dislocations along its length, it is convenient to define the dislocations' Burger's vectors in terms of the rotated co-ordinate set $(\hat{x},\hat{z})$. The functions D_x and D_z may be transformed to $D_{\hat{x}}$ and $D_{\hat{z}}$ by use of a rotation matrix:

$$\begin{pmatrix} D_{\hat{x}} \\ D_{\hat{z}} \end{pmatrix} = \begin{bmatrix} \cos\theta & -\sin\theta \\ \sin\theta & \cos\theta \end{bmatrix} \begin{pmatrix} D_x \\ D_z \end{pmatrix}. \tag{9.6}$$

The surface displacement gradient $(\partial z/\partial x)_{crack}$ of a continuous distribution of dislocations of magnitude $(B_{\hat{x}}(\hat{z}), B_{\hat{z}}(\hat{z})\ 0 \le \hat{z} \le l)$ may be found by integration:

$$\left(\frac{\partial z}{\partial x}\right)_{crack} = \int_0^l \left[D_{\hat{x}}(x,\hat{\zeta})\, B_{\hat{x}}(\hat{\zeta}) + D_{\hat{z}}(x,\hat{\zeta})\, B_{\hat{z}}(\hat{\zeta})\right]\, d\hat{\zeta}. \tag{9.7}$$

where the arguments of the functions are related as follows: $x_d = \hat{\zeta}\sin\theta - c$, $z_d = \hat{\zeta}\cos\theta$.

The two surface displacement gradients due to the crack and the contact may now be superimposed and set equal to the derivative of the profile (ie. the gradient) of the indenter. If the indenter is constrained so that its end-face remains parallel to the free surface of the undeformed half-space, this derivative may be set to zero, hence

$$\left(\frac{\partial z}{\partial x}\right)_{contact} + \left(\frac{\partial z}{\partial x}\right)_{crack} = 0 \qquad |x| \le a, z = 0 \tag{9.8}$$

9.2.2 Crack face tractions

Attention is now turned to the state of stress at the crack. The boundary conditions are met here when the superposition of the component stress fields due to the surface loading and due to the dislocations result in crack faces that are free of normal and shear tractions. First, it is necessary to evaluate the tractions arising along the line of the crack which are induced by the surface loading. To do this, the following standard results will

be used. The stress field within an elastic half-space due to tractions distributed along its surface between $x = -a$ and $x = a$ is (Johnson (1985))

$$\sigma_{xx}(x,z) = -\frac{2z}{\pi}\int_{-a}^{a}\frac{p(\xi)(x-\xi)^2}{R^2}\,d\xi - \frac{2}{\pi}\int_{-a}^{a}\frac{q(\xi)(x-\xi)^3}{R^2}\,d\xi \tag{9.9}$$

$$\sigma_{zz}(x,z) = -\frac{2z^3}{\pi}\int_{-a}^{a}\frac{p(\xi)}{R^2}\,d\xi - \frac{2z^2}{\pi}\int_{-a}^{a}\frac{q(\xi)(x-\xi)}{R^2}\,d\xi \tag{9.10}$$

$$\tau_{xz}(x,z) = -\frac{2z^2}{\pi}\int_{-a}^{a}\frac{p(\xi)(x-\xi)}{R^2}\,d\xi - \frac{2z}{\pi}\int_{-a}^{a}\frac{q(\xi)(x-\xi)^2}{R^2}\,d\xi \tag{9.11}$$

where

$$R = (x-\xi)^2 + z^2. \tag{9.12}$$

Thus, the state of stress along the line of the crack due the indenter may be found, making use of equation 9.2. This then has to be transformed into the rotated axis set $(\hat{x},\hat{z})$ so that the traction components $\tau_{\hat{x}\hat{z}}, \sigma_{\hat{x}\hat{x}}$ may be found. Mohr's circle may be used to provide the necessary rotation and can be expressed conveniently in matrix form:

$$\begin{pmatrix} \sigma_{\hat{x}\hat{x}} \\ \sigma_{\hat{z}\hat{z}} \\ \tau_{\hat{x}\hat{z}} \end{pmatrix} = \frac{1}{2}\begin{bmatrix} 1+\cos 2\theta & 1-\cos 2\theta & -2\sin 2\theta \\ 1-\cos 2\theta & 1+\cos 2\theta & 2\sin 2\theta \\ \sin 2\theta & -\sin 2\theta & 2\cos 2\theta \end{bmatrix}\begin{pmatrix} \sigma_{xx} \\ \sigma_{zz} \\ \sigma_{xz} \end{pmatrix}. \tag{9.13}$$

By distributing appropriate densities of glide and climb dislocations along the length of the crack it is possible to cancel the unsatisfied tractions appearing there. As discussed above, the Airy stress function of a single dislocation (of magnitude (b_x, b_z) at (x_d, z_d)) has been found by Dundurs and Mura (1964). From it the stress field can be derived with the following outcome:

$$s_{xx}(x,z) = \lambda[b_x\,G_{xxx}(x-x_d,z,z_d) + b_z\,G_{zxx}(x-x_d,z,z_d)] \tag{9.14}$$

$$s_{zz}(x,z) = \lambda[b_x\,G_{xzz}(x-x_d,z,z_d) + b_z\,G_{zzz}(x-x_d,z,z_d)] \tag{9.15}$$

$$t_{xz}(x,z) = \lambda[b_x\,G_{xxz}(x-x_d,z,z_d) + b_z\,G_{zxz}(x-x_d,z,z_d)] \tag{9.16}$$

where $\lambda = \mu/\pi(\kappa+1)$, $\kappa = 3-4\nu$ in plane strain, and the functions $G_{ijk}(x-x_d,z,z_d)$ (i denotes the direction of the Burger's vector and jk denote the resulting stress) are

recorded in an appendix of (Nowell & Hills, 1987) (where the use of dislocations to model cracks is described in full). These stresses may be expressed in terms of the rotated coordinate set $(\hat{x}, \hat{z})$ by application of Mohr's circle, as:

$$\begin{pmatrix} s_{\hat{x}\hat{x}} \\ s_{\hat{z}\hat{z}} \\ t_{\hat{x}\hat{z}} \end{pmatrix} = \frac{\lambda}{2} \begin{bmatrix} 1+\cos 2\theta & 1-\cos 2\theta & -2\sin 2\theta \\ 1-\cos 2\theta & 1+\cos 2\theta & 2\sin 2\theta \\ \sin 2\theta & -\sin 2\theta & 2\cos 2\theta \end{bmatrix} \begin{bmatrix} G_{xxx} & G_{zxx} \\ G_{xzz} & G_{zzz} \\ G_{xzx} & G_{zxz} \end{bmatrix} \begin{bmatrix} \cos\theta & \sin\theta \\ -\sin\theta & \cos\theta \end{bmatrix} \begin{pmatrix} b_{\hat{x}} \\ b_{\hat{z}} \end{pmatrix}$$

$$\equiv \begin{bmatrix} K_{\hat{x}\hat{x}\hat{x}} & K_{\hat{z}\hat{x}\hat{x}} \\ K_{\hat{x}\hat{z}\hat{z}} & K_{\hat{z}\hat{z}\hat{z}} \\ K_{\hat{x}\hat{x}\hat{z}} & K_{\hat{z}\hat{x}\hat{z}} \end{bmatrix} \begin{pmatrix} b_{\hat{x}} \\ b_{\hat{z}} \end{pmatrix} \tag{9.17}$$

Hence, a continuous distribution of dislocations $(B_{\hat{x}}(\hat{z}), B_{\hat{z}}(\hat{z}))$ along the $\hat{z}$-axis between $\hat{z}=0$ and $\hat{z}=l$ gives rise to normal and shear stresses along the crack faces:

$$S_{\hat{z}\hat{z}}(\hat{z}) = \int_0^l B_{\hat{x}}(\hat{\zeta})\, K_{\hat{x}\hat{z}\hat{z}}(\hat{z},\hat{\zeta}) + B_{\hat{z}}(\hat{\zeta})\, K_{\hat{z}\hat{z}\hat{z}}(\hat{z},\hat{\zeta})\, d\hat{\zeta} \tag{9.18}$$

$$T_{\hat{x}\hat{z}}(\hat{z}) = \int_0^l B_{\hat{x}}(\hat{\zeta})\, K_{\hat{x}\hat{x}\hat{z}}(\hat{z},\hat{\zeta}) + B_{\hat{z}}(\hat{\zeta})\, K_{\hat{z}\hat{x}\hat{z}}(\hat{z},\hat{\zeta})\, d\hat{\zeta} \tag{9.19}$$

where $K_{\hat{x}\hat{z}\hat{z}}$, $K_{\hat{z}\hat{z}\hat{z}}$, $K_{\hat{x}\hat{x}\hat{z}}$, $K_{\hat{z}\hat{x}\hat{z}}$ are defined in equation 9.17. Their arguments are related to those of the G_{ijk} functions as follows: $x - x_d = (\hat{z}-\hat{\zeta})\sin\theta$, $z = \hat{z}\cos\theta$, $z_d = \hat{\zeta}\cos\theta$. Superimposing the stress field due to the indenter (equation 9.13) and that due to the dislocations (equations 9.18 and 9.19), the crack face boundary conditions are satisfied when

$$S_{\hat{z}\hat{z}}(\hat{z}) + \sigma_{\hat{x}\hat{x}}(\hat{z}) = 0 \tag{9.20}$$

$$T_{\hat{x}\hat{z}}(\hat{z}) + \tau_{\hat{z}\hat{x}}(\hat{z}) = 0 \tag{9.21}$$

at every point along the line of the crack. Equations 9.8, 9.20 and 9.21 form a set of simultaneous integral equations which cannot be solved analytically and so a numerical method must be employed.

9.3 Numerical treatment

Erdogan, Gupta and Cook (1973) describe a method for solving singular integral equations such as those present here. Their method was successfully used to solve a contact problem in Chapter 5. The power and versatility of this method is such that it is possible to incorporate the characteristics of the solution that are anticipated and treat the Cauchy kernels without loss of accuracy. In addition, a solution for the contact tractions and the crack dislocations may be found simultaneously. The continuous traction and dislocation distributions are each approximated by a truncated series of Chebyshev polynomials, where the number of terms in the series corresponds to the order of polynomial employed. For each distribution, it is first necessary to normalize the problem with respect to the region of integration. The application of a Gaussian quadrature formula is then made and additional equations generated to render the problem determinate. Once formulated, the discretized version of the problem is essentially a set of simultaneous, linear, algebraic equations, which may be inverted by a computer library routine. Equations 9.8, 9.20 and 9.21 are three simultaneous integral equations which define three unknown functions, viz. the contact pressure $p(x)$ and the dislocation density functions $B_{\hat{x}}(\hat{z}), B_{\hat{z}}(\hat{z})$. Each equation has both Cauchy and non-Cauchy terms, but it is the former which characterise the kind of solution we expect for each function. Hence, equation 9.8 gives principally the contact pressure distribution (equation 9.1 illustrates the Cauchy integral in terms of the pressure) whilst the dominant parts of equations 9.20 and 9.21 may be found indirectly from the equations for G_{ijk} defined in equations 9.14, 9.15 and 9.16.

9.3.1 Discretization of the surface tractions

The surface tractions will be considered first. Equations 9.1 and 9.2 constitute a singular integral equation of the second kind and may be put in standard form by normalizing

using the substitutions $r=\xi/a$, $s=x/a$, $\tilde{p}=a\,p(x)/P$, where P is the normal load:

$$\left(\frac{\partial z}{\partial x}\right)_{contact} = -\frac{(1-\nu)P}{\pi\,\mu\,a}\int_{-1}^{1}\frac{\tilde{p}(r)}{s-r}\,dr + \frac{(1-2\nu)P}{2\mu\,a}f\,\tilde{p}(s) \tag{9.22}$$

Johnson (1985) presents a solution to this equation when the displacement gradient is zero. This may be used as the basis of a solution to the present problem and assume it has the form:

$$\tilde{p}(s) = (1-s)^{-\frac{1}{2}-\gamma}(1+s)^{-\frac{1}{2}+\gamma}\,\phi'(s) \tag{9.23}$$

where $\cot\pi\gamma = 2(1-\nu)/f(1-2\nu)$ and $\phi'(s)$ is a bounded function. However, it is expected that the value of γ in equation 9.23 will be small and experience has shown that the solution may be well represented by choosing a simpler fundamental solution of the form:

$$\tilde{p}(s) = (1-s)^{-\frac{1}{2}}(1+s)^{-\frac{1}{2}}\,\phi(s) \tag{9.24}$$

permitting the use of the Gauss-Chebyshev quadrature. The discretized form of equation 9.22 becomes:

$$\left(\frac{\partial z}{\partial x}\right)_{contact} = -\frac{(1-\nu)P}{\mu\,a\,n}\sum_{i=1}^{n}\frac{1}{s_k-r_i}\phi(r_i) + \frac{(1-2\nu)P}{2\mu\,a}f\,\tilde{p}(s_k) \tag{9.25}$$

where

$$r_i = \cos\left(\tfrac{2i-1}{2n}\pi\right) \quad i=1,n \tag{9.26}$$

and

$$s_k = \cos\left(\tfrac{k}{n}\pi\right) \quad k=1,n-1. \tag{9.27}$$

A disadvantage of the simplification cited above is that the unknown function (here $\tilde{p}(s)$) is required both at the integration points (in the form $(\phi(r_i))$ and at the collocation

points (as $\tilde{p}(s_k)$). In order to determine the latter, the interpolation formula of Krenk (1975) is required, which gives:

$$\phi(s_k) = \frac{2}{n} \sum_{i=1}^{n} \left(\sum_{j=1}^{n} c_j \right) \phi(r_i) \tag{9.28}$$

where

$$c_j = \begin{cases} \frac{1}{2} & j = 1 \\ \cos\left[\frac{(j-1)k}{n}\pi\right] \cos\left[\frac{(2i-1)(j-1)}{2n}\pi\right] & j > 1. \end{cases} \tag{9.29}$$

Substituting this result into equation 9.25 produces

$$\left(\frac{\partial z}{\partial x}\right)_{contact} = \frac{(1-\nu)P}{\mu\, a\, n} \left[\sum_{i=1}^{m} \left(-\frac{1}{s_k - r_i} + \frac{1-2\nu}{(1-\nu)} f (1 - s_k^2)^{-\frac{1}{2}} \left(\sum_{j=1}^{m} c_j \right) \right) \phi(r_i) \right]. \tag{9.30}$$

The stress field within the half-plane induced by the surface tractions is described by equations 9.9, 9.10 and 9.11 which contain non-Cauchy integrals (except along the line of contact), so that the quadrature used above can be applied there. After normalization with the additional substitutions $t = z/a$ and $T = R/a^2$, and discretization these equations become:

$$\sigma_{xx}(s,t) = -\frac{2P}{a\, n} \sum_{i=1}^{n} \frac{t(s-r_i)^2 + f(s-r_i)^3}{T^2} \phi(r_i) \tag{9.31}$$

$$\sigma_{zz}(s,t) = -\frac{2P}{a\, n} \sum_{i=1}^{n} \frac{t^3 + f\, t^2 (s-r_i)}{T^2} \phi(r_i) \tag{9.32}$$

$$\tau_{xz}(s,t) = -\frac{2P}{a\, n} \sum_{i=1}^{n} \frac{t^2(s-r_i) + f\, t (s-r_i)^2}{T^2} \phi(r_i) \tag{9.33}$$

9.3.2 Discretization of the crack dislocations

The representation of the dislocation distributions is considered next. From physical and mathematical considerations, one would expect the dislocation densities to be unbounded at the crack tip and bounded but non-zero at the mouth, unless the crack mouth is at the edge of the contact. This situation, leading to a singularity at the crack mouth, which is required to balance complementary shear stresses, has been investigated by Korsunsky

(n.d.), but will be avoided here by maintaining a finite space between the mouth of the crack and the contact.

The approximation used in (Nowell & Hills, 1987), in which it was assumed that the dislocation densities fall to zero at the free surface has a negligible effect upon the stress intensity factors at the tip, but does influence the surface displacement, and so cannot be made here. The modification devised by Dewynne (n.d.) will be employed and will now be described briefly.

First, equations 9.18 and 9.19 are written in standard form by use of the substitutions $v = (2\hat{z}/l) - 1$ and $u = (2\hat{\zeta}/l) - 1$

$$S_{\hat{z}\hat{z}}(v) = \int_{-1}^{1} B_{\hat{x}}(u)\, K_{\hat{x}\hat{z}\hat{z}}(v,u) + B_{\hat{z}}(u)\, K_{\hat{z}\hat{z}\hat{z}}(v,u)\, du \tag{9.34}$$

$$T_{\hat{x}\hat{z}}(v) = \int_{-1}^{1} B_{\hat{x}}(u)\, K_{\hat{x}\hat{x}\hat{z}}(v,u) + B_{\hat{z}}(u)\, K_{\hat{z}\hat{x}\hat{z}}(v,u)\, du. \tag{9.35}$$

The dislocation densities are then written in the usual way as the product of an unknown function $\psi(v)$ and the relevant weighting function $(1+v)^{1/2}(1-v)^{-1/2}$. However, an additional term is suggested by Dewynne (n.d.), which is a triangular distribution of magnitude $\Delta/2(1-v)$, where Δ is an unknown constant.

The use of Gauss-Jacobi quadrature permits equations 9.34 and 9.35 to be discretized, which become:

$$\begin{aligned} S_{\hat{z}\hat{z}}(v_k) &= \sum_{i=1}^{m} \frac{2\pi}{2m+1}(1+u_i)\left[K_{\hat{x}\hat{z}\hat{z}}(v_k,u_i)\,\psi_{\hat{x}}(u_i) + K_{\hat{z}\hat{z}\hat{z}}(v_k,u_i)\,\psi_{\hat{z}}(u_i)\right] \\ &\quad + \frac{\Delta_{\hat{x}}}{2}\int_{-1}^{1} K_{\hat{x}\hat{z}\hat{z}}(v_k,u)(1-u)\,du + \frac{\Delta_{\hat{z}}}{2}\int_{-1}^{1} K_{\hat{z}\hat{z}\hat{z}}(v_k,u)(1-u)\,du \end{aligned} \tag{9.36}$$

$$\begin{aligned} T_{\hat{x}\hat{z}}(v_k) &= \sum_{i=1}^{m} \frac{2\pi}{2m+1}(1+u_i)\left[K_{\hat{x}\hat{x}\hat{z}}(v_k,u_i)\,\psi_{\hat{x}}(u_i) + K_{\hat{z}\hat{x}\hat{z}}(v_k,u_i)\,\psi_{\hat{z}}(u_i)\right] \\ &\quad + \frac{\Delta_{\hat{x}}}{2}\int_{-1}^{1} K_{\hat{x}\hat{x}\hat{z}}(v_k,u)(1-u)\,du + \frac{\Delta_{\hat{z}}}{2}\int_{-1}^{1} K_{\hat{z}\hat{x}\hat{z}}(v_k,u)(1-u)\,du \end{aligned} \tag{9.37}$$

where

$$u_i = \cos\left(\frac{2i+1}{2m+1}\pi\right) i = 1, m \tag{9.38}$$

and

$$v_k = \cos\left(\frac{2k}{2m+1}\pi\right) k = 1, m. \tag{9.39}$$

The surface displacement gradient resulting from the dislocations is described by equation 9.7. As with the equations describing stress field induced by the surface tractions, this integral is non-Cauchy, so the quadrature employed above may be used to evaluate it. After normalization and discretization, equation 9.7 becomes:

$$\begin{aligned}\left(\frac{\partial z}{\partial x}\right)_{crack} &= 2l\sum_{i=1}^{m}(D_{\hat{x}}(x,u_i)\,\psi_{\hat{x}}(u_i) + D_{\hat{z}}(x,u_i)\,\psi_{\hat{z}}(u_i)) \\ &\quad + l\,\Delta_{\hat{x}}\int_{-1}^{1} D_{\hat{x}}(x,u)(1-u)\,du + l\,\Delta_{\hat{x}}\int_{-1}^{1} D_{\hat{x}}(x,u)(1-u)\,du \end{aligned} \tag{9.40}$$

The remaining integrals in equations 9.36, 9.37 and 9.40 may be evaluated numerically by a computer library routine.

9.3.3 Additional equations

The number of unknown functions and variables that have been generated by the above analysis are now reviewed. The continuous distribution of surface tractions has been discretized to a series of Chebyshev polynomials $\phi(r_i)$ with n terms. The dislocations have been similarly discretized to two series of Chebyshev polynomials $\psi_{\hat{x}}(u_i), \psi_{\hat{z}}(u_i)$ with m terms each and two triangles of magnitude $\Delta_{\hat{x}}, \Delta_{\hat{z}}$ at the mouth of the crack.

The discretization process has generated $n-1$ equations for the condition of a compatible surface displacement gradient beneath the indenter and $2m$ equations for the requirement that the crack faces be free of tractions. Therefore, three side conditions are needed to render the overall problem determinate.

Equilibrium considerations generate the equation:

$$\int_{-a}^{a} p(x)\,dx = P, \tag{9.41}$$

which, after normalization and discretization, becomes:

$$\sum_{i=1}^{n} \frac{\pi}{n}\phi(r_i) = 1. \tag{9.42}$$

Two further equations may be generated by forcing $\psi_{\hat{x}}(v)$ and $\psi_{\hat{z}}(v)$ to zero as $v \to -1$; the validity of this is proved by Dewynne (n.d.). Krenk's formulae (1975) provide the necessary interpolation to find the values of $\psi_{\hat{x}}$ and $\psi_{\hat{z}}$ at $v=-1$:

$$\psi(-1) = \sum_{i=1}^{m} \psi(u_{m+1-i}) \sin\left(\frac{2m-1}{2m+1}\pi\right) / \sin\left(\frac{i}{2m+1}\pi\right) \tag{9.43}$$

The equations may now be inverted by a computer library routine as a set of simultaneous linear equations.

9.3.4 Evaluation of stress intensity factors

Once the distributions of dislocations have been found, the stress intensity factors at the crack tip may be found by interpolation (see Krenk (1975) for proof).

$$K_I = 2\sqrt{2\pi l}\frac{\mu}{\kappa+1}\psi_{\hat{x}}(1) \tag{9.44}$$

$$K_{II} = 2\sqrt{2\pi l}\frac{\mu}{\kappa+1}\psi_{\hat{z}}(1) \tag{9.45}$$

where

$$\psi(1) = \frac{2}{2m+1}\sum_{i=1}^{m} \psi(u_i)\cot\left(\frac{2i-1}{2(2m+1)}\pi\right)\sin\left(\frac{m(2i-1)}{2m+1}\pi\right) \tag{9.46}$$

9.4 Results and conclusions

Using the method described above, the following results were found: mode I and mode II stress intensity factors for a range of crack lengths and orientations. For comparison, three

loading conditions were considered: a) a Boussinesq traction distribution (corresponding to an uncoupled solution); b) tractions developed by the indentation of an unflawed half-plane where coupling was considered between the normal and shear tractions (whose analytic result can be found in (Johnson, 1985)); c) tractions where coupling was considered between the half-plane and the indenter and interactions between the crack and the contact were permitted. In every calculation, the half-plane was assumed to have a Poisson's ratio of 0.3. The coefficient of friction was given the value of 0.75, which is about the largest one would expect in practice and which ensures that the crack remains open to the root, thereby producing the maximum change in compliance.

Figures 9.2 and 9.3 respectively show the mode I and mode II stress intensity factors for a crack of length $\frac{1}{2}a$ at various angles of inclination to the z-axis and a range of distances from the centre of the contact.It can be seen that for each geometry the difference between the three solutions is small and that any difference between solutions of coupled and uncoupled contacts is emphasised when interactions between crack and contact are included. Figure 9.4 shows a comparison of K_I for a vertical crack of varying length at a distance $0.05a$ outside the edge of the contact for each loading condition, and Figure 9.5 shows a similar comparison for a crack angled at -45^o. It can be seen that for a small range of crack lengths although the uncoupled solution significantly underestimates the coupled solution, there is very little additional difference when interactions between crack and contact are included. The largest difference in mode I and mode II stress intensity factors produced through taking account of the interactions between crack and contact occurs for medium length cracks. When the crack is small and hence the crack tip is very near to the corner of the indenter, the change in compliance produced by the presence of the crack is negligible. As a result interactions between small cracks and contacts do not affect the stress intensity factors[1]. Larger cracks produce a much greater change in the compliance

[1]The mode I stress intensity factor for a very small, surface breaking, vertical crack may be written $K_I = 1.1215\sigma_{xx}\sqrt{\pi l}$. The difference in the order of the singularity between the coupled and Boussinesq traction distributions for a coefficient of friction of 0.75 results in a maximum increase in σ_{xx} of 15%

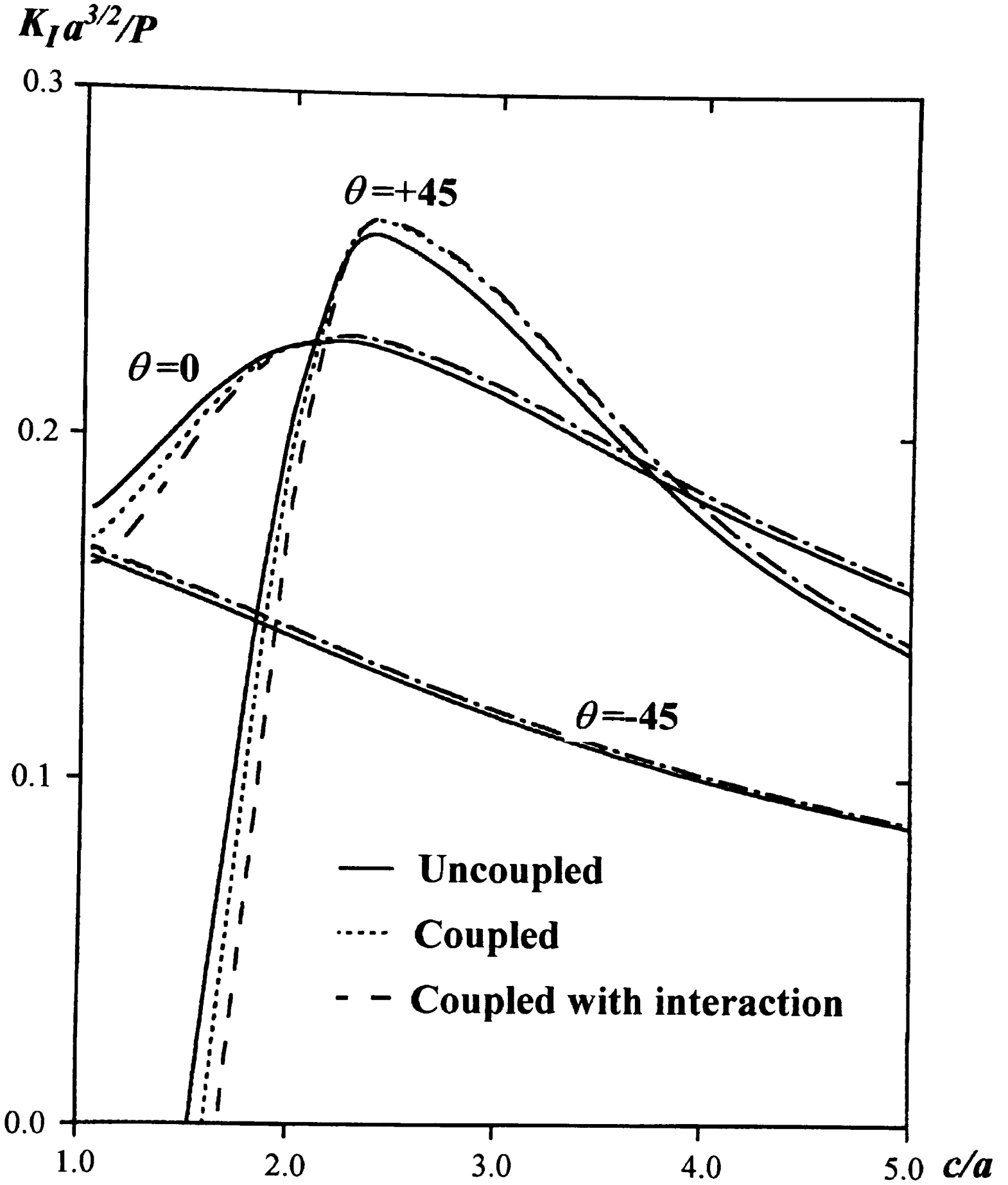

Figure 9.2: Variation of K_I with crack location at various angles ($l = 0.5a$). For $\theta = 45$, K_I falls to zero for $c/a \approx 1.5$ indicating crack tip closure.

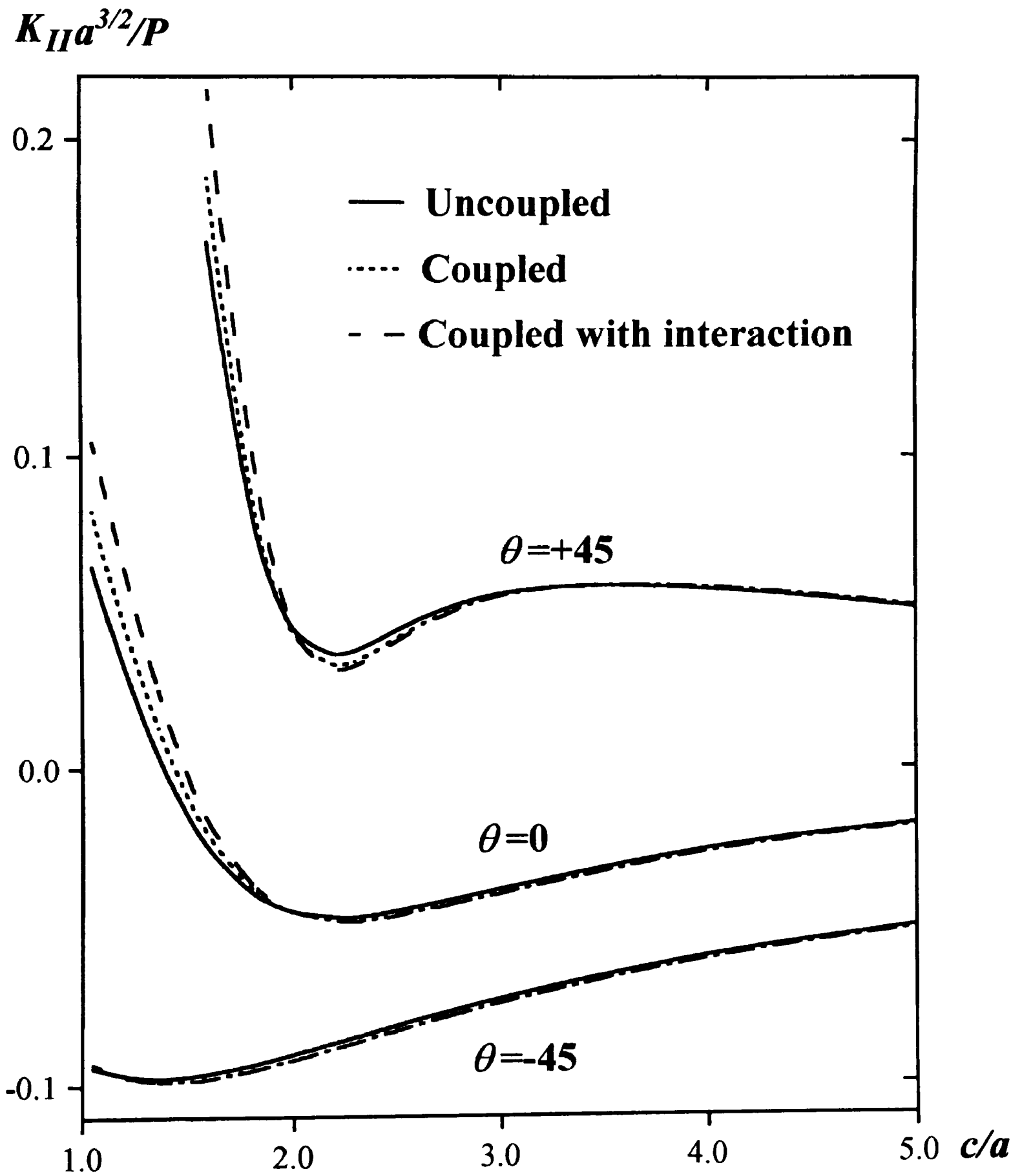

Figure 9.3: Variatio n of K_{II} with crack location at various angles ($l = 0.5a$). For $\theta = 45$, K_{II} is not considered when the crack tip is closed.

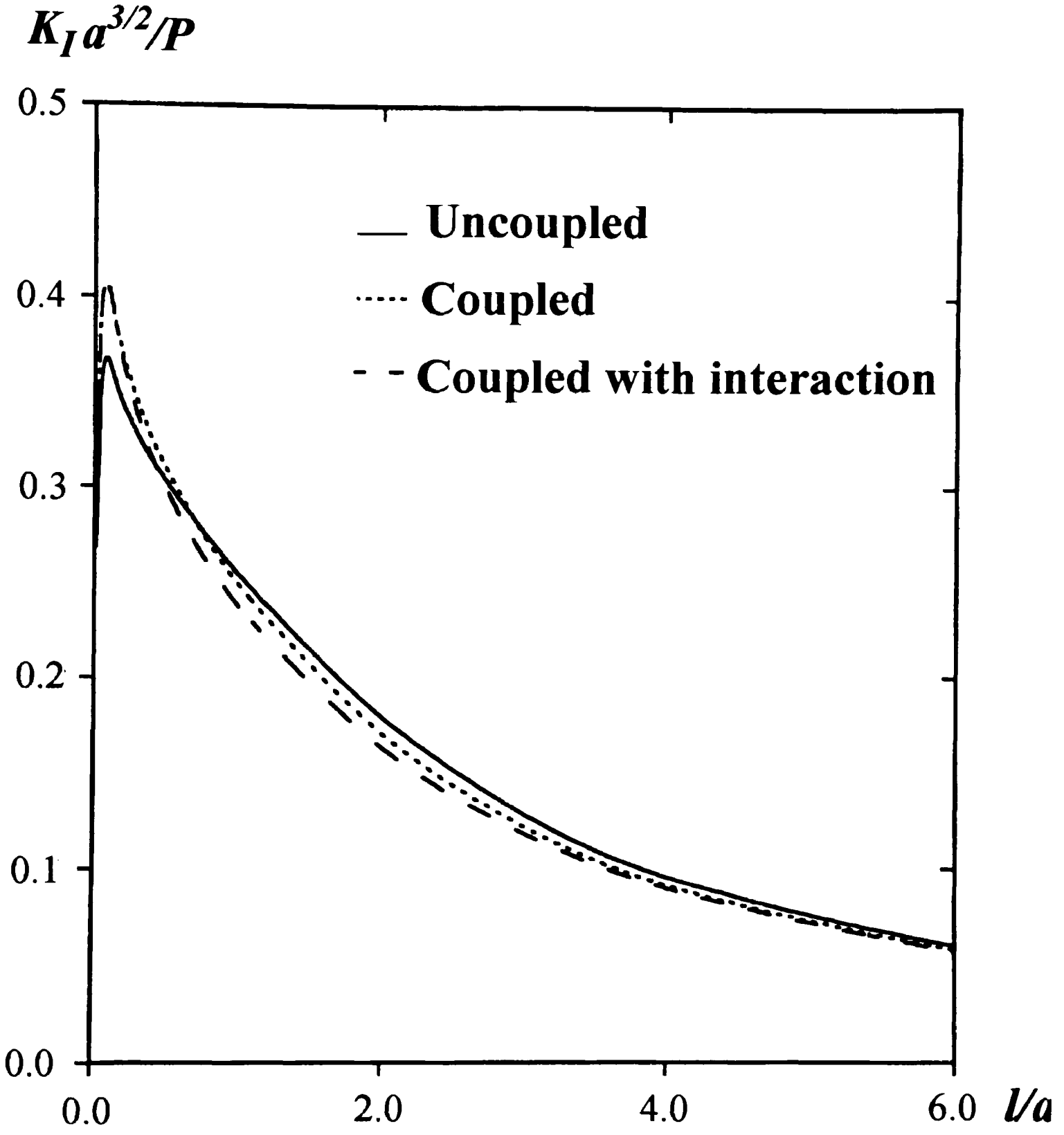

Figure 9.4: Variation of K_I for a vertical crack with crack length ($c = 1.05a$).

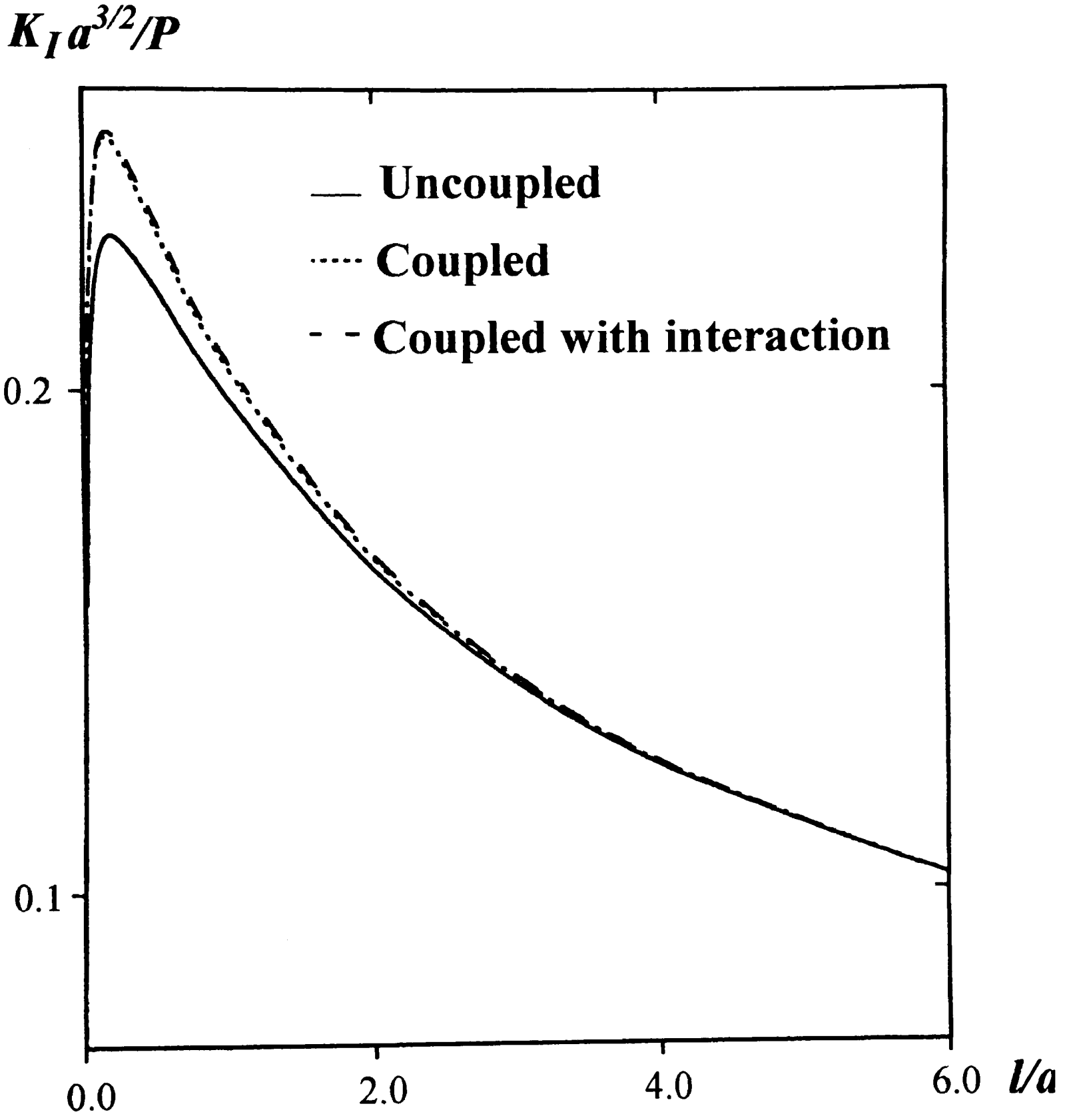

Figure 9.5: Variation of K_I with crack length ($\theta = -45^o$ and $c = 1.05a$).

of the half-plane, however, the local differences in the traction distribution are negligible at the distance of the crack tip due to St. Venant's principle. The effect of the crack on the traction distribution can be quite marked as shown in Figure 9.6 which compares the pressure distribution for each loading condition for a vertical crack near to the indenter. The increase in tractions at the rear of the indenter is due to the local crack opening displacement which generates a peak in the negative z direction. For the geometries investigated, there is only a small set of combinations of all the different parameters which gives rise to a significant difference in stress intensity factors for coupled loading compared with an uncoupled approximation. Although the inclusion of interactions between crack and contact emphasize this difference, if it is considered that an uncoupled approximation is sufficiently accurate, then any interactions between crack and contact may be neglected in addition to any coupling between half-plane and indenter. However, if coupling must be included to obtain the required accuracy, consideration must be given to the effect of the change in compliance which results from the presence of the crack.

---

at the edge of the contact (which decreases rapidly away from the edge).This change is obscured by the linear dependence of K_I on the square root of the crack length, which forces K_I to zero as the crack length is decreased. Hence, all three loading conditions produce similar results for very small cracks.

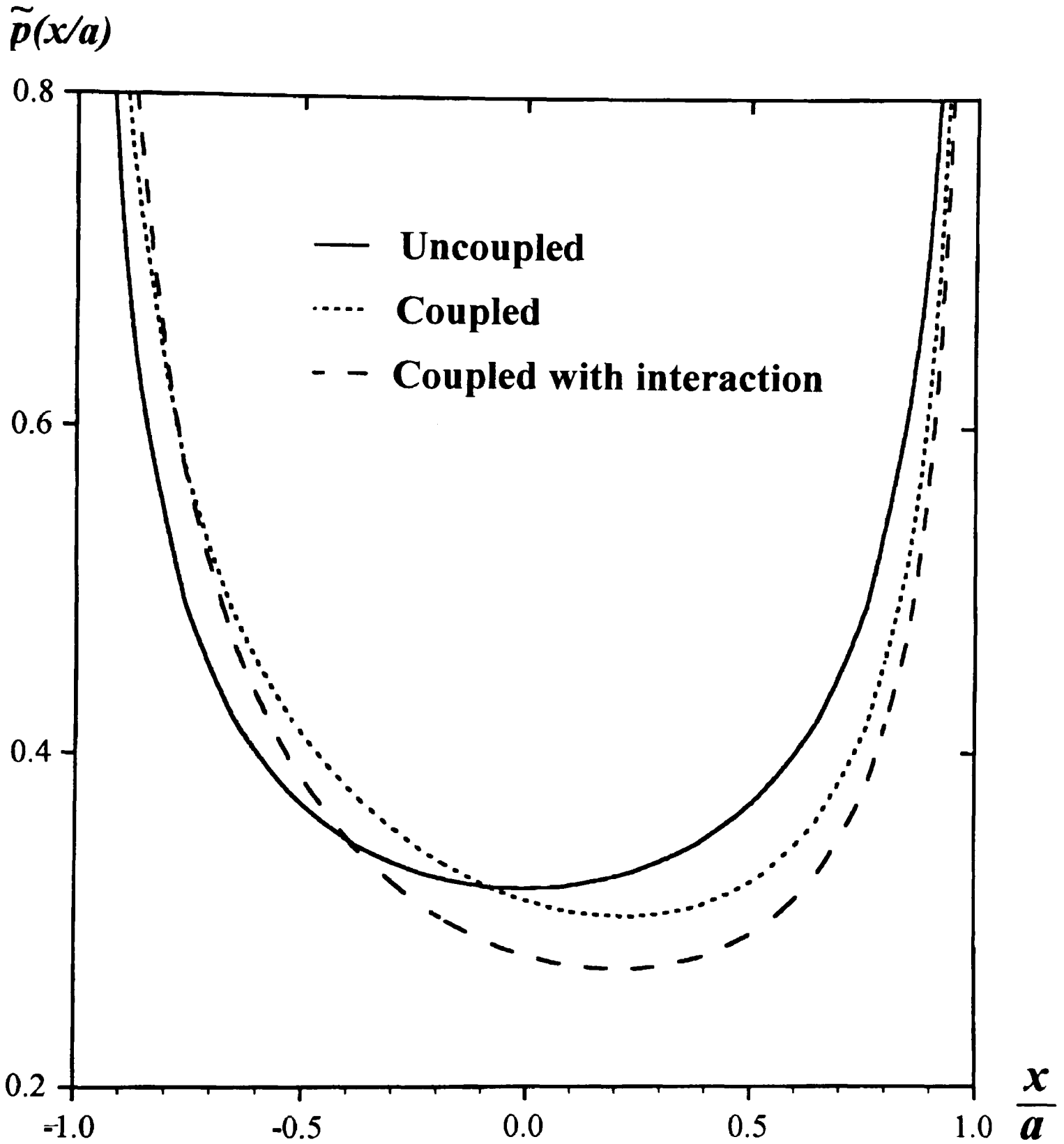

Figure 9.6: Traction distribution for each loading condition ($l = 0.5a$ and $c = 1.05a$).

Chapter 10

Fracture Behind a Sliding Sphere

10.1 Introduction

The stress fields which arise due to frictional contacts can cause failure due to yield or fracture. A Hertzian-type contact subject to normal load alone can generate a ring of tension for certain combinations of material properties (Johnson *et al.*, 1973), which can induce a ring crack (Roesler, 1957) which may in turn develop into the frustum of a cone (Roesler, 1957; Frank & Lawn, 1967). However, unless the indented material is truly brittle, yield is achieved first and the resulting plastic flow relieves the stress field.

A *sliding* Hertzian contact generates a much larger zone of tension in its wake and this region is far more favourable for the development of cracks. The surface flaws so induced are horseshoe shaped and form at regular intervals in the wake of the contact; a typical example is shown in Figure 10.1 (Atkins, 1991). It is the aim of this Chapter to relate the fracture toughness of the indented material to the depth and spacing of the flaws, the contact pressure and the coefficient of friction. Thus it may be possible to deduce the fracture toughness of a brittle material from a simple sliding indentation test.

A simplified representation of the actual geometry is employed which models the crack and the stress field along the plane through the centre of the contact parallel to the sliding direction. Thus the actual three dimensional problem is reduced to one in two dimensions. This enables the crack to be modelled as a continuous distribution of Burgers' vectors

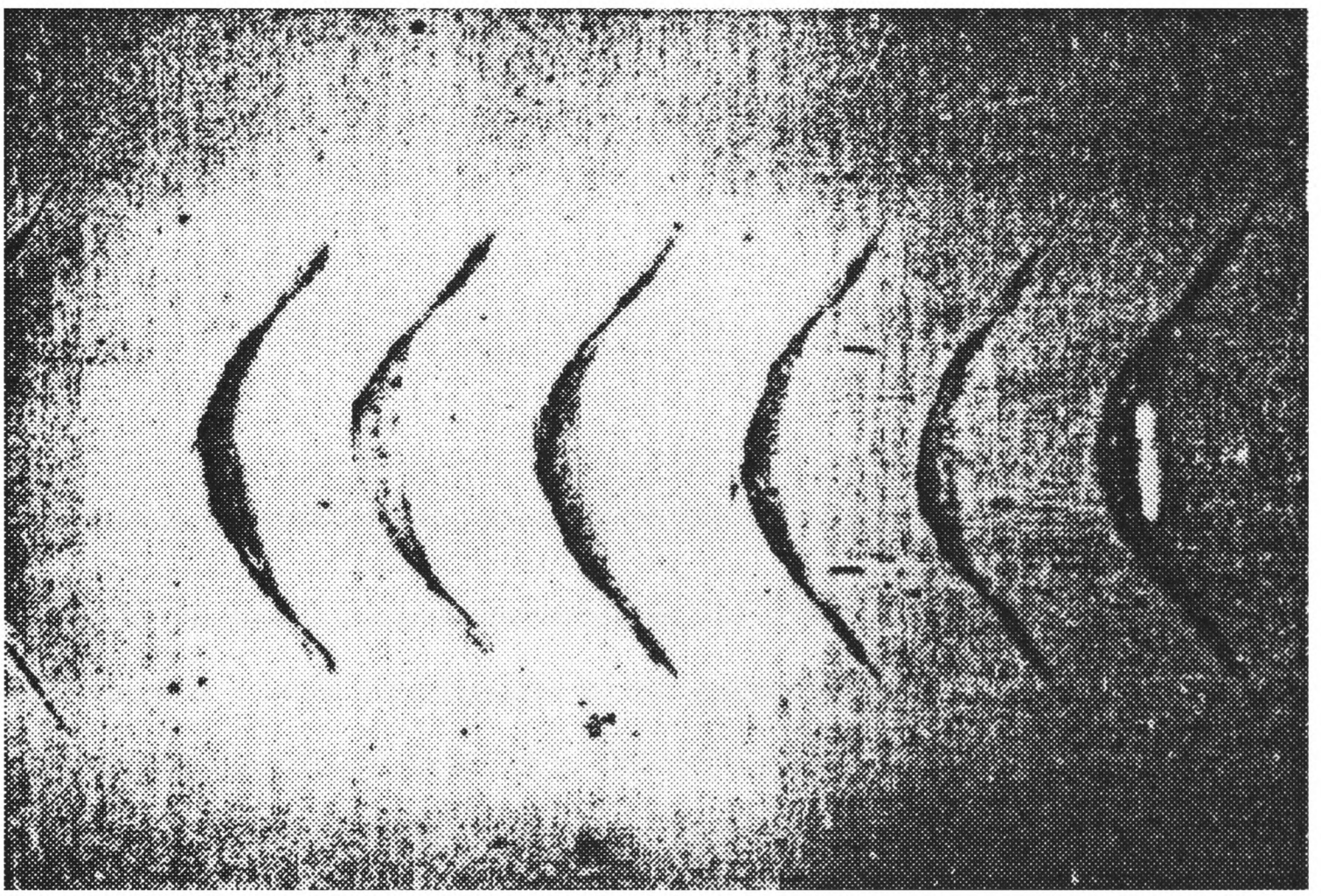

Figure 10.1: Optical micrograph of the friction track obtained by sliding a steel ball over glass (left to right).

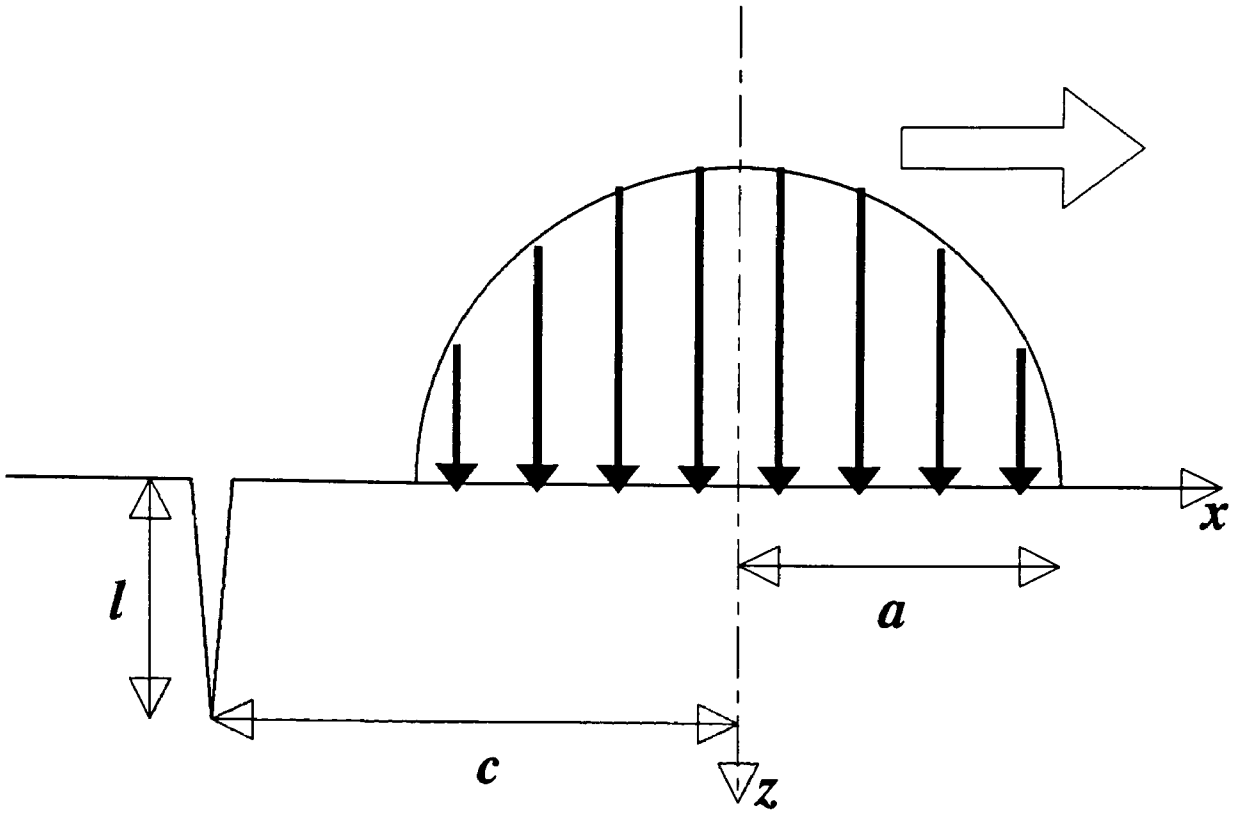

Figure 10.2: Schematic of the geometry of the indenter propelling a single crack.

which may be evaluated using the powerful method of Erdogan *et al* (1973).

Since there is a large simplification in the geometry modelled, it is not considered necessary to use the stress field found in Chapter 7 for sliding contact between a sphere and a dissimilar elastic half-space. Instead the stress field generated by a sliding Hertzian contact is used, which was first found in analytic form by Hamilton and Goodman (1966) and was later presented in a more tractable form by Hamilton (1983). In Chapter 7 it was demonstrated that such an approximation is valid provided that the product of Dundurs' constant and the coefficient of friction is small. Interactions between the crack and the contact are also neglected, an approximation which was justified in Chapter 9.

10.2 Formulation

The geometry of the simplified problem is shown in Figure 10.2. A Hertzian contact of half-width a is sliding in the positive x direction. In its wake is a crack, parallel to the

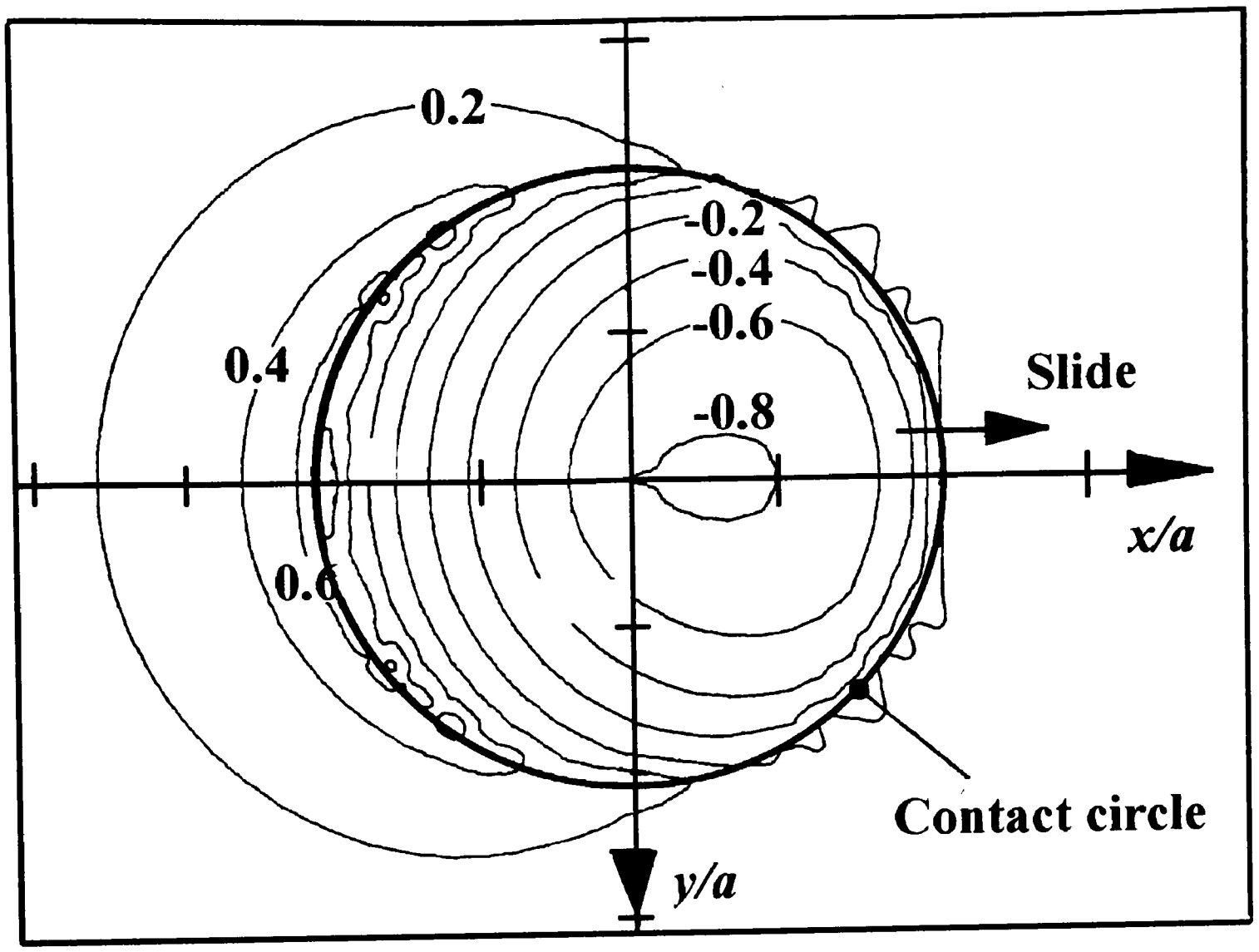

Figure 10.3: Contours of most positive principal stress at surface, normalized with respect to p_0, the peak Herzian pressure.

z-axis, of length l whose mouth is a distance c from the centre of the contact.

The stress field due to the contact alone may be inspected to aid understanding of the mode of crack growth. Figure 10.3 shows the contours of the most positive principal stress at the surface of the half-space and it is clear that the region of significant tension lies in a crescent shape at the rear of the contact. This may be compared with the form of the actual cracks (Figure 10.1) and indicates that the cracks grow due to mode I loading. Figure 10.4 shows the most positive principal stress in the $x - z$ plane. Figures 10.5 and 10.6 show the trajectories of the principal stresses at the surface and the $x - z$ plane respectively. These confirm that, on the basis of the unaffected stress field, the cracks

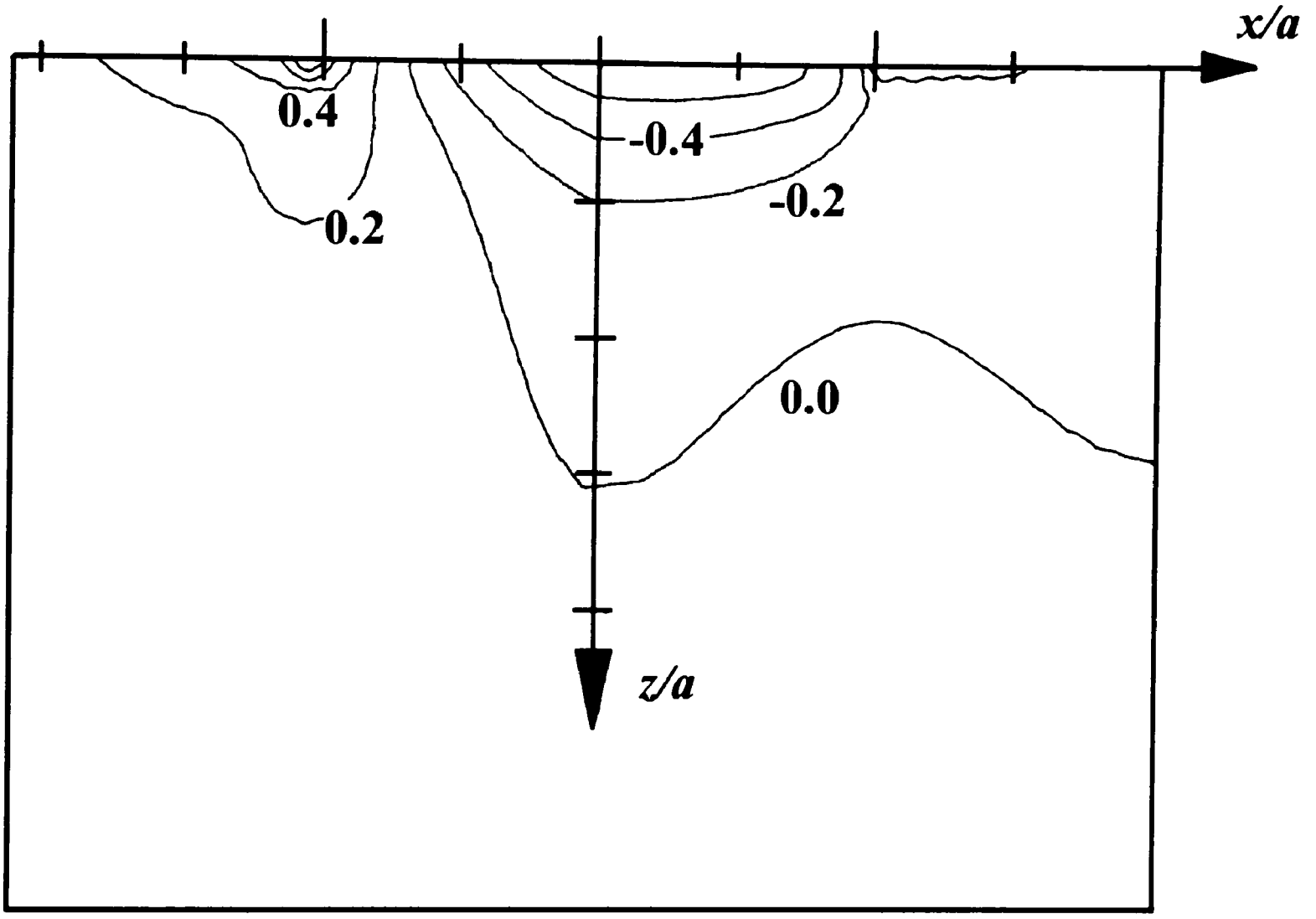

Figure 10.4: Contours of most positive principal stress across mid section, normalized with respect to p_0, the peak Hertzian pressure.

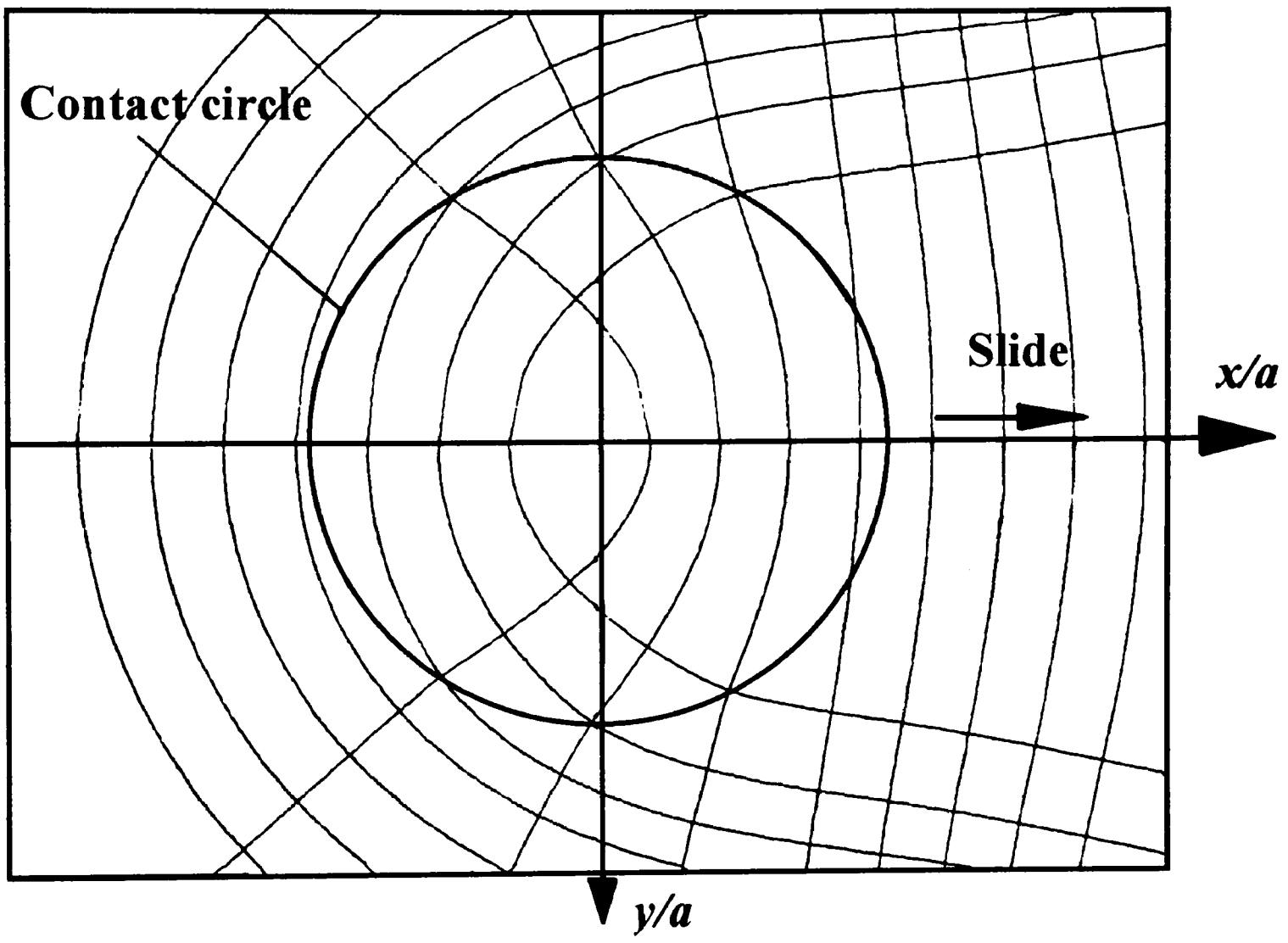

Figure 10.5: Trajectories of principal stresses at surface.

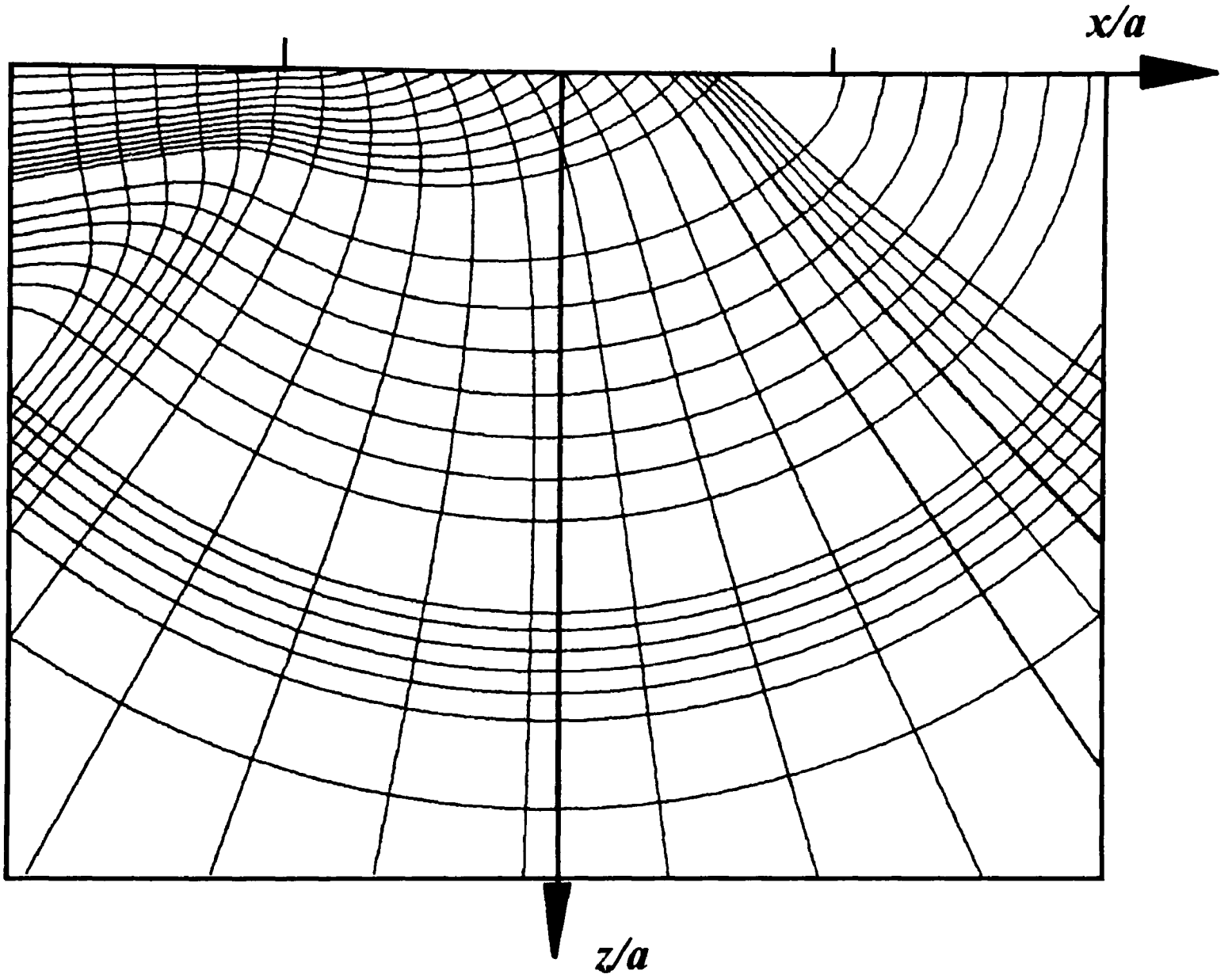

Figure 10.6: Trajectories of principal stresses across mid section.

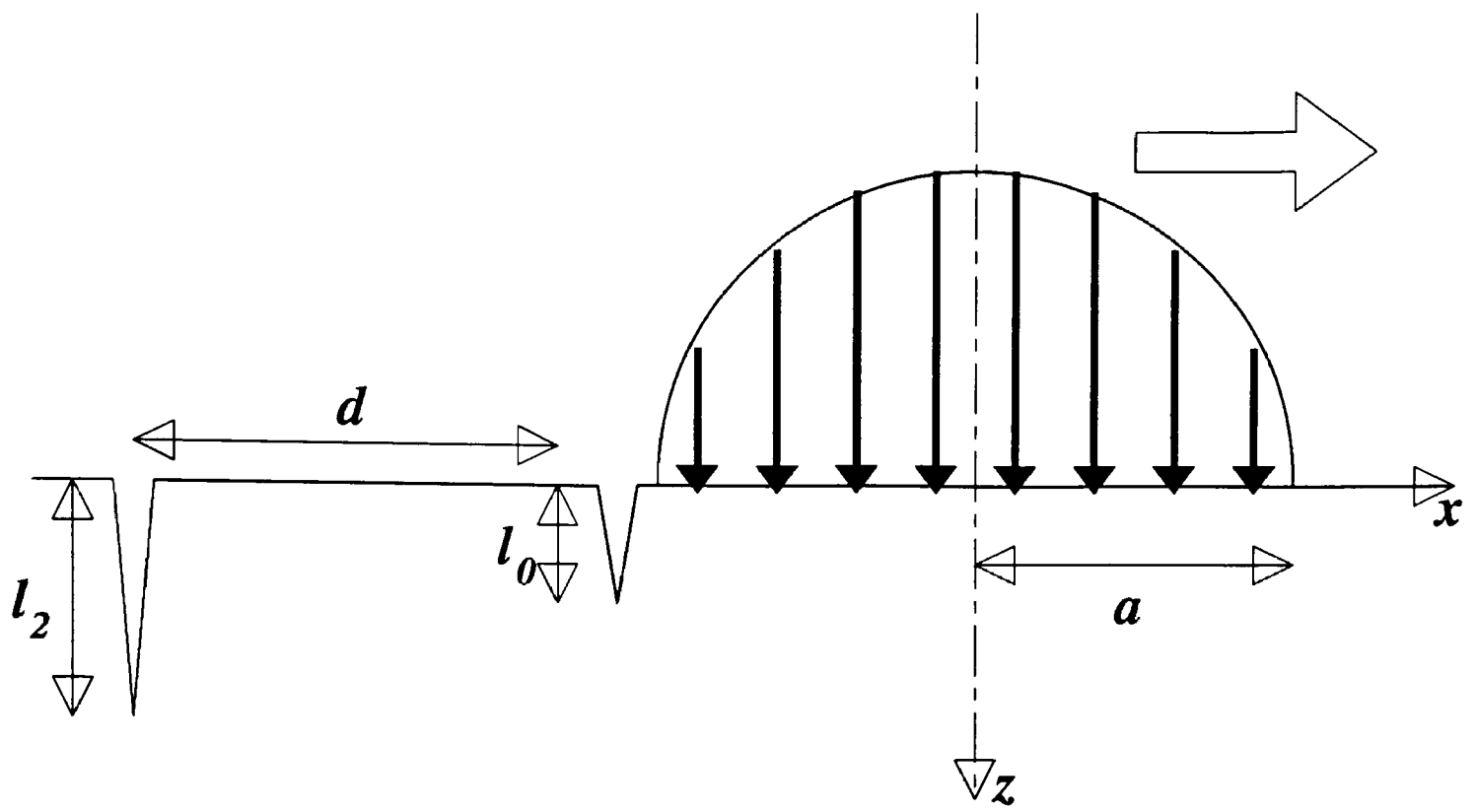

Figure 10.7: Schematic of the indenter propelling a second crack in the presence of the first.

will grow in horseshoe shapes at the surface and approximately vertically in the $x - z$ plane.

The crack itself may be modelled by finding a continuous distribution of climb and glide dislocations along the length of the crack which render its faces stress free. A detailed discussion of this approach is given in Chapter 9 and is not repeated here.

The situation is only slightly more complex when two cracks are modelled. The geometry for this case is shown in Figure 10.7. It is assumed that the crack furthest from the contact has arrested and its effect on the stress field at the second crack may be found using the same influence functions described in Chapter 9. The continuous distributions of Burgers' vectors along each crack must be found simultaneously and this is achieved by doubling the number of discretized simultaneous equations and including the effect of each crack on the other.

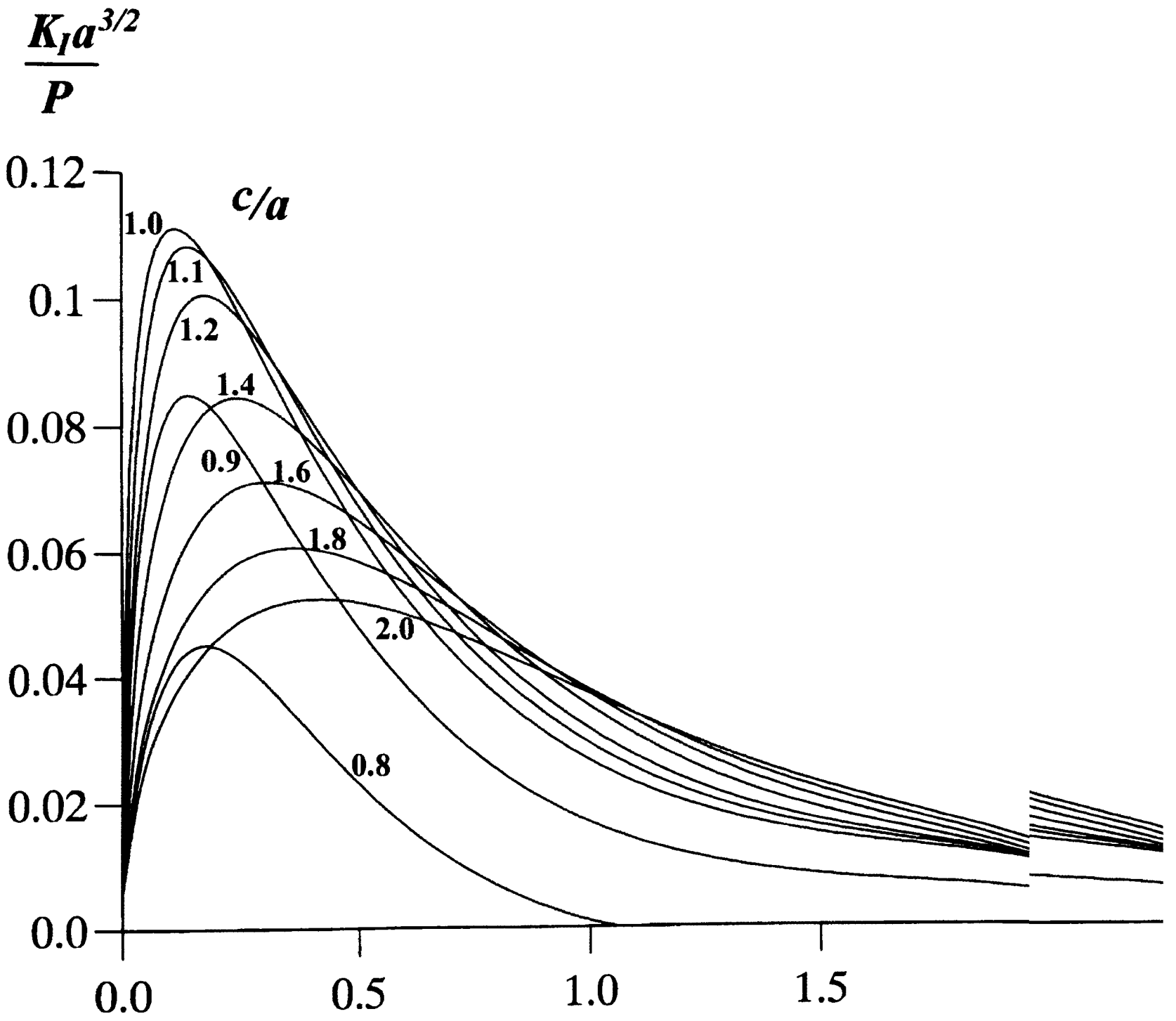

Figure 10.8: Stress intensity factor experienced by a single crack. gle crack.

10.3 Results

10.3.1 Single cracks

Figure 10.8 shows the normalised mode I stress intensity factor for a single crac a single c crack length at a range of locations both within the contact area and behind. and behi coefficient of friction is 0.5 and Poisson's ratio is 0.25. At any position where tition wher field tends to open the crack there is a peak size of crack which corresponds to thesponds to value of K_I. If the crack is larger or smaller than the peak size, the stress intensistress inte

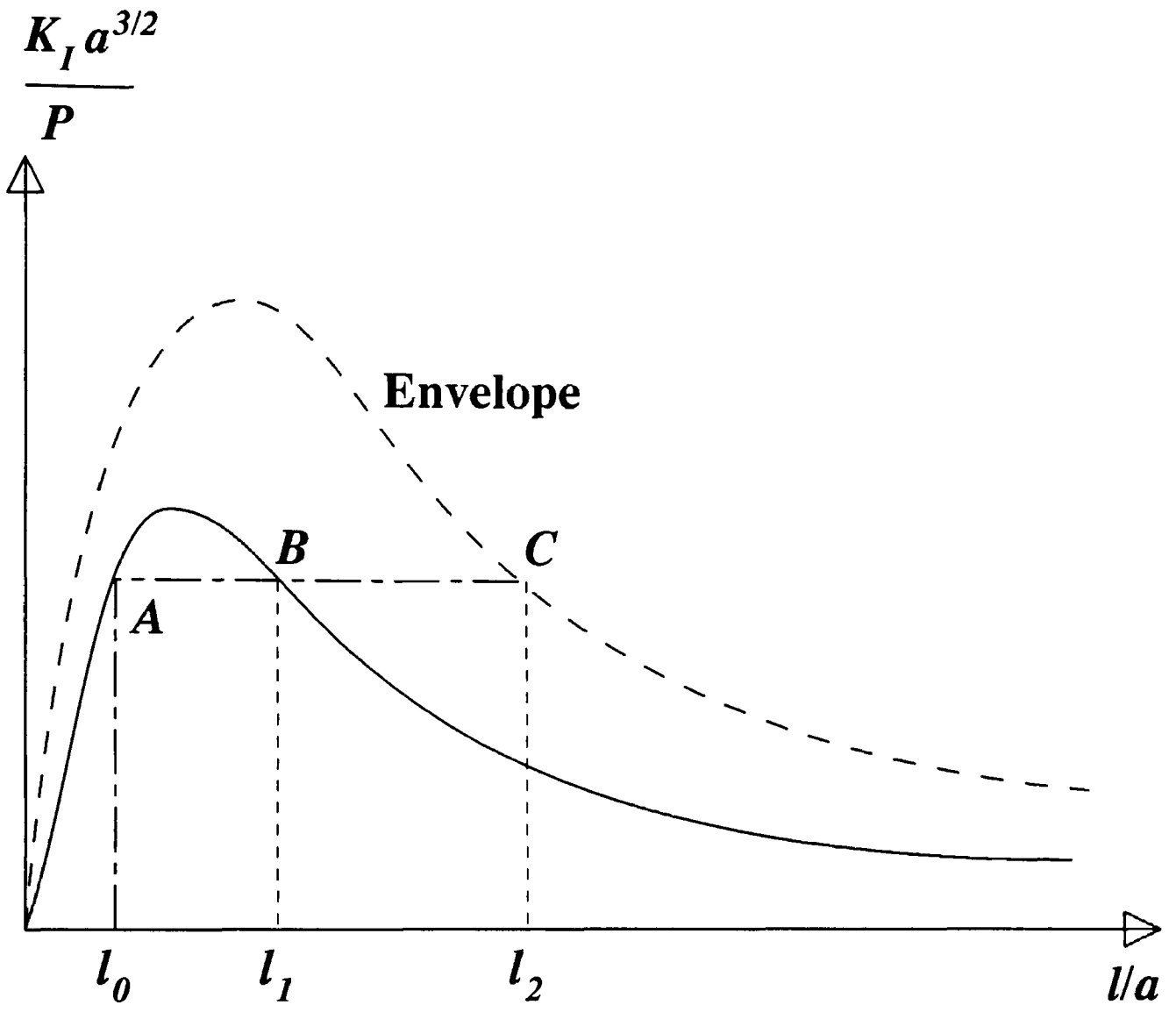

Figure 10.9: Schematic of Figure 10.8 to facilitate interpretation.

is reduced. The envelope (shown schematically in Figure 10.9) which just encloses all the data in Figure 10.8 corresponds to the maximum stress intensity factor versus each size of crack at the location necessary to make K_I maximum.

Suppose there is an initial flaw of length l_0 in a material of critical stress intensity factor K_{IC}. If the point (l_0, K_{IC}) plotted on Figure 10.9 lies above the envelope or to its left then the crack will not extend as the indenter passes over it. However, if l_0 is increased or K_{IC} reduced then there will be some point when crack growth is possible.

Consider what happens as the indenter passes over such a crack. At some location when the indenter is over the crack K_I corresponding to the length of the crack and its relative location will equal K_{IC} (point A on Figure 10.9). Immediately the crack will grow to length l_1 (point B)[1] where it will arrest. As the indenter continues away from the crack, the crack will grow in a stable manner until it reaches the far side of the envelope (point C) and no further growth will occur. Thus the final length of the crack l_2 is independent of its initial size and hence can be used to deduce the fracture toughness of the material in a test.

An upper bound on the maximum initial flaw size can be deduced if K_{IC} is known and no crack growth occurs. Figure 10.10 shows the left hand side of the envelope which is plotted for three approximations of the stress intensity factor at the crack tip. The upper and lower lines correspond to the following equation:

$$K_I = 1.1215\sigma_0\sqrt{\pi l} \tag{10.1}$$

where σ_0 is the stress in a half-space in uniform tension and is given the value at the surface and at the crack tip respectively. The middle line corresponds to the numerical solution presented above. It is clear that if equation 10.1 is used in conjunction with surface stress then the stress intensity factor is significantly over-estimated. This is due to the rapid decay in the actual stress field with depth.

10.4 Multiple cracks

The stress intensity factor for a second crack is shown in Figure 10.11 for various initial sizes for a range of final sizes versus crack spacing. It is assumed that the first crack arrested at point C on Figure 10.9. The point of initiation of growth of the second crack depends on its initial length, l_0, the crack spacing, d, and the final length of the first

[1] This assumes that the growth of the crack is quasi-static. In practice the crack growth will be unstable and will tend to overshoot B. However, this is of no significance provided the overshoot does not exceed C since the crack will extend to that point in a stable manner anyway.

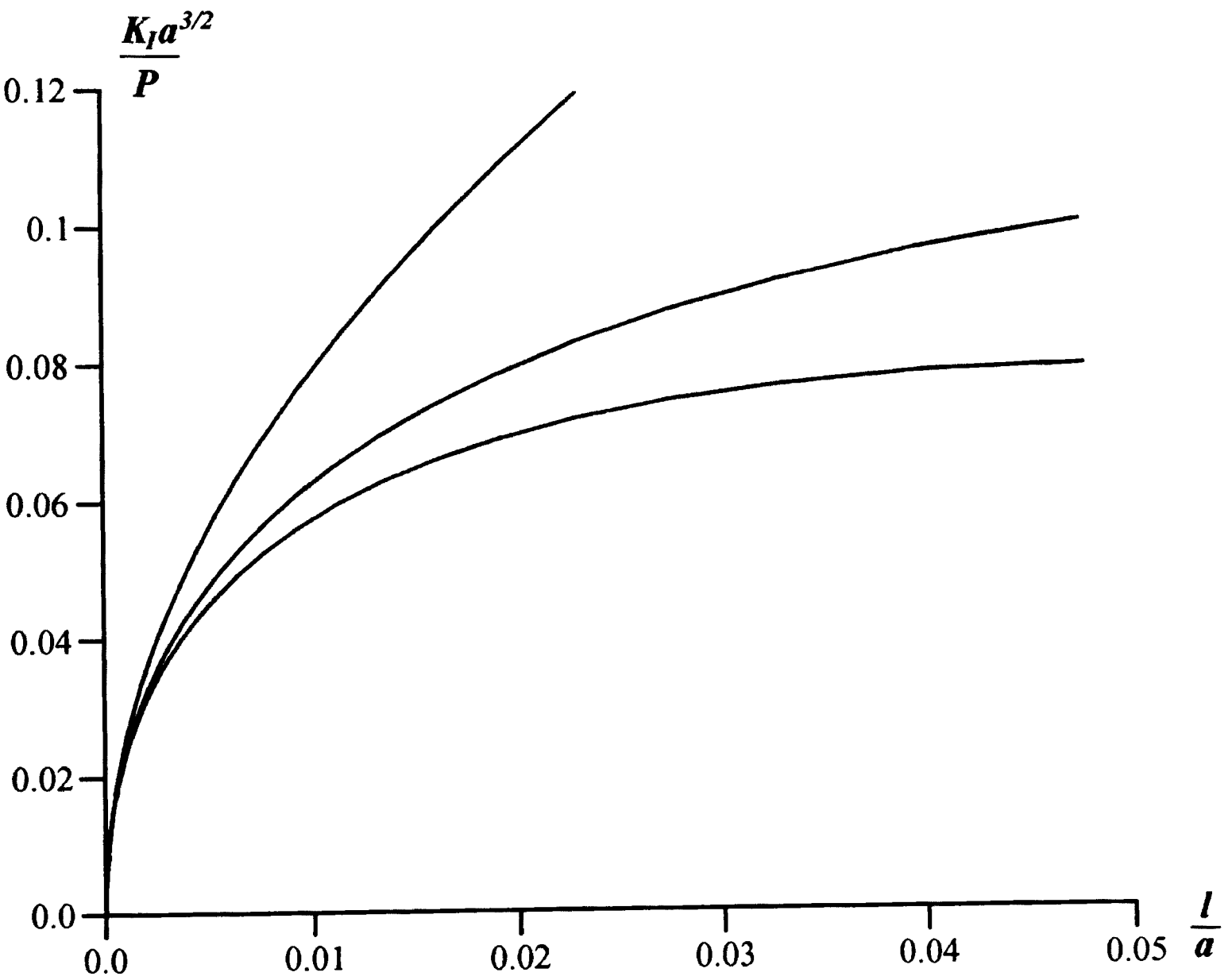

Figure 10.10: Stress intensity factors for very small cracks at the trailing edge of the contact. The upper and lower lines are approximations assuming that the half-space is in uniform tension equal to the actual stress at the surface and at the crack tip respectively. The middle line corresponds to the numerical solution and uses the actual stress distribution.

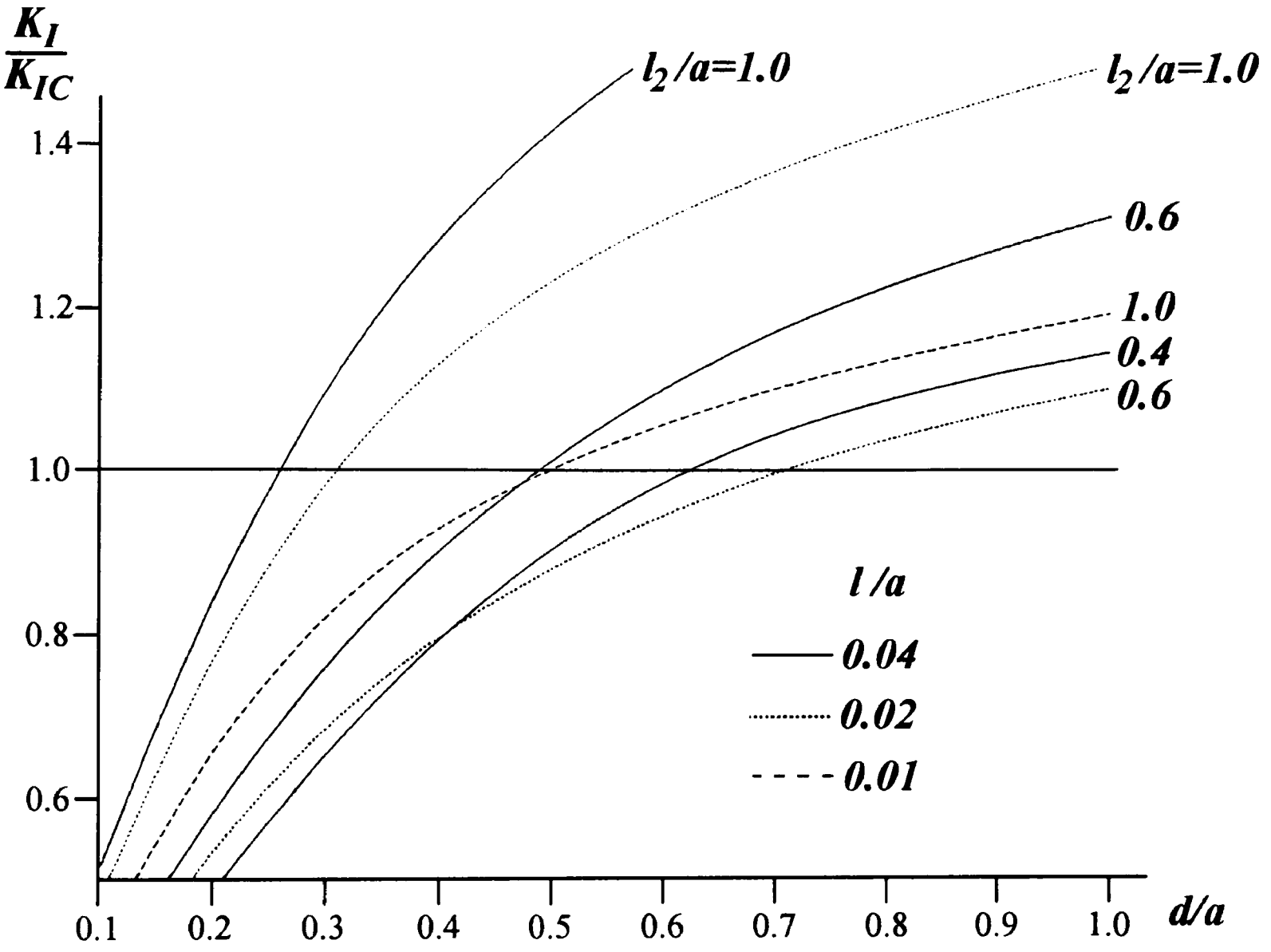

Figure 10.11: Stress intensity factor experienced by second crack in the presence of a self-arrested first crack.

crack l_2 (which of course depends on K_{IC}). The evaluation of crack spacing provides an additional check on the estimate of the initial flaw sizes. This assumes that the density of initial flaws is sufficiently high that there is always one present at the minimum crack spacing. If this is not the case then the spacing between cracks will be erratic.

10.5 Conclusion

This Chapter has presented a quantitative explanation of the formation, depth and spacing of horseshoe cracks formed in a brittle material behind a sliding spherical indenter. In principle, it should be possible use the method in a scheme to find the fracture toughness of a brittle material by a simple test If the final depth of the crack can be measured. In addition the minimum initial flaw sizes can be estimated by the spacing of the cracks, which will also provide some insight into their distribution.

Chapter 11

Conclusions

This study has addressed a range of phenomena associated with dry frictional contacts. Particular emphasis has been devoted to the effect of elastic dissimilarity. In many cases coupling between the normal and shear tractions is considered in full. The conclusions from each general area are discussed in turn below.

11.1 Frictional manipulation

The motion of bodies resting on three discrete points of support and subject to an arbitrary impressed force may be predicted. When the impressed force acts in the plane containing the points of support the analysis may be extended to bodies with many points of support and in the limit to distributed contact provided that the normal reactions or pressure distribution are known. Bodies have a tendency to rotate about points of support and this type of motion is stable in comparison with more general translation and rotation.

The motion of three-footed bodies pushed by a force in a plane parallel to and above the ground may also be predicted and it is possible to show when a planar approximation is valid. The tendency of a body to rotate about a point of support may be increased by introducing friction at the pushing contact and changing the height at which the pushing force acts.

11.2 Two dimensional contacts

The effects of friction and dissimilar elastic properties on the rolling contact of two cylinders have been found using a fully coupled formulation and compared with similar results using the Goodman approximation. Of particular interest is the eccentricity of the contact zone which can arise and generate a significant resisting moment which balances the nett power supplied and the frictional losses.

11.3 Three dimensional contacts

A sequential release method has been developed which may be used to solve many three dimensional contact problems. The number of material properties required to describe a general contact has been contracted to two independent composite parameters and the coefficient of friction. As part of the solution process, the traction distributions may be found as well as the bounds of the contact and the transitions between local stick and slip zones.

11.3.1 Incomplete contact

The region of contact between an inclined rigid punch and an elastic half-space has been found as the angle of tilt is increased. A single plan of the punch was considered in this study but any geometry and profile may be addressed.

11.3.2 Sliding sphere

Fully coupled contact between a sphere sliding over a dissimilar elastic half-space has been analyzed. The traction distributions and the region of contact have been found and these have been used to evaluate the resulting stress field. The differences compared with a standard Hertzian solution increase with the product of Dundurs' constant and the coefficient of friction. The peak stresses which may lead to failure due to yield or fracture tend to be greater in the more compliant body than an uncoupled analysis would predict.

11.3.3 Oscillating sphere

The Mindlin-type contact has been re-evaluated for contact involving both elastically similar and dissimilar materials. In both cases traction distributions have been found which are compatible with local slip directions. For the case of dissimilar materials the effect of pre-existing tractions, present after normal indentations, has a profound effect on the tangential traction distribution. This effect "shakes down" after a few cycles.

11.4 Fracture

The large stress gradients near frictional contacts can induce fracture in brittle materials and some aspects of this have been analyzed in this study.

11.4.1 Interactions between cracks and contacts

The change in compliance of a half-plane due to the presence of a crack has been shown to have an effect on the contact pressure and this is especially true for long cracks close to the contact. However, such large cracks have tips well removed from the contact and the modification in traction distribution tends not to affect the stress intensity factors.

11.4.2 Horseshoe cracks

It has been proposed that the size and spacing of horseshoe cracks in the wake of a sliding spherical indenter can be used to estimate the fracture toughness and initial flaw size in brittle materials.

11.5 Further work

There are several areas addressed in this study which lend themselves to further research. An obvious course would be to integrate the solution for three dimensional contacts with the frictional manipulation problem. In this way the motion of general three dimensional objects with distributed contacts could be predicted. Both halves of the problem are

computer intensive and at the time of writing sufficient computer resource was not widely available.

The sequential release method itself could be applied to a far greater number of three dimensional contact problems. The stability of an inclined body resting on an elastic surface is but one example. Indeed it is a powerful approach that can be applied to contacts of arbitrary area and traction distribution and can cope with stick/slip transitions. The use of sliding indenters to determine fracture toughness of brittle materials may also be worth pursuing. Comprehensive testing should first be undertaken to validate the simplified analysis. If greater accuracy is required, consideration should be given to the effects of elastic dissimilarity and interactions between the cracks and the indenter.

Appendix A

Influence Functions

In this Appendix the influence functions for a rectangle of uniform normal and tangential tractions are presented. They were evaluated by integrating Equations 5.21–5.29.

A.1 Surface displacements

Figure A.1 shows a rectangle at the surface of a half-space, which extends from $-a$ to a along the x-axis and from $-b$ to b along the y-axis. The normal surface displacements u_{zz}, u_{zx} due to a uniform normal pressure p_u and a shearing traction q_{ux} (acting parallel to the x-axis), respectively, applied over the area of the rectangle are:

$$\begin{aligned}\frac{2\pi\mu}{(1-\nu)p_u}u_z^z(x,y) &= (y+b)\ln\left(\frac{x+a+\gamma_0}{x-a+\delta_0}\right)-(y-b)\ln\left(\frac{x+a+\beta_0}{x-a+\alpha_0}\right)\\ &\quad +(x+a)\ln\left(\frac{y+b+\gamma_0}{y-b+\beta_0}\right)-(x-a)\ln\left(\frac{y+b+\delta_0}{y-b+\alpha_0}\right) \quad \text{(A.1)}\\ \frac{4\pi\mu}{(1-2\nu)q_{ux}}u_x^z(x,y) &= (y+b)\ln\left(\frac{\delta_0}{\gamma_0}\right)+(y-b)\ln\left(\frac{\beta_0}{\alpha_0}\right)\\ &\quad +2(x-a)(\theta_4^0-\theta_1^0)-2(x+a)(\theta_3^0-\theta_2^0) \quad \text{(A.2)}\end{aligned}$$

where

$$\begin{aligned}\alpha_0^2 &= (x-a)^2+(y-b)^2\\ \beta_0^2 &= (x+a)^2+(y-b)^2\end{aligned}$$

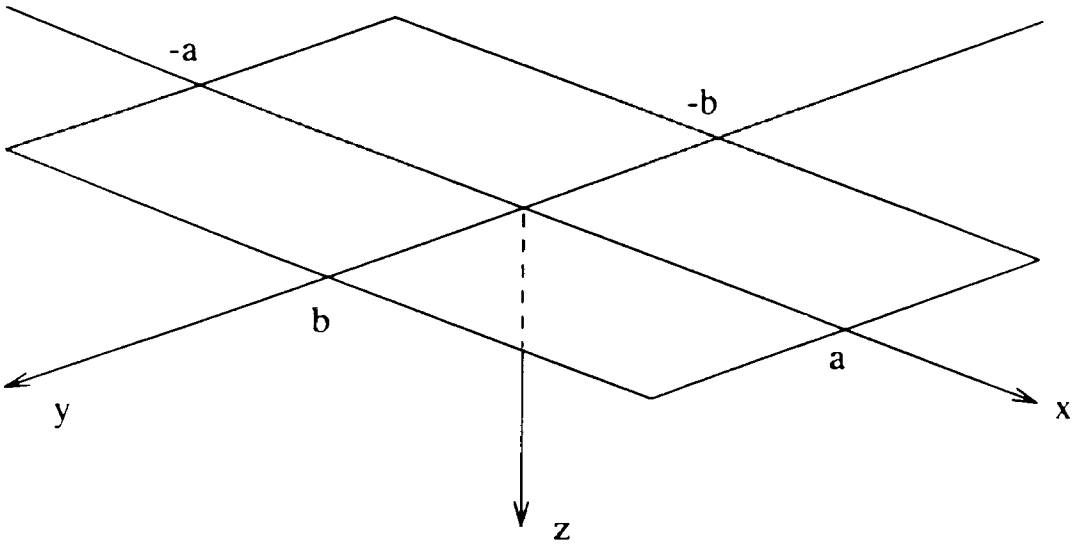

Figure A.1: Rectangular element of uniform tractions.

$$\begin{aligned} \gamma_0^2 &= (x+a)^2 + (y+b)^2 \\ \delta_0^2 &= (x-a)^2 + (y+b)^2 \end{aligned} \tag{A.3}$$

and

$$\begin{aligned} \theta_1^0 &= \tan^{-1}\left(\frac{y-b+\alpha_0}{x-a}\right) \\ \theta_2^0 &= \tan^{-1}\left(\frac{y-b+\beta_0}{x+a}\right) \\ \theta_3^0 &= \tan^{-1}\left(\frac{y+b+\gamma_0}{x+a}\right) \\ \theta_4^0 &= \tan^{-1}\left(\frac{y+b+\delta_0}{x-a}\right) \qquad -\frac{\pi}{2} \le \theta_i \le \frac{\pi}{2} \end{aligned} \tag{A.4}$$

Normal displacements due to a rectangle of uniform shearing traction parallel to the y-axis are not required in this study but may be derived from the above equations simply by replacing x, y, a, b with y, x, b, a respectively. Tangential displacements due to normal tractions are also not required in this study. However, they may be found by integrating Equation 5.23 of Chapter 5 over the area of the rectangle. Tangential displacements u_x^x, u_y^x in the x and y directions repectively due to a rectangle of uniform shearing traction acting parallel to the x-axis are

$$\frac{u_x^x}{q_{ux}} = \frac{1}{2\pi\mu}\left\{(y+b)\ln\frac{x+a+\gamma_0}{x-a+\delta_0} + (y-b)\ln\frac{x-a+\alpha_0}{x+a+\beta_0}\right.$$
$$\left. +(1-\nu)(x+a)\ln\frac{y+b+\gamma_0}{y-b+\beta_0} + (1-\nu)(x-a)\ln\frac{y-b+\gamma_0}{y+b+\delta_0}\right\} \quad \text{(A.5)}$$

$$\frac{u_y^x}{q_{ux}} = -\frac{\nu}{2\pi\mu}(\beta_0+\delta_0-\alpha_0-\gamma_0) \quad \text{(A.6)}$$

The corresponding x and y-direction displacement for a rectangle of uniform shearing traction parallel to the y-axis is

$$\frac{u_x^y}{q_{uy}} = \frac{\nu}{2\pi\mu}(\beta_0+\delta_0-\alpha_0-\gamma_0) \quad \text{(A.7)}$$

$$\frac{u_y^y}{q_{uy}} = \frac{1}{2\pi\mu}\left\{(x+a)\ln\frac{y+b+\gamma_0}{y-b+\beta_0} + (x-a)\ln\frac{y-b+\alpha_0}{y+b+\delta_0}\right.$$
$$\left. +(1-\nu)(y+b)\ln\frac{x+a+\gamma_0}{x-a+\delta_0} + (1-\nu)(y-b)\ln\frac{x-a+\gamma_0}{y+b+\beta_0}\right\}. \quad \text{(A.8)}$$

Two points are worth noting: the transverse displacements due to a rectangle of uniform shearing traction are zero at the centre of the rectangle and the y displacement field produced by uniform x direction tractions is identical in magnitude but of opposite sign to the y displacement field produced by uniform x direction tracitons when the tractions act over the area of square, i.e.

$$\left(\frac{u_y^x}{q_{ux}}\right)_{x=0,y=0} = 0 \quad \text{(A.9)}$$

$$\frac{u_x^y}{q_{uy}} = -\frac{u_y^x}{q_{ux}} \qquad \text{when } a=b \quad \text{(A.10)}$$

A.2 Stress field within the half-space

The stress field generated in the elastic half-space by the rectangle of uniform pressure p_u is

$$\frac{\sigma_{xx}^z}{p_u} = \frac{2\nu}{\pi}(\theta_1+\theta_3-\theta_2-\theta_4) + \frac{z}{2\pi}\left[\left(\frac{a-x}{(a-x)^2+z^2}\right)\left(\frac{b-y}{\alpha_1}+\frac{b+y}{\delta_1}\right) + \left(\frac{a+x}{(a+x)^2+z^2}\right)\left(\frac{b-y}{\beta_1}+\frac{b+y}{\gamma_1}\right)\right]$$
$$-\frac{(1-2\nu)}{2\pi}\left[\tan^{-1}\left(\frac{b-y}{a-x}\right) + \tan^{-1}\left(\frac{b+y}{a-x}\right) - \tan^{-1}\left(\frac{z(b-y)}{\alpha_1(a-x)}\right) - \tan^{-1}\left(\frac{z(b+y)}{\delta_1(a-x)}\right)\right.$$

$$+\tan^{-1}\left(\frac{b-y}{a+x}\right)+\tan^{-1}\left(\frac{b+y}{a+x}\right)-\tan^{-1}\left(\frac{z(b-y)}{\beta_1(a+x)}\right)-\tan^{-1}\left(\frac{z(b+y)}{\gamma_1(a+x)}\right)\Bigg] \tag{A.11}$$

$$\frac{\sigma^z_{yy}}{p_u} = \frac{2\nu}{\pi}(\theta_1+\theta_3-\theta_2-\theta_4)+\frac{z}{2\pi}\left[\left(\frac{b-y}{(b-y)^2+z^2}\right)\left(\frac{a-x}{\alpha_1}+\frac{a+x}{\beta_1}\right)+\left(\frac{b+y}{(b+y)^2+z^2}\right)\left(\frac{a-x}{\delta_1}+\frac{a+x}{\gamma_1}\right)\right]$$

$$-\frac{(1-2\nu)}{2\pi}\left[\tan^{-1}\left(\frac{a-x}{b-y}\right)+\tan^{-1}\left(\frac{a+x}{b-y}\right)-\tan^{-1}\left(\frac{z(a-x)}{\alpha_1(b-y)}\right)-\tan^{-1}\left(\frac{z(a+x)}{\beta_1(b-y)}\right)\right.$$

$$\left.+\tan^{-1}\left(\frac{a-x}{b+y}\right)+\tan^{-1}\left(\frac{a+x}{b+y}\right)-\tan^{-1}\left(\frac{z(a-x)}{\delta_1(b+y)}\right)-\tan^{-1}\left(\frac{z(a+x)}{\gamma_1(b+y)}\right)\right] \tag{A.12}$$

$$\frac{\sigma^z_{zz}}{p_u} = \frac{1}{\pi}(\theta_1+\theta_3-\theta_2-\theta_4)-\frac{z}{2\pi}\left[\left(\frac{a-x}{(a-x)^2+z^2}\right)\left(\frac{b-y}{\alpha_1}+\frac{b+y}{\delta_1}\right)+\left(\frac{a+x}{(a+x)^2+z^2}\right)\left(\frac{b-y}{\beta_1}+\frac{b+y}{\gamma_1}\right)\right.$$

$$\left.+\left(\frac{b-y}{(b-y)^2+z^2}\right)\left(\frac{a-x}{\alpha_1}+\frac{a+x}{\beta_1}\right)+\left(\frac{b+y}{(b+y)^2+z^2}\right)\left(\frac{a-x}{\delta_1}+\frac{a+x}{\gamma_1}\right)\right] \tag{A.13}$$

$$\frac{\sigma^z_{xy}}{p_u} = -\frac{(1-2\nu)}{2\pi}\ln\left(\frac{(z+\alpha_1)(z+\gamma_1)}{(z+\beta_1)(z+\delta_1)}\right)-\frac{z}{2\pi}\left(\frac{1}{\alpha_1}-\frac{1}{\beta_1}+\frac{1}{\gamma_1}-\frac{1}{\delta_1}\right) \tag{A.14}$$

$$\frac{\sigma^z_{yz}}{p_u} = -\frac{z}{2\pi}\left[\frac{z}{(b-y)^2+z^2}\left(\frac{a-x}{\alpha_1}+\frac{a+x}{\beta_1}\right)-\frac{z}{(b+y)^2+z^2}\left(\frac{a-x}{\delta_1}+\frac{a+x}{\gamma_1}\right)\right] \tag{A.15}$$

$$\frac{\sigma^z_{zx}}{p_u} = -\frac{z}{2\pi}\left[\frac{z}{(a-x)^2+z^2}\left(\frac{b-y}{\alpha_1}+\frac{b+y}{\delta_1}\right)-\frac{z}{(a+x)^2+z^2}\left(\frac{b-y}{\beta_1}+\frac{b+y}{\gamma_1}\right)\right]. \tag{A.16}$$

The corresponding field produced by a rectangle of shearing traction acting parallel to the x-axis is

$$\frac{\sigma^x_{xx}}{q_{ux}} = \frac{1}{\pi}\ln\left(\frac{(y+b+\gamma_1)(y-b+\alpha_1)}{(y-b+\beta_1)(y+b+\delta_1)}\right)+\frac{z(1+2\nu)}{2\pi}\left\{(y+b)\left[\frac{1}{\gamma_0^2}-\frac{1}{\delta_0^2}-z\left(\frac{\gamma_1^2+(x+a)^2}{\gamma_1\gamma_0^2[z^2+(x+a)^2]}\right.\right.\right.$$

$$\left.\left.\left.-\frac{\delta_1^2+(x-a)^2}{\delta_1\delta_0^2[z^2+(x-a)^2]}\right)\right]+(y-b)\left[\frac{1}{\alpha_0^2}-\frac{1}{\beta_0^2}-z\left(\frac{\alpha_1^2+(x-a)^2}{\alpha_1\alpha_0^2[z^2+(x+a)^2]}-\frac{\beta_1^2+(x+a)^2}{\beta_1\beta_0^2[z^2+(x+a)^2]}\right)\right]\right\}$$

$$-\frac{\nu}{\pi}\left(\frac{(x+a)^2}{(y+b+\gamma_1)\gamma_1}+\frac{(x-a)^2}{(y-b+\alpha_1)\alpha_1}-\frac{(x-a)^2}{(y+b+\delta_1)\delta_1}-\frac{(x+a)^2}{(y-b+\beta_1)\beta_1}\right) \tag{A.17}$$

$$\frac{\sigma^x_{yy}}{q_{ux}} = \frac{\nu}{\pi}\ln\left(\frac{(y+b+\gamma_1)(y-b+\alpha_1)}{(y-b+\beta_1)(y+b+\delta_1)}\right)+\frac{z(1-2\nu)}{2\pi}\left(-\frac{y+b}{\gamma_1(z+\gamma_1)}-\frac{y-b}{\alpha_1(z+\alpha_1)}+\frac{y+b}{\delta_1(z+\delta_1}\right)+\frac{y-b}{\beta_1(z+\beta_1)}\Bigg)$$

$$+\frac{\nu}{\pi}\left(-\frac{y+b}{\gamma_1}-\frac{y-b}{\alpha_1}+\frac{y+b}{\delta_1}+\frac{y-b}{\beta_1}\right) \tag{A.18}$$

$$\frac{\sigma^x_{zz}}{q_{ux}} = -\frac{z}{2\pi}\left[\frac{z}{(a-x)^2+z^2}\left(\frac{b-y}{\alpha_1}+\frac{b+y}{\delta_1}\right)-\frac{z}{(a+x)^2+z^2}\left(\frac{b-y}{\beta_1}+\frac{b+y}{\gamma_1}\right)\right] \tag{A.19}$$

$$\frac{\sigma^x_{xy}}{q_{ux}} = \frac{1}{2\pi}\ln\left(\frac{(x+a+\gamma_1)(x-a+\alpha_1)}{(x-a+\delta_1)(x+a+\beta_1)}\right)+\frac{z(1-2\nu)}{2\pi}\left(-\frac{x+a}{\gamma_1(z+\gamma_1)}-\frac{x-a}{\alpha_1(z+\alpha_1)}+\frac{x-a}{\delta_1(z+\delta_1)}+\frac{x+a}{\beta_1(z+\beta_1)}\right)$$

$$+\frac{\nu}{\pi}\left(-\frac{x+a}{\gamma_1}-\frac{x-a}{\alpha_1}+\frac{x-a}{\delta_1}+\frac{x+a}{\beta_1}\right) \tag{A.20}$$

$$\frac{\sigma^x_{yz}}{q_{ux}} = -\frac{z}{2\pi}\left(\frac{1}{\gamma_1}+\frac{1}{\alpha_1}-\frac{1}{\beta_1}-\frac{1}{\delta_1}\right) \tag{A.21}$$

$$\frac{\sigma^x_{zx}}{q_{ux}} = \frac{1}{\pi}(\theta_1+\theta_3-\theta_2-\theta_4)+\frac{z}{2\pi}\left[\left(\frac{a-x}{(a-x)^2+z^2}\right)\left(\frac{b-y}{\alpha_1}+\frac{b+y}{\delta_1}\right)+\left(\frac{a+x}{(a+x)^2+z^2}\right)\left(\frac{b-y}{\beta_1}+\frac{b+y}{\gamma_1}\right)\right] \tag{A.22}$$

where

$$\begin{aligned}
\theta_1 &= \tan^{-1}\left(\frac{x-a+y-b+\alpha_1}{z}\right)\\
\theta_2 &= \tan^{-1}\left(\frac{x+a+y-b+\beta_1}{z}\right)\\
\theta_3 &= \tan^{-1}\left(\frac{x+a+y+b+\gamma_1}{z}\right)\\
\theta_4 &= \tan^{-1}\left(\frac{x-a+y+b+\delta_1}{z}\right) \qquad -\frac{\pi}{2}\le\theta_i\le\frac{\pi}{2}
\end{aligned} \tag{A.23}$$

and

$$\begin{aligned}
\alpha_1^2 &= (x-a)^2+(y-b)^2+z^2\\
\beta_1^2 &= (x+a)^2+(y-b)^2+z^2\\
\gamma_1^2 &= (x+a)^2+(y+b)^2+z^2\\
\delta_1^2 &= (x-a)^2+(y+b)^2+z^2.
\end{aligned} \tag{A.24}$$

Although not required in this study, it is possible to derive the equivalent stress field due to a rectangle of traction acting parallel to the y-axis. This may be achieved by performing the appropriate integrations of the equations of Chapter 5 or by replacing x, y, a, b with y, x, b, a, respectively, in the equations above.

A.3 Surface stress at contact boundary

One disadvantage of using piecewise constant traction elements is that the stress field at the edges of the elements are undefined. Hence, it is impossible to obtain a comprehensive surface stress distribution at a mesh of such elements. If the stress field must be calcualted at the surface, a special procedure must be employed. The one used here essentially models part of the piecewise constant traction distribution with a continuous distribution which

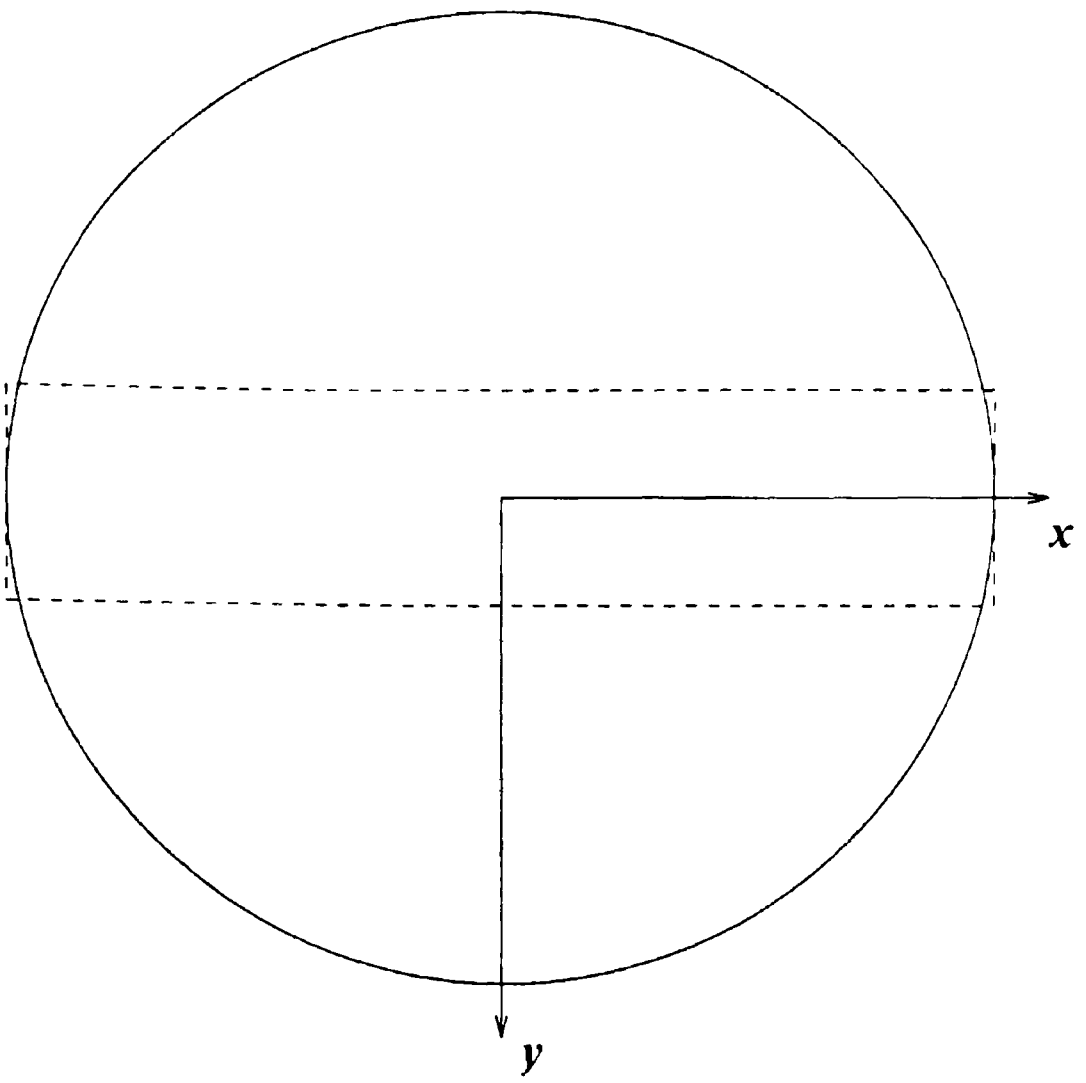

Figure A.2: Contact region showing the location of the special traction element.

falls smoothly to zero at the edges of the contact. In Chapter 7 it is necessary to evaluate the stress field at the trailing edge of the contact. This may be done by replacing the elements lying along the x-axis with a special element over which the traction distributions vary continuously and smoothly. The location of the special element and the traction distribution acting over it are shown in Figures A.2 and A.3 respectively. The stress field produced by this element may be evaluated by taking the sum, over the length of the element, of the effect of infinitesimally small strips of traction. In the limit this sum becomes an integral.

From the previous section it is straightforward to derive the stress field due to a rectangle of uniform pressure and shearing traction (parallel to the x-axis) which extends

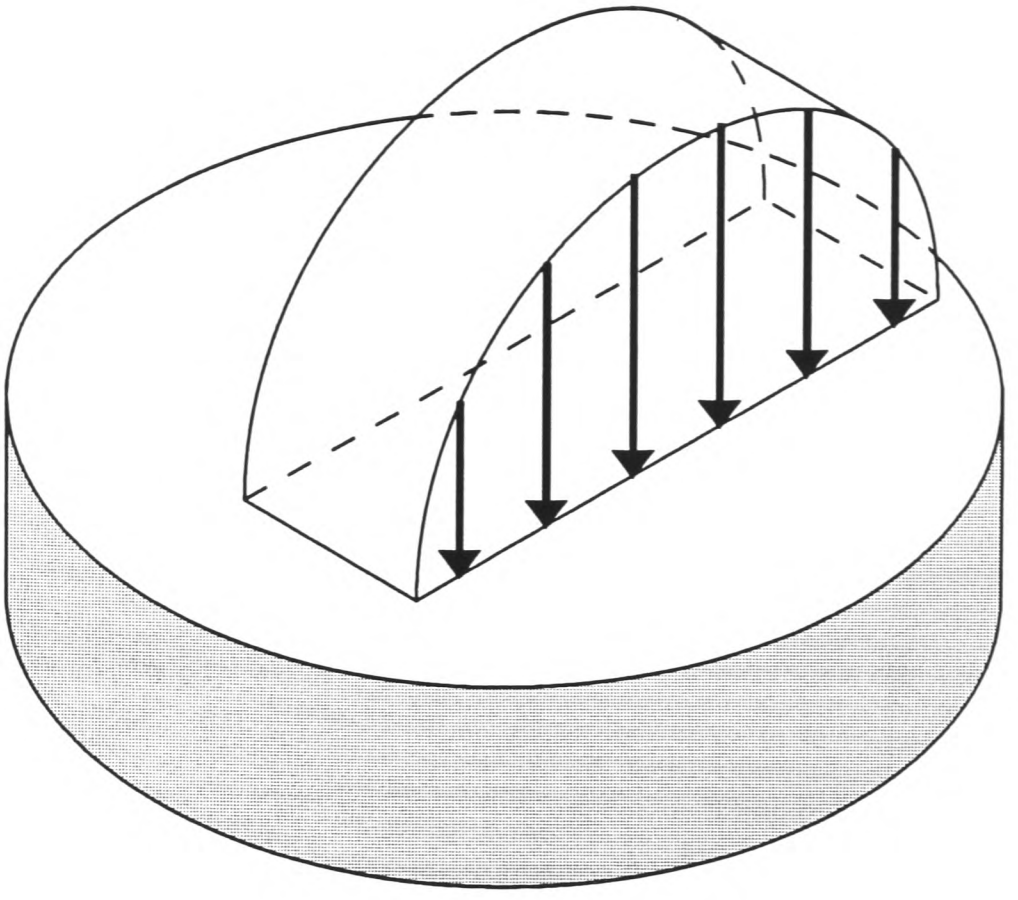

Figure A.3: Form of the traction distribution acting over the special element.

from 0 to a along the x-axis and from $-b$ to b along the y-axis at the surface of an elastic half-space. The non-zero derivatives of its components with respect to a for $y = 0$ and $z = 0$ are:

$$\frac{d}{da}\frac{(\sigma^z_{xx})}{p_u} = \frac{(1-2\nu)}{\pi}\left(\frac{b}{b^2+(a-x)^2}\right) \tag{A.25}$$

$$\frac{d}{da}\frac{(\sigma^z_{yy})}{p_u} = -\frac{(1-2\nu)}{\pi}\left(\frac{b}{b^2+(a-x)^2}\right) \tag{A.26}$$

$$\frac{d}{da}\frac{(\sigma^x_{xx})}{q_{ux}} = \frac{2b}{\pi\delta_0}\left(\frac{1}{a-x}+\frac{\nu(a-x)}{\delta_0^2}\right) \tag{A.27}$$

$$\frac{d}{da}\frac{(\sigma^x_{yy})}{q_{ux}} = \frac{2\nu\, b}{\pi\delta_0}\left(\frac{1}{a-x}-\frac{(a-x)}{\delta_0^2}\right) \tag{A.28}$$

Hence, the stress field may be evaluated at any point along the x-axis by integrating the product of the local tractions and the deriviatives above over the traction element. Because of the Cauchy nature of the eqautions required to derive the above, if x lies within contact then the following constants must be added to the integrals:

$$\begin{aligned}
\sigma^z_{xx} &: -p(x) \\
\sigma^z_{yy} &: -2\nu\, p(x) \\
\sigma^z_{zz} &: -p(x) \\
\sigma^x_{zx} &: -q_x(x)
\end{aligned}$$

For example if the traction distribution acting over the special element $2b$ wide was $p(a)$ and $q_x(a)$ from a_1 to a_2, then the σ_{xx} component of stress at $(x,0,0)$ within the contact would be:

$$\sigma_{xx}(x,0,0) = \int_{a1}^{a2} \left(\frac{(1-2\nu)}{\pi} \left(\frac{b}{b^2+(a-x)^2} \right) p(a) + \frac{2b}{\pi\delta_0} \left(\frac{1}{a-x} + \frac{\nu(a-x)}{\delta_0^2} \right) q_x(a) \right) da - p(x) \tag{A.29}$$

Bibliography

Ahmadi, L. M., Keer, L. M., and Mura, T. 1983. "Non-Hertzian contact stress analysis for an elastic half space—normal and sliding contact". *Int. Jnl. Solids and Structures*, Vol. 19, pp. 357–373.

Amontons, G. 1699. "De la resistance causee dans les machines". *Histoires Acad. Roy. Sci., Paris*, Vol. 12, p. 206.

Atkins, A. 1991. *Cracks induced by sliding a rigid sphere over a glass plate.* Private communication.

Bentall, R. H., and Johnson, K. L. 1967. "Slip in the rolling contact of two dissimilar elastic rollers". *International Journal of the Physics of Solids*, Vol. 9, pp. 389–404.

Beuckner, H. F. 1970. "A novel principle for the computation of stress intensity factors". *ZAMM*, Vol. 50, pp. 529–546.

Boussinesq, J. 1885. "Applications des potentials à l'etuude de l'équilibre et du mouvemnt des solides élastique".

Bowden, F. P., and Tabor, D. 1942. "The theory of metallic friction and the role of shearing and ploughing". *Council Sci. and Ind. Research, Comm. of Australia, Bulletin*, Vol. 145.

Bower, A. F. 1988. "The influence of crack face friction on surface initiated rolling contact fatigue cracks". *ASME Journal of Tribology*, Vol. 11, pp. 1–8.

Bryant, M. D., Miller, G. R., and Keer, L. M. 1984. "Line contact between a rigid indenter and a damaged elastic body". *Quarterly Journal of Applied Mathematics*, Vol. 37, pp. 467–478.

Carter, F. W. 1926. "On the action of a locomotive driving wheel". *Proc. Roy. Soc. London*, Vol. A112, pp. 151–157.

Cattaneo, C. 1938. "Sul contatto di due corpi elastici: distribuzione locale degli sforzi". *Rendiconti dell'Accademia natzionale dei Lincei*, Vol. 27, pp. 342–348, 434–436, 474–478.

Cerruti. 1882. *Accademia dei Lincei, Roma.*

Coulomb, E. 1785. "Theorie des machines simples". *Mem. Math. Phys., Paris*, Vol. 10, p. 161.

Dewynne, J.N. *The opening displacement of surface-breaking plane cracks.* Under review *Int. Journal of Fracture.*

Dubourg, M. C. 1989. *Le contact unilateral avec frottment le long de fissures de fatigue dans les liasons mechaniques.* Ph.D. thesis, L'Institut National des Sciences Appliquées de Lyon.

Dundurs, J., and Mura, T. 1964. "Interaction between an edge dislocation and a circular inclusion". *Journal of the Mechanical Physics of Solids*, Vol. 12, pp. 177–189.

Dundurs, J., and Sendeckyj, G. P. 1965. "Behaviour of an edge dislocation near a bimetallic interface". *Journal of Applied Physics*, Vol. 32, pp. 3353–3354.

Duvaut, G., and Lions, J.-L. 1972. *Les inéquations en mécanique et en physique.* Paris: Dunod.

Erdmann, M. A., and Mason, M. 1986. An exploration of sensorless manipulation. *In: IEEE International Conference on Robotics and Automation.*

Erdogan, F., Gupta, G. D., and Cook, T. S. 1973. Numerical solution of singular integral equations. *Pages 368–425 of:* Sih, G. C (ed), *Methods of analysis and solutions of crack problems.* Noordhoff.

Ernst, H., and Merchant, M. E. 1938. "Die Reibungskraft in der wahren Kontaktflache". *Wiss. Veroff Siemens Werke*, Vol. 17, p. 38.

Ernst, H., and Merchant, M. E. 1940. Surface friction between metals—a basic factor in the metal cutting process. *Page 76 of: Proc. Special Summer Conf. Friction and Surface Finish.* MIT Press, Cambridge, Mass.

Fichera, G. 1984. "Problemi elastostici co vincoli unilaterale: il problema di Signorini con ambigue codizioni al contorno". *Memorie Accademie Nazionale dei Lincei*, Vol. 8, pp. 91–140.

Frank, F. C., and Lawn, B. R. 1967. "On the theory of Hertzian fracture". *Proc. Roy. Soc.*, Vol. A299, pp. 291–306.

Gilroy, D. R., and Hirst, W. 1969. "Brittle fracture of glass under normal and sliding loads". *Brit. Jnl. Appl. Phys. Ser. 2*, Vol. 2, pp. 1784–1787.

Goodman, L. E. 1962. "Contact stress analysis of rough spheres". *Jnl. Appl. Mech.*, Vol. 84, pp. 515–522.

Goshima, T., and Keer, L. M. 1990. "Thermoelastic contact between a rigid indenter and a damaged elastic body". *ASME Journal of Tribology*, Vol. 112, pp. 382–391.

Goyal, S. 1989. *Planar sliding of a rigid body with dry friction: limit surfaces and dynamics of motion.* Ph.D. thesis, Cornell University, Ithaca, NY.

Goyal, S., Ruina, A., and Papadopoulos, J. 1989 (May). Limit surface and moment function discriptions of planar sliding. *In: Proceedings IEEE International Conference on* Robotics and Automation, *Scotsdale, Arizona.*

Greenwood, J. A., and Williamson, J. B. P. 1966. "Contact of nominally flat surfaces". *Proc. Roy. Soc.*, Vol. A295, p. 300.

Hamilton, G. M. 1983. "Explicit equations for the stresses beneath a sliding spherical contact". *Proc. Instn. Mech. Engnrs.*, Vol. 197, pp. 53–59.

Hamilton, G. M., and Goodman, L. E. 1966. "The stress field created by a circular sliding contact". *ASME Journal of Applied Mechanics*, Vol. 88, pp. 371–376.

Hardy, W. B., and Hardy, J. K. 1919. "Note on static friction and on the lubricating properties of certain chemical substances". *Phil. Mag.*, Vol. 6, p. 32.

Hartnett, M. J. 1980. A general numerical solution for elastic body contact problems. *Pages 51–56 of:* Cheng, H. S., and Keer, L. M. (eds), *Solid contact and lubrication*, vol. 39. ASME AMD.

Hertz, H. 1882. "On the elastic contact of rigid elastic solids". *J. Reine und Angewandte Mathematik.*

Hills, D. A., and Nowell, D. 1989. "Stress intensity calibrations for closed cracks". *Journal of Strain Analysis*, Vol. 24(1), pp. 37–43.

Hills, D. A., and Sackfield, A. 1985. "Sliding contact between dissimilar elastic cylinders". *ASME Journal of Tribology*, Vol. 107, pp. 463–466.

Hills, D. A., and Sackfield, A. 1987. "The stress field induced by normal contact between dissimilar spheres". *ASME Journal of Applied Mechanics*, Vol. 109, pp. 8–14.

Hüber, M. T. 1904. "On the theory of elastic solid contact". *Annalen der Physik*, Vol. 14, pp. 153–163.

Johnson, K. L. 1985. *Contact mechanics.* Cambridge: Cambridge University Press.

Johnson, K. L., O'Connor, J. J., and Woodward, A. C. 1973. "The effect of indenter elasticity on the Hertzian fracture of brittle materials". *Proc. Roy. Soc.*, Vol. A334, pp. 95–117.

Kalker, J. J. 1971. "A minimum principle for the law of dry friction, with application to elastic cylinders in rolling contact". *ASME Journal of Applied Mechanics*, Vol. 38, pp. 875–880.

Kalker, J. J. 1979. "The computation of three-dimensional rolling contact with dry friction". *International Journal for Numerical Methods in Engineering*, Vol. 14, pp. 1293–1307.

Kalker, J. J. 1990. *Three dimensional elastic bodies in rolling contact.* Dordrecht: Kluwer Academic Publishers.

Klarbring, A. 1986. "A mathematical programming approach to three-dimensional contact problems with friction". *Computer Methods in Applied Mechanics and Engineering*, Vol. 50, pp. 175–200.

Korsunsky, A. *Singularities at crack-contact interfaces.* Personal correspondence.

Krenk, S. 1975. "On the use of the interpolation polynomial for solutions of singular integral equations". *Quaterly Journal of Applied Mathematics*, Vol. 32, pp. 479–484.

Lawn, B. R. 1967. "Partial cone crack formation in brittle material with a sliding spherical indenter". *Proc. Roy. Soc.*, Vol. A299, pp. 307–317.

Li Yingzhi, and Hills, D. A. 1987. "The Hertzian cone crack". *ASME Jnl. App. Mech.*, Vol. 109, pp. 8–14.

Liu, C., and Paul, B. 1989. "Fully developed sliding of rough surfaces". *ASME Journal of Tribology*, Vol. 111, pp. 445–451.

Love, A. E. H. 1929. "Stress produced on in a semi-infinite solid by pressure on part of the boundary". *Phil. Trans. Royal Society*, Vol. A228, p. 377.

MacMillan, W. D. 1936. *Dynamics of rigid bodies.* New York: McGraph-Hill.

Mason, M. T. 1982. *Manipulator grasping and pushing operations.* Ph.D. thesis, Massachusetts Institute of Technology.

Mason, M. T. 1986. "Mechanics and planning of manipulator pushing operations". *International Journal of Robotics Research*, Vol. 5(3), pp. 53–71.

M'Ewen, E. 1949. "Stresses in elastic cylinders along a generatrix". *Philosophical magazine*, Vol. 40, p. 454.

Mindlin, R. D. 1949. "Compliance of elastic bodies in contact". *ASME Journal of Applied Mechanics*, Vol. 16, pp. 259–268.

Mouginot, R. 1987. Sliding Hertzian fracture. Proc. I. Mech. E. Int. Conf. Tribology. *Pages 995–1001 of: Lubrication and wear fifty years on C197/87.*

Mouwakeh, M. 1989. *Etude quantitative des phenomenes de glissements dans un contact sec a deux corps par comparison avec la propagation d'une fissure interfaciale.* Ph.D. thesis, L'Institut National des Sciences Appliques de Lyon.

Nowell, D., and Hills, D. A. 1987. "Open cracks at or near free edges". *Journal of Strain Analysis*, Vol. 22(3), pp. 177–185.

Nowell, D., and Hills, D. A. 1988. "Tractive rolling of dissimilar elastic cylinders". *Int. Jnl. Mech. Sci.*, Vol. 30(6), pp. 427–439.

Nowell, D., Hills, D. A., and O'Connor, J. J. 1987 (July). An analysis of fretting fatigue. I. Mech. E. conference on tribology, friction, lubrication and wear. *In: Proc. I. Mech. E., C131/87.*

Nowell, D., Hills, D. A., and Sackfield, A. 1988. "Contact of dissimilar elastic cylinders under normal and tangential loading". *Int. Jnl. Mech. Phys. Solids*, Vol. 36(1), pp. 59–75.

Paul, B., and Hashemi, J. 1981. "Contact pressures in closely conforming elastic bodies". *ASME Journal of Applied Mechanics*, pp. 543–548.

Peshkin, M. A. 1986. *Planning robotic manipulation strategies for sliding objects.* Ph.D. thesis, Carnegie-Mellon University.

Peshkin, M. A., and Sanderson. 1988. "The motion of a pushed, sliding workpiece". *IEEE Journal of Robotics and Automation*, Vol. 4(6), pp. 569–598.

Poritsky, H. 1950. "Stresses and deflections of cylindrical bodies in contact with application to contact of gears and locomotive wheels". *ASME Journal of Applied Mechanics*, Vol. 17, pp. 191–200.

Powell, M. J. D. 1970. A hybrid method for nonlinear algebraic equations. *In:* Rabinowitz, P. (ed), *numerical methods for nonlinear algebraic equations.* Gordon and Breach.

Prescott, J. 1923. *Mechanics of particles and rigid bodies.* London: Longmans, Green, and Co.

Reynolds, O. 1875. "On rolling friction". *Phil. Trans. Royal Society*, Vol. 166, p. 155.

Roesler, F. C. 1957. "Brittle fractures near equilibrium". *Proc. Roy. Soc.*, Vol. A299, pp. 981–992.

Sackfield, A., and Hills, D. A. 1983. "A note on the Hertz contact problem—a correlation of standard formulae". *Journal of Strain Analysis*, Vol. 18, pp. 195–197.

Smith, J. O., and Liu, C. K. 1953. "Stresses due to normal and tangential loads on an elastic solid with application to some contact stress problems". *ASME Journal of Applied Mechanics*, Vol. 21, pp. 157–166.

Spence, D. A. 1973. "An eigen value problem for elastic contact with finite friction". *Proc. Cambridge Philosophical Society*, Vol. 73, pp. 249–268.

Spence, D. A. 1975. "The Hertz contact problem with finite friction". *Journal of Elasticity*, Vol. 5, pp. 297–319.

Szalwinski, C. M. 1985. "Flexibility of a contact area of an isotropic body". *ASME Journal of Applied Mechanics*, Vol. 52, pp. 62–66.

Timoshenko, S. P., and Goodier, J. N. 1970. *Theory of elasticity.* McGraw-Hill. Pages 409–420.

Tomlinson, G. A. 1929. "A molecular theory of friction". *Phil. Mag.*, Vol. 7, p. 905.

Van Groenou, A. B., and Kadijk, S. E. 1988. "Sliding sphere wear test on nickel zinc and manganese zinc ferrites". *Wear*, Vol. 126, pp. 91–110.